November 2015

Biophysical Characterization of Katanin's Regulation of Microtubules

Megan E. Bailey
University of Massachusetts - Amherst

Biophysical Characterization of Katanin's Regulation of Microtubules

A Dissertation Presented

by

MEGAN E. BAILEY

Submitted to the Graduate School of the
University of Massachusetts Amherst in partial fulfillment
of the requirements for the degree of

DOCTOR OF PHILOSOPHY

SEPTEMBER 2015

Molecular and Cellular Biology

Biophysical Characterization of Katanin's Regulation of Microtubules

A Dissertation Presented

by

MEGAN E. BAILEY

Approved as to style and content by:

_____
Jennifer L. Ross, Chair

_____
Peter Chien, Member

_____
Edward P. Debold, Member

_____
Thomas J. Maresca, Member

_____
Elizabeth R. Dumont, Director
Molecular and Cellular Biology Program

DEDICATION

To my husband and my family.

ACKNOWLEDGMENTS

I would like to thank Dr. Jennifer Ross for her guidance and continued support throughout my PhD. Her commitment to teaching and mentoring is inspirational. I feel lucky to have been able to work under her mentorship.

Thank you to my family for their continued support in everything I have done (including my art history degree). They have made a real effort to understand my research and why I find it exciting and for this I thank them. I would like to especially thank my sister, Katelin Bailey, for commiserating and reminding me to keep pushing forward as we both endure our PhDs.

I would like to thank my husband, Samuel Johansson, for coming on this crazy journey with me. He has been positive and encouraging throughout the process, and genuinely interested despite the missed dinners, long hours, and forgotten plans. Thank you for all the support.

Without my committee's helpful input this PhD would not have been possible. I would like to especially like to thank Peter Chien. He has spent many hours helping me troubleshoot and interpret ATPase assay data. Also thank you to Jing Liu from the Chien lab for helping me successfully perform the ATPase assays. I would also like to thank Ned Debold and Tom Maresca for their useful advice and support throughout my research.

ABSTRACT

BIOPHYSICAL CHARACTERIZATION OF KATANIN'S REGULATION OF MICROTUBULES

SEPTEMBER 2015

MEGAN E. BAILEY

B.S., WILLIAMS COLLEGE

Ph.D., UNIVERSITY OF MASSACHUSETTS AMHERST

Directed by: Dr. Jennifer L. Ross

Microtubules, as an essential part of the cytoskeleton, require proper function as well as correct spatial and temporal localization. In order to achieve correct organization, microtubule-associated proteins (MAPs) regulate microtubule dynamics. Katanin, a known microtubule-severing enzyme from the AAA family of proteins, plays a role in regulating microtubules, but the mechanisms of microtubule control and the mechanism of severing activity remain to be elucidated.

In the following studies I examine mechanisms of katanin-based regulation of microtubule dynamics using a single molecule biophysics approach. I use this simplified in vitro approach to change specific parameters to investigate how katanin targets microtubules with defects, how free tubulin regulates katanin severing activity, and how katanin and tau regulate dynamic microtubules. This work provides us with new insights as to how katanin targets both stable and dynamic microtubules as well as how katanin is regulated by other cellular components.

TABLE OF CONTENTS

Page

LIST OF TABLES

Table Page

LIST OF FIGURES

CHAPTER 1

INTRODUCTION

1.1 Biophysics

Biophysics is an interdisciplinary field that applies the theories and techniques of physics to study biological questions. Biophysics is an inherently quantitative field, and allows us to provide quantitative answers to questions that have typically been able to only be answered with qualitative techniques. The field of biophysics is expanding and is currently working on questions in various systems within the cell. One question that can be difficult to answer in a crowded cellular environment is how proteins fold, but is more feasible in vitro using biophysical techniques. Additional questions about DNA to RNA transcription, axonal firing, as well as how motor proteins transport cargo throughout the cell are able to be addressed using biophysical techniques and significant progress is being made toward understanding the molecular mechanisms of these processes.

In this dissertation I aim to describe how I employed biochemical and biophysical techniques to better understand regulation of microtubule organization. Microtubule severing enzymes are a known family of microtubule-associated proteins (MAPs) that regulates both the dynamics and the organization of microtubule cytoskeleton. I specifically aim to investigate how these enzymes target microtubules for severing, and how they regulate dynamic microtubules. To address these questions, I used purified severing enzymes and microtubules to begin to reconstitute this system in vitro. I can begin to introduce complexity by changing the type of microtubules, or adding additional MAPs to the system to better understand how these unique enzymes may regulate microtubules in vivo. This work will hopefully give us a better understanding of the mechanisms severing enzymes use and we can begin to answer more complex

questions about regulating an entire network of microtubules.

1.2 Microtubules

The cell is full of complex machinery that require proteins, enzymes and organelles to be in specific places at specific times for proper function. Many of these functions require the microtubule network, which is the primary highway system that is used to transport materials across the cell, to aid the complex machinery. In addition to transport, microtubules are essential for cell motility, cell division, and structural support.

Microtubules are hollow tubes, that in vivo are predominately composed of 13 protofilaments, however, in vitro microtubules can vary in protofilament number from 12-16 when stabilized with Taxol, and can vary further depending on polymerization conditions (Mandelkow et al. 1986; Amos and Schlieper 2005). Each protofilament is composed of heterodimers of alpha and beta tubulin (Nogales, Wolf, and Downing 1998), which self-associate in a head-to-tail manner (Fig 1.1A). Alpha tubulin is always at the minus end of the microtubule and beta tubulin is at the plus end (Fan et al. 1996; Hirose, Fan, and Amos 1995). The structure of a protofilament has been solved using cryo-EM by making crystals from zinc sheets of tubulin. This resulted in anti-parallel arrays of protofilaments, which are believed to have similar protofilament structure (Löwe et al. 2001).

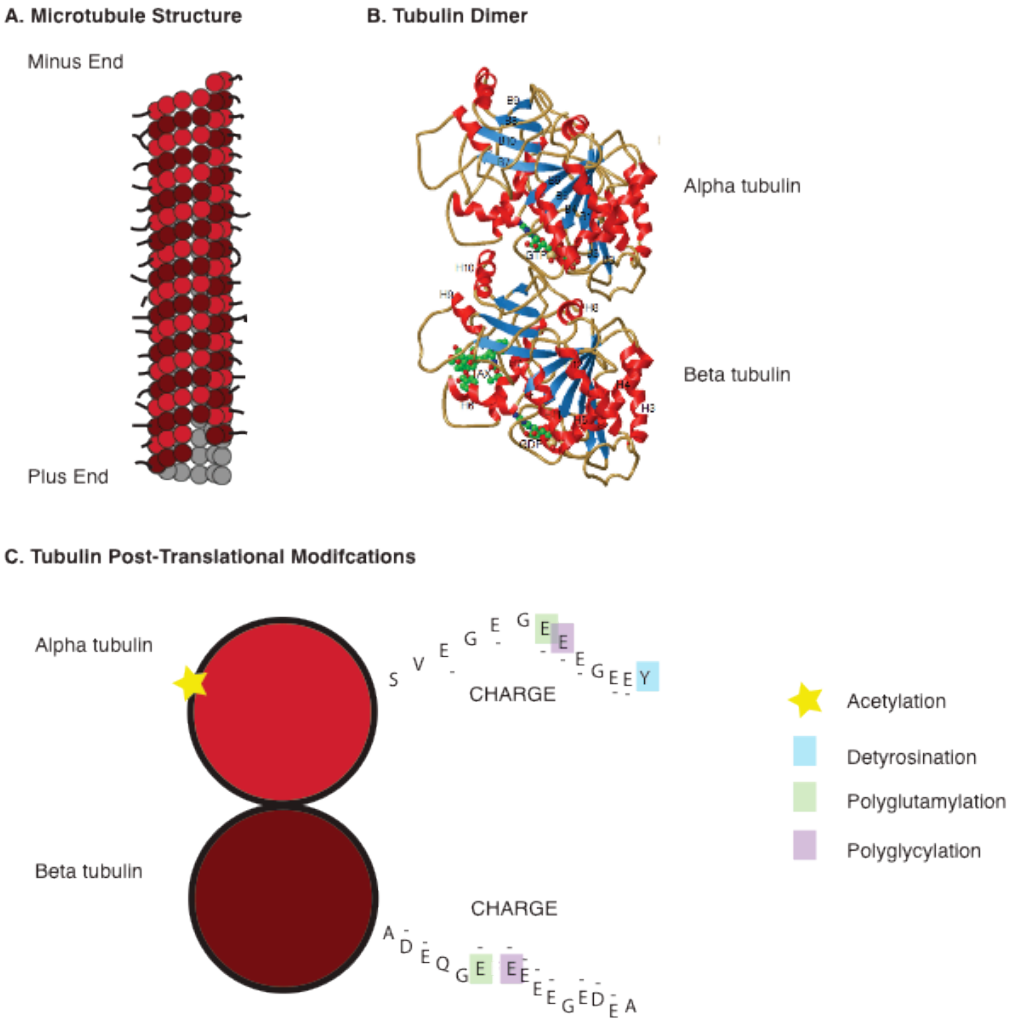

Figure 1.1 Microtubule and Tubulin Structure.

(**A**) Diagram of a 13-protofilament microtubule. Red is alpha tubulin and dark red is beta tubulin. The CTTs of tubulin extend off the microtubule. In the presence of GTP, tubulin will assemble in a head to tail fashion, alpha tubulin at the minus end and beta tubulin at the plus end, to form protofilaments and the protofilaments will eventually fold into a hollow tube made up of 13 protofilaments. (**B**) Ribbon diagram of the structure of the tubulin dimer. Shows the locations where GTP and Taxol interact with the alpha and beta tubulin. Images reproduced with permission from Nogales et al (Nogales1998). (**C**) Diagram of the potential post translational modifications of alpha and beta tubulin. Many of the post translational modifications occur on the CTTs of tubulin, with the exception of acetylation, which occurs on the lumen side of the alpha tubulin. The charged amino acids on each of the tails are labeled.

Microtubules are characterized by a helical structure with lateral (side-to-side) interactions between protofilaments predominately with alpha-alpha or beta-beta association, also known as B type lattice (Song and Mandelkow 1993). Due to the offset of the protofilaments from the helical rotation, there is a seam that runs that length of the microtubule, where there are alpha-beta interactions, or A lattice (Fig. 1.1) (Song and Mandelkow 1993). The longitudinal interactions (top-to-bottom) between tubulin dimers tend to be stronger interactions, since disassembly of microtubules is characterized by peeling back of protofilament loops (Mandelkow, Mandelkow, and Milligan 1991).

Alpha and beta tubulin are very similar in sequence and only differ along the longitudinal axis in structure. Both monomers are approximately 46 x 40 x 65 Å (Nogales et al. 1999). Each monomer has three characteristic domains. The N-terminal domain is the nucleotide binding domain, a smaller domain in the middle, where stabilizing agents tend to bind, and a helical C-terminal domain (Nogales et al. 1999). The C-terminal domain, or the C-terminal tail (CTT), is made up of helices H11 and H12, which are relatively disordered and is where many microtubule associated proteins (MAPs) dock (Nogales, Wolf, and Downing 1998). While tails of alpha and beta tubulin are both acidic and negatively charged, their sequence differs, allowing them to be differentially modified and for the MAPs to interact specifically with one or the other (Reviewed in Janke 2014; Nogales, Wolf, and Downing 1998).

Although the alpha and beta subunit both have binding sites for GTP, only the beta site is able to be hydrolyzed (Mitchison 1993; Nogales, Wolf, and Downing 1998; Nogales et al. 1999). Therefore, two molecules of GTP bind to tubulin dimers, one at the non-exchangeable (N-site) on alpha tubulin, embedded within the stable dimer, and another at the exchangeable (E site) on beta tubulin (Weisenberg, Deery, and Dickinson 1976; Nath, Eagle, and Himes 1986). The nucleotide interacts with the next monomer

near the longitudinal interface (Nogales, Wolf, and Downing 1998). When the microtubule is polymerizing, a new dimer adds to the plus end of the microtubule. Loop T7 and helix H8 in alpha tubulin of this dimer interact with the beta tubulin at the end of the growing microtubule, acting like an GAP (GTPase Activating Complex) and consequently hydrolyzing the GTP on the beta tubulin (Löwe et al. 2001). Since the GTP on the new dimer is not actually hydrolyzed yet, there is typically a layer of GTP tubulin at the plus ends of the microtubules, called a "GTP cap" (Nogales et al. 1999). Since the minus end of the microtubule consists of alpha tubulin, it is unlikely to have a GTP cap unless there is a high concentration of free tubulin present (Nogales et al. 1999).

GTP hydrolysis can cause protofilaments to bend into the rings that we observe when microtubules disassemble. GTP hydrolysis causes the dimers to bend backwards, however, if neighboring protofilaments are still bound to the dimer, this association can constrain the protofilament so it does not bend (Nogales et al. 1999). Since the lateral interaction of GDP-tubulin are weaker, if enough dimers have had GTP hydrolyzed, this can cause rapid depolymerization, or peeling back of filaments to release the stored energy from the conformational changes (Nogales et al. 1999). The idea of a GTP cap was confirmed experimentally years before the crystal structure, by observing microtubules that were cut with a UV beam in vitro (Walker, Pryer, and Salmon 1991). The microtubule plus ends would rapidly depolymerize, however, the minus ends, remained the same length or even elongated (Walker, Pryer, and Salmon 1991).

1.3 Post-Translational Modifications of Tubulin

Alpha and beta tubulin are highly conserved. In order to generate diversity to regulate the wide variety of functions that microtubules are involved in, there are two mechanisms that have been created. First, there are different isoforms of alpha and beta tubulin that

can be expressed and second, there are a variety of post-translational modifications (PTMs) that can modify alpha and beta tubulin differentially. (Reviewed in Janke 2014). PTMs can affect overall tubulin assembly, MAP binding to regulate microtubule dynamics, or even microtubule motor motility (Sirajuddin, Rice, and Vale 2014). Some of the major PTMs that occur on tubulin are acetylation, detyrosination/tyrosination, polyglutamylation, and polyglycylation.

Tubulin acetylation involves the addition of an acetyl group onto lysines. This PTM is enriched in stable microtubule populations and was first discovered on alpha tubulin K40 in *Chlamydomonas reinhardtii* (L'Hernault and Rosenbaum 1985). It is possible that are there more acetylation sites, however they have not been confirmed (Choudhary et al. 2009). While acetylation is found more frequently in more stable microtubules, and has been shown to be more resistant to drug induced depolymerization (Matsuyama et al. 2002), it does not actually affect the structure of the microtubule (Howes et al. 2014). K40 is located on the inside of the microtubule and would likely affect binding the microtubules to the inside the microtubule. However, it has also been shown to regulate intracellular transport by kinesin motors (Reed et al. 2006). Recently it has been also shown that an increase in microtubule acetylation decrease the motility of axonemal dynein (Alper et al. 2014).

Unlike acetylation, detyrosination is known to only occur on alpha tubulin. Alpha tubulin has a tyrosine at the C-terminus that can be removed (Hallak et al. 1977). Detyrosinated tubulin is found on parts of mitotic spindle microtubules (Gundersen and Bulinski 1986) as well as in more stable and older microtubules in neurons (Cambray-Deakin and Burgoyne 1987; Brown et al. 1993; Robson and Burgoyne 1989). Detyrosination increases the stability against MCAK and KIF2 (Peris et al. 2009; Sirajuddin, Rice, and Vale 2014). There is also a significant increase in binding affinity

and processivity of Kinesin-I and CENP-E, a kinetochore motor, in vitro on detyrosinated microtubules {Liao:1998vg, Dunn:2008ig, Konishi:2009ja, Kaul:2014cu, (Barisic et al. 2015).

Polyglutamylation is the addition of a secondary chain of glutamate residues to glutamate resides within the alpha or beta tubulin tails. Polyglutamylation is found extensively in neuronal microtubules (Audebert et al. 1993; Audebert et al. 1994), as well as the axonemes of cilia (Fouquet et al. 1994), and at centrioles (Bobinnec et al. 1998). Severing enzymes have been shown to regulate polyglutamylated microtubules (Sharma et al. 2007; Lacroix et al. 2010).

Polyglycylation involves adding a secondary chain of glycine residues to the CTTs of either alpha or beta tubulin. It is still unclear how glycylation regulates microtubules, but axonemes without glycylation disassemble soon after assembling (Rogowski et al. 2009; Bosch Grau et al. 2013).

1.4 Microtubule dynamics

Microtubules are known to be dynamic polymers that grow and shrink and this property allows them to perform the diverse functions and dynamic reorganization. Microtubule dynamics were first studied in vitro in 1984 when Mitchison and Kirshner grew dynamic microtubules off of axonemes. The axonemes were fixed every 10 seconds and visualized with electron microscopy (Mitchison and Kirschner 1984). These experiments were further confirmed using dark field light microscopy and differential interference contrast light microscopy (Horio and Hotani 1986; Walker et al. 1988). From these studies, they were able to infer kinetics of assembly of dynamic microtubules. This work revealed that different microtubules within the same slide were able to simultaneously grow and shrink at the same time points, which has been named

“dynamic instability” (Mitchison and Kirschner 1984). Even in conditions where the tubulin is above the critical concentration microtubules will shrink rapidly, which is called a “catastrophe” (Fig. 1.2). When the microtubule begins to grow again, that is called a “rescue” (Mitchison and Kirschner 1984).

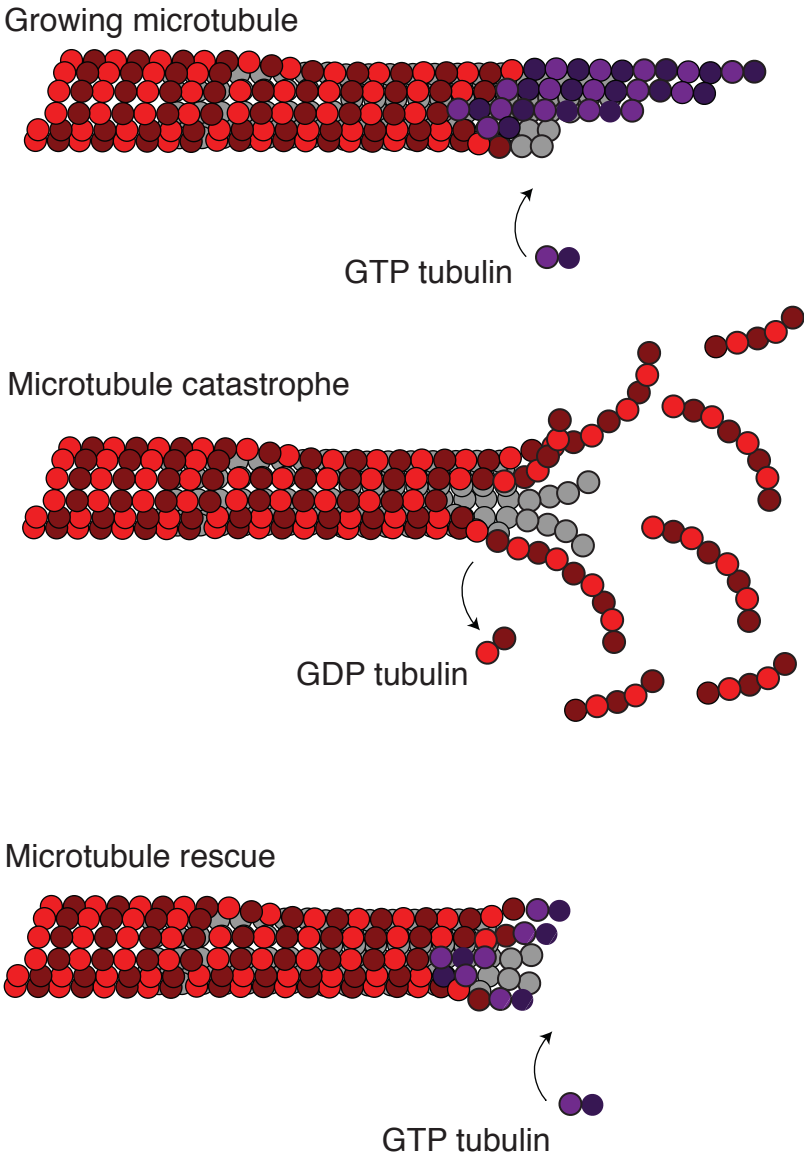

Figure 1.2 Microtubule Dynamics.

Diagrams of the states a dynamic microtubule can undergo. Microtubules can grow with addition of GTP tubulin. The growth will occur predominately on the plus end, however, in vitro can also occur on the minus ends of microtubules. When the microtubule loses the GTP cap, it can undergo a shrinking event, called a catastrophe. This can also be aided by destabilizing MAPs that cause more frequent catastrophes. Catastrophes can be rescued, which is a growth event following a catastrophe. This often occurs because a stabilizing MAP stabilizes the microtubule by adding additional GTP tubulin to the end. Rescues can also occur more frequently in conditions of excess tubulin.

These dynamic length changes are temperature dependent as well (Caplow, Shanks, and Ruhlen 1988). Microtubules will disassemble more rapidly at lower temperatures and tend to grow more at higher temperatures. However, they will still undergo dynamic events in both conditions. In vivo, microtubules generally grow out from an organizing center like the centrosome. In vitro, microtubules can undergo dynamic instability on both ends as long as the tubulin concentration is above a critical concentration (Schiff, Fant, and Horwitz 1979).

While it is generally thought that microtubules in vivo are attached at the minus end to centrosomes or another nucleating center and undergo dynamic instability primarily on the plus ends, there is evidence that microtubules can undergo dynamic instability in the form of treadmilling during interphase and during mitosis (Reviewed in Waterman-Storer and Salmon 1997). Treadmilling was originally a phenomenon proposed for actin where the filament has a constant on rate of subunits adding to one end and disassembly of subunits on the other end (Wegner 1976). Tubulin can treadmill in the plus end direction at a rate of 4 μm per hour (Walker et al. 1988). Bulk in vitro microtubule assays have demonstrated that microtubules can undergo treadmilling with MAPs in vitro, but at a slower rate of 1 μm per hour (Margolis and Wilson 1978). Further, microtubules can treadmill in a minus end direction with MAPs (Hotani and Horio 1988). These prior results showed that microtubule-associated proteins (MAPs) would likely change the kinetic properties of dynamic instability and treadmilling.

1.5 Microtubule Stabilization

There are multiple ways of stabilizing microtubules so that they do not undergo growth and shrinkage events. Often paclitaxel (Taxol), a small molecule chemotherapy drug, is used to stabilize microtubules made in vitro. It is known through a variety of

structural studies that Taxol likely binds to a hydrophobic patch on beta tubulin that is next to the core helix and M-loop in beta tubulin on the inside surface of the microtubule (Wang and Nogales 2005; Nogales et al. 1999; Snyder et al. 2001). The same location on alpha tubulin is blocked due to the extended L-loop. There are several proposed mechanisms for how Taxol stabilizes microtubules. One theory is that Taxol holds the M-loop in place and stabilizes the contacts between protofilaments (Nogales et al. 1999; Li et al. 2002). Another possibility is that Taxol can position the domains in an orientation that promotes straight protofilaments (Amos and Löwe 1999). There are a variety of other microtubule-stabilizing drugs, but many of them bind in the same pocket of beta tubulin as Taxol (Haar et al. 1996; Hamel et al. 1999; Long et al. 1998).

It is also known that GMPCPP, a GTP analogue, can stabilize microtubules (Hyman et al. 1992). GMPCPP replaces an oxygen between the β and γ phosphate with a carbon. GMPCPP is a slowly hydrolyzable analog of GTP that can stabilize microtubules by keeping beta tubulin in the GTP-bound state. Often, microtubules are made in vitro with GMPCPP to simulate GTP bound tubulin. They are also used frequently as seeds to help nucleate and polymerize dynamic microtubules.

1.6 Microtubule-Associated Proteins (MAPs)

Microtubule-associated proteins (MAPS) are proteins that are known to interact with microtubules and can regulate their stability, target microtubules, or even mediate interactions with other cellular proteins. Another way to stabilize microtubules both in vivo and in vitro is with MAPs. MAPs can stabilize microtubules by several different mechanisms: by preventing catastrophes, rescuing a depolymerizing microtubules, or by decreasing the overall shrinking speed.

Plus TIPs are a class of MAPS that bind to growing microtubule plus ends and

track the TIPs and often can stabilize the microtubules by binding to the cell cortex (Schuyler and Pellman 2001; Reviewed in Gundersen, Gomes, and Wen 2004). EB1 and EB3 are both plus-tip MAPs that stabilize microtubules by preventing catastrophes (Komarova et al. 2009).

XMAP215 can significantly increase the polymerization speed of microtubules (Gard and Kirschner 1987a). It has been shown to increase both the growth and shrinkage rates in cells as well (Vasquez, Gard, and Cassimeris 1994; Tournebize et al. 2000). It can enhance both polymerization and depolymerization by binding to the tubulin dimer and promoting incorporation into the growing microtubule (Brouhard et al. 2008).

Tau is another MAP that is known to stabilize microtubules by binding along the lattice of microtubules. Tau comes in six isoforms, all of which are found in axons. It has very little secondary structure (Cleveland, Hwo, and Kirschner 1977; Schweers et al. 1994), but there are three essential domains: the negatively-charged N-terminal projection domain that extends out from the microtubule and spaces out microtubules (Chen et al. 1992), the positively charged proline-rich region that interacts with the surface of the microtubule (Trinczek et al. 1995; Goode et al. 1997; Brandt and Lee 1993) and the repeat region that binds to the interior of the microtubules (Chau et al. 1998; Serrano et al. 1985; Maccioni, Rivas, and Vera 1988). There is some evidence that tau does not function as a monomer, but as a dimer, zippering together N-terminal regions of tau (Rosenberg et al. 2008). Similar to Taxol, Tau binds and fills the hydrophobic pocket of the β-tubulin that interacts with nearby dimers on other protofilaments.

In addition to stabilizing MAPs, there are also destabilizing MAPs. Destabilizing MAPs can destabilize microtubules in several ways. Destabilizers can inhibit polymerization, cause more frequent catastrophes, or promote disassembly of the

filaments. MCAK, a member of the kinesin-13 family, is an example of a catastrophe-promoting factor. It has been shown that MCAK is ATP-dependent and causes more frequent catastrophes both in cells and in vitro. More recent work has shown that in vitro MCAK and EB3 can make microtubule plus ends in vitro more dynamic (Montenegro Gouveia et al. 2010). Unlike other depolymerizing kinesins, MCAK does not cause catastrophes based on microtubule length, instead it reduces the number of steps it takes to catastrophe and promotes more rapid catastrophes (Gardner et al. 2011). Since the crystal structure of kinesin-13 motors fits better on curved protofilaments, the experimental evidence suggests that MCAK shortens the transition time between growth and catastrophe (Ogawa et al. 2004; Shipley et al. 2004). The Kinesin-8 family is also known to destabilize microtubules, however, they are sensitive to the length of the microtubule and slows growth more on longer microtubules (Gardner et al. 2011).

Stathmin is a negative regulator of microtubules, but regulates microtubules by causing more depolymerization and sequestering tubulin. However, Stathmin has also been reported to be a catastrophe-inducing factor (Belmont and Mitchison 1996). Both experimental evidence and the crystal structure of Stathmin shows that it is able to form a ternary structure and sequester two alpha-beta tubulin dimers (Jourdain et al. 1997; Curmi et al. 1997; Gigant et al. 2000). The N-terminal domain of Stathmin caps the alpha-tubulin so that tubulin cannot be added to the ends of the microtubule (Steinmetz et al. 2000).

Another family of MAPs that destabilizes microtubules is the microtubule severing enzyme family. These enzymes are able to sever and depolymerize microtubules from both ends. Severing enzymes belong to the AAA (ATPases associated with different cellular activities) family of proteins that take advantage of ATP binding and hydrolysis to drive conformational changes for proper enzymatic function (Frickey and Lupas 2004).

There are three known severing enzymes that are found across many organisms: katanin, spastin, and fidgetin.

1.7 Microtubule Severing Enzymes

Microtubule severing enzymes all have a similar C-terminal region that contains the AAA domain. This region is involved in the catalytic activity. It contains the canonical walker A and walker B motifs and P-loop, which are involved in ATP binding and hydrolysis in AAA proteins (Frickey and Lupas 2004). However, the three enzymes differ in their N-terminus. Katanin p60, the catalytic subunit of katanin, is known to contain a microtubule interacting and trafficking (MIT) domain (Iwaya et al. 2010). This region is likely responsible for binding to microtubules. It is known that spastin also contains an MIT domain, although this domain does not interact with microtubules like katanin (White et al. 2007). The MIT domain of fidgetin has not been identified yet.

At the extreme N-terminus of p60 is a domain that interacts with katanin's partner protein, p80 (Fig. 1.3). Katanin p80 is a regulatory protein that is important for regulating p60's severing activity and targeting it to the correct locations in cells. P80 also has domains that interact with other MAPs, such as Dynein (Toyo-Oka et al. 2005). The N-terminus contains WD repeats that can negatively regulate katanin's severing activity (F. McNally 2000). The N-terminus of p80 is also important for targeting to centrosomes (F. McNally 2000). The C-terminus of p80 interacts with the N-terminus of p60 to promote severing activity (F. McNally 2000). Interestingly, partner regulatory proteins have not been identified yet for spastin or fidgetin.

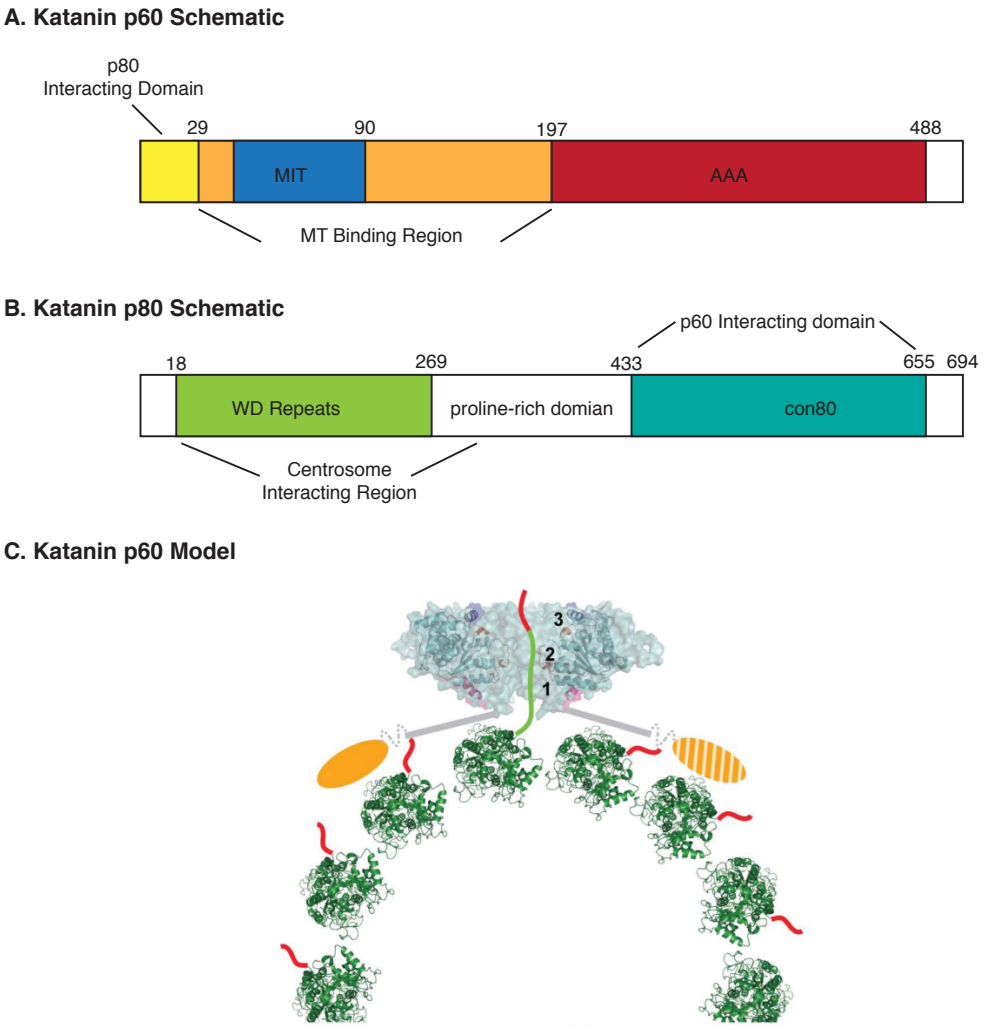

Figure 1.3 Katanin Structure and Model.

(**A**) Schematic of some of the important domains in p60. The N-terminus is comprised of a p80 interacting domain, the microtubule-interacting and trafficking (MIT) domain, as well as the putative microtubule binding domain. The C-terminus contains the AAA domain, which is responsible for the catalytic activity. (**B**) Schematic of known p80 domains. p80 is made up of WD repeats on the N-terminus. This is also the region that is known to target the protein and interact with centrosomes. There is a proline-rich domain the middle, and con80 on the C-terminus is the minimal section necessary for interaction with p60. (**C**) Based on the structural evidence from spastin, a model has been proposed that can be applied to katanin as well since they are similar in sequence and function. The severing enzyme forms a hexamer with a pore in the center. The N-terminal region of the enzyme docks on the microtubules and allowing the CTTs of tubulin to interact with the three pore loops in the pore. The pore loops tug on the CTT of tubulin and unfold the tubulin. This can cause a cascade of events that will result in a severed microtubule. Image reproduced with permission from Roll-Mecak and Vale, 2008.

Microtubule severing enzymes were discovered two decades ago, when a protein in Xenopus egg extracts that used ATP was shown to sever Taxol-stabilized microtubules (Vale 1991). Two years later katanin was identified and purified from sea urchin eggs (F. J. McNally and Vale 1993). It is hypothesized that severing enzymes form a transient hexamer in the presence of ATP to sever microtubules (Hartman et al. 1998; Hartman and Vale 1999; Roll-Mecak and Vale 2008), however, the mechanism is not understood.

In the last decade additional information about how these enzymes interact with their substrates. Subtilisin-treated microtubules, which are missing the CTTs of tubulin are unable to be severed implying that the CTTs are the location for severing enzyme binding and activity (F. J. McNally and Vale 1993; Roll-Mecak and Vale 2008; Eckert, Le, et al. 2012; White et al. 2007). Interestingly, spastin, can interact with either of the alpha or beta CTTs alone or on beads, but prefers to bind to beta tubulin tails (Roll-Mecak and Vale 2008; White et al. 2007). Recent evidence suggests that katanin requires both the alpha and beta tubulin equally (Johjima et al. 2015). The CTTs of tubulin are thought to interact with the pore loops of severing enzyme AAA proteins since mutations in spastin's pore loops, a region of the AAA domain, result in a lack of severing activity (Roll-Mecak and Vale 2008; White et al. 2007).

Based on the crystal structure of spastin's AAA domain as well as biochemical and biophysical evidence there has been a model proposed for how severing enzymes might sever (Roll-Mecak and Vale 2008). The model suggests that the enzymes would hexamerize on a microtubule, in the presence of ATP, forming a pore in the middle of the hexamer. The N-terminal domains of the enzymes would dock on the sides of the microtubule allowing the enzyme to thread the CTTs of tubulin through the pore and begin to disassemble the microtubule.

Severing enzymes require ATP to sever microtubules (Hartman and Vale 1999; Roll-Mecak and Vale 2008; Eckert, Le, et al. 2012), and microtubules can stimulate the ATPase activity (F. J. McNally and Vale 1993; Hartman and Vale 1999). Other steps or mechanisms of severing activity are not known. For instance, the order of binding and forming a hexamer are still unclear. Recent biochemical and computational work on spastin has begun to dissect the ATPase cycle and precisely pinpoint how many subunits are required for severing activity (Eckert, Link, et al. 2012; Le, Eckert, and Woehlke 2013a).

Theoretical and experimental evidence suggests that katanin targets microtubules that have defects. It has been theorized that severing enzymes would not be able to achieve the severing speeds observed in vitro without specific targeting (Davis et al. 2002). This has been supported by experimental data that katanin targets the interfaces of microtubules that have been annealed together (Díaz-Valencia et al. 2011). However, it remains to be elucidated what types of defects katanin actually targets and whether the other severing enzymes target defects as well.

Severing enzymes are found in many organisms, but have diverse roles. Severing enzymes were first discovered in mitotic Xenopus oocyte extracts (Vale 1991). However, even prior to this discovery, *mei-1* and *mei-2* (now known to be katanin homologs) were identified in *C. elegans* during a screen for embryonic lethal mutants (Mains et al. 1990). When *C.* elegans developed null mutations in *mei-1* and *mei-2,* microtubules around the chromosomes are disorganized (Clandinin and Mains 1993; Clark-Maguire and Mains 1994). Katanin is found to be on meiotic chromosomes and spindle pole and when expressed at low levels, results in spindles that are elongated and display orientation defects (Fig. 1.6) (Srayko et al. 2006; K. McNally et al. 2006; Clark-Maguire and Mains 1994; K. McNally et al. 2014). These results have led to the concept that katanin plays a

role in generating new small microtubules that act to nucleate new microtubules to enhance the microtubule network in spindles (Roll-Mecak and Vale 2006; Srayko et al. 2006).

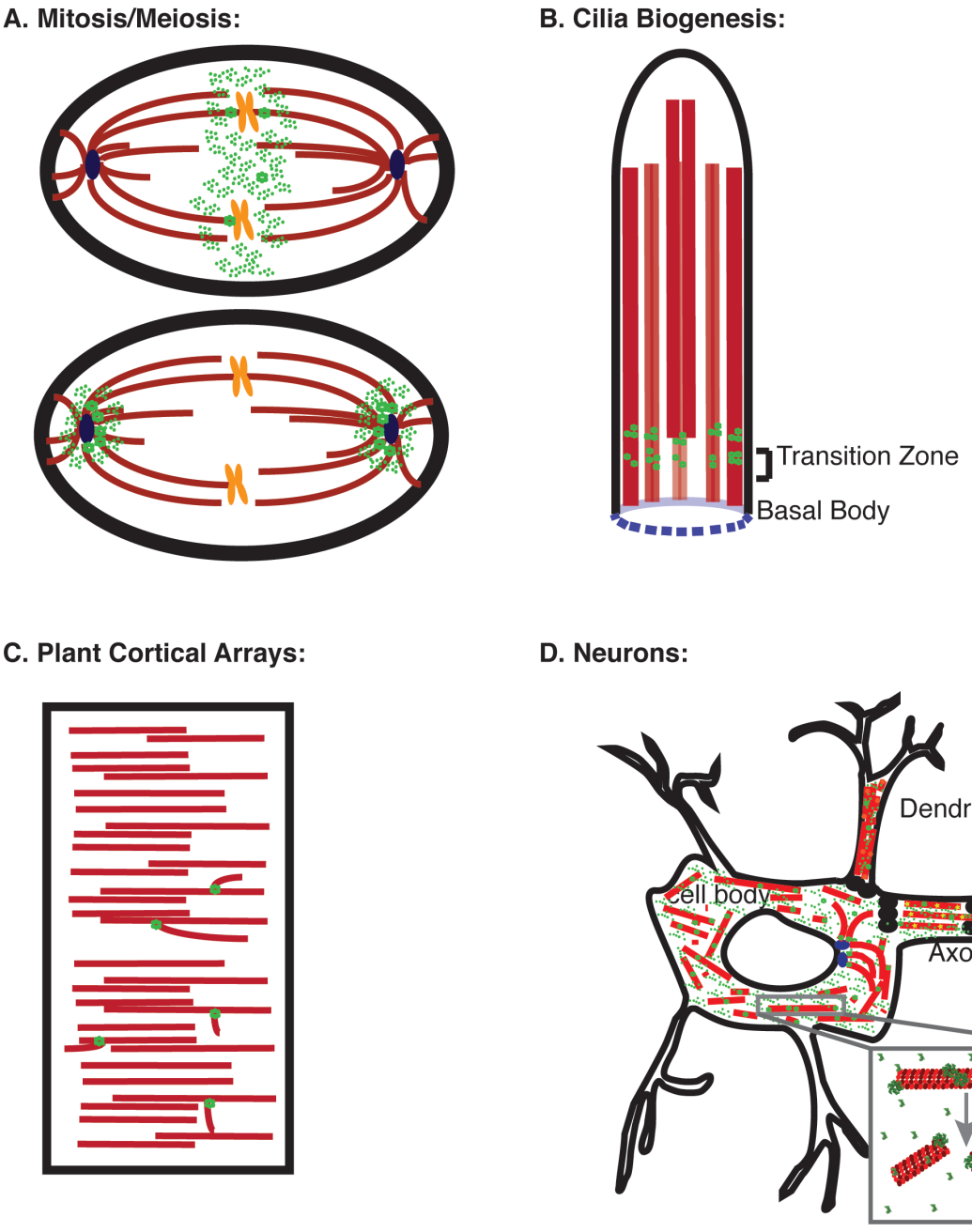

Figure 1.4 Selected Functions of Katanin.

Some of the functions that katanin is involved in regulating. (**A**) Katanin is active in mitosis and meiosis. Regulating the kinetochore microtubules at the kinetochores during mitosis and regulating microtubule outgrowth at the centrosomes during meiosis. (**B**) Katanin regulates cilia biogenesis. When it is absent, the central axonemal microtubules do not form properly. It is also important for disassembling cilia at the start of mitosis, so that mitosis can continue properly. (**C**) Katanin contributes to cortical array alignment.

When katanin is missing, there is a lack of organization in cortical arrays. (**D**) Katanin is found in all areas of neurons, however, is most abundant in the axon, where it is thought to regulate microtubule length.

Katanin also functions in mitosis in S2 cells (D. Zhang et al. 2007). In fact, all three severing enzymes, katanin, spastin and fidgetin are involved in movement of chromosomes toward the mitotic spindle (D. Zhang et al. 2007). Spastin and fidgetin are found at the centrosomes and stimulate microtubule minus end depolymerization (Mukherjee et al. 2012; D. Zhang et al. 2007). Both enzymes are involved in releasing gamma γ-tubulin complexes from the minus ends (Mukherjee et al. 2012; D. Zhang et al. 2007). Interestingly, katanin is found to be primarily a plus-end depolymerizer that works on anaphase chromosomes, by releasing the kinetochore microtubules from the chromosomes (D. Zhang et al. 2007). *X. laevis* and *X. tropicalis* mitotic spindle size is highly dependent on katanin activity levels (Loughlin et al. 2011). Specifically, phosphorylation in the N-terminal region of *X. laevis* katanin inhibits depolymerization activity resulting in longer spindles (Loughlin et al. 2011; Whitehead, Heald, and Wilbur 2012).

Katanin is also found in the cell body in *Chlamydomonas* where it regulates microtubules in cilia. When the central microtubule pair is missing, the cilia are immotile (Dymek, Lefebvre, and Smith 2004; Lohret, McNally, and Quarmby 1998). Interestingly, when katanin is mutated in *Chlamydomonas* or *Tetrahymena*, the cilia lack the middle doublet microtubules immobilizing the cilia. In Chlamydomonas*,* the cilia are also unable to be disassembled before the onset of mitosis (Dymek, Lefebvre, and Smith 2004; Lohret, McNally, and Quarmby 1998). It is likely that katanin plays a role in disassembly of the cilia by releasing microtubules from the basal body (Sharma et al. 2007; Rasi et al. 2009; Lechtreck, Gould, and Witman 2013). Recently, katanin has also been shown to regulate cilia number in human development (Hu et al. 2014).

Katanin has also been implicated in cell migration. In *Drosophila*, when katanin is absent, the migration rates increase (D. Zhang et al. 2011). Katanin is thought to play a

role at the cell cortex in regulating microtubule length at the plus ends of microtubules (D. Zhang et al. 2011). It has also shown to decrease cell movement in rat epithelial cells (Sudo and Maru 2008), but enhances cell movement in prostate cancer (Ye et al. 2011).

Katanin is active in plants where it organizes cortical microtubule arrays (Nakamura, Ehrhardt, and Hashimoto 2010; Q. Zhang et al. 2013). In plants, microtubules are nucleated from gamma-tubulin complexes that bind to the sides of already growing microtubules (Reviewed in Kollman et al. 2011). The minus-end is released by katanin severing, and the minus end shrinks while the plus-end grows, causing a treadmilling of microtubules around the edge of the cell (Reviewed Ehrhardt and Shaw 2006). Microtubules inside the plant cells are lined to the cellulose-deposition machinery outside the cell. Katanin mutants often result in fragile plants with poorly constructed cell walls around the individual cells (Burk et al. 2001). A loss-of-function mutation delays formation of the microtubule arrays at the cortex, Katanin overexpression causes bundles of microtubules, which eventually depolymerize (Stoppin-Mellet, Gaillard, and Vantard 2006; Burk et al. 2001). Katanin has been shown to be important for releasing the gamma-tubulin complex from the sides of growing microtubules. Katanin mutants showed minus ends of microtubules were not properly released form the nucleation sites (Nakamura and Hashimoto 2009).

Both katanin and spastin have been shown to have roles in neurons. Katanin is found throughout the axon and cell body where it is thought to have an important role in breaking up long microtubules into smaller microtubules and dimers to enable dynamic reorganization of the microtubule network, including branching and new growth cones (Ahmad et al. 1999; Yu et al. 2008). If katanin is inhibited, microtubules are not released from the centrosome and the overall length of microtubules increases (Ahmad et al. 1999; Karabay et al. 2004). Katanin mutations in drosophila also lead to increased

dendritic expansion (Mao et al. 2014). Spastin also localizes in axons and is involved in axonal branching (Yu et al. 2008). Uncontrolled severing in axons could have catastrophic effects. Therefore, it is likely that both katanin and spastin would be tightly regulated. Tau, a MAP found in axons has been shown to protect microtubules from severing (Qiang et al. 2006). When tau is phosphorylated, it does not bind as well to microtubules and could leave microtubules open for katanin severing (Qiang et al. 2010). This further contributes to the theory that katanin could be implicated in Alzheimer's diseases (Baas and Qiang 2005; Sudo and Baas 2011).

Microtubules severing enzymes need to be regulated to ensure proper cellular functioning. Katanin has been shown to be regulated in *X.* laevis by phosphorylation of the N-terminal domain to negatively regulate severing activity (Loughlin et al. 2011; Whitehead, Heald, and Wilbur 2012). However, it has not been revealed if there are other phosphorylation sites that regulate katanin activity. There is also evidence that katanin could be targeted to specific locations on microtubules by post-translational modifications of tubulin. Katanin and spastin can both be regulated by polyglutamylation and perhaps also by glycylation (Lacroix et al. 2010; Sharma et al. 2007). Additionally, acetylation enhances katanin's severing activity in fibroblasts (Sudo and Baas 2010). There are still many open questions surrounding how tubulin post-translational modifications can regulate severing activity and whether there are additional mechanisms that have yet to be revealed.

1.8 Broad Relevance/Disease Impacts

It is important to study microtubule regulation and in particular regulation of severing enzymes because both are essential for cell survival. Uncontrolled microtubule severing would likely destroy cells because they would become disorganized, lose their

shape, and ultimately be unable to function properly. Spastin is best known for its involvement in Hereditary Spastic Paraplegia, which is a neurodegenerative disease that causes spasticity in lower limbs and eventual neuron degeneration (McDermott et al. 2000). Approximately 40% of the cases of Hereditary Spastic Paraplegia have been linked to mutations in spastin (McDermott et al. 2000). In prostate cancer, katanin has been shown to be overexpressed and actually speeds up cell migration movement and may enhance metastasis (Ye et al. 2011). One study has hypothesized that katanin is regulated by phosphorylation of tau (Qiang et al. 2010). When tau is phosphorylated, it can no longer bind to the microtubule and therefore exposes potential sites for katanin to sever. It has also been suggested that katanin can contribute to tauopathies, such as Alzheimer's disease (Baas and Qiang 2005). Fidget mice, with a fidgetin mutation, have skeletal, auditory, and ocular defects, likely due to a single retrotransposon (Truslove et al.1956; Yang et al. 2006; Cox et al. 2000). Recent evidence has also suggested that Fidgetin-Like 2 is involved in wound healing (Charafeddine et al. 2015). Misregulation of severing enzymes can lead to severe diseases or lethality across all different types of organisms, however, we still do not fully understand how they are regulated or regulate microtubule organization. In order to correct misregulation we associate with diseases it is essential we be able to fill in gaps in our knowledge about the mechanism that katanin uses to regulate microtubule dynamics.

1.9 Motivation

Despite the numerous studies that have been conducted to understand the mechanistic details and cellular functions of katanin, there is still a large amount of information that remains unknown. While there is evidence to support the proposed model of how severing occurs, it has not been proven. More importantly, we do not know

how katanin targets microtubules. It is very likely that katanin does have specific modes of regulation, since it has been shown to mostly generate a population of short microtubules and selectively depolymerize or sever microtubule ends.

There has also not been any characterization of how katanin regulates dynamic microtubules. Since many of the processes katanin has been shown to be involved in require dynamic microtubules, it is likely that katanin will also target these microtubules. However, biophysical characterization of these interactions would help us better understand how this destabilizing MAP regulates microtubule dynamics.

We still do not know how katanin p60 is regulated beyond its partner protein, p80. There is some evidence that katanin could be regulated by the neuronal MAP, tau (Qiang et al. 2006; Yu et al. 2008; Sudo and Baas 2011) however, there is no direct single molecule evidence for how this regulation occurs. In vitro single molecule assays would help us better understand how tau may regulate katanin's interactions with microtubules.

There are still many remaining open questions about how katanin can regulate microtubule dynamics and how katanin itself is regulated. Katanin has been implicated in diseases, such as prostate cancer and Alzheimer's disease. In order to better understand these diseases and find realistic solutions for them, it is important to know more about the basic science behind the relevant proteins. In this dissertation we hope to gain a greater understanding of the basic mechanisms katanin uses to target microtubules, both stable and dynamic, and how this unique enzyme is regulated.

CHAPTER 2

KATANIN TARGETING TO DEFECT MICROTUBULES

2.1 Introduction

Microtubule severing enzymes are essential regulators of the microtubule cytoskeleton. They impact the overall organization of the microtubule network. This includes axon outgrowth, mitosis, cell migration, and organization of non-centrosomal arrays in plants (Ahmad et al. 1999; Karabay et al. 2004; Srayko et al. 2006; K. McNally et al. 2006; Nakamura, Ehrhardt, and Hashimoto 2010; D. Zhang et al. 2011). These enzymes remodel essential networks, not by destroying microtubules, but by generating shorter microtubules that can be used as seeds for a variety of diverse purposes (Roll-Mecak and Vale 2006; Srayko et al. 2000).

Katanin was the first discovered microtubule severing enzyme (Vale 1991). The prevailing theory for how katanin severs microtubules is that ATP-bound monomers to oligomerize into a hexamer. The hexamer binds to the microtubule by threading the CTT (CTT) of tubulin through its pore (Roll-Mecak and Vale 2008). The ATPase activity works to pull the tubulin through the pore unraveling and dissociating the tubulin dimer. The mechanism is based on the activity of other AAA enzymes, such as Clp proteins, that unfold proteins by similar threading mechanisms (Frickey et al. 2004).

In addition to severing, we have demonstrated that katanin can end sever, or depolymerize microtubules ends in an ATP-dependent manner (D. Zhang et al. 2011; Díaz-Valencia et al. 2011). This activity would be especially important when trying to regulated the microtubule length, such as in interphase cells, at the cortex, where the microtubules should not over grow. In order for the microtubule network to remain intact, katanin must be targeted spatially to specific locations, by binding partners, such as its

partner protein p80, or by specific signals along microtubule tracks (Hartman et al. 1998; F. J. McNally and Thomas 1998; K. P. McNally, Bazirgan, and McNally 2000). Previous work has shown that katanin can target defects in microtubules (Davis et al. 2002; Díaz-Valencia et al. 2011), but it is unknown what types of lattice defects are important for targeting. Here, we tested several types of microtubules with a variety of defects to probe how well katanin severs each type. We used in vitro reconstitution assays to probe whether katanin targets microtubules with protofilaments shifts or that lack the CTT of tubulin. Using data from biophysical and biochemistry assays we can determine whether katanin preferentially severs these abnormal microtubules and provide a possible mechanism for katanin based microtubule depolymerization.

2.2 Results

2.2.1 Experimental Set-Up

The most direct way to test the mechanism katanin uses to sever and depolymerize microtubules is to purify the enzyme and perform in vitro severing assays. This approach allows direct observation of microtubule severing and removes many additional variables that complicate cellular studies. We made 10 µL flow chambers using double stick tape, a coverslip and a slide (Fig. 2.1). We attached microtubules to the cover slip by first flowing in rigor kinesin or anti-tubulin antibodies (Fig. 2.1). To prevent non-specific interactions we blocked the surface with a BSA wash before adding in the microtubules. After microtubules were added, we washed the chamber with activity buffer to remove any microtubules that were not stuck to the surface. Next, we added katanin to the chamber and imaged in epifluorescence or Total Internal Reflection Fluorescence microscopy (TIRF) (Fig. 2.1).

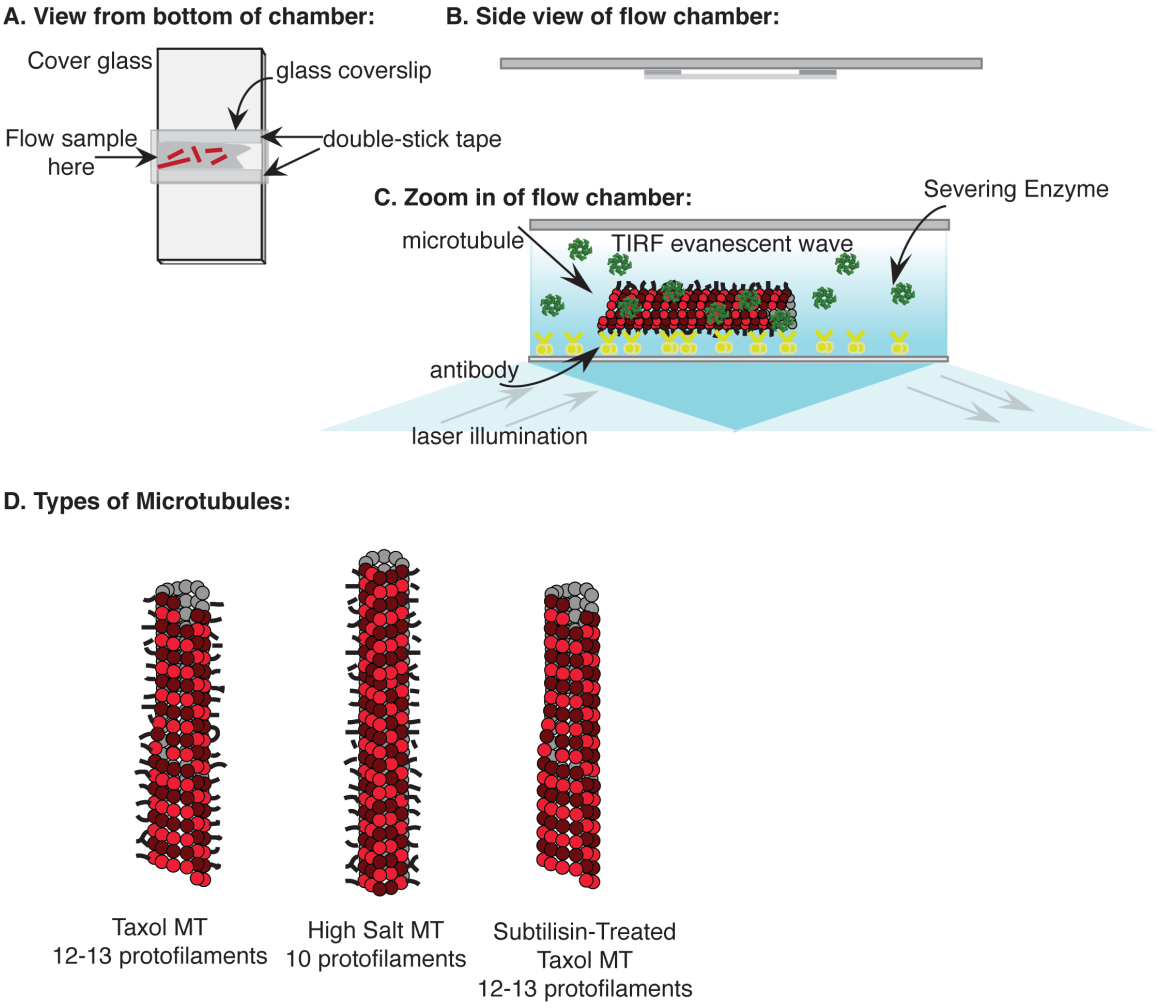

Figure 2.1 Chamber Diagram.

(**A**) Diagram of flow chamber created with double-stick tape, coverslip, and cover glass. We flowed the sample in one side of the chamber and wicked the excess liquid from the other end to draw the sample through. (**B**) Side view of the chamber. (**C**) Zoom in of the side of the flow chamber. We adhered the microtubules to the surface of the chamber using kinesin. Once the severing enzyme is added to the chamber, we can image using epifluorescence, or Total Internal Reflection Fluorescence (TIRF) microscopy as depicted. In TIRF microscopy, the laser is directed in and reflected out of the chamber at the same angle allowing for less background fluorescence and better resolution of single molecules. (**D**) Diagrams of the types of microtubules we made to test whether katanin

targets specific microtubule defects. Taxol microtubules are our “normal” microtubules that typically have 12-13 protofilaments. “High Salt” microtubules are made with 580 mM NaCl and typically have 10 protofilaments and more frequent seem defects. Subtilisin-treated microtubules (“Subtilisin MTs”) are Taxol-stabilized microtubules that have the CTTs of tubulin removed.

In order to test the activity of katanin on different types of microtubule defects, we created several types of microtubules. “High salt” microtubules are microtubules that are nucleated and polymerized in 580 mM NaCl (Fig. 2.1D). These microtubules have been shown to have predominantly only 10 protofilaments and more frequent protofilament shifts (Bohm et al. 1990). Electron Microscopy evidence revealed that high salt microtubules have equal proportions of A and B type lattices and all the microtubules analyzed had even numbers of seams (Dias and Milligan 1999). The even number of seams ensures that the pseudo-helical tubulin pattern is uninterrupted (Dias and Milligan 1999). While high salt microtubules are an example of protofilament shift defects, “Subtilisin” microtubules are microtubules that are missing the CTTs of tubulin. Subtilisin-treated microtubules are made by treating Taxol-stabilized microtubules with a protease inhibitor, subtilisin, which removes the CTTs of both alpha and beta tubulin (Fig. 2.1D). It has been shown that the CTT is essential for severing enzyme activity (Roll-Mecak and Vale 2008; White et al. 2007; Roll-Mecak and McNally 2010). We expect that subtilisin-treated microtubules would not be able to be severed, as has been previously described (F. J. McNally and Vale 1993; Eckert, Le, et al. 2012). However, it is also possible that katanin could bind to other locations on the microtubule to either sever or depolymerize the microtubule. In addition, we made Taxol-stabilized microtubules, which predominately have 13 protofilaments and are treated as our “normal” microtubule control (Fig. 2.1D). By performing in vitro severing assays with microtubules containing defects, we can begin to dissect how katanin regulates microtubules.

2.2.2 Katanin requires ATP to sever Taxol-stabilized microtubules.

First we show that katanin is functioning on Taxol-stabilized microtubules in the severing assays, which have been used previously to characterize severing enzymes

(Loughlin et al. 2011; Whitehead, Heald, and Wilbur 2012; Eckert, Le, et al. 2012; Le, Eckert, and Woehlke 2013b; F. J. McNally and Thomas 1998; K. P. McNally, Bazirgan, and McNally 2000; Buster, McNally, and McNally 2002; Stoppin-Mellet, Gaillard, and Vantard 2002; Díaz-Valencia et al. 2011; D. Zhang et al. 2011; K. McNally et al. 2014). Previous studies have shown that katanin can sever and depolymerize stabilized microtubules in vitro (F. J. McNally and Vale 1993; Loughlin et al. 2011; Whitehead, Heald, and Wilbur 2012; P. Zhang et al. 2010; Díaz-Valencia et al. 2011; F. J. McNally and Thomas 1998). Fig. 2.2 shows that WT-p60 is able to sever microtubules and within ~100 seconds. In control severing assays without any katanin no microtubule severing occurs, since the time series shows that the entire microtubule is present at the end of the assay. The walker B mutant, E306Q-p60, a mutant version of katanin that is unable to hydrolyze ATP, is also not able to sever microtubules. The time series of the severing assay with the E306Q-p60 shows that the entire microtubule is still in tact. This data reveals that any microtubule severing we observe is due to katanin severing and the enzyme is functioning as previously reported for X. laevis p60 (Xl-p60) (Loughlin et al. 2011; Whitehead, Heald, and Wilbur 2012).

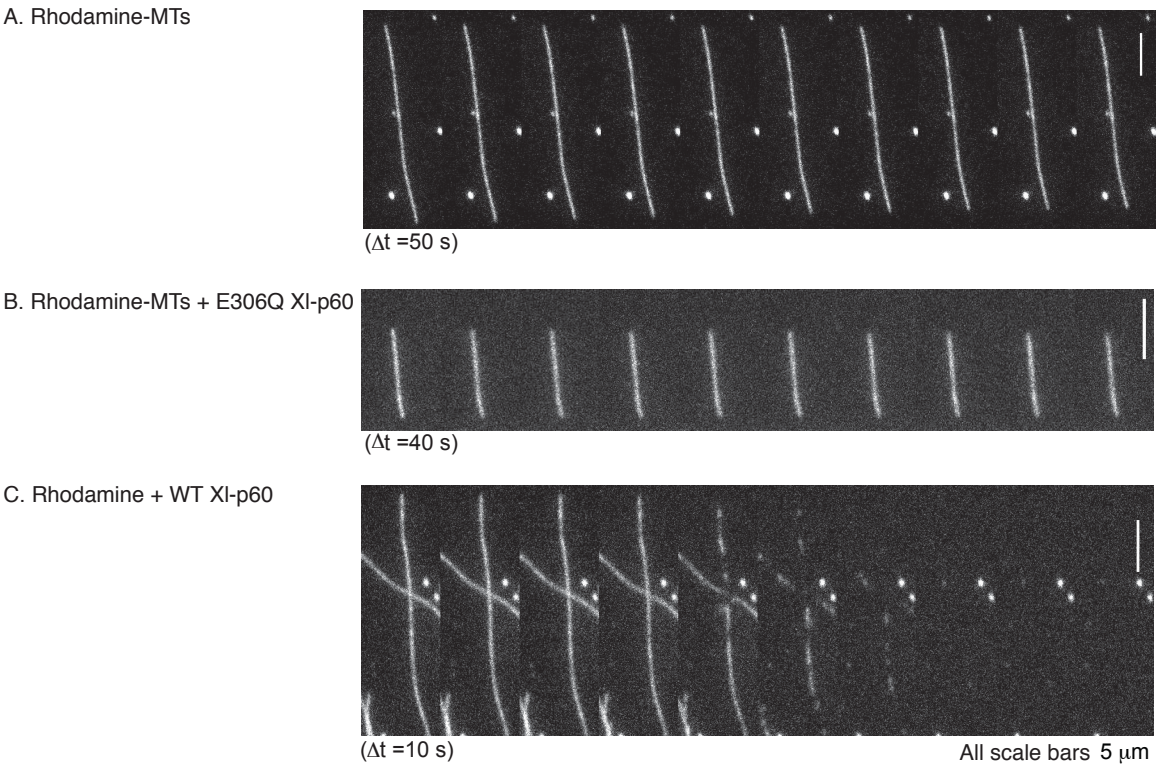

Figure 2.2 Representative Time Series of Severing on Taxol-stabilized Microtubules.

Time series of representative Taxol-stabilized microtubules in a severing assay alone (**A**), with E306Q-Xl-p60 (**B**), or with WT-Xl-p60 (**C**). The time between images is as stated below each time series and all the scale bars are 5 μm.

We can quantify the severing activity by tracking the mean fluorescence intensity of the microtubule over the course of the severing assay and correlate the fluorescence with the fraction of microtubule remaining. We plotted the ratio of the fluorescence intensity at each frame to the initial frame where WT-Xl-p60 was added to quantify the loss of polymer over time (Fig. 2.3A). Quantification of the loss of polymer in severing assays with WT-Xl-p60 shows that the microtubules are completely destroyed. The walker B mutant katanin, E306Q-Xl-p60, is unable to sever the microtubules and we observe no loss polymer from the ends, known as depolymerization. We also observe no loss of polymer from severing or depolymerization when there is no enzyme present in the assay. We can find the rate of decay by fitting the data with an exponential decay function:

$$I(t) = I_0 \exp(-t/\tau), \quad \text{Eq. 2.1}$$

where I is the intensity as a function of time, t, I_0 is the amplitude at time zero, and τ is the characteristic time constant for the decay (Fig. 2.3B). When there is no katanin in the assay the data is best fit by a linear equation:

$$I(t) \sim I_0 (1 - (t/\tau)) \quad \text{Eq. 2.2}$$

and has a slow characteristic decay time (Fig. 2.3B). Using these parameters, we found that WT-Xl-p60 has a fast decay time with a decay constant of τ = 69.6 s ± 2.72 with the goodness of fit: R^2 = 0.959. Whereas microtubules alone or microtubules + E306Q p60 both have slow decay times of τ = 2724.9 s ± 48.293 with the goodness of fit: R^2 = 0.9704 and τ = 4177.9 s ± 75.532 with the goodness of fit: R^2 = 0.949 respectively, indicating the microtubules remain intact over the time frame of this assay.

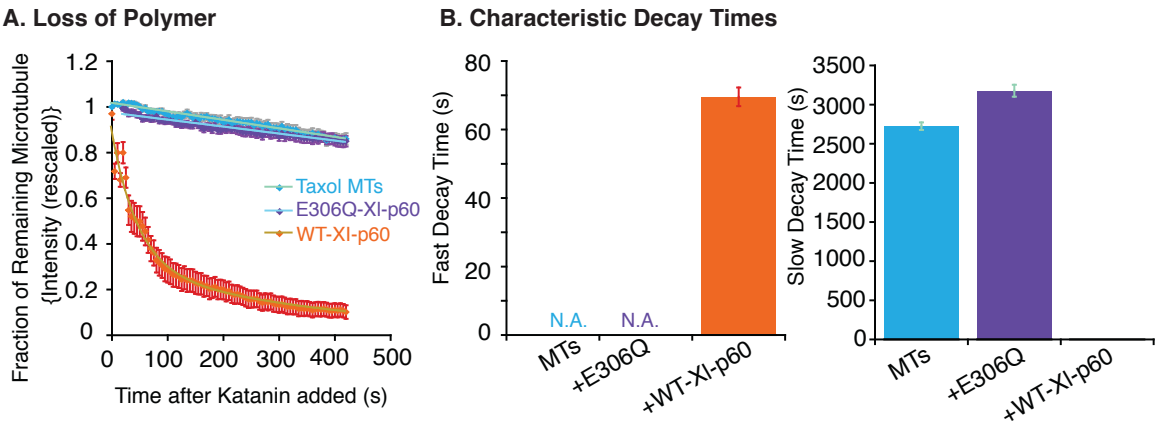

Figure 2.3 Quantification of Severing on Taxol-stabilized Microtubules.

(**A**) Total loss of microtubule polymer over time for each of the conditions. Images were collected every 5 seconds for 10 minutes and then ImageJ was used to analyze the images. The first three minutes of each movie was used a control to make sure that the microtubules were stable and not falling apart due to something other than MBP-katanin p60. We quantified loss of polymer for Taxol-stabilized microtubules (light blue, N=33 in 6 different chambers); purple is Taxol-stabilized microtubules + E306Q-Xl-p60 (purple, N=53 6 different chambers); orange is Taxol-stabilized microtubules + WT-Xl-p60 (orange, N=51 in 8 different chambers). Only chambers with WT-Xl-p60 were completely destroyed during the assay. The error bars represent the standard error of the mean. (**B**) The loss of polymer data was fit with either linear equation (Eq. 2.2) or single exponential decay (Eq. 2.1). The error bars represent the uncertainty associated with the fit parameters.

2.2.3 Katanin severs high salt microtubules as efficiently as Taxol-stabilized microtubules.

We performed severing assays using high salt microtubules to test whether katanin severs microtubules with seam defects. Time series of experiments show that WT-p60 severs high salt microtubules. Assays with high salt microtubule alone or high salt microtubules in the presence of E306Q-p60 show no breaks in the microtubules (Fig. 2.4).

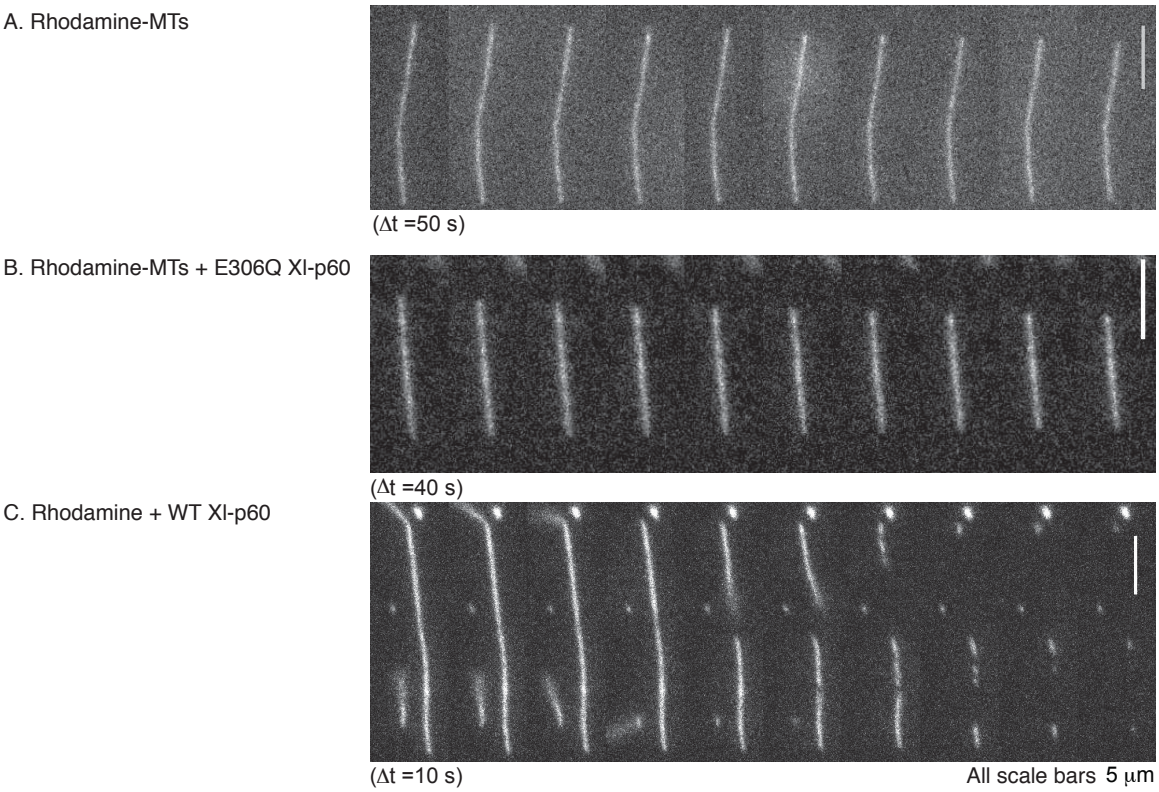

Figure 2.4 Representative Time Series of Severing on High Salt Microtubules.

Time series of representative high salt microtubules in a severing assay alone (**A**), with E306Q-Xl-p60 (**B**), or with WT-Xl-p60 (**C**). The time between images is as stated below each time series and all the scale bars are 5 μm.

Quantification of the overall rate of polymer loss confirms that WT-p60 is able to completely destroy high salt microtubules over the course of the severing assay (Fig. 2.5A). There is some minor loss of polymer in severing assays with E306Q-XI-p60, which is likely due to depolymerization. The decay constants show similar trends, where WT-p60 has a fast decay time of τ = 53.445 s ± 2.124 with the goodness of fit: R^2 = 0.973 and E306Q-XI-p60 has a decay time of τ = 2091.8 s ± 37.605 with the goodness of fit: R^2 = 0.97014 (Fig 2.5B). However, the high salt microtubules depolymerize slightly on their own and have an initial fast decay time of τ = 97.207 s ± 9.1879 with the goodness of fit: R^2 = 0.91551 (Fig. 2.5B).

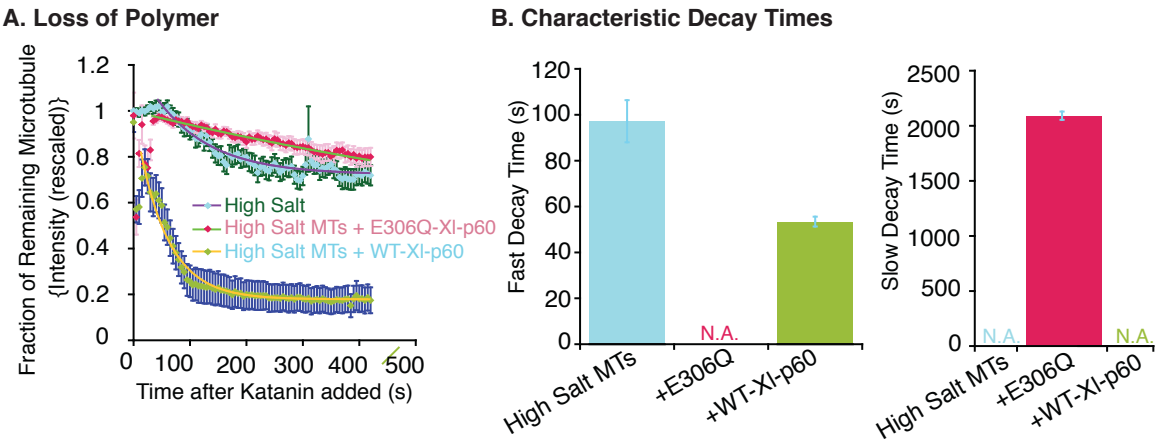

Figure 2.5 Quantification of Severing on High Salt Microtubules.

(**A**) This is a plot of the quantification of the total loss of microtubule polymer over time for each of the conditions. Images were collected every 5 seconds for 10 minutes and then ImageJ was used to analyze the images. The first three minutes of each movie was used a control to make sure that the microtubules were stable and not falling apart due to something other than MBP-katanin p60. Green is severing assays with high salt microtubules and no severing enzyme (N=32 in 2 different chambers); pink is high salt microtubules + E306Q-Xl-p60 (N=28 in 6 different chambers); lime green is high salt microtubules + WT-Xl-p60 (N=30 in 7 different chambers). Only chambers with WT-Xl-p60 were completely destroyed during the assay. The error bars represent the standard error of the mean. (**B**) The loss of polymer data was fit with either linear equation (Eq. 2.2) or an exponential decay (Eq. 2.1). The error bars are the uncertainty associated with the fit parameters from quantification and fitting in (A).

To determine if there was any difference in the severing activity between the standard Taxol-stabilized microtubules and high salt microtubules, we quantified the microtubule remaining on the same plot for each condition. We show that high salt microtubules are less stable than Taxol stabilized microtubules because they lose ~20% of their length during the severing assays, when there is no severing enzyme present (Fig. 2.6A). However, both E306Q-p60 and WT-p60 displayed similar rates of deterioration on Taxol-stabilized and high salt microtubules (Fig. 2.6B and C). From this data we can infer that high salt microtubules are inherently less stable than Taxol-stabilized microtubules, but are not preferentially targeted by WT-Xl-p60.

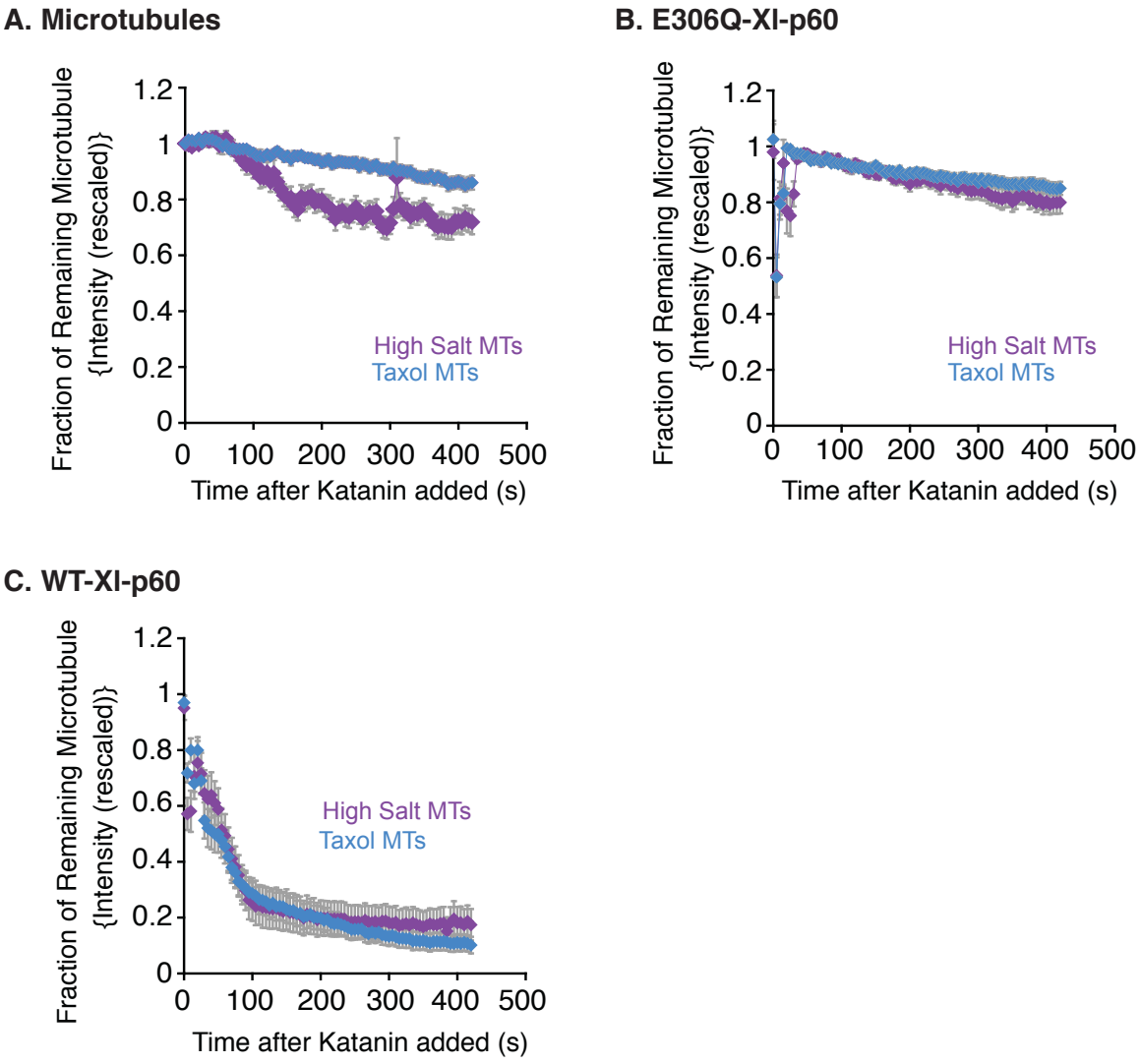

Figure 2.6 Comparison of Taxol-stabilized and High Salt Microtubules Loss of Polymer.

In order to compare overall rates of total loss of polymer between standard Taxol-standardized and the "defective" high salt microtubules we plot the quantification for each type of microtubule under the same conditions on the same graph. Blue data is Taxol microtubules and purple data is high salt microtubules. All error bars represent the standard error of the mean. (**A**) Quantification of loss of polymer in severing assays without any severing enzyme. The N for high salt microtubules is 32 in 2 different chambers and for Taxol-stabilized microtubules N=33 in 6 different chambers. (**B**) Quantification of loss of polymer in severing assays with E306Q-Xl-p60. High salt microtubules N=28 in 6 different chambers and for Taxol-stabilized microtubules N=53 in 6 different chambers. (**C**) Loss of polymer plots for assays on microtubules with WT-Xl-p60. The number of high salt microtubules measured + WT-Xl-p60 is N=30 in 7 different chambers and for Taxol-stabilized microtubules + WT-Xl-p60 it is 51 in 8 different chambers.

From our severing assay data we can also determine the total number of microtubules severed and the time of the first severing event on each individual microtubule. This ensures that the overall severing activity we observed and quantified is not in just a small subsection of the microtubule population. First we plotted the total number of microtubules severed at least once during the assays (Fig. 2.7A). Even when WT-Xl-p60 is in the severing assay there are some microtubules that are not severed, however, the majority of microtubules are severed at least once. Microtubules without any severing enzyme, or with the ATPase mutant E306QQ-Xl-p60 are not severed at all during the assay.

We also noted the time it took for the first severing event to occur. It is conceivable that under some conditions all microtubules will be severed at least once, but it could take significantly longer for that event to occur. Any microtubules that were not severed within the movie were calculated as if they took the entire length of the assay, 420 seconds. The majority of both the Taxol-stabilized and high salt microtubules were severed in assay with WT-Xl-p60, but no microtubules were severed under any of the other control conditions. All of the above data corroborate that WT-Xl-p60 is required for severing of both Taxol-stabilized and high salt microtubules. In addition, Xl-p60 does not target high salt microtubules any more frequently than Taxol-stabilized microtubules.

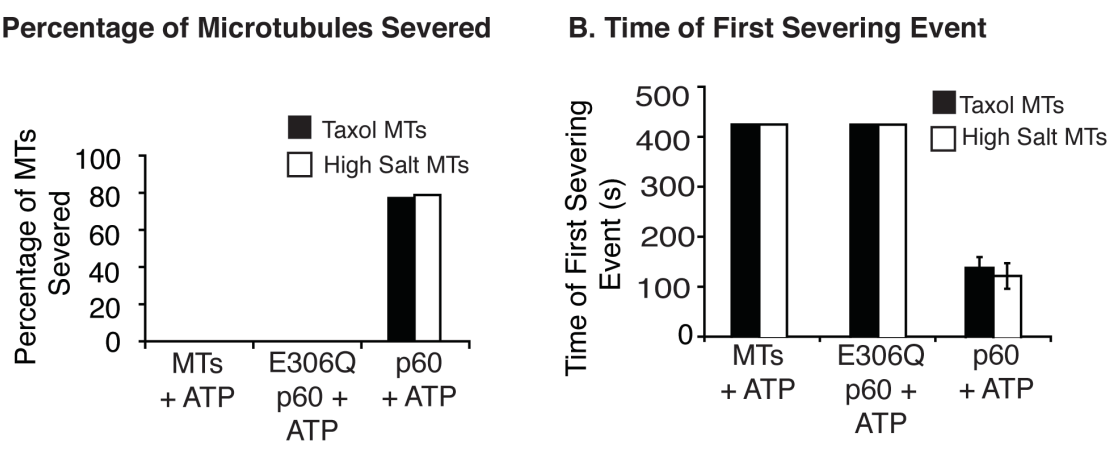

Figure 2.7 Quantification of Severing Parameters for Taxol-stabilized and High Salt Microtubules.

(**A**) Plot of quantification of the percentage of microtubules severed during the severing assays. This was calculated by counting the number of microtubules severed at least once during the assay. Both Taxol-stabilized and high salt microtubules were only severed when WT-Xl-p60 was present. (**B**) We calculated the time of the first severing event by noting the time at which the first break in the microtubule occurred. The time for the first severing event was around 100 seconds for both Taxol-stabilized and high salt microtubules. The N values are as follows: Taxol-stabilized microtubules N=33; Taxol-stabilized microtubules + E306Q-Xl-p60 N=53; Taxol-stabilized microtubules + WT-Xl-p60 N=51; high salt microtubules N=32; high salt microtubules + E306Q-Xl-p60 N=28; high salt microtubules + WT-Xl-p60 N=30. Error bars represent the standard error of the mean.

2.2.4 Katanin Activity on Subtilisin Microtubules

We investigated another type of defect microtubule that is missing the CTTs of alpha and beta tubulin. We treated Taxol-stabilized microtubules with subtilisin, a serine protease, that cleaves off the CTTs of both alpha and beta tubulin. Previous studies have shown that katanin is able to bind to subtilisin-treated microtubules and pellet with them (F. J. McNally and Vale 1993), but cannot sever such microtubules (F. J. McNally and Vale 1993; Eckert, Le, et al. 2012). Eckert et al. observed that at low concentrations of katanin there was no binding to microtubules, however, at high concentrations of katanin, katanin bound all over subtilisin-treated microtubules. Both the pelleting assays and the microscopy evidence suggest that katanin is able to bind to microtubules, although likely weakly, through a mechanism that does not involve the CTTs of tubulin.

Since it is known that katanin does not sever subtilisin-treated microtubules, we wanted to further examine whether the CTT is required for depolymerization, or end severing events. The evidence from the time series (Fig. 2.8) indicates that the subtilisin-treated microtubules alone or with the E306Q-Xl-p60 do not get severed, but may depolymerize. As previously reported, there is also no severing in assays with WT-Xl-p60 either, however, we do observe some depolymerization.

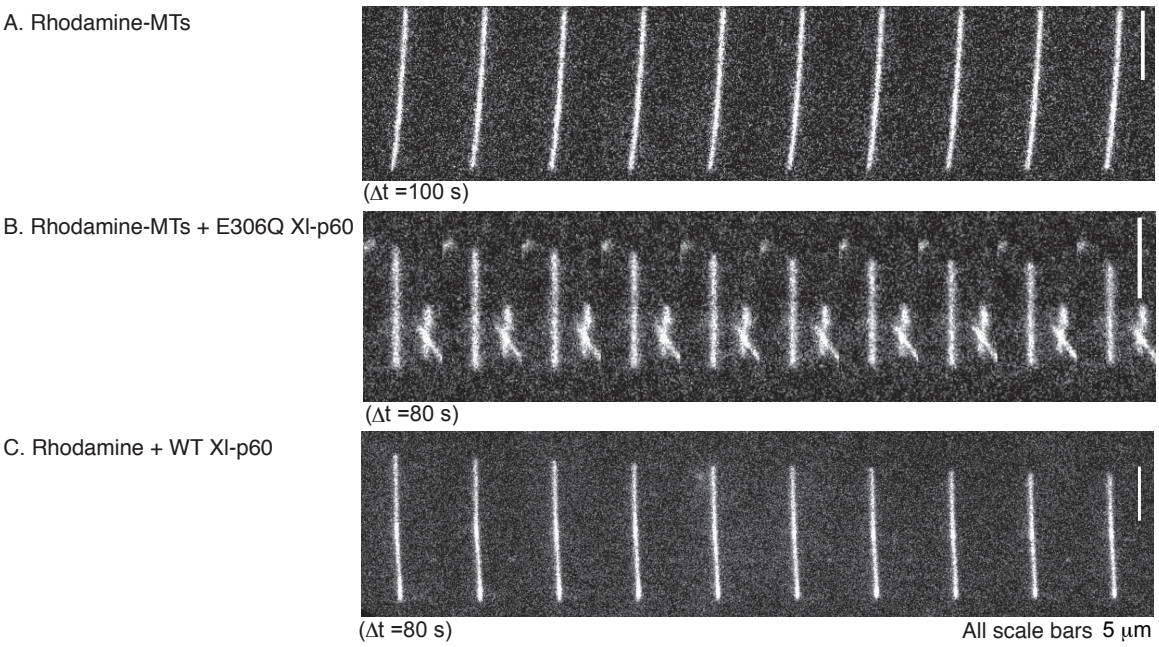

Figure 2.8 Representative Time Series of Severing on Subtilisin-Treated Microtubules.

Time series of representative subtilisin-treated microtubules in a severing assay alone (**A**), with E306Q-Xl-p60 (**B**), or with WT-Xl-p60 (**C**). The time between images is as stated below each time series and all the scale bars are 5 μm.

Quantification of the loss of polymer data for subtilisin microtubules shows the microtubules themselves are relatively stable. They show no loss of polymer over the course of the assay, and have a long characteristic decay time, which would be infinite over the time scale of our assays (Fig. 2.9). We observed a small amount of polymer loss in assays with E306Q-Xl-p60. This is best represented by the slow decay constant τ = 506.08 s ± 189.03 with the goodness of fit: R^2 = 0.905 (Fig. 2.9). Assays with WT-Xl-p60 also lose polymer, and have a relatively fast decay constant τ = 106.47 s ± 8.5026 with the goodness of fit: R^2 = 0.93915 (Fig. 2.9). However, since there is still ~50% of the microtubules remaining at the end of the assays, there is a significant vertical offset to this exponential decay allowing the decay to level to a non-zero value (Appendix A.1). This data can be fit to the equation:

$$I(t) = I_0 \exp(-t/\tau) + I_\infty, \qquad \text{Eq. 2.3}$$

Where the parameters are the same as Eq. 2.1 and is the I_∞ intensity level at which the decay asymptotes as time goes to infinity.

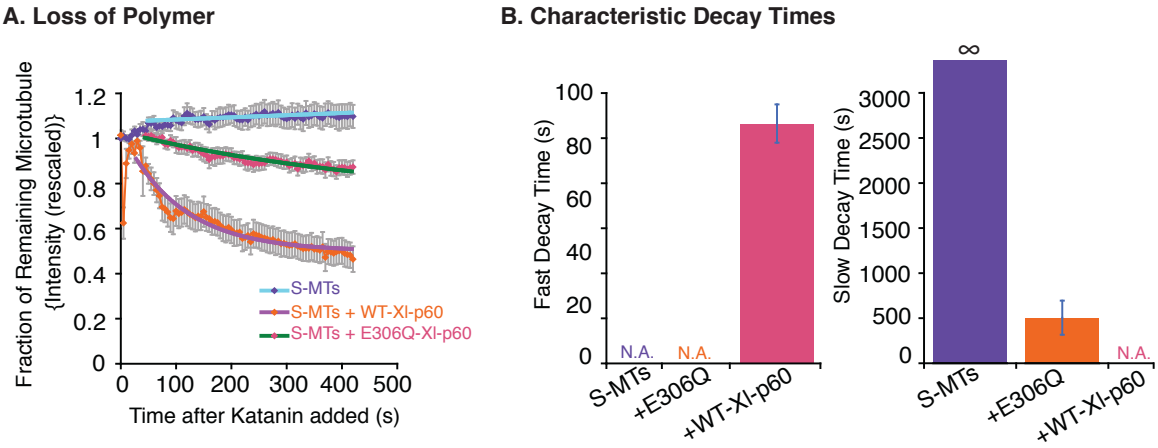

Figure 2.9 Quantification of Severing on Subtilisin-treated Microtubules.

(**A**) This is a plot of the quantification of the total loss of microtubule polymer over time for each of the conditions with subtilisin-treated microtubules. Images were collected every 5 seconds for 10 minutes and then ImageJ was used to analyze the images. Purple is severing assays with subtilisin-treated microtubules and no severing enzyme (N=32 in 4 different chambers); pink is subtilisin-treated microtubules + E306Q-Xl-p60 (N=27 in 5 different chambers); orange is subtilisin-treated microtubules + WT-Xl-p60 (N=31 in 10 different chambers). Microtubules were not completely destroyed under any of the conditions. The error bars represent the standard error of the mean. (**B**) The loss of polymer data was fit with either linear approximate (Eq. 2.2) or a single exponential with a non-zero long-time asymptote (Eq. 2.3) to distinguish the overall decay times. The error bars are the uncertainty associated with the decay time fit parameters.

We plotted the rates of polymer loss for each condition on the same plot in order to compare Taxol-stabilized microtubules and subtilisin microtubules (Fig. 2.10). We found that subtilisin microtubules are consistently more stable than Taxol-stabilized microtubules under all conditions (Fig. 2.10). With WT-XI-p60 the subtilisin microtubules lose polymer, but not at the same rate as Taxol microtubules.

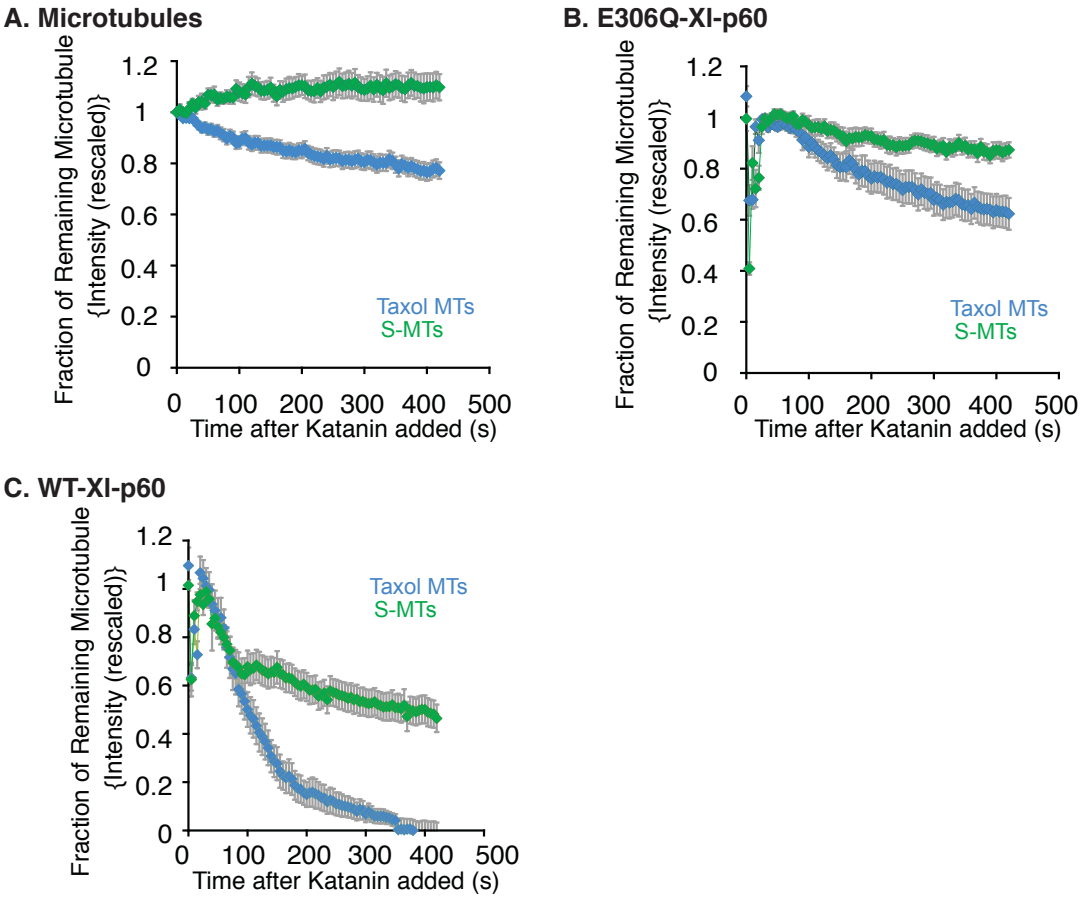

Figure 2.10 Comparison of Taxol-stabilized and Subtilisin-Treated Microtubules Loss of Polymer.

In order to compare overall rates of total loss of polymer between standard Taxol-standardized and the “defective” subtilisin-treated microtubules, which are missing the CTTs of tubulin, we plot the quantification for each type of microtubule under the same conditions on the same graph. Blue data is Taxol microtubules and green data is subtilisin-treated microtubules. All error bars represent the standard error of the mean. (**A**) Quantification of loss of polymer in severing assays without any severing enzyme. The N for subtilisin-treated microtubules is N=32 in 4 different chambers and for Taxol-stabilized microtubules N=42 in 6 different chambers. (**B**) Quantification of loss of polymer in severing assays with E306Q-Xl-p60. The N for subtilisin-treated microtubules is N=27 in 5 different chambers and for Taxol-stabilized microtubules N=31 in 5 different chambers. (**C**) Loss of polymer plots for assays on microtubules with WT-Xl-p60. The number of subtilisin-treated microtubules + WT-Xl-p60 is N=31 in 10 different chambers and for Taxol-stabilized microtubules + WT-Xl-p60 it is N=37 in 8 different chambers.

From the severing assays we also calculated the total number of microtubules severed. We found that only assays with WT-Xl-p60 and Taxol-stabilized microtubules are microtubules severed (Fig. 2.11A). This indicates that the loss of polymer for subtilisin microtubules that we observed in Fig. 2.9 was due to depolymerization. We also quantified the time to the first severing event, which suggested that severing only occurred on Taxol-stabilized microtubules with WT-Xl-p60 (Fig 2.11B). This further confirms that katanin cannot sever subtilisin-treated microtubules, so any loss of polymer we see is due to depolymerization. Since we observe depolymerization in the presence of katanin and ATP, that the enzyme is likely using an alternate ATP and katanin dependent mechanism to perform depolymerization.

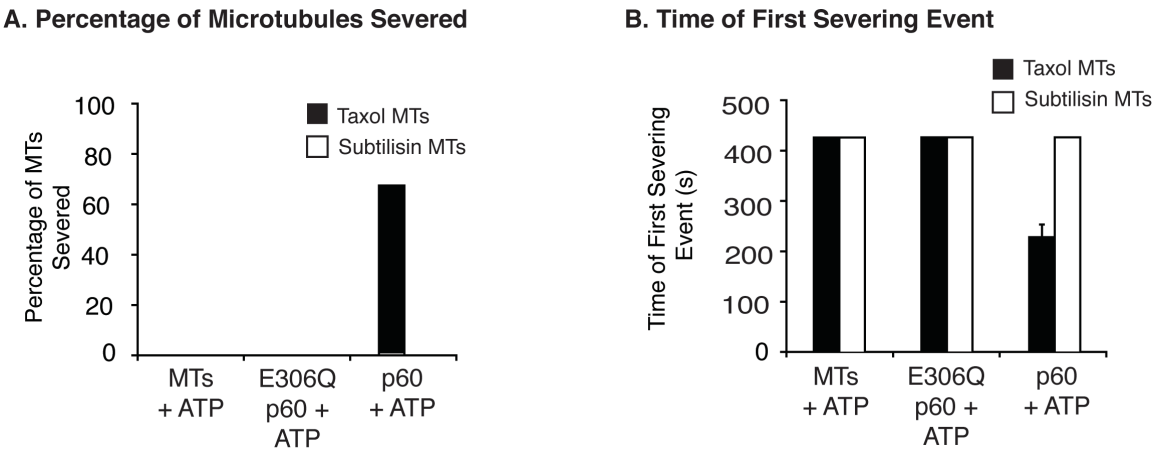

Figure 2.11 Quantification of Severing Parameters for Taxol-stabilized and Subtilisin-Treated Microtubules.

(**A**) Plot of quantification of the percentage of microtubules severed during the severing assays. This was calculated by counting the number of microtubules severed at least once during the assay. Only Taxol-stabilized microtubules were severed, and they were only severed when WT-Xl-p60 was present. (**B**) We calculated the time of the first severing event by noting the time at which the first break in the microtubule occurred. The time for the first severing event was around 100 seconds for both Taxol-stabilized and subtilisin-treated microtubules. The number of experiments performed are as follows: Taxol-stabilized microtubules N=42; Taxol-stabilized microtubules + E306Q-Xl-p60 N=31; Taxol-stabilized microtubules + WT-Xl-p60 N=37; subtilisin-treated microtubules N=32; subtilisin-treated microtubules + E306Q-Xl-p60 N=27; subtilisin-treated microtubules + WT-Xl-p60 N=31. Error bars represent the standard error of the mean.

2.2.5 Katanin Activity depends on ATP Concentration.

There is no prior microscopic evidence that the microtubule severing activity increases with increasing ATP substrate. In order to directly test the severing activity as a function of ATP concentration, we performed ATPase assays with 28 μM, 100 μM, 500 μM, and 2 mM ATP. The time series reveals that microtubules are completely destroyed with WT-Xl-p60 and 500 μM or 2 mM ATP over the time frame of our assays (Fig. 2.12).

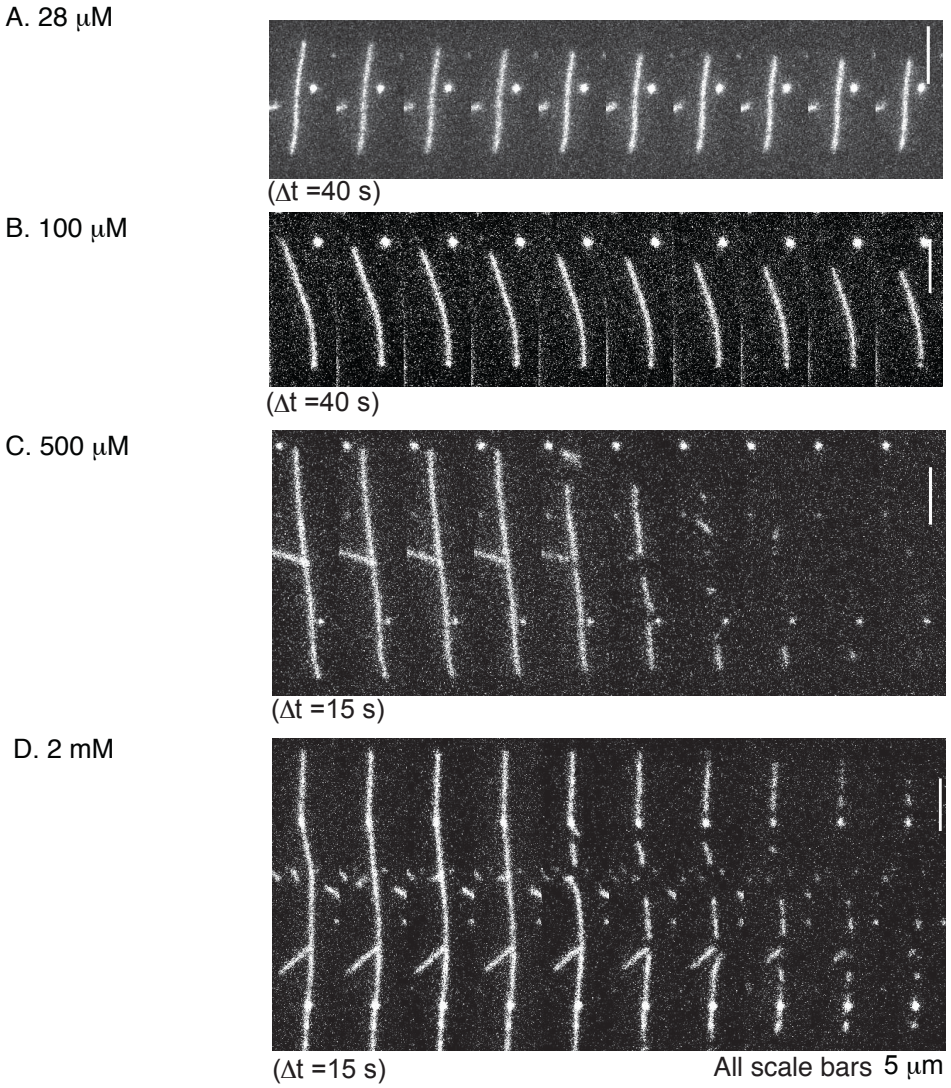

Figure 2.12 Representative Time Series of Severing on Taxol Microtubules with Different Concentrations of ATP.

Time series of representative Taxol-stabilized microtubules in a severing assay with WT-Xl-p60 and different concentrations of ATP: (**A**) with 28 μM, (**B**) 100 μM, (**C**) 500 μM, (**D**) 2 mM.

We confirmed the visual results in Fig. 2.12 by quantifying the loss of polymer of the range of ATP concentrations and found that the most lost of polymer occurs between 500 μM-2 mM ATP (Fig. 2.13A). ATP concentrations above or below this range have only ~ 50% of the microtubule destroyed during the assay. The characteristic decay times calculated from fitting the data to linear or exponential decays indicated similar outcomes. The decay times for 500 μM ATP and 2 mM ATP are $\tau = 116.16$ s ± 5.44 with the goodness of fit: $R^2 = 0.98$ and $\tau = 146.76$ s ± 3.87 with the goodness of fit: $R^2 = 0.99$ respectively (Fig. 2.13B). All other lower ATP concentrations have slow characteristic decay times and significant offsets because they do not decay completely (Fig. 2.13B).

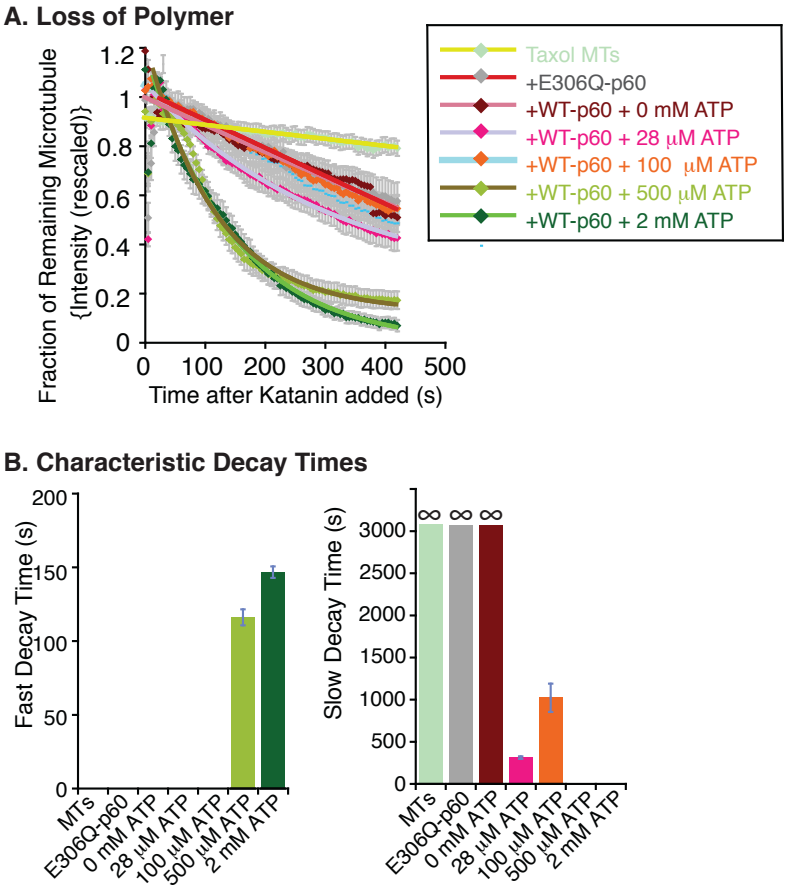

Figure 2.13 Analysis of Loss of Polymer as a Function of ATP Concentration.

(**A**) Quantification of overall loss of polymer in severing assays as a function of ATP concentrations. This is plotted as the fraction of microtubule remaining over time by comparing the intensity of the microtubule at each time point to the intensity of the microtubule at the first frame WT-p60 is added. The error bars represent the standard error of the mean. The N values for each condition is as follows: light green is Taxol-stabilized MTs + 2 mM ATP (N=50); grey is Taxol-stabilized MTs + E306Q-p60 + 2 mM ATP (N=33); dark red is Taxol-stabilized MTs + WT-p60 + 0 mM ATP (N=36); pink is Taxol-stabilized MTs + WT-p60 + 28 μM ATP (N=42); orange is Taxol-stabilized MTs + WT-p60 + 100 μM ATP (N=35); lime green is Taxol-stabilized MTs + WT-p60 + 500 μM ATP (N=53); green is Taxol-stabilized MTs + WT-p60 + 2 mM ATP (N=55). Microtubules were destroyed fastest and most completely in the presence of 500 μM and 2 mM ATP. Error bars represent the standard error of the mean. (**B**) Each data set in (A) was fit to a linear (Eq. 2.2) or single exponential decay (Eq. 2.1, 2.3). The representative decay times are plotted in seconds by their time scale. Fast time scales are on the left and slow time scales are on the right. The characteristic decay times reflect the data in (A) and show that the fastest decay occurs with 500 μM and 2 mM ATP. All other decay times are significantly longer. The error bars represent the error associated with the decay time. All fit parameters are found in Appendix A.8.

We also quantified the total number of microtubules severed for each ATP concentration. There is a peak in the total number of microtubules severed around 2 mM ATP, which drops significantly at lower concentrations of ATP (Fig. 2.14A). The time of the first severing event also depends on ATP concentration. The lowest average time to first severing event is between 500 μM-2 mM ATP. The time it takes to achieve the first severing event increases for ATP concentrations below this range (Fig. 2.14B). At ATP concentrations where there is not a complete loss of polymer, there is still only 50% of the microtubule remaining, regardless of the number of microtubules severed. Therefore, we can infer that the loss of polymer occurring is due to depolymerization and it does not appear to not depend on ATP concentration.

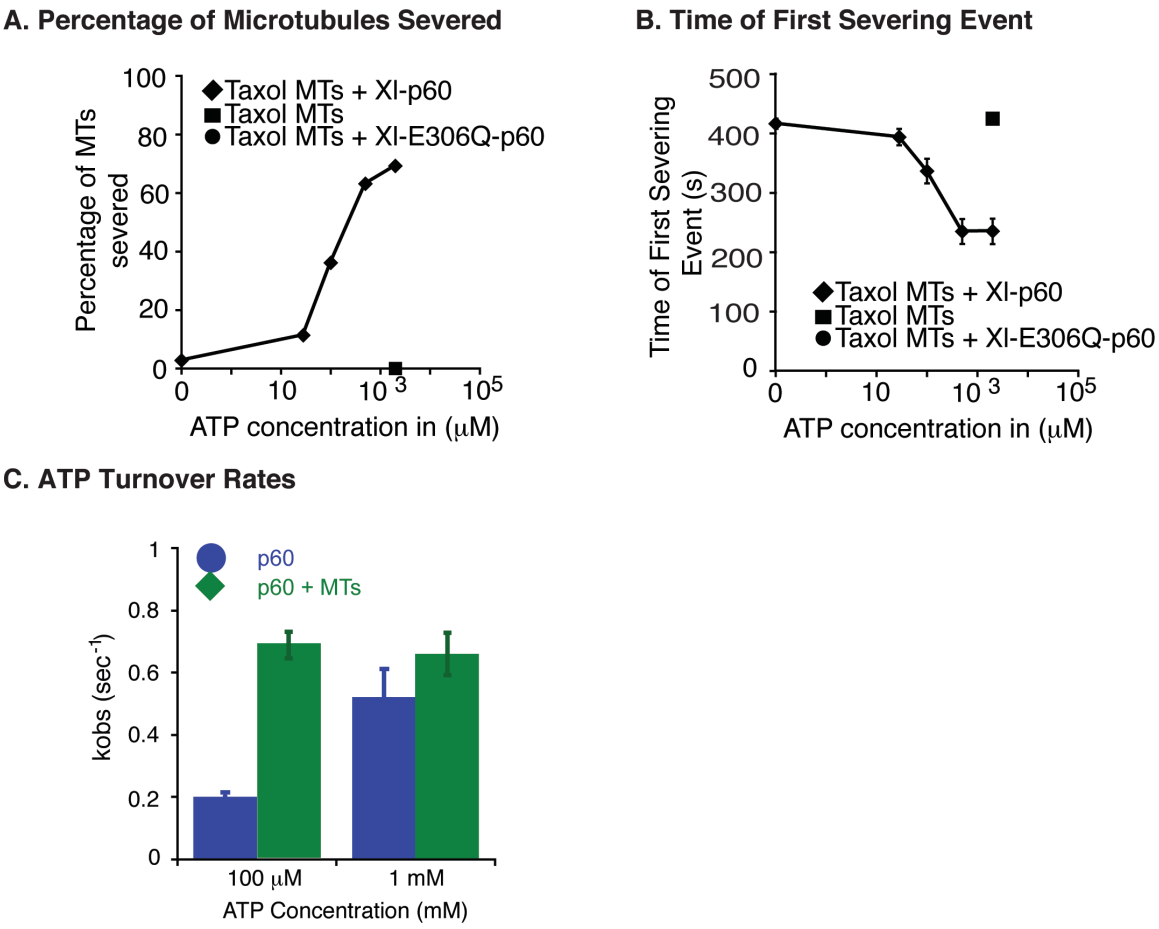

Figure 2.14 The Total Microtubules Severed and ATP Turnover Rates are Dependent on ATP Concentration.

(**A**) The total number of microtubules severed at least once was quantified to show that it was not one subsection of the population showing the trends we observe. The highest percentage of microtubules severed was with 500 μM and 2 mM ATP. The percentages decrease when the ATP concentration is raised or lowered. The error bars represent the standard error of the mean. The number of experiments preformed for each condition is as follows: light green is Taxol-stabilized MTs + 2 mM ATP (N=50); grey is Taxol-stabilized MTs + E306Q-p60 + 2 mM ATP (N=33); dark red is Taxol-stabilized MTs + WT-p60 + 0 mM ATP (N=36); pink is Taxol-stabilized MTs + WT-p60 + 28 μM ATP (N=42); orange is Taxol-stabilized MTs + WT-p60 + 100 μM ATP (N=35); lime green is Taxol-stabilized MTs + WT-p60 + 500 μM ATP (N=53); green is Taxol-stabilized MTs + WT-p60 + 2 mM ATP (N=55). Error bars represent the standard error of the mean. (**B**) The time to the first severing event is plotted as a function of ATP concentration. The time of the first severing event is shortest with 500 μM and 2 mM ATP. All other ATP concentrations were severed at long time points. If the microtubules were not severed at

all we plotted this as 420 seconds, the longest time point in our assays. The data reflect the same trends as Figure 2.13. (**C**) is quantification of the k_{obs} for 2 μM WT-p60 and 2 μM WT-60 + 1 μM MTs. This was calculated by using the V_{max} to calculate the k_{obs}. The equation we used is $V_{max}(sec^{-1}) = k_{ob} * [WT\text{-}p60 \text{ in } \mu M]$. Each data set was repeated at least three times. The error bars represent the standard error of the mean.

Previous work has shown that ATP is required for severing activity, however, it is unknown how much ATP is needed for optimal severing or depolymerization activity. McNally et al., measured the ATPase rate in the presence of 100 μM ATP and 50 μg/mL *S. purpuratus* katanin p81-p60 as 160 nM PO_4 min/mg (F. J. McNally and Vale 1993). Hartman et al. performed similar assays with 0.04 μM *S. purpuratus* p60 and found that the ATPase rate increased as a function of microtubule concentration until 2 μM microtubules, where it hydrolyzed a maximum of 3 ATP/katanin/second (Hartman et al. 1998). More recently, Whitehead et al. revealed that with *X. laevis* p60 the ATPase rate increased with increasing microtubule concentration as well as ATP concentration to 5 mM ATP (Whitehead, Heald, and Wilbur 2012). To correlate the severing activity we observe in our severing assays with the ATPase activity, we chose two concentrations of ATP: 100 μM and 1 mM, and measured the ATPase rate of 2 μM p60 with 1 μM of Taxol-stabilized microtubules. We observed that under these conditions, katanin has peak basal ATPase at 1 mM (Fig. 2.14C). In ATPase assays with 100 μM ATP, we observe a 4-fold increase in ATPase activity when p60 is microtubule stimulated. However, at 1 mM ATP, we observe minimal microtubule stimulation. These results show that the ATPase rate correlated well with the severing activity that we observe since we see a peak around 1 mM ATP. We can infer that the severing activity is highly dependent on both ATP and microtubule concentration.

2.3 Discussion

There are both theoretical and experimental evidence for katanin targeting defects in microtubules (Davis et al. 2002; Díaz-Valencia et al. 2011). Here we have presented two different types of defect microtubules which katanin targets in different ways. We show that: (1) katanin does not prefer microtubules with protofilament shifts and seam

defects, (2) Subtilisin-treated microtubules cannot be severed, but are depolymerized at a faster rate than either Taxol-stabilized or high salt microtubules, (3) Severing activity is dependent on ATP concentration, but depolymerization requires only minimal ATP. We propose that katanin can bind along the length of the filament, likely through interactions with the CTT, and can cause dimers to be removed (Fig. 2.15). However, katanin can also act at the end of filaments to enhance the rates of dimer dissociation.

Previously it has been proposed that severing enzymes bind to microtubules and can sense the curvature of the microtubule in order to sever (Roll-Mecak and Vale 2008). However, both in our previous work where katanin severs GMPCPP microtubules, which typically have 14-15 protofilaments (Diaz-Valencia 2011), and this study where we observed high salt microtubules, with 9-10 protofilaments, we observe similar rates of severing as with normal Taxol-stabilized microtubules. Therefore, it is unlikely that katanin is sensing a curvature since all three types of microtubules have a different characteristic curvature. However, it is possible that p60 is able to sense a broad range of curvatures. In the case of polarity-marked microtubules being severed more frequently at seams, it is more likely that katanin is recognizing a hole in the microtubule, since these microtubules are known to have gaps where the ends anneal (unpublished data). Therefore, katanin would be targeting a hole in the lattice and positively regulate severing activity at that location.

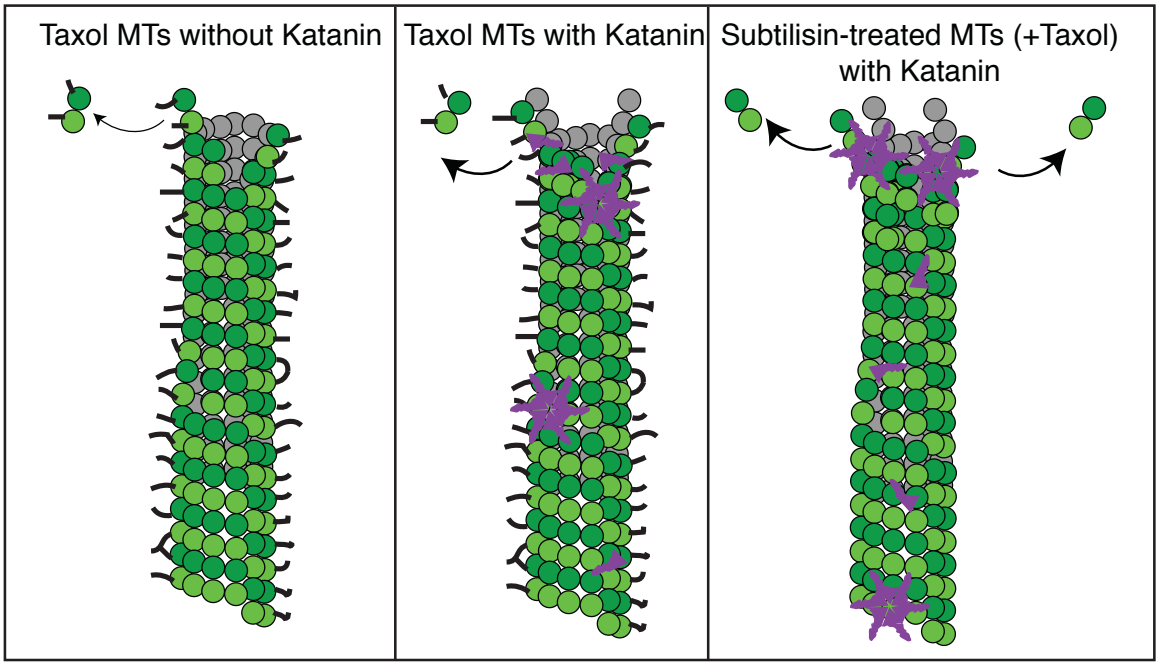

Figure 2.15 Model of Katanin-Dependent Depolymerization.

This is a model for katanin-dependent depolymerization. (**A**) Taxol-stabilized microtubules will naturally undergo a very low rate of depolymerization (**B**) When katanin is added to Taxol microtubules, it can either sever microtubules in the middle, or depolymerize microtubules from the ends. The severing activity likely requires formation of a hexamer, while depolymerization may not. (**C**) When katanin is added to subtilisin-treated microtubules it is unable to sever microtubules. However, when ATP is present, it does depolymerize microtubules. There are several possible mechanisms for how this depolymerization activity could be achieved. First, it could enhance the inherent fluctuations of the dimers so that occur at a faster rate. Second, katanin could cause a conformational change in the tubulin dimers so that is less likely to bind to its neighbors. Finally, katanin could drive a wedge between the dimer and its neighbor and dislodge it from the end of the microtubule. Additionally, it could be enhancing depolymerizing activity by some combination of these mechanisms.

In our model for how katanin can both sever and depolymerize microtubules, we know that Taxol is used to stabilize microtubules, however we observe a low rate of dimer dissociation from the ends. In our severing assays the overall background concentration of tubulin is low and although Taxol is stabilizing the microtubules, there is a chemical potential gradient of dimer loss. This rate of dimer loss is slightly faster with the high salt microtubules, suggesting that they may be less stable (Fig. 2.5). In the case of both Taxol-stabilized microtubules and high salt microtubules the rate of dimer loss remains the same when the ATPase mutant katanin is added, but due to the nature of our assays it is hard to deconvolve the depolymerization from the severing activity with WT-katanin (Fig. 2.6). Interestingly, subtilisin-treated microtubules have a lower rate of loss of polymer on their own and also with the ATPase mutant katanin, but the loss increases with WT katanin (Fig. 2.9). Since subtilisin-treated microtubules cannot be severed, the rates of loss of polymer can be attributed to depolymerization. Therefore, it is reasonable to suggest that katanin is acting through a mechanism that does not involve the CTTs of tubulin to depolymerize microtubules. We propose that katanin acts as a hexamer on the dimers on the end to enhance dissociation by one of these mechanisms: (1) katanin binding enhances the fluctuations of these dimers, (2) katanin binding causes a conformational change in the tubulin that lowers the affinity of the dimers for its neighbors, or (3) katanin binding simply drives a wedge between the end dimers and the filament. These possible, and not necessarily mutually exclusive, mechanisms rely both on katanin binding and a low level of ATP hydrolysis.

Our proposed mechanism is similar to how actin-severing enzymes act to cut without ATP. ADF-cofilin can bind to the side of the filament and loosen the bonds between neighboring monomer ultimately cutting the filament (McCullough et al. 2008; McCullough et al. 2011). This mechanism is less likely to work for microtubule severing,

because there are six times as many protofilaments in a microtubule to cut through to sever. The most vulnerable place for this type of mechanism is at the microtubule ends, where the barrier to removing a dimer is much lower, due to the lack of longitudinal and possibly lateral neighbors. Even without severing enzyme, we observe a very low rate of depolymerization that is likely due to thermal fluctuations.

Our lab and others have previously shown that katanin does depolymerize microtubules in an ATP dependent manner (Díaz-Valencia et al. 2011; Eckert, Le, et al. 2012), however, we believe that ATP only enhances the binding of katanin to the microtubules. Other groups have also shown that ATP can enhance katanin's affinity for microtubules (F. J. McNally and Vale 1993; Hartman and Vale 1999; Díaz-Valencia et al. 2011). If even small amounts of ATP are able to increase katanin binding, then it seems likely that the rate of depolymerization would also increase. Our data support that ATP can enhance katanin's severing activity within a certain range of ATP. We found that katanin had the most severing activity when the assays were supplemented with 500 μM - 2 mM ATP, and if there is less ATP the severing activity decreased (Fig. 2.12 and Fig. 2.14). However, interestingly over all ATP concentrations outside the optimal range, there was a 50% decrease in polymer mass during the severing assay, which is likely due to depolymerization (Fig. 2.13 and Fig. 2.14). Therefore, we believe that the depolymerization activity is increased by ATP, but is not dependent on the ATP concentration. Previous work from other groups has shown that katanin is sensitive to microtubule concentration. If there are too many microtubules present, the ATPase activity actually decreases for both p60 and p60/p80 (Hartman et al. 1998). Recent studies on spastin's chemical activity have suggested that spastin needs at least two wild type monomers to interact, and likely as neighbors, in order to achieve normal levels of ATPase activity (Eckert, Link, et al. 2012). Since the Hill coefficient is increased in the

presence of microtubules, it is likely that microtubules could help stimulate the cooperative interactions of the monomers (Eckert, Link, et al. 2012). Further, increasing concentrations of mutant spastin affects the turnover rate and suggests that the subunits likely exert an allosteric effect on each other (Eckert, Link, et al. 2012). Modeling of this cooperativity has proved difficult as we are still uncertain of all the states involved (Le, Eckert, and Woehlke 2013a) Future work will need to focus on determining mechanistic details of how the ATPase cycle works and how the cycle is connected to severing and depolymerization activity.

Conclusions

We have revealed some new insights on how katanin may target microtubules for both severing and depolymerization activity and that these activities may be mechanistically different. We have further showed that data from ATPase assays seems to mirror severing activity. We have provided a model for how katanin may depolymerize microtubules in an ATP-dependent manner. However, more in depth studies need to be performed to dissect the validity of this model.

2.4 Methods

2.4.1 Protein Purification

We received the pMAL-c5x-*X.* laevis p60 from the Heald lab. We used an IPTG inducible expression system was used for expression and purification. The plasmid was transformed into BL21 Competent *E. coli* (New England BioLabs). An LB starter culture was grown overnight and added to a 500mL culture the next day. This culture was grown at 37°C until it reached an OD of 0.8 and then it was induced with 1 mM IPTG. The culture was allowed to continue to grow at 16°C for 16 hours. The cells were lysed in resuspension buffer (20 mM Hepes pH 7.7, 250 mM NaCl, 0.5 mM BME, 10% glycerol,

0.25 mM ATP) via sonication. The lysate was incubated with amylose resin (New England BioLabs) for 1-2 hours. The lysate/resin mixture was added to the column and allowed to enter the column completely. Once excess lysate had passed through the column, the column was washed twice with 20 mL of resuspension buffer (20 mM Hepes pH 7.7, 250 mM NaCl, 0.5 mM BME, 10% glycerol, 0.25 mM ATP). Then the protein is eluted in elution buffer (20 mM Hepes pH 7.7, 250 mM NaCl, 0.5 mM BME, 10% glycerol, 0.25 mM ATP, 10 mM Maltose). The approximate concentration was measured by a Bradford assay.

2.4.2 Taxol-stabilized Microtubule Polymerization

Taxol-stabilized microtubules were made by combining a 1:3-1:20 ratio of labeled rhodamine tubulin (Cytoskeleton) or homemade Dylight 649 (Thermo Scientific) tubulin with home purified unlabeled tubulin. The unlabeled tubulin was purified from porcine brains using the method described in (Peloquin et al., 2005). Both the unlabeled and labeled tubulin were resuspended in PEM-100 (100 mM K-Pipes, pH 6.8, 2 mM $MgSO_4$, 2 mM EGTA) to a concentration of 5 mg/mL. Both were incubated on ice for 10 minutes. Then the labeled and unlabeled tubulin was combined and spun at 366,000 xg, 4°C for 10 minutes. To polymerize the microtubules 1 mM GTP was added to the tubulin and it was incubated at 37°C for 20 minutes. To further stabilize the microtubules, 50 μM Taxol was added and they were incubated for 20 minutes at 37°C. The microtubules were centrifuged at 16,200 xg, 27°C for 10 minutes. The pellet was resuspended in PEM-100 and 50 μM Taxol.

2.4.3 High Salt Taxol-stabilized Microtubule Polymerization

High Salt Taxol-stabilized microtubules were polymerized by the same procedure as Taxol-stabilized Microtubules, but during the polymerization step 580 mM NaCl was

added in addition to the GTP.

2.4.4 Subtilisin-treated Taxol-stabilized Microtubule Polymerization

Subtilisin-treated Taxol-stabilized microtubules were polymerized by the same procedure as Taxol-stabilized Microtubules, with several additional steps. Once the microtubules are polymerized, they are incubated with 100 mg/mL subtilisin for 45 minutes. The reaction is stopped using 2 mM PMSF. The microtubules were centrifuged for 30 minutes at 16,200 xg 27°C for 30 minutes and the pellet was resuspended in PEM-100 and 1 mM GTP.

2.4.5 In vitro assays

I made a 10 µL flow chamber with double stick tape (3M), a coverglass (fisherbrand) and a silanized coverslip (fisherbrand). The coverslips were biologically cleaned (Dixit and Ross 2010). Coverslips assembled into chambers were coated with 2% dimethyldichlorosilane (GE Healthcare) to block the surface and prevent proteins from sticking to the surface of the coverslips. I first incubated 2% (w/v) MAB1864 tubulin antibody in Katanin Activity Buffer (20 mM Hepes pH 7.7, 10% glycerol, 2 mM $MgCl_2$) for 5 minutes. Next I added 5% (w/v) Pluronic F-127 in Katanin Activity Buffer (20 mM Hepes pH 7.7, 10% glycerol, 2 mM $MgCl_2$) to additionally block the surface. Then rhodamine or dylight 649 microtubules were incubated in the chamber for 5 minutes. To remove excess microtubules, complete Katanin Activity Buffer (20 mM Hepes pH 7.7, 10% glycerol, 2 mM $MgCl_2$, 2 mM ATP, 0.025 mg/mL BSA, 0.05% F-127, 10 mM DTT, 15 mg/mL glucose, 0.15 mg/mL catalase, 0.05 mg/mL glucose oxidase) was washed through the chamber. After 3 minutes of imaging, motility mix with p60 (20 mM Hepes pH 7.7, 10% glycerol, 2 mM $MgCl_2$, 2 mM ATP, 0.025 mg/mL BSA, 0.05% F-127, 10 mM DTT, 15 mg/mL glucose, 0.15 mg/mL catalase, 0.05 mg/mL glucose oxidase, 100nM

gfp-p60).

2.4.6 ATPase Assays

ATPase assays were performed as described in (Whitehead, Heald, and Wilbur 2012). I incubated 100 μM p60 and microtubules ranging from 0.5-5 μM in Katanin Activity Buffer (20 mM Hepes pH 7.7, 10% glycerol, 2 mM $MgCl_2$) with additional 1 mM DTT, 1 mM, $MgCl_2$, 6.5 μM Taxol in a 384 well plate (Corning), at 340 nm, 30°C with an ATPase mix containing 1 mM ATP, PEP, LDH/PK for 10 minutes. Using this data I found the V_{max} (maximum rate of ATP hydrolysis) and used this rate to plot the overall k_{obs} (rate of observed ATP hydrolysis)

$$k_{obs} = V_{max}/[p60] \qquad \text{Eq 2.4}$$

2.4.7 Loss of Polymer Data Analysis

Loss of polymer analysis was performed in ImageJ. First I used the line tool to draw a segmented line, 3 pixels wide, over the length of the microtubule. I used the macro "measure stacks" to measure the mean intensity of the line for each frame of the movie. The line was moved to a piece of background near the microtubules to measure the mean intensity of the background. To find the amount of microtubule remaining at each frame, the background intensity was subtracted from the mean microtubule intensity. Then the intensity was normalized to the first frame in focus after p60 was added to the chamber.

2.4.8 Percentage of Microtubules Severed Analysis

The percentage of microtubules severed analysis was performed by counting the total

number of microtubules in the movie and the number of microtubules that were severed at least once during the course of the movie.

2.4.9 Time to First Severing Event Analysis

The time to first severing event analysis was performed by noting the frame that we first see a break in the microtubule for each microtubule that was severed at least one time during the movie.

CHAPTER 3

FREE TUBULIN INHIBITS KATANIN ACTIVITY

3.1 Introduction

Microtubules are essential, rigid biopolymers that form part of the cytoskeleton used to support and organize the interior of cells. Along with their associated proteins and enzymes, microtubules are essential for a variety of processes including mitosis, cell migration, and intracellular transport. Since microtubules are involved in diverse processes, it is important for them to be dynamically organize and rearrange based on the state of the cell. It has long been known that microtubules have intrinsic dynamics termed dynamic instability, wherein the filaments grow and shrink stochastically (Desai and Mitchison 1997). Microtubules will undergo dynamic instability spontaneously in vitro, and microtubule associated proteins (MAPs) have been shown to modify the dynamics to regulate how these cytoskeletal filaments are remodeled. It is assumed that alteration of microtubule dynamics by MAPs allows for better spatial and temporal control in the cell.

There are a plethora of MAPs in the cell including MAPs that stabilize microtubules, aiding in nucleation of filaments, and allowing microtubules to grow, as well as destabilizing MAPs that depolymerize microtubules, cause more frequent catastrophes, or even sever microtubules. A novel family of enzymatic MAPs used to sever microtubules is termed microtubule severing enzymes family. Microtubule severing enzymes are members of the (ATPases Associated with various cellular Activities) AAA+ enzyme family that hexamerize and utilize ATP to perform their function (Frickey and Lupas 2004). Microtubule severing enzymes use their catalytic activity to dismantle microtubules both in vitro and in vivo (Hartman et al. 1998; Hartman and Vale 1999).

Within the family of microtubule-severing enzymes, there are three known members: katanin, spastin, and fidgetin.

Katanin was the first discovered microtubule severing enzyme, and it is unique because katanin is composed of a 60 kD catalytic subunit, p60, and a 80 kD regulatory subunit, p80 (F. J. McNally and Vale 1993; Hartman et al. 1998). Katanin has been shown to be crucial for a variety of functions in several different types of cells. Katanin was discovered as a component of a Xenopus mitotic extract egg extract that caused the destruction of Taxol-stabilized microtubules (Vale 1991) and later purified from sea urchin embryos and identified (F. J. McNally and Vale 1993). Katanin-p80 works as a regulatory protein that targets p80 to the centrosomes via the WD40 domains in the N-terminal region (K. P. McNally, Bazirgan, and McNally 2000; Hartman et al. 1998). In egg extracts, katanin controls the spindle length in *X. tropicalis* and *X. laevis*, which in *X. laevis* is regulated by N-terminal phosphorylation (Loughlin et al. 2011; Whitehead, Heald, and Wilbur 2012). Katanin has also been shown to be involved in regulating microtubule length and releasing microtubules from centrosomes in neurons for proper neuronal development to occur (Ahmad et al. 1999). Katanin mutants are responsible for fragile plant defects affecting patterning of cell wall deposition materials (Murata et al. 2005; Nakamura and Hashimoto 2009), loss of motile function of cilia in ciliary diseases (Dymek, Lefebvre, and Smith 2004; Sharma et al. 2007), and longer than normal meiotic spindles in *C. elegans* meiosis, which eventually lost their biorientation (K. McNally et al. 2014; K. McNally et al. 2006). Recently, we have shown that katanin regulates microtubule length at the cortex of S2 cells and affects cell migration (D. Zhang et al. 2011).

Despite katanin having been discovered almost 25 years ago, there are many open questions about its biochemical and biophysical mechanisms. Katanin is an

ATPase that has been reported to be stimulated by the presence of the microtubule substrate, requires ATP to oligomerize, and is inhibited by high concentrations of microtubules (F. J. McNally and Vale 1993; Hartman et al. 1998; Stoppin-Mellet, Gaillard, and Vantard 2002). The active site for severing is likely the carboy-terminal tail (CTT) of the tubulin dimer, since katanin is unable to sever microtubules treated with subtilisin to cleave the CTT (F. J. McNally and Vale 1993; Eckert, Le, et al. 2012). Katanin requires ATP to oligomerize similar to NSF, anther known AAA enzyme (Hartman and Vale 1999). In vitro work combined with modeling has shown indirectly and directly that katanin targets to microtubule defects (Davis et al. 2002; Díaz-Valencia et al. 2011).

Much of our understanding of katanin is based on information we know about the other severing enzymes. Both spastin and katanin require ATP and the CTT of tubulin to function (Roll-Mecak and Vale 2005; Roll-Mecak and Vale 2008; Eckert, Le, et al. 2012). It has also been shown that spastin severing is inhibited by CTTs and all three pore loops in spastin's AAA domain are crucial for severing activity (Roll-Mecak and Vale 2008; White et al. 2007). Based on the crystal structure of spastin, a model of how it severs was proposed. In the presence of ATP, the severing enzyme docks on the microtubule using the N-terminal microtubule binding domains. The monomers form a hexameric ring, however, it is unclear whether this occurs before or after docking on the microtubule. The center of the ring forms a pore with three pore loops that are thought to interact with the CTTs of tubulin and tug the tails to unfold the tubulin and ultimately cause microtubule breakdown (Roll-Mecak and Vale 2008). Recent work on spastin has begun to dissect the ATPase cycle and precisely pinpoint how many subunits are required to have ATP in order to sustain severing (Eckert, Link, et al. 2012; Le, Eckert, and Woehlke 2013a). Despite the mechanistic details that have been uncovered, there is

very little that is known about how severing enzymes interact with other individual MAPs, or even tubulin itself.

3.2 Results

3.2.1 Experimental Set-up

In the following studies we used a purified GFP-labeled human version of katanin p60 to perform quantitative measurements of katanin binding and severing activity on microtubules. We find that tubulin is a potent inhibitor of katanin severing activity, even low levels of free tubulin can inhibit katanin-based severing of Taxol-stabilized microtubules. Performing direct imaging of GFP-katanin binding, we show that the free tubulin competes with the microtubule filament for binding and that even the CTTs can effectively compete for binding to cause severing inhibition. Using such CTT constructs, we show that different isoforms of tubulin are more or less potent at inhibiting severing with beta-tubulin CTTs being the most effective and detyrosinated alpha tubulin CTTs being the least inhibitory. Our studies shed new light on possible inhibitory feedback mechanism of katanin that might function in the cell to shut down katanin activity so that it does not destroy all the microtubules of the cell.

3.2.2 Human p60 is as effective as X. laevis p60.

Microtubule severing assays have been performed previously to characterize severing enzymes (Loughlin et al. 2011; Whitehead, Heald, and Wilbur 2012; Eckert, Le, et al. 2012; Eckert, Link, et al. 2012; F. J. McNally and Thomas 1998; K. P. McNally, Bazirgan, and McNally 2000; Buster, McNally, and McNally 2002; Stoppin-Mellet, Gaillard, and Vantard 2002; Díaz-Valencia et al. 2011; D. Zhang et al. 2011; K. McNally et al. 2014; Johjima et al. 2015). First, in order to show that our purified katanin is

functioning we performed microtubule-severing assays in vitro on Taxol-stabilized microtubules. We compared our new GFP-labeled human version of p60 (Hu-p60) to a previously characterized p60 from X. leaves (Xl-p60) (Loughlin et al. 2011; Whitehead, Heald, and Wilbur 2012). Qualitatively, we find that severing by Hu-p60 is as fast as by Xl-p60, a majority of the microtubules are severed by the third frame in the series ~100 s, as seen in the representative time series (Fig. 3.1A-B).

Time Series of Severing Assays

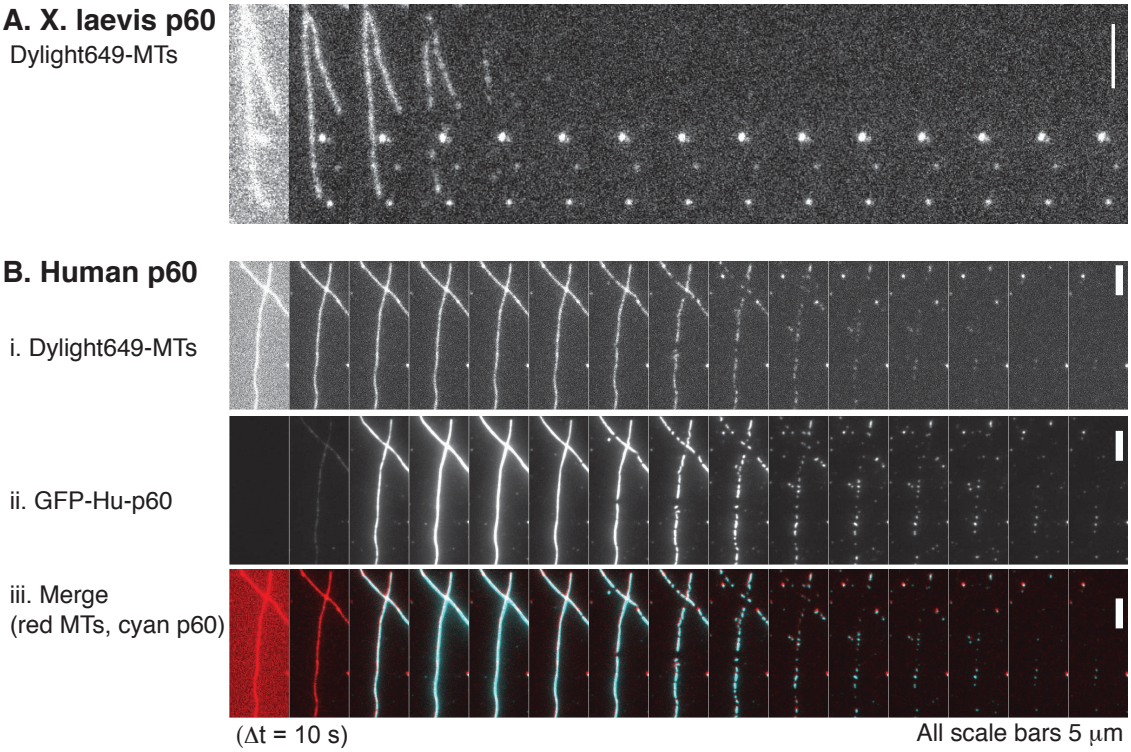

Figure 3.1 Representative Time Series of X. laevis p60 and Human p60.

(**A**) Example time series of severing assays with X. laevis p60 (Xl-p60). The severing assays were 10 minutes long with a frame taken every 5 seconds. The times series depicts a frame every 10 seconds. The scale bars are 5 μm. Time series of Dylight649 microtubules (MTs) in a severing assay with Xl-p60. By the end of the movie the microtubules are completely destroyed. The first frame is bright and out of focus due to the enzyme being flowed into the chamber. (**B**) Example time series of severing assays with human-p60 (GFP-Hu-p60). (i) Time series of Dylight649-MTs in a severing assay with GFP-Hu-p60. Microtubules are completely destroyed by the end of the assay. The first frame is bright and out of focus due to the enzyme being flowed into the chamber. (ii) Time series of the same assay in (i) of the GFP channel showing GFP-Hu-p60 binding along the microtubules. The GFP-Hu-p60 was added during the first frame in the time series and within two frames is completely decorating the microtubules. (iii) A merge of (i) and (ii). Red is the microtubules and cyan is GFP-Hu-p60. The severing assays were 10 minutes long with a frame taken every 5 seconds. The times series depicts a frame every 10 seconds. The scale bars are 5 μm.

Similar to other methods of tracking microtubule severing, we used the average fluorescence intensity of the microtubule to plot the fraction of microtubule remaining over time (Loughlin et al. 2011; Whitehead, Heald, and Wilbur 2012; K. P. McNally, Bazirgan, and McNally 2000; Buster, McNally, and McNally 2002; Stoppin-Mellet, Gaillard, and Vantard 2002; K. P. McNally, Buster, and McNally 2002; K. McNally et al. 2014) or the total number of microtubules remaining over time (F. J. McNally and Thomas 1998). Using fluorescence intensity of the microtubule signal as a read-out for the microtubule remaining, we quantified the loss of polymer over time (Fig. 3.2A). We found the rate of decay by fitting the data with an exponential decay function of the form:

$$I(t) = I_0 \exp(-t/\tau), \quad \text{Eq. 3.1}$$

where I is the intensity as a function of time, t, I_0 is the amplitude at time zero, and τ is the characteristic time constant for the decay (Fig. 3.2B). If it does not decay to zero, we can use a vertical offset, to the equation:

$$I(t) = I_0 \exp(-t/\tau) + I_\infty, \quad \text{Eq. 3.2}$$

where I_∞ is the intensity asymptote at infinity. In some data sets, we needed a double exponential decay to best fit the data:

$$I(t) = I_1 \exp(-t/\tau_1) + I_2 \exp(-t/\tau_2), \quad \text{Eq. 3.3}$$

When there is no katanin present, the data has a single, long characteristic decay time, and can basically be fit to a linear approximation for an exponential decay:

$$I(t) \sim I_0 (1 - (t/\tau)), \quad \text{Eq. 3.4}$$

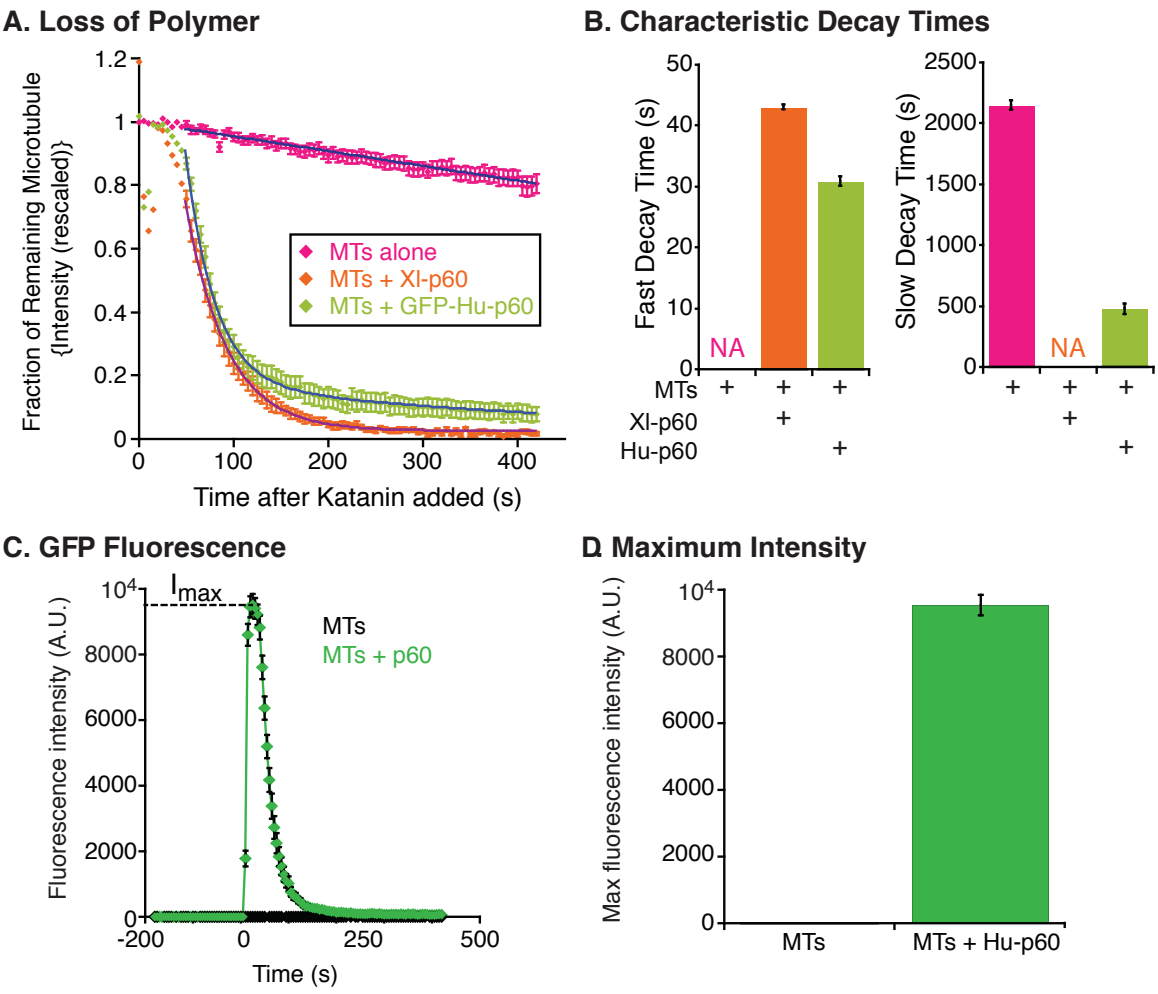

Figure 3.2 Human p60 is as Effective as X. laevis p60.

(**A)** Plot of quantification of fraction of microtubule remaining over the course of the severing assay for Dylight649-MTs + Xl-p60, Dylight649-MTs + Hu-p60 and Dylight649-MTs without any severing enzyme. Each of the data sets are fit to a line, single, exponential decay, or double exponential decay. Fit parameters are in Appendix A.3. The N values for these assays are as follows: Xl-p60 + MTs (N=55), Hu-p60 + MTs (N=73), MTs (N=56). The error bars for the data sets represent the standard error of the mean. (**B**) Graph of the characteristic decay time for each condition. This plot was made by fitting each data set from part (A) with a line, single exponential decay, or double exponential decay. On the left side the fast decay times are plotted and on the right side are the slow decay times. Error bars represent the error associated with the decay time. (**C**) Plot of background subtracted fluorescence intensity of GFP-Hu-p60 over the course of a severing assay. The dotted line represents I_{max}, the maximum fluorescence intensity, which corresponds to maximum Hu-p60 binding to microtubules. The N values for these assays are as follows: Hu-p60 + MTs (N=73), MTs (N=52). (**D**) The bar chart of the maximum fluorescence intensity of GFP-Hu-p60 and the MTs control. All error bars represent the standard error of the mean. Using this fit, we find the decay constant, tau to be: 2143.6 ± 36.96 with a goodness of fit of R^2 = 0.983. When Xl- p60, is added to the

severing assays, the data is best fit by a single exponential curve, Eq. 3.2. Using these parameters, we find the decay constant is τ_1 = 42.967 ± 0.4042, with an R^2 = 0.998. Interestingly, when Hu-p60 is present, a double exponential decay is required for the best fit, Eq. 3.3. suggesting that there are two different phases in the data. There is a fast phase initially which is characterized by a steep slope and a characteristic decay time of τ_1 = 30.743 ± 0.7491 followed by a slow phase with a long decay time τ_2 = 471.04 s ± 40.035 with the goodness of fit: R^2 = 0.997. It is especially intriguing that Xl-p60 and Hu-p60 follow distinctly different decay behavior. This could suggest that are working in different in different ways mechanistically. The fit parameters can be found in Appendix A.3.

Since the human construct is GFP-labeled, it provided us with additional information about how and when katanin binds to microtubules over the course of the severing assay (Fig. 3.1B). Plotting the average intensity of GFP-Hu-p60 fluorescence on the microtubule over time correlates with Hu-p60 severing microtubules (Fig. 3.2C), and showed that the peak of katanin binding occurs as severing began. As severing proceeded to completion, the fluorescence intensity associated with binding also dropped rapidly. To best portray the data, we chose to represent the binding data as the point of maximum fluorescence intensity or binding (Fig. 3.2D). The loss of polymer and GFP-intensity metrics will be used throughout to represent severing assays under differ conditions.

3.2.3 Total Time for Katanin to Complete Severing is Concentration Dependent.

To determine how the severing rate depends on Hu-p60 concentration, we performed severing assays with high temporal resolution and increasing concentrations of katanin. Severing activity is fast and tightly coupled to katanin binding (Fig. 3.1). In order to characterize the fast kinetics, we imaged continuously in the GFP Hu-p60 channel at approximately 25 frames per second. An example of the time series of the severing assay is depicted in Fig. 3.3. From these assays we determined the time-dependent activities including: association time, time to first severing event, total severing time, and severing activity time (Fig, 3.3).

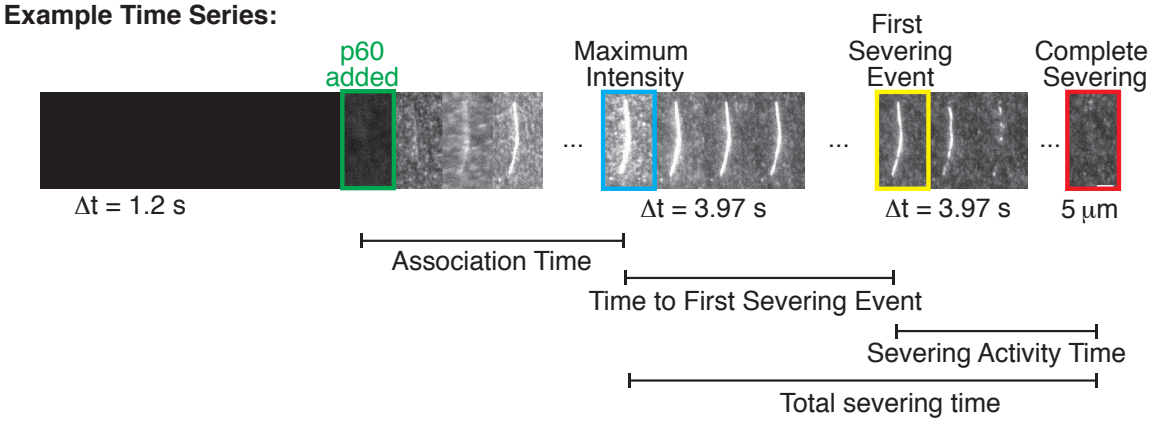

Figure 3.3 Representative Time Series of Concentration Dependence.

Example time series of GFP-Hu-p60 binding and severing. We highlight the initial frame where the GFP-Hu-p60 is added (green box), the GFP intensity if maximum (blue box), the first resolvable severing event (yellow box), and the frame at which the microtubule is completely lost to katanin activity (red box). The time between the insertion of p60 and the maximum intensity is the association time. The time between the maximum intensity and the first resolvable severing event is the time to first severing event. The time between the first severing event and the complete loss of microtubule signal we call that severing activity time. The total time for severing is the time from the maximum intensity and the complete loss of microtubule.

The association time is the time is takes for the protein to bind to the microtubule after being injected into the flow chamber. We defined the association time as the time between the frame when the GFP-Hu-p60 was added to the chamber and the frame displaying the maximum intensity of GFP fluorescence (Fig. 3.2C). We were careful to image microtubules in a region of the chamber that were a similar distance from the edge of the chamber (approximately 10 mm) where protein was injected, so as to not affect the results due to flow. The association rate data is fit to a hyperbolic function equation of the form:

$$k_a = k_{\max} \frac{[c]}{k_{1/2} + [c]} \qquad \text{Eq 3.5}$$

where k(c) is the association rate, k_{max} is the maximum association rate at infinite katanin concentration, $k_{1/2}$ is the characteristic concentration of katanin at which the rate is half and [c] is the concentration of the katanin. The best fit had $k_{a,max}$ = 0.145 ± 0.008 1/s, $k_{1/2}$ = 50 ± 10 nM, and a goodness of fit of 0.91 and χ^2 = 0.0003. The $k_{1/2}$ = 50 ± 10 nM could be used as an estimate of the affinity, K_D, of the katanin for the microtubule.

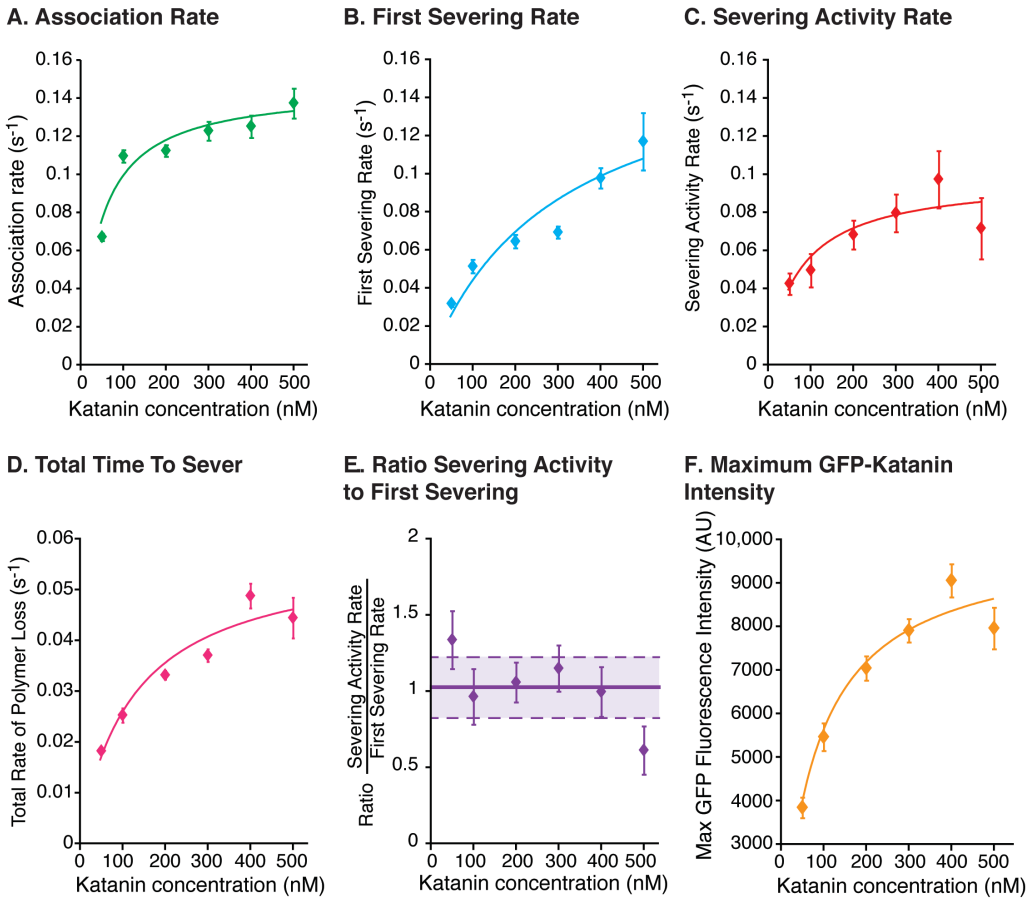

Figure 3.4: Fast Katanin Severing Activities Are Concentration Dependent.

(**A**) Quantification of the association rate as a function of GFP-Hu-p60 concentration with fit to equation 5. The number of experiments performed are as follows for (A)-(E): 50 nM (N=7), 100 nM (N=54), 200 nM (N=45), 300 nM (N=53), 400 nM (N=33), 500 nM (N=10). Error bars represent the standard error of the mean. (**B**) Quantification of the time to first severing rate as a function of GFP-Hu-p60 concentration with fit. Error bars represent the standard error of the mean. (**D**) Quantification of the total severing rate as a function of GFP-Hu-p60 concentration. Error bars represent the standard error of the mean. (**E**) Ratio of the severing activity rate to the rate of first severing. Error bars represent aggregated uncertainties from both the severing activity rate and the first severing rate added in quadrature. In the range of concentrations used, the mean is about 1 (solid line) with a standard deviation of about 0.2 (shaded region). (**F**) Maximum intensity of katanin in the GFP channel as a function of added katanin concentration with fit to equation 5. The N values are as follows: 50 nM (N=36), 100 nM (N=54), 200 nM (N=45), 300 nM (N=53), 400 nM (N=33), 500 nM (N=10). Error bars represent the standard error of the mean. Fit parameters are found in Appendix A.4.

We quantified the time to first severing as the time between the max intensity frame and the first clear severing event distinguishable (Fig. 3.3). Again, we examine the inverse of this time, the first severing rate (Fig. 3.4B). This rate also depends on the amount of katanin added and is Michaelis-Menten-like. The best fit had $k_{first,max}$ = 0.17 ± 0.05 1/s, $k_{1/2}$ = 300 ± 160 nM, and a goodness of fit of 0.89 and χ^2 = 0.0005. Comparing this data to the association rate data, we can see that it takes 6 times as much concentration to sever (300 nM) as it does to bind (50 nM). Interestingly, that fits perfectly with the 6-fold oligomerization stoichiometry for katanin, which is thought to be a hexamer. This data supports a model where individual monomers of katanin can bind to microtubules independently, but hexamerization is required for severing.

We quantified the severing activity time and the total severing time. The severing activity time is the time is takes for the microtubule to be completely destroyed once severing has initiated (Fig. 3.4C). The total severing time is the sum of the time to first sever and the severing activity time (Fig. 3.4D). Inverting these times, and plotting as a function of katanin concentration, we find that both rates increases with the concentration of katanin added, with a best fit using Eq. 3.5. For the severing activity, the best fit parameters are $k_{severing,max}$ = 0.10 ± 0.01 1/s, $k_{1/2}$ = 80 ± 40 nM, and a goodness of fit of 0.77 and χ^2 = 0.0004. For the total severing, the best fit parameters are $k_{severing,max}$ = 0.057 ± 0.006 1/s, $k_{1/2}$ = 130 ± 40 nM, and a goodness of fit of 0.93 and χ^2 = 0.00005. Interestingly, we noticed a similarity in the data for the first severing rates and the severing activity rates. Indeed, when we calculated the ratio of these two data for each concentration, the ratio was about one (Fig. 3.4E). This implies that the first severing and severing activity rates are likely measures of the same activity of hexamerization and removal of dimers.

Finally, we could also quantify the maximum GFP fluorescence of katanin binding during severing with the background fluorescence intensity removed (Fig. 2G). We fit the data to a binding curve (Supp. Table 2). Using the average maximum value of intensity, and the fit, we can find that the half-maximum intensity occurs at 80 ± 20 nM, giving an estimate for the K_D value for katanin binding. This is in agreement (within uncertainty) with the value found from the both the severing activity and the association rate data implying that these concentrations are probably similar and measuring the affinity of the enzyme for the microtubule (Fig. 2B).

3.2.4 Free Tubulin Inhibits Katanin Binding to Microtubules.

Many microtubule associated proteins (MAPs) are able to distinguish between microtubules and free tubulin and will selectively bind to one or the other. For example, the N-terminus of doublecortin cannot bind soluble tubulin, whereas the C-terminus binds to both microtubules and soluble tubulin (Kim et al. 2003). Both Stu2p, a member of the XMAP215 family and E-like can sequester tubulin dimers (Al-Bassam et al. 2006; Bartolini 2005). Some evidence that severing proteins may not bind selectively to microtubules is that spastin is inhibited by tubulin CTTs in severing assays (White et al. 2007; Roll-Mecak and Vale 2008). Further, both spastin and katanin do not sever subtilisin-treated microtubules. Pelleting assays with free tubulin and microtubules has shown that katanin severing activity is inhibited by tubulin (Vale 1991; F. J. McNally and Vale 1993; Eckert, Le, et al. 2012; Roll-Mecak and Vale 2005). Therefore, since these enzymes are very similar, it would not be surprising if katanin severing was also inhibited by tubulin.

To test the hypothesis that free tubulin can inhibit severing of filaments, we added free tubulin to the severing assays with Hu-p60 or Xl-p60 katanin. Surprisingly small

concentrations of free tubulin (50 nM) showed significant reduction of severing, and any concentration of free tubulin above 500 nM was completely inhibitory to severing (Fig. 3.5).

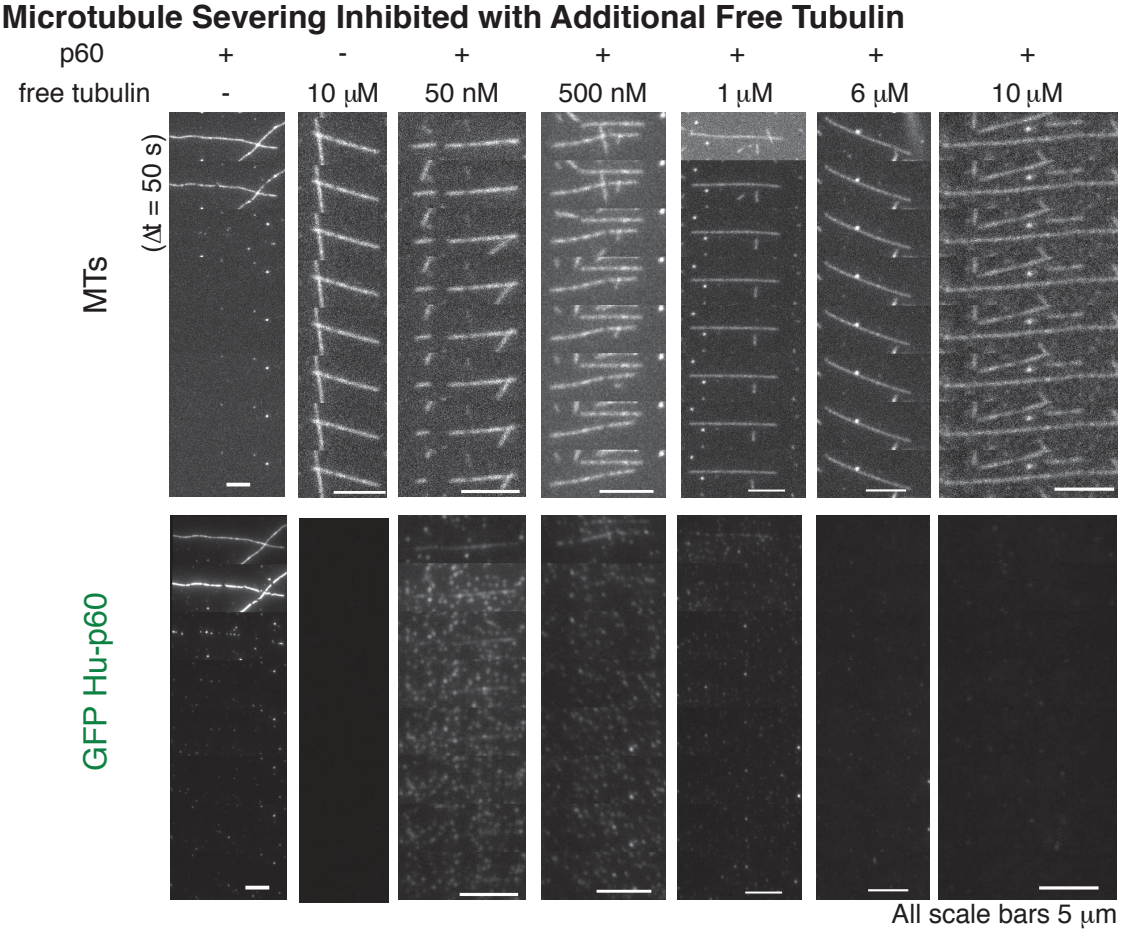

Figure 3.5 Representative Time Series of Katanin's Severing Activity Inhibited by Free Tubulin.

Example time series of severing assays with katanin +/- free tubulin at concentrations from 50nM to 10 μM. The severing assays were 10 minutes long with a frame taken every 5 seconds. The time series are frames every 50 seconds as stated in figure A. The scale bars are 5 μm.

Examination of the GFP-Hu-p60 shows that the inhibition of severing is due to a loss of katanin binding to microtubules (Fig. 3.5). We quantified and plotted the fraction of microtubule remaining as a function of tubulin concentration (Fig. 3.6A,B). Even at the lowest concentration of free tubulin (50 nM) there is significant inhibition of the severing and depolymerization activity of katanin (Fig. 3.6A,B).

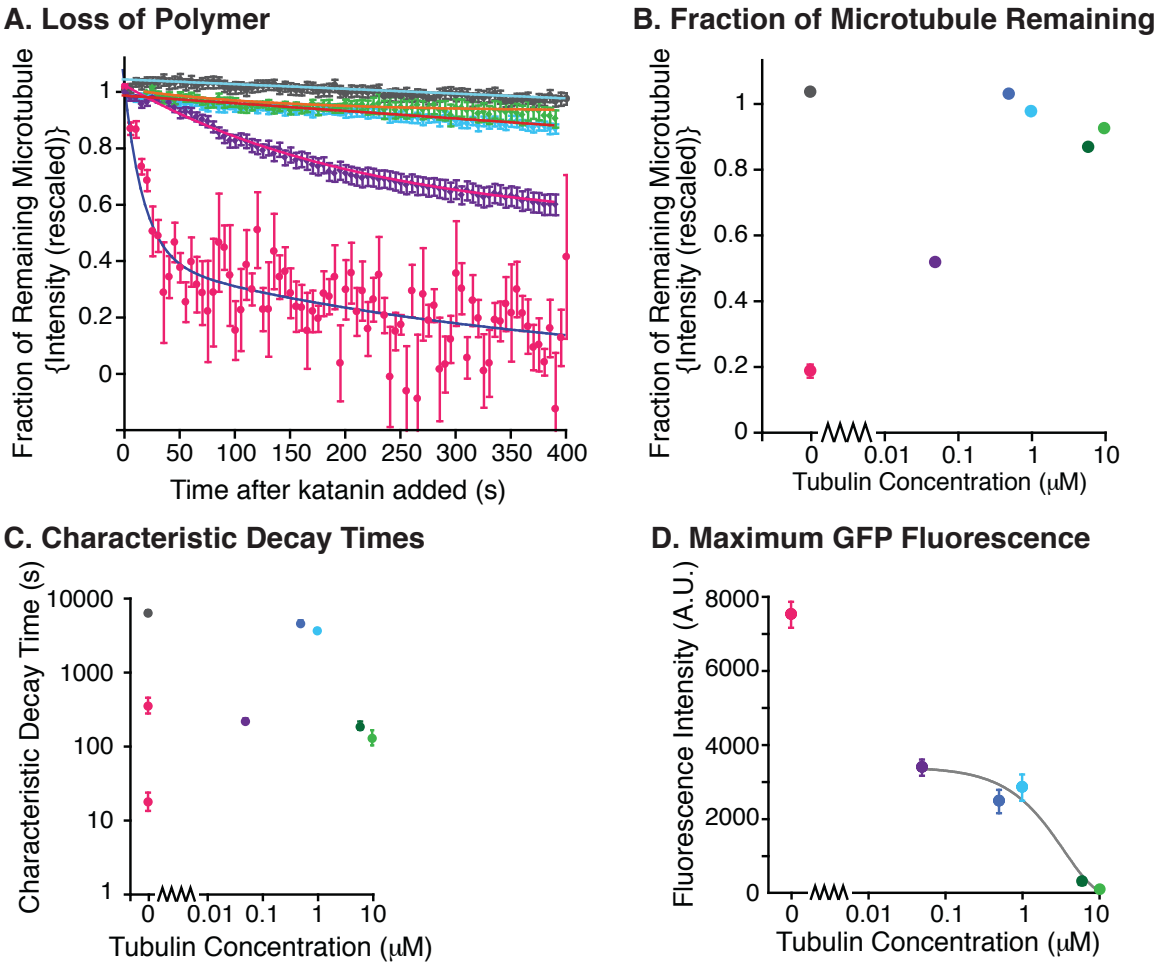

Figure 3.6 Quantification of Katanin's Severing Activity Inhibited by Free Tubulin.

(**A**) This is a plot of representative tubulin concentrations quantifying the fraction of microtubules. The plot shows that a majority of the microtubule is remaining at the end the severing assay when there is any tubulin added to the assay. The data was fit to exponential decay lines to find additional information about the characteristic decay times. The color key is as follows: pink is katanin, purple is katanin + 50 nM free tubulin, dark blue is 500 nM free tubulin, light blue is katanin + 1 μM free tubulin, dark green is katanin + 6 μM free tubulin, light green is katanin + 10 μM free tubulin. From the fits we were able to also find the fraction of microtubule remaining, which is plotted in (**B**). The fit parameters are in Appendix A.5. (**C**) is the characteristic decay times from the fits. Only when there is no free tubulin are there multiple decay constants. (**D**) This is a plot of the peak GFP fluorescence for free tubulin concentrations of 50nM to 10 μM. When there is any free tubulin is in the severing assay, the average GFP fluorescence decreases to half the overall fluorescence intensity of the control assay, which has no free tubulin in the chamber. The exponential decay fit shows the dependence of katanin binding on the free tubulin concentration.

We quantified the loss of polymer and fit the data to single decays, linear approximations, or double exponential decays, depending on the best fit (fit parameters with uncertainties and goodnesses of fit can be found in Appendix A.5). Using the fit parameters we quantified the fraction of polymer remaining to find that as more tubulin is added, the fraction of microtubule increased to 1 (Fig. 3.6A), implying that all the polymer was remaining and no severing or depolymerization was occurring. Further, the characteristic decay times also increased, showing that the loss of polymer that did exist took longer to be lost (Fig. 3.6D).

We also quantified the maximum fluorescence of GFP-Hu-p60 binding and found a significant decrease in katanin binding with increasing concentrations of free tubulin (Fig. 3.5 and Fig. 3.6D). There is an initial rapid decrease in severing activity when even small concentrations of free tubulin (50 nM) are added. We plotted the max intensity as a function of added free tubulin and find that it decreases monotonically with increasing concentration of inhibitory tubulin. We fit the data to an exponential decay (Eq 1) to determine the characteristic decay concentration of 3.1 ± 0.9 μM. This concentration represents a critical concentration of inhibition, K_i. For comparison, the critical concentration of tubulin alone is about 1.8 μM, but the critical concentration for Taxol-stabilized microtubules is 0.08 μM (Schiff, Fant, and Horwitz 1979; Shelanski, Gaskin, and Cantor 1973). This explains why Taxol-stabilized microtubules that have very little free tubulin in the background are easily severed. On the other hand, dynamic microtubules will be much more difficult to sever, because the free tubulin in the background will inhibit severing at equilibrium. Interestingly, the concentration of free tubulin in a cell is thought to be between 20-24 μM (Gard and Kirschner 1987b), adding

more mystery to the activity of katanin in cells.

The same pattern of severing inhibition held true for the unlabeled *X. laevis* construct (Fig. 3.7) suggesting that the severing activity is similarly affected by the presence of free tubulin.

A. Loss of Polymer

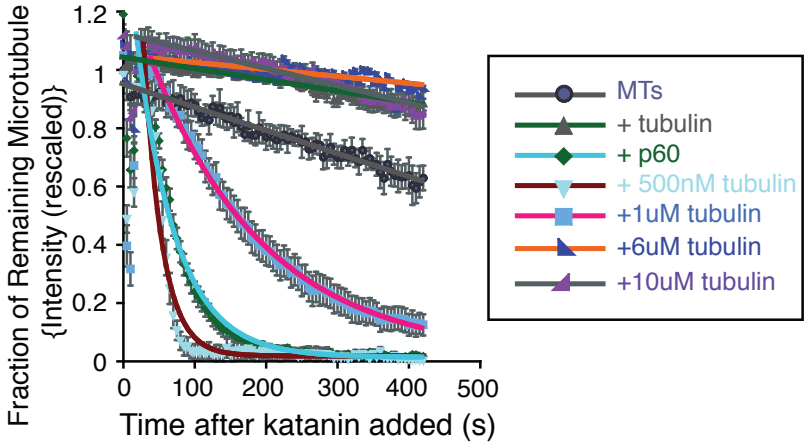

B. Characteristic Decay Times

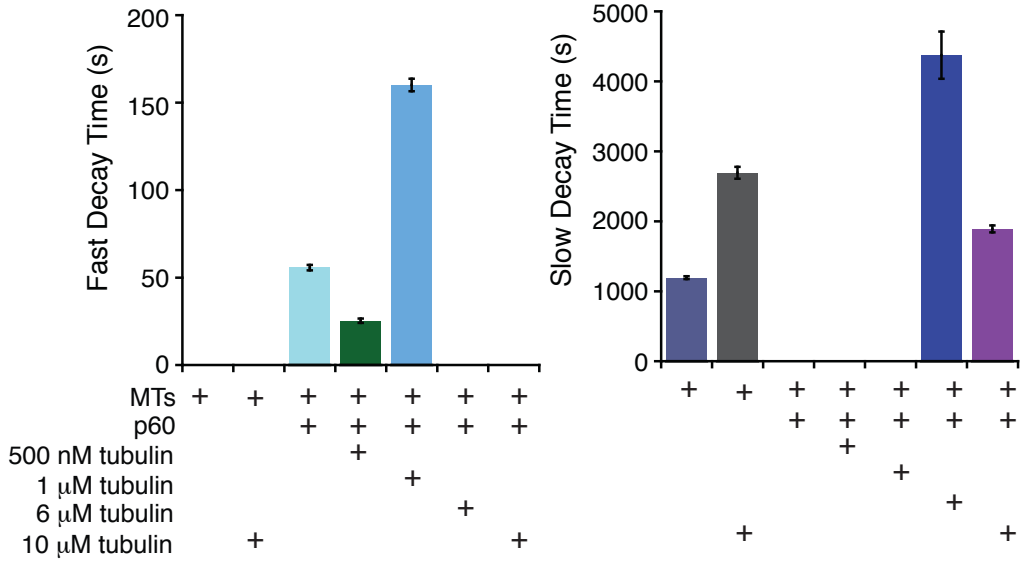

Figure 3.7 X. laevis Katanin is Inhibited by Free Tubulin.

(**A**) Plot of the quantification of the fraction of microtubule remaining for Xl-p60. The error bars represent the standard error of the mean. Each condition is fit to a linear or single exponential decay. The fit parameters are found in appendix A.2. The number of experiments for each condition are as follows: MTs (N=4), MTs + 10 μM tubulin (N=10), MTs + Xl-p60 (N=55), MTs + Xl-p60 + 500 nM free tubulin (N=17), MTs + Xl-p60 + 1 μM free tubulin (N=14), MTs + Xl-p60 + 6 μM free tubulin (N=10), MTs + Xl-p60 + 10 μM free tubulin (N=15). (**B**) Plot of the decay times found from the fits in (A). The fast decay times are plotted on the left and the slow decay times are plotted on the right. The error bars represent the error associated with the fit.

3.2.5 Katanin has a Higher Affinity for Free Tubulin than Microtubules in Severing Assays.

We have shown that free tubulin can inhibit binding of katanin when the free tubulin and katanin are added simultaneously (Fig. 3.5-3.6). In the experiments described in figures 3.5 and 3.6, katanin and tubulin are pre-mixed before addition to the imaging chamber. Thus, the katanin could be binding to the free tubulin before being added to the assay. In order to directly test if free tubulin can compete with microtubule polymer for binding, we created a flow-in experiment to directly observe if katanin bound to the microtubule can be competed off by free tubulin. We pre-bound the GFP-Hu-p60 to the microtubules with ATPγS, a slowly hydrolyzable analog of ATP that allows katanin to bind to microtubules but not sever. Then we added 0 nM (buffer only), 50 nM, 500 nM, 1 μM, 6 μM, and 10 μM free tubulin to the chamber and monitored the GFP fluorescence on the microtubules over time (Fig. 3.8).

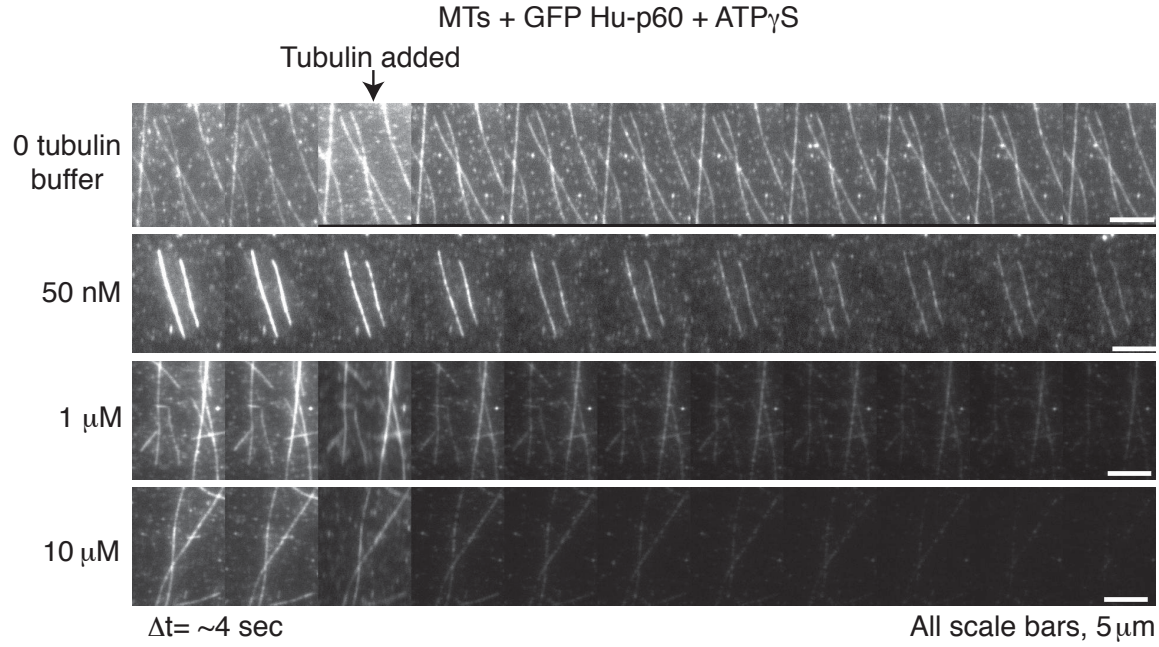

Figure 3.8 Representative Time Series of Free Tubulin Flow Through Experiments.

Example time series of assays with katanin +/- free tubulin at concentrations of 0 nM, 50nM 1 μM and 10 μM free tubulin. The data was taken by imaging continuously for several minutes. The time between frames in the time series is 4 seconds. Katanin was pre-bound to microtubules with ATPγS prior to starting imaging, allowing the enzyme to bind, but not sever microtubules. The tubulin was added as indicated in the third frame of the time series. The scale bars are 5 μm.

We quantified the GFP fluorescence over time and could fit the loss of GFP fluorescence to a double exponential decay equation (Eq. 3.3, Fig. 3.9A). For all concentrations of free tubulin, the double exponential decay fit best (fit parameters, uncertainty, and goodnesses of fit can be found in Appendix A.6). From the image data and the quantification, it is clear that the loss of overall fluorescence increases as a function of free tubulin (Fig. 3.9B). We plotted the short and long decay times from the double exponential fits to determine their physical meaning (Fig. 3.9B). The short time data had no dependence on the amount of free tubulin added and was about 18 ± 2 s. Since the same time scale was observed for the buffer control, has no dependence on the amount of tubulin added, and was fast, we conclude that the fast time scale is due to flow alone. Some of the background fluorescence will be swept away with the flow, and that will be fast and the same for all data sets.

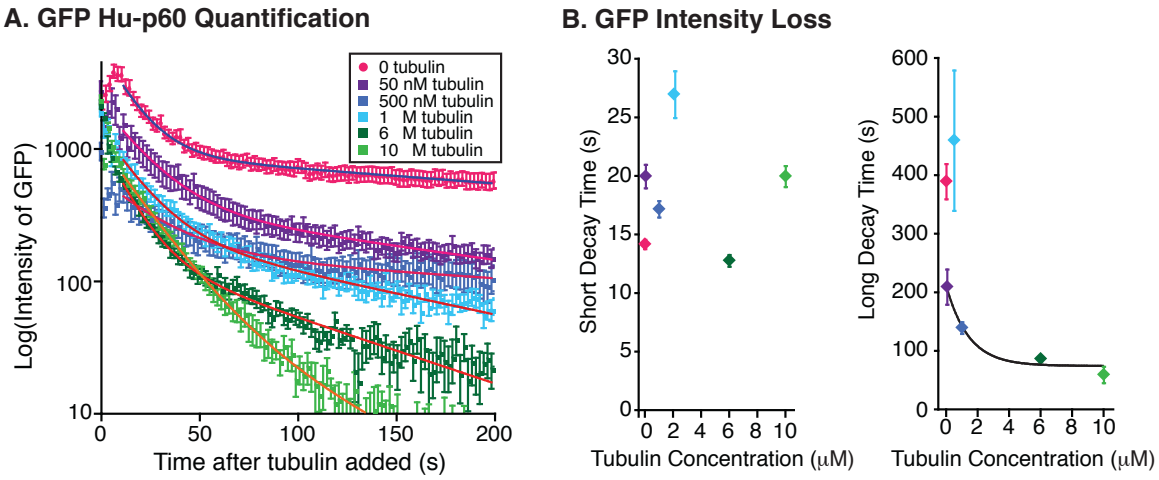

Figure 3.9 Katanin Has a Higher Affinity for Free Tubulin than Microtubules.

(**A**) Quantification of the average GFP fluorescence remaining on the microtubules after free tubulin was added to the assay. Error bars represent the standard error of the mean. The data shows there is a significant decrease in GFP fluorescence on the microtubules when there is any free tubulin added to the assay. Each data set was fit to an exponential decay curve. The parameters can be found in Appendix A.6. (**B**) Plot of the characteristic decay times for each condition. The short decay times are on the left and the long decay times are on the right. The long decay times are fit to an exponential decay curve and can be related to the off rate of katanin as a result of tubulin competition. The number of experiments for each condition are as follows: katanin (N=20), katanin + 50 nM free tubulin (N=23), katanin + 500 nM free tubulin (N=22), katanin + 1 μM free tubulin (N=25), katanin + 6 μM free tubulin (N=25), katanin + 10 μM free tubulin (N=11).

The long decay times show a dependence on the amount of free tubulin added and decreases with increasing amounts of free tubulin. The long time decay time represents the dissociation of free tubulin due to both depletion of background GFP-Hu-p60 during the flow and competition between the microtubule filament and free tubulin for GFP-Hu-p60 binding. The long decay time has a dependence on the amount of free tubulin added and can be fit with a single exponential decay of the form:

$$\tau([c]) = A\exp(-[c]/c^*) + \tau_\infty, \qquad \text{Eq. 3.6}$$

where A is the amplitude, [c] is the concentration of tubulin, c* is the characteristic concentration, and τ_∞ is the high concentration limit of the long time. The best fit parameters are A = 140 ± 20 s, c* = 1.4 ± 0.7 μM, τ_∞ = 70 ± 10 s, with a goodness of fit of 0.98 and a χ^2 = 320. From these fits, we can surmise that the characteristic concentration for tubulin competition, c*, is similar to the critical concentration of tubulin for dynamic microtubules, implying again that severing dynamic microtubules is unlikely. The data asymptotes at high concentrations to a time of about 70 s, implying that this is the minimal time for competition to occur.

It is interesting to point out that even the control with buffer only and no free tubulin had a long time decay constant (Fig. 3.9B). This is because the background concentration of GFP-Hu-p60 was reduced during the flow. The slower loss of fluorescence from the microtubule is due to dissociation that re-establishes the dynamic equilibrium and reinstates the background concentration of unbound GFP-Hu-p60. From the data, it is clear that 200 s is enough time to establish the final equilibration level, which is similar before and after the flow (Fig. 3.9A,B), and implies a high affinity for microtubule substrate in the ATP-state. The ability of the free tubulin to compete off the GFP-Hu-p60 implies that katanin has an even higher affinity for free tubulin - even in the ATP-state.

3.2.6 Katanin Recognizes Sequence of CTT of Free Tubulin.

Katanin-p60 has been proposed to have two possible microtubule-binding sites: the microtubule interacting and trafficking (MIT) site at the N-terminus of p60 and the pore loop region in the AAA domain that binds to the tubulin carboxy-terminal tail. In human katanin the MIT has been mapped to amino acids 55-180, and the AAA pores are amino acids 197-88 (F. J. McNally and Thomas 1998; Eckert, Le, et al. 2012; Johjima et al. 2015). Next, we wanted to distinguish whether katanin was binding to the free tubulin due to it recognizing and therefore binding to the specific shape or folded structure of the free tubulin or whether katanin was recognizing a specific sequence of tubulin, most likely through the CTT. To address this question, we unfolded free tubulin using acid denaturation and brought the samples back to neutral pH to use in the assay (please see the methods for more information). Since tubulin requires a chaperone to fold, the neutralized protein is likely improperly folded or unfolded. In order to specifically probe if the CTT was needed, we also made denatured free tubulin with the CTTs cleaved off by treating microtubules with the protease, subtilisin, prior to denaturing the microtubules. We performed the same experiment where we added GFP-Hu-p60 with free tubulin at 50 nM, denatured tubulin at 50 nM, or subtilisin-treated denatured tubulin at 50 nM. We monitored both the microtubule signal to inspect severing and polymer loss and the GFP-channel to quantify katanin binding (Fig. 3.10). As is clear from the time series (Fig. 3.10), both free tubulin and denatured tubulin are able to effectively inhibit katanin's severing activity and binding. However, the subtilisin-treated denatured tubulin did not inhibit severing and allowed for more GFP-Hu-p60 to bind microtubules.

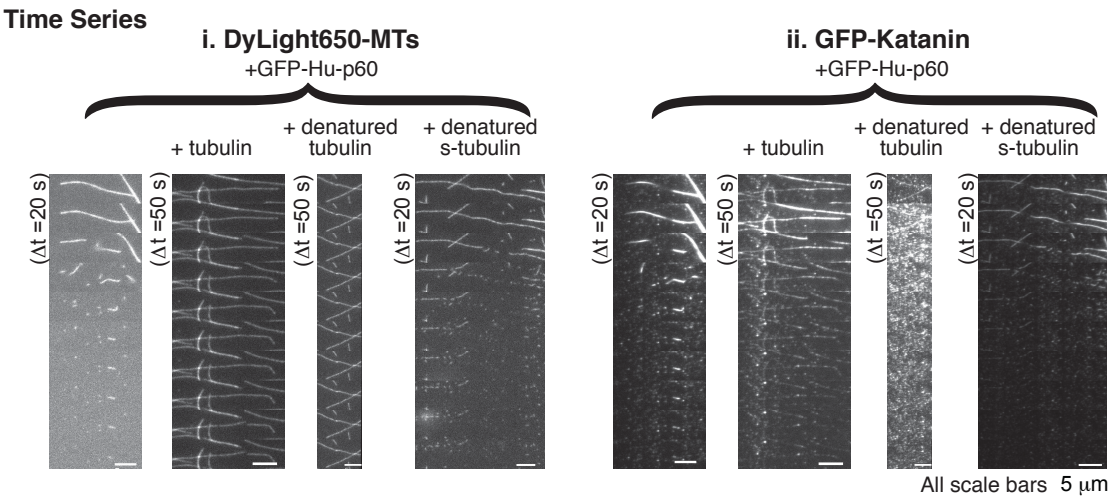

Figure 3.10 Representative Time Series of Katanin Inhibited By Denatured-Tubulin and Denatured Subtilisin-Treated Tubulin.

Example time series of severing assays with GFP-Hu-p60 +/- free tubulin, denatured tubulin, or denatured subtilisin-treated tubulin (denatured s-tubulin). The severing assays were 10 minutes with a frame taken every 5 seconds. (i) Time series of the Dylight649-MTs for each of the conditions. The time series are frames every 20 seconds or 50 seconds as stated in figure A. The scale bars are 5 μm. (ii) Time series of GFP-Hu-p60 for each of the conditions. The time series are frames every 20 seconds or 50 seconds as stated. The scale bars are 5 μm.

For experiments with denatured tubulin, we quantified the fraction of microtubules remaining over time and fit each data set to the exponential decays (Fig. 3.10, 3.11A,B, fit parameters in Appendix A.7). Microtubules in the presence of either the free tubulin or denatured tubulin lose very little polymer (Fig. 3.10, 3.11A,B). Interestingly, when subtilisin-treated denatured free tubulin is present the severing activity is almost completely recovered to the same level as the control assays without free tubulin present implying that the CTTs are needed for inhibition. We can fit the data to exponential decays or linear approximations to exponential decays to find decay rates for each data set. The decay time is initially fast for severing in the absence of free tubulin τ_1 = 28.189 ± 0.7861 s followed by a slow phase with a long decay time τ_2 = 735.61 ± 167.36 s, as before, but is significantly slower when folded free tubulin τ_1 = 51.127 ± 2.2252 s, or denatured free tubulin is added τ_1 = 2855.4 ± 75.727 s. When the tubulin is subtilisin-treated before denaturing, the rate of severing is again fast τ_1 = 32.705 ± 1.0343 s followed by a slow phase with a long decay time τ_2 = 482.33 ± 36.938 s (Fig. 3.11B).

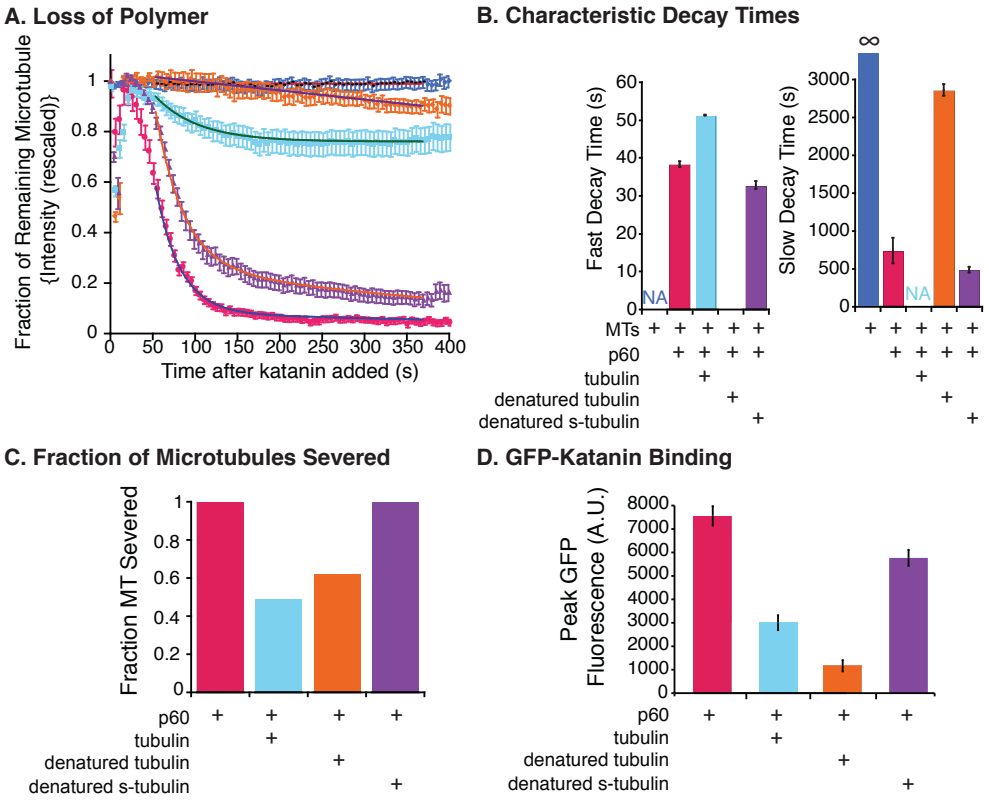

Figure 3.11 Katanin is Effectively Inhibited by Denatured Tubulin But Not Subtilisin-Treated Denatured Tubulin.

(**A**) Quantification of the fraction of the microtubule remaining over time for each of the following conditions: Dylight649-MTs + GFP-Hu-p60, Dylight649-MTs + GFP-Hu-p60 + 50 nM tubulin, Dylight649-MTs + GFP-Hu-p60 + 50 nM denatured free tubulin, Dylight649-MTs + GFP-Hu-p60 + 50 nM denatured subtilisin-treated free tubulin. This plot shows that the denatured free tubulin and free tubulin are the best inhibitors, while the subtilisin-treated free tubulin only slightly reduced the severing activity. Each data set is fit to a line, single exponential decay, or double exponential decay. Parameters for the fits are in Appendix A.7. The error bars on the data set represent the standard error of the mean. (**B**) Each data set from (A) was fit with an exponential decay curve. The two plots are of the characteristic decay times both fast (left) and slow (right) for each data set. Error bars represent the error associated with the decay time. (**C**) For each data set we counted the total number of microtubules severed at least once during the severing assays. We plotted the fraction of the total number of microtubules that were severed at least once. This corresponds with the data from A-B, suggesting that the denatured tubulin was the best inhibitor of severing activity. (**D**) Plot of the peak GFP fluorescence for each condition. The highest GFP fluorescence peak was severing assays with Hu-60 with no tubulin or CTTs present in the assay. The lowest peak fluorescence was when denatured tubulin was in the severing assay, suggesting that it prevents katanin from binding to the microtubules. This corresponds with the data in A-C suggesting that the denatured tubulin is the most effective inhibitor of severing activity. The N values for

each condition are as follows: GFP-Hu-p60 (N=50), GFP-Hu-p60 + 50 nM free tubulin (N=57), GFP-Hu-p60 + 50 nM denatured tubulin (N=42), GFP-Hu-p60 + 50 nM denatured subtilisin-treated tubulin (N=46). Error bars represent the standard error of the mean.

We also quantified the total number of microtubules that displayed at least one severing event (Fig. 3.10). The denatured tubulin inhibits severing the best, whereas when subtilisin-tubulin is present, almost all the microtubules are severed (Fig. 3.11C). The time series of the GFP-katanin shows a decrease in fluorescence intensity when free tubulin, denatured free tubulin, or the subtilisin-treated denatured free tubulin are present. Quantification of the maximum GFP fluorescence demonstrates that the lack of severing activity is due to a lack of katanin binding to the microtubules (Fig. 3.11D) and is directly proportional to the overall loss of polymer (Fig. 3.11A). Combining these results, we can infer that katanin does not recognize the shape of the folded tubulin. Rather, the binding of katanin to the CTT is required for effective inhibition of binding and severing.

3.2.7 Katanin has a Higher Affinity for Beta than Alpha Tubulin CTT.

We have demonstrated that the CTT of microtubules is essential for effective inhibition of severing activity (Fig. 3.10, 3.11). Each tubulin dimer has two CTTs, one alpha and one beta. We sought to investigate which CTT tail is a better inhibitor of katanin and thus a better competitor for the katanin binding. To address these questions we created peptide sequences of the alpha and beta CTTs from human tubulin type beta-1. Using click chemistry (Kolb, Finn, and Sharpless 2001), we covalently bound the CTT constructs to BSA protein to make CTT-BSA chimeras (Rostovtseva et al. 2008). A background concentration of BSA protein already exists in our assays, so the addition of BSA is controlled.

We added the CTT-BSA chimeras to severing assays to test the effect of the alpha or beta CTTs on the binding and severing of GFP-Hu-p60. We observed distinct differences in the ability to sever depending if the CTT constructs were alpha or beta.

Specifically, very few severing events occurred when the beta tails were present (Fig. 3.12). When the alpha tails were present we saw severing events and some loss of polymer from the ends of filaments, suggesting that the alpha tails are not as effective at inhibiting the severing activity (Fig. 3.12).

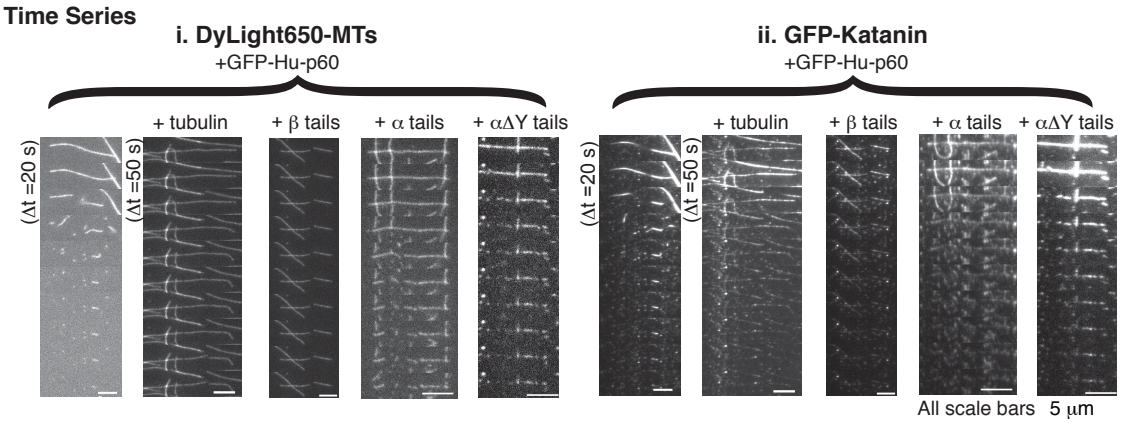

Figure 3.12 Representative Time Series of Severing Assays with Tubulin CTTs.

Example time series of severing assays with human p60 +/- free tubulin. (i) Time series of Dylight649-MTs in severing assays for Dylight649-MTs + GFP-Hu-p60, Dylight649-MTs + GFP-Hu-p60 + 50 nM tubulin, Dylight649-MTs + GFP-Hu-p60 + 50 nM beta tubulin CTT constructs, Dylight649-MTs + GFP-Hu-p60 + 50 nM alpha tubulin CTT constructs, or Dylight649-MTs + GFP-Hu-p60 + 50 nM alpha tubulin CTT constructs minus the last tyrosine. (ii) Example time series of GFP-Hu-p60 in severing assays for Dylight649-MTs + GFP-Hu-p60, Dylight649-MTs + GFP-Hu-p60 + 50 nM tubulin, Dylight649-MTs + GFP-Hu-p60 + 50 nM beta tubulin CTT constructs, Dylight649-MTs + GFP-Hu-p60 + 50 nM alpha tubulin CTT constructs, or Dylight649-MTs + GFP-Hu-p60 + 50 nM alpha tubulin CTT constructs minus the last tyrosine. The severing assays were 10 minutes with a frame taken every 5 seconds. The time series are frames every 20 seconds or 50 seconds as stated. The scale bars are 5 μm.

The quantified data indicated that beta tails were better inhibitors the severing than alpha tails (Fig. 3.13A). For severing inhibition experiments, we can also quantify the fraction of microtubules that displayed at least one severing event. The trend was identical to the total loss of polymer and confirms that the beta tubulin CTT inhibits better than alpha CTT (Fig. 3.13C).We also quantified binding of the GFP-Hu-p60 to microtubules from our images in the GFP-channel. The maximum GFP fluorescence for katanin binding follows the exact same trend as total polymer loss (Fig. 3.13D) and filaments severed (Fig. 3.13C), again demonstrating that binding is directly proportional to and required for severing (Fig. 3.13D).

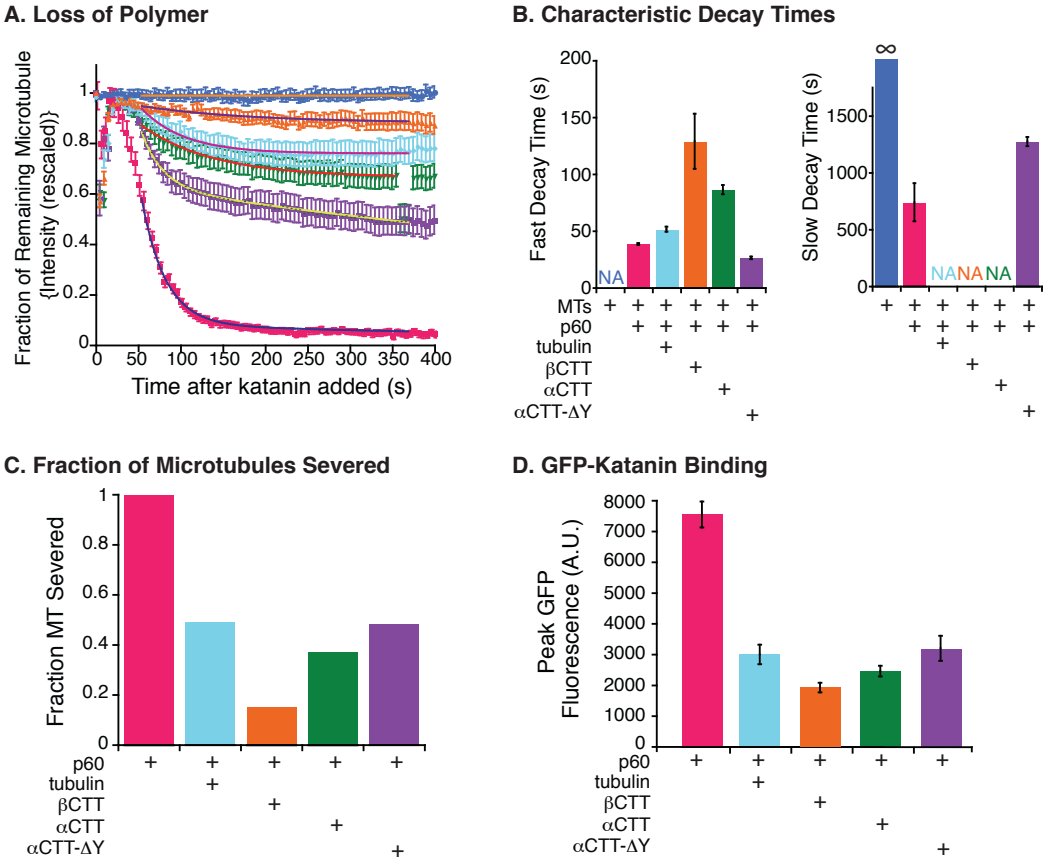

Figure 3.13: Katanin is Most Effectively Inhibited by Beta Tubulin CTTs.

(**A**) Plot of the fraction of the microtubule remaining over time for each of the following conditions: Dylight649-MTs + GFP-Hu-p60, Dylight649-MTs + GFP-Hu-p60 + 50 nM tubulin, Dylight649-MTs + GFP-Hu-p60 + 50 nM beta tubulin CTT constructs, Dylight649-MTs + GFP-Hu-p60 + 50 nM alpha tubulin CTT constructs, or Dylight649-MTs + GFP-Hu-p60 + 50 nM alpha tubulin CTT constructs minus the last tyrosine. The error bars represent the standard error of the mean. Each data set was fit with a line, single exponential decay, or double exponential decay. Parameters for the fit equations are in Appendix A.8. This plot shows that the beta tubulin CTTs are the most effective inhibitors of severing activity, followed by alpha CTTs and alpha CTTs minus the last tyrosine. (**B**) Each data set from (**A**) was fit with a line or exponential decay curve. This is a plot of the characteristic decay constants for each data set. On the left is the fast decay times, and on the right is the slow decay times. The error bars represent the error associated with the decay times. (**C**) For each data set we counted the total number of microtubules severed at least once during the severing assays. We plotted the fraction of the total number of microtubules that were severed at least once. This corresponds with the data from A-B, suggesting that beta tubulin CTTs are the best inhibitors of severing. (D) This is a plot of the peak GFP fluorescence for each condition. The highest

GFP fluorescence peak was with no tubulin or CTTs present in the assay. The lowest peak was with the beta tubulin CTTs in the severing assay, suggesting that the beta tubulin CTTs are preventing katanin from binding to the microtubules. This corresponds with the data in A-C suggesting that the beta tails are the most effective inhibitors of severing activity. The N values for each condition are as follows: GFP-Hu-p60 (N=50), GFP-Hu-p60 + 50 nM free tubulin (N=57), GFP-Hu-p60 + 50 nM beta CTT constructs (N=40), GFP-Hu-p60 + 50 nM alpha CTT constructs (N=59), GFP-Hu-p60 + 50 nM alpha CTT constructs minus the last CTTs (N=33). Error bars represent the standard error of the mean.

3.2.8 Katanin has Lower Affinity for Detyrosinated Alpha Tubulin.

Using the same CTT polypeptide to BSA chimeras, we were able to make a version of the alpha CTT with the final tyrosine missing. Such detyrosinated tubulin is typically a marker of reduced microtubule dynamics in cells (Kreis 1987). We added the detyrosinated alpha CTT-BSA chimeras to severing assays and found that the microtubules were still severed (Fig. 3.12), but the overall rate of severing and overall loss of polymer was reduced compared to controls with GFP-Hu-p60 alone (Fig. 3.13B-D). The total polymer lost, percentage of filaments severed, and amount of GFP-Hu-p60 binding were also directly proportional again showing that the inhibition of severing was again due to a reduction in katanin binding in the presence of detyrosinated alpha tubulin CTT-BSA chimeras.

3.3 Discussion

We used quantitative methods to analyze a human version of the enzymatic portion of the microtubule severing enzyme, katanin. The methods allow us to analyze both the severing activity and the binding activity individually, for the first time. We find that binding is tight and directly proportional to severing activity. Further, inhibition of severing, as we report and as has been reported previously for a similar protein, spastin, is completely due to inhibition of binding to severing enzymes to the microtubule substrate. Our analysis provides more detailed information on the activity of katanin than ever allowed before.

Our results demonstrate that katanin is effectively inhibited by free tubulin in vitro at tubulin concentrations well below the cellular concentration. The cellular concentration of tubulin has been estimated to be at approximately 2 mg/ml (18 μM) (Gerhard and Weber 1978). Even if half of the tubulin is in the form of microtubules, there is still 10 μM

of free tubulin available in cells. We observed that katanin's severing activity was inhibited even at 50 nM free tubulin (Fig. 3.5, 3.6). Our assays typically used 50 - 100 nM katanin, so the lowest concentration was effectively 1:1 tubulin to katanins. This is a much lower concentration than previously probed as the p60-p80 complex was shown to bind to microtubules over free tubulin when there was a 1:5 ratio of p60-p80 to tubulin (F. J. McNally and Vale 1993). Spastin severing was inhibited by 10-fold molar excess of tubulin tails (White et al. 2007). In addition, 0.5 mM beta tail peptide significantly inhibited spastin severing activity (Roll-Mecak and Vale 2008). Our results imply you would need at least as much katanin as free tubulin to cause any type of severing or microtubule regulation in a live cell. In our prior work, we showed that Drosophila katanin was highly enriched at the cell cortex and it acted there to keep microtubules short in S2 cells (D. Zhang et al. 2011). Thus activity of katanin in living cells will require a relatively high concentration of katanin or a relatively low concentration of free tubulin. Depending on the cell type and developmental stage, different cells could display either. For instance, the S2 cells specifically localized the katanin to the cortex to increase the local concentration (D. Zhang et al. 2011). On the other hand, the concentration of free tubulin is relatively low in locations with mostly stable microtubules, such as neuronal axons, where altering the microtubule dynamics is enough to alter the polarity of the neuron (Witte, Neukirchen, and Bradke 2008; reviewed in Conde and Cáceres 2009). Overall, our work suggests that the ratio of katanin to free tubulin is an effective means to regulate katanin's activity in cells. Since you would only want to locally destroy microtubules, localizing high concentrations of katanin about a threshold ratio of katanin to free tubulin would allow such activity.

We found that katanin has a higher affinity for free tubulin regardless of whether katanin is in solution or pre-bound to microtubules (Fig. 3.8, 3.9). This is surprising given

that severing proteins were originally discovered by adding mitotic extracts to Taxol-stabilized microtubules, which presumably have a high concentration of free tubulin. In extracts, severing was observed within minutes (Vale 1991). It was previously shown that in microtubule pelleting assays with 200 µg/ml microtubules, 200 µg/ml free tubulin and 40 µg/ml p60-p80, katanin still pelleted with the microtubule polymers and not with the soluble tubulin (F. J. McNally and Vale 1993). This suggests that in this assay katanin has a higher affinity for microtubules than free tubulin. However, there is also p80 present in these assays making it difficult to directly compare directly to our experiments.

There are several possible explanations for how katanin can continue to function in cells despite being inhibited by free tubulin. The first explanation is that p80, the regulatory subunit of katanin, is helping to target katanin to the microtubules. It has been shown that katanin is targeted to centrosomes by p80 in both sea urchin embryos (F. J. McNally et al. 1996) and in fibroblasts (Hartman et al. 1998). Additionally, p80's WD-40 repeats are sufficient to target GFP to centromeres (Hartman et al. 1998). The C-terminal domain of p80 is required for microtubule binding and interacting with p60, while the N-terminal WD-40 domains are required for correct localization of the complex and can negatively regulate severing activity (K. P. McNally, Bazirgan, and McNally 2000). It is also known that the p80 subunit enhances the affinity of p60 for microtubules in vitro as shown by microtubule pelleting assays (K. P. McNally, Bazirgan, and McNally 2000). In vivo, a fully functional set of p60 and p80 subunits are required for efficient targeting and severing activity (K. P. McNally, Bazirgan, and McNally 2000). Therefore, it is likely that katanin p60 could be targeted to microtubules in the presence of its partner protein, p80. This evidence provides one plausible explanation for how katanin can sever microtubules in vivo despite displaying a high affinity for free tubulin in vitro. Future in

vitro experiments with both p60 and p80 should be performed to determine if the katanin heterodimer can overcome the inhibition by the free tubulin heterodimer or alter/enhance localization of katanin to the microtubule lattice.

Another possible mechanism for how katanin could function in vivo is if other MAPs are bound to the free tubulin making it inaccessible to katanin. There are several examples of MAPs that bind to tubulin monomers. Many, but not all, of these MAPs are involved in stabilizing microtubules or contribute to growing microtubules by recruiting tubulin dimers to the growing end of the microtubule. Tau is known to bind to soluble tubulin dimers and binds even more tightly to tubulin when there are disease mutations in tau (Elbaum-Garfinkle et al. 2014). Stathmin, a microtubule catastrophe factor, also binds to free tubulin dimers (Belmont and Mitchison 1996) and may even sequester them (Howell et al. 1999). Stu2p, a member of the XMAP215 family, is also known to sequester free tubulin (Al-Bassam et al. 2006). E-like, a novel protein similar to the chaperone cofactor E, causes depolymerization of microtubules by sequestering and even degrading the free tubulin pool (Bartolini 2005). CLASP, another stabilizing MAP similar to XMAP215, also is able to bind free tubulin dimers directly. Further, it can bind to the microtubule polymer itself and the free tubulin at the same time to recruit tubulin to the growing ends of microtubules (Al-Bassam et al. 2010). If most of the free tubulin available in the cell is bound up and sequestered by other MAPs, it is conceivable that katanin severing activity would not be inhibited by the tubulin because the tubulin would be inaccessible.

Phosphorylation is a way that many mitotic proteins are controlled. X. *laevis* p60 has been shown to have an N-terminal phosphorylation site that can regulate severing activity (Loughlin et al. 2011; Whitehead, Heald, and Wilbur 2012). However, this site negatively regulates severing, by causing a down-regulation of severing near

kinetochores and chromatin (Loughlin et al. 2011). This site has also only been shown in the X. *laevis* p60 and does not occur in the human version of p60. There are other possible phosphorylation sites, however, no other confirmed sites in human p60 so far.

A final possible mechanism for katanin's functionality in the cells is that katanin is found mostly in areas cells where there is less free tubulin. Katanin is highly expressed in embryonic tissue, when there is high cell proliferation and axons are being formed (Yu et al. 2005). Katanin p80 and p60 are most highly expressed in the CNS, but the levels of p60 are higher than that of p80 (Yu et al. 2005). Katanin is also expressed in non-neuronal tissues at lower levels than in neuronal tissues, but the ratio of p60 to p80 is much higher (Yu et al. 2005). In cultured neuronal cells, p80 is enriched predominately in the cell body, and p60 is found at higher levels in axons (Yu et al. 2005). In cultured neurons, the early axons were not as susceptible to severing as other parts of the neuron (Yu et al. 2005). This data suggests that katanin p60's severing activity is tightly regulated in time and space and is likely regulated by other proteins, such as p80. Since p80 is not found in the exact same location as p60, it is unlikely that targeting p60 is its only role, but it also suggests that there are other factors regulating p60 so that severing in controlled. It is likely that katanin is also regulated by MAPs that bind to microtubules and protect them from severing activity (Qiang et al. 2006). Given all this information and the data we have collected, how can katanin sever microtubules? Katanin is needed for axonal outgrowth and for branching in the processes as well as to control the overall length of microtubules. Therefore, it must be regulated by some variety of factors to ensure that severing occurs only at the precise time and locations needed. In axons the microtubules tend to be more stable and less dynamic than in other cells. It is likely that since the microtubules tend to be more stable, there is also less free tubulin present in these areas. Katanin would therefore not be affected nearly as much by free tubulin and

in fact may be the source of tubulin dimers to produce the new processes.

We demonstrated that the katanin enzyme is more effectively inhibited by denatured tubulin (Fig. 3.10, 3.11). We can infer from this result that katanin is not recognizing the overall shape of tubulin, but part of the protein sequence. This inhibition is abolished when the CTTs are removed from tubulin (Fig. 3.10, 3.11). Previous work has shown that katanin and spastin are both unable to sever subtilisin-treated microtubules (F. J. McNally and Vale 1993; Eckert, Le, et al. 2012; Roll-Mecak and Vale 2005). Many AAA proteins recognize the carboxy terminus of their substrate and thread them through the central pore of the hexamer (Gottesman et al. 1998; Hoskins et al. 1998; Ishikawa et al. 2001). In the proposed model for how severing enzymes function, katanin would form a hexamer on the microtubules via the CTT of tubulin and, with the ATP as an energy source, proceed to thread the tubulin through the hexameric pore unfolding and destroying the dimer in the process (Roll-Mecak and Vale 2008). Our results imply that the inhibition and thus binding of katanin is not aided by a secondary binding site mediated through the MIT domain or other katanin structure.

Given the results we have shown that tubulin can compete with katanin prior to it binding to microtubules. We propose a model, diagrammed in figure 3.14, in which we can describe katanin inhibition as K_i. Under uninhibited conditions Hu-p60 (E) will bind to microtubules (S) to create ES and then will proceed with severing. The product (P) of this reaction is a mixture of microtubules and tubulin bound to p60. We have found that there are two separate inhibition schemes. First, katanin can be inhibited by free tubulin (I) prior to binding to microtubules. In this case the tubulin-bound katanin (EI) prior to ES formation. We have also shown that tubulin will competitively compete for binding after Hu-p60 binds to microtubules, and inhibit binding. Since the transition for ES to EI is rapid and we do not have a direct readout for ESI vs. EI, we can only report on the rate

the entire reaction takes to complete. We do not see any recovery of microtubule binding after it has bound tubulin, either so it seems to be working as an irreversible inhibitor, under the conditions in our assay.

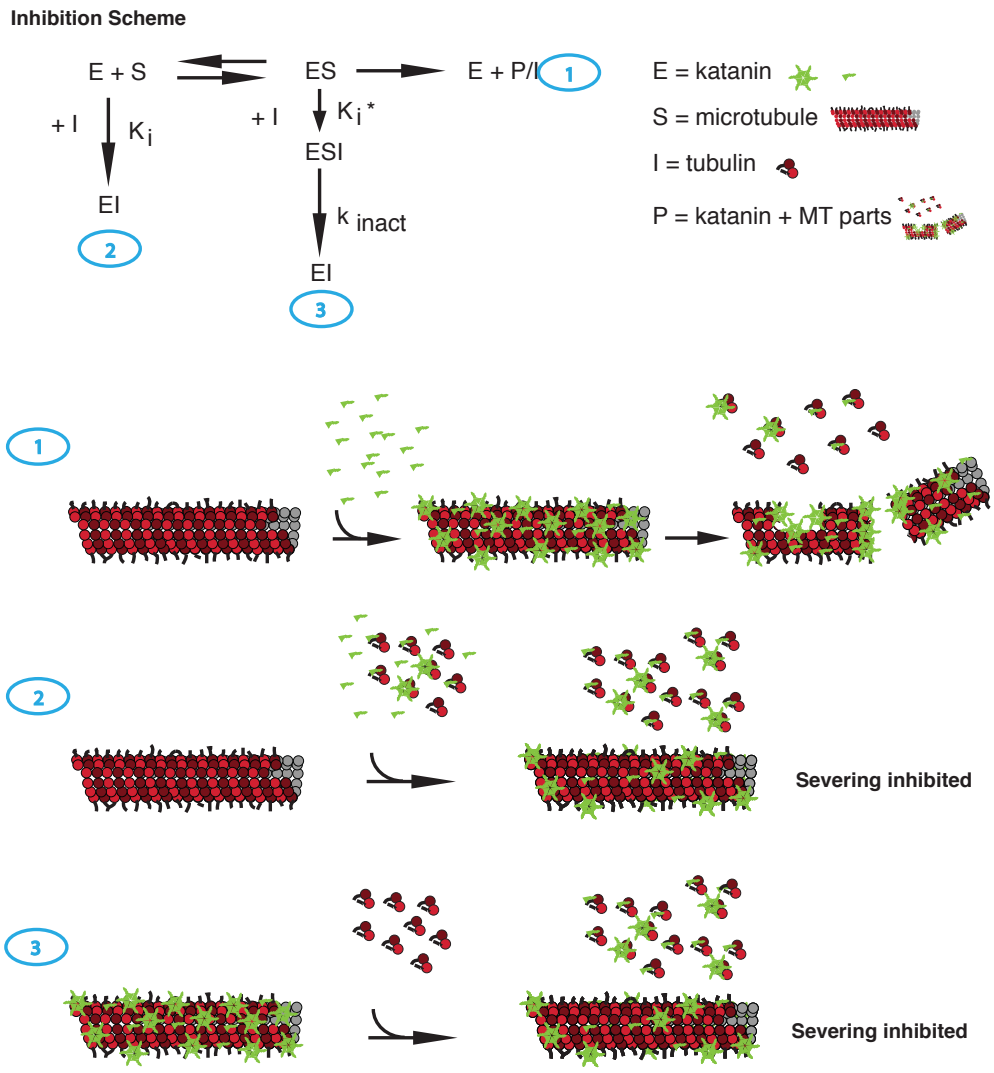

Figure 3.14 Model of Katanin's Inhibition by Free Tubulin.

We can represent to microscopy results we observe in terms of enzyme kinetics. In the uninhibited reaction, the severing enzyme (E) binds to the microtubules (S) to create (ES) and severs microtubules leaving a mixture of microtubule pieces and tubulin dimers (P). Katanin can be inhibited in two ways. If katanin interacts with the free tubulin (I) before binding to microtubules this can cause inhibition. Or if the katanin is bound to the microtubules and then free tubulin is added, this can also cause inhibition. Because the transition from ES to EI occurs rapidly and we have no direct readout for ESI vs. EI, we can only report the rate that the entire reaction takes to complete.

Katanin severing activity is inhibited by constructs containing just the CTTs of tubulin. Our results demonstrate that the sequence of the CTT alters the ability to inhibit where the beta sequence is the most inhibitory, the alpha sequence is the next best, and the detyrosinated tubulin, while still able to inhibit severing, is the least effective (Fig. 3.12, 3.13). Our results are consistent with prior results reported for spastin where CTT peptides were able to bind spastin (White et al. 2007) and CTT peptides could inhibit spastin severing (Roll-Mecak and Vale 2008). Interestingly, we find distinct differences in our results with katanin compared to prior work with spastin. First, previous studies showed that spastin did not bind to free tubulin, only tails alone or microtubules (White et al. 2007). Further, prior studies showed that only relatively high concentrations (500 μM) of beta-tubulin CTT peptide could inhibit spastin severing, but the same concentration of alpha CTTs could not (Roll-Mecak and Vale 2008). In contrast, we have clearly demonstrated that katanin can bind to free tubulin of both alpha and beta. Further, alpha and beta are both able to inhibit severing noticeably at fairly low concentrations of CTTs (50 nM). Our results imply that katanin is easier to "switch off" in the cell through a direct interaction with free tubulin than spastin. This could be because spastin is actually a membrane-associated protein, so it is sequestered on cellular membranes and likely not as capable of interacting with microtubules (White et al. 2007).

We showed that detyrosination of the alpha tubulin CTT is less inhibitory than unmodified alpha (Fig 3.12, 3.13). Our results could imply that detyrosinated tubulin is a less attractive substrate for katanin binding. Katanin is clearly distinct from spastin, which bound tyrosinated and detyrosinated tubulin CTTs equally well (White et al. 2007). Spastin, however, was not detectably inhibited by alpha-Tyr CTT constructs, but there was some inhibition with an anti-Glu antibody (Roll-Mecak and Vale 2008). Although our work does not directly test if katanin can bind to different types of tubulin, the inhibition is

mediated by a direct competition with the microtubule substrate. Our results imply that katanin binds somewhat to detyrosinated tubulin, but better to tyrosinated tubulin. If this result holds for katanin binding to tubulin in the microtubule lattice, it would imply that katanin would target tyrosinated tubulin over detyrosinated tubulin, and could be a mechanism to improve the stability of detyrosinated (Glu) microtubules. On the other hand, this mechanism would be less effective, since katanin clearly preferentially binds to beta tubulin CTTs and could target to all beta CTTs over either type of alpha CTT.

Post-translational modifications of tubulin can act as road signs for many different MAPs and can allow the microtubules to be differentially regulated based on the modification type and location. For example, detyrosinated microtubules are less dynamic and slower to incorporate new tubulin than tyrosinated microtubules (Kreis 1987). There are many MAPs that do not bind as well to tubulin in this form. In neurons, microtubules are both tyrosinated and detyrosinated. The plus end tips of growing microtubules in axons are enriched in tyrosinated tubulin, while the main body of the microtubule that remains more stable, is made up primarily of detyrosinated tubulin (Wloga and Gaertig 2010; Janke and Kneussel 2010; Hammond, Cai, and Verhey 2008; Fukushima et al. 2009). It is known that MCAK prefers to depolymerize tyrosinated tubulin, but when overexpressed will depolymerize detyrosinated tubulin (Peris et al. 2009). Other motors like KIF5 (kinesin-1) can also be regulated by tyrosination. When tubulin tyrosination is inhibited, kinesin-1 becomes distributed throughout dendrites and axons as it can no longer distinguish between dendrites and axons (Konishi and Setou 2009). Even stabilizing MAPs, such as CLIP-170, can be sensitive to tyrosination as this particular MAP will only localize at the ends of tyrosinated microtubules (Peris et al. 2006).

There are many other types of post-translational modifications of tubulin that can

regulate how MAPs bind to microtubules. Most modifications occur on the CTTs including detyrosination, poly-glutamylation and poly-glycylation. Acetylation of tubulin occurs on the lumen surface. Each type of post-translational modification has been shown to affect the activity of severing enzymes both in vivo (Sharma et al. 2007; Lacroix et al. 2010; Sudo and Baas 2010) and in vitro (F. J. McNally and Vale 1993; Roll-Mecak and Vale 2005; White et al. 2007; Eckert, Le, et al. 2012). Given this evidence, it is likely that post-translational modifications of tubulin play a role in regulation of katanin. It is still unclear whether this regulation is direct, by serving as targets for enhanced severing, or indirect by inhibition of katanin or influencing the binding of other MAPs that may inhibit or enhance katanin severing activity. Future studies using the CTT-BSA constructs with other engineered modified CTTs that mimic native post-translational modifications will begin to unravel these signals.

Conclusions

Our results conclude that katanin's severing activity is concentration dependent. It is inhibited by free tubulin and specifically and differentially by the CTTs of tubulin. Future studies need to be performed to address how katanin is regulated by p80 in vitro and whether this activity changes the severing activity and inhibition we report here. Overall, the regulation of microtubules and severing enzymes is complicated and still not well understood.

3.4 Methods

3.4.1 Protein Purification

We received the pMAL-c5x-*X.* laevis p60 from the Heald Lab, and it was purified as previously described (Loughlin 2011). We also made an optimized human p60 construct

with an, MBP-GFP-p60. An IPTG inducible expression system was used for expression and purification. The plasmid was transformed into BL21 Competent *E. coli* (New England BioLabs). An LB starter culture was grown overnight and added to a 500 mL culture the next day. This culture was grown at 37°C until it reached an OD of 0.8 and then it was induced with 1 mM IPTG. The culture was allowed to continue to grow at 16°C for 16 hours. The cells were lysed in resuspension buffer (20 mM Hepes pH 7.7, 250 mM NaCl, 0.5 mM BME, 10% glycerol, 0.25 mM ATP) via sonication. The lysate was incubated with amylose resin (New England BioLabs) for 1-2 hours. The lysate/resin mixture was added to the column and allowed to enter the column completely. Once excess lysate had passed through the column, the column was washed twice with 20 mL of resuspension buffer. The protein is eluted in elution buffer (20 mM Hepes pH 7.7, 250 mM NaCl, 0.5 mM BME, 10% glycerol, 0.25 mM ATP, 10 mM Maltose). The approximate concentration was determined by a bradford assay.

3.4.2 Taxol-stabilized Microtubule Polymerization

Taxol-stabilized microtubules were made by combining a 1:3-1:20 ratio of labeled rhodamine tubulin (Cytoskeleton) or homemade Dylight 649 (Thermo Scientific) tubulin with home purified unlabeled tubulin. The unlabeled tubulin was purified from Porcine brains using a previously described method (Peloquin et al., 2005). Both the unlabeled and labeled tubulin were resuspended in PEM-100 (100 mM K-Pipes, pH 6.8, 2 mM $MgSO_4$, 2 mM EGTA) to a concentration of 5 mg/mL. Both were incubated on ice for 10 minutes. Then the labeled and unlabeled tubulin were combined and spun at 366,000 xg, 4°C for 10 minutes. To polymerize the microtubules 1 mM GTP was added to the tubulin and it was incubated at 37°C for 20 minutes. To further stabilize the microtubules, 50 μM Taxol was added and they were incubated for 20 minutes at 37°C. The

microtubules were centrifuged at 16,200 xg, 27°C for 10 minutes. The pellet was resuspended in PEM-100 and 50 μM Taxol.

3.4.3 Denatured Tubulin

The denatured tubulin was made by adding 1M HCl to the tubulin. Then the tubulin was brought back up to pH 6.8 using KOH.

3.4.4 Subtilisin-treated Denatured Tubulin

Subtilisin-treated Taxol-stabilized microtubules were polymerized by the same procedure as Taxol-stabilized Microtubules, with several additional steps. Once the microtubules are polymerized, they are incubated with 100 μg/mL subtilisin for 45 minutes. The reaction is stopped with 2 mM PMSF. The microtubules are centrifuged for 30 minutes at 16,200 xg 27°C for 30 minutes and the pellet is resuspended in PEM-100 and 1 mM GTP. The subtilisin-treated denatured tubulin was made by adding 1 M HCl to the subtilisin-treated microtubules. Then the tubulin was brought back up to pH 6.8 using KOH.

3.4.5 In vitro assays

We made a 10 μL flow chamber with double stick tape (3M), a coverglass (fisherbrand) and a silanized coverslip (fisherbrand). The coverslips were biologically cleaned (Dixit and Ross 2010) and coated with 2% dimethyldichlorosilane (GE Healthcare) to block the surface and prevent proteins from sticking to the surface of the coverslips. We first incubated 2% (w/v) MAB1864 tubulin antibody in Katanin Activity Buffer (20 mM Hepes pH 7.7, 10% glycerol, 2 mM $MgCl_2$) for 5 minutes. Next we added 5% (w/v) Pluronic F-127 in Katanin Activity Buffer to additionally block the surface. Then rhodamine or dylight 649 microtubules were incubated in the chamber for 5 minutes. To remove excess

microtubules, motility mix (20 mM Hepes pH 7.7, 10% glycerol, 2 mM $MgCl_2$, 2 mM ATP, 0.025 mg/mL BSA, 0.05% F-127, 10 mM DTT, 15 mg/mL glucose, 0.15 mg/mL catalase, 0.05 mg/mL glucose oxidase) was washed through the chamber. After 3 minutes of imaging, motility mix with p60 was flowed into the chamber (20 mM Hepes pH 7.7, 10% glycerol, 2 mM $MgCl_2$, 2 mM ATP, 0.025 mg/mL BSA, 0.05% F-127, 10 mM DTT, 15 mg/mL glucose, 0.15 mg/mL catalase, 0.05 mg/mL glucose oxidase, 100 nM GFP-p60).

3.4.6 Loss of Polymer Data Analysis

Loss of polymer analysis was performed in ImageJ. First, we used the line tool to draw a segmented line, 3 pixels wide, over the length of the microtubule. We used the macro "measure stacks" to measure the mean intensity of the line for each frame of the movie. The line was moved to a piece of background near the microtubules to measure the mean intensity of the background. To find the amount of microtubule remaining at each frame, the background intensity was subtracted from the mean microtubule intensity. Then the intensity was normalized to the first frame in focus after p60 was added to the chamber.

3.4.7 Percentage of Microtubules Severed Analysis

The percentage of microtubules severed analysis was performed by counting the total number of microtubules in the movie and the number of microtubules that were severed at least once during the course of the movie.

3.4.8 Maximum GFP Fluorescence

The maximum GFP fluorescence was performed in ImageJ. We used the line tool to draw a segmented line, 3 pixels wide, over the length of the microtubule in the GFP channel. I used the macro "measure stacks" to measure the mean intensity of the line for

each frame of the movie. The line was moved to a piece of background near the microtubules to measure the mean intensity of the background. To find fluorescence intensity of katanin on the microtubules, the background intensity was subtracted from the mean GFP fluorescence intensity. The maximum GFP fluorescence was found from the maximum point on this plot.

CHAPTER 4

KATANIN'S REGULATION OF DYNAMIC MICROTUBULES

4.1 Introduction

Microtubule length control is crucial in cells because of their involvement in many essential processes. Microtubule length is regulated by microtubule-associated proteins (MAPs) that can both stabilize and destabilize filaments. While there have been several studies on the affects of stabilizers on dynamic microtubules in vitro (selected publications: Levy et al. 2005; Vitre et al. 2008; Lopus et al. 2012; Manna et al. 2008; Zanic et al. 2013), there are only a few on how destabilizing MAPs interact with dynamic microtubules (Gardner et al. 2011; Montenegro Gouveia et al. 2010).

Microtubule severing enzymes are a class of enzymes that are known to disassemble microtubules by severing and depolymerization in vitro (Vale 1991; F. J. McNally and Vale 1993; Díaz-Valencia et al. 2011; D. Zhang et al. 2011). Katanin is known to have two subunits, p60, the catalytic subunit and p80, the regulatory subunit (F. J. McNally and Vale 1993; Hartman et al. 1998). Katanin is important for regulation of spindle length (Loughlin et al. 2011), microtubules at the cortex during interphase (D. Zhang et al. 2011), and neuronal outgrowth (Ahmad et al. 1999; Karabay et al. 2004). Yet, how katanin regulates dynamic microtubules in vitro has not been studied. In vivo, it is likely that katanin coordinates with stabilizing MAPs to regulate microtubules.

To understand how katanin may regulate dynamic microtubules we performed two sets of experiments on dynamic microtubules. First, we performed experiments with 7 μM, 10 μM, 20 μM tubulin to test how katanin (p60), regulates microtubules by itself. Second, we performed dynamic instability experiments with 7 μM tubulin and both katanin and tau, a known microtubule stabilizer, to test how they may work together to

regulate microtubule dynamics.

4.2 Results

4.2.1 Dynamic Instability of Microtubules in vitro

In order to explore how katanin regulates dynamic microtubules in conjunction with stabilizing MAPs, we used vitro dynamic instability assays imaged directly using total internal reflection fluorescence (TIRF) microscopy (Fig. 4.1). We used a similar experimental procedure as described in previous chapters, except, we coated the slides with PLL-PEG-Biotin (Fig. 4.1A-C). This layer of polymers coated the slide, to help eliminate non-specific interactions with the glass slides, and allowed for biotin labeled microtubule seeds to be immobilized on the surface with a streptavidin (Fig. 4.1B). After the microtubules seeds were immobilized to the surface, we added tubulin dimers and GTP to promote microtubule growth and dynamics. Additional MAPs, such as the katanin or tau can be added in addition to dimers. We purified WT-MBP-katanin (p60) and tau 4RL from bacteria to perform in vitro assays (see Materials and Methods section 4.4). This set up allowed us to evaluate specific controllable conditions, such as different tubulin concentrations or enzyme concentrations. It also provides us with a system to monitor the changes of individual microtubules over time.

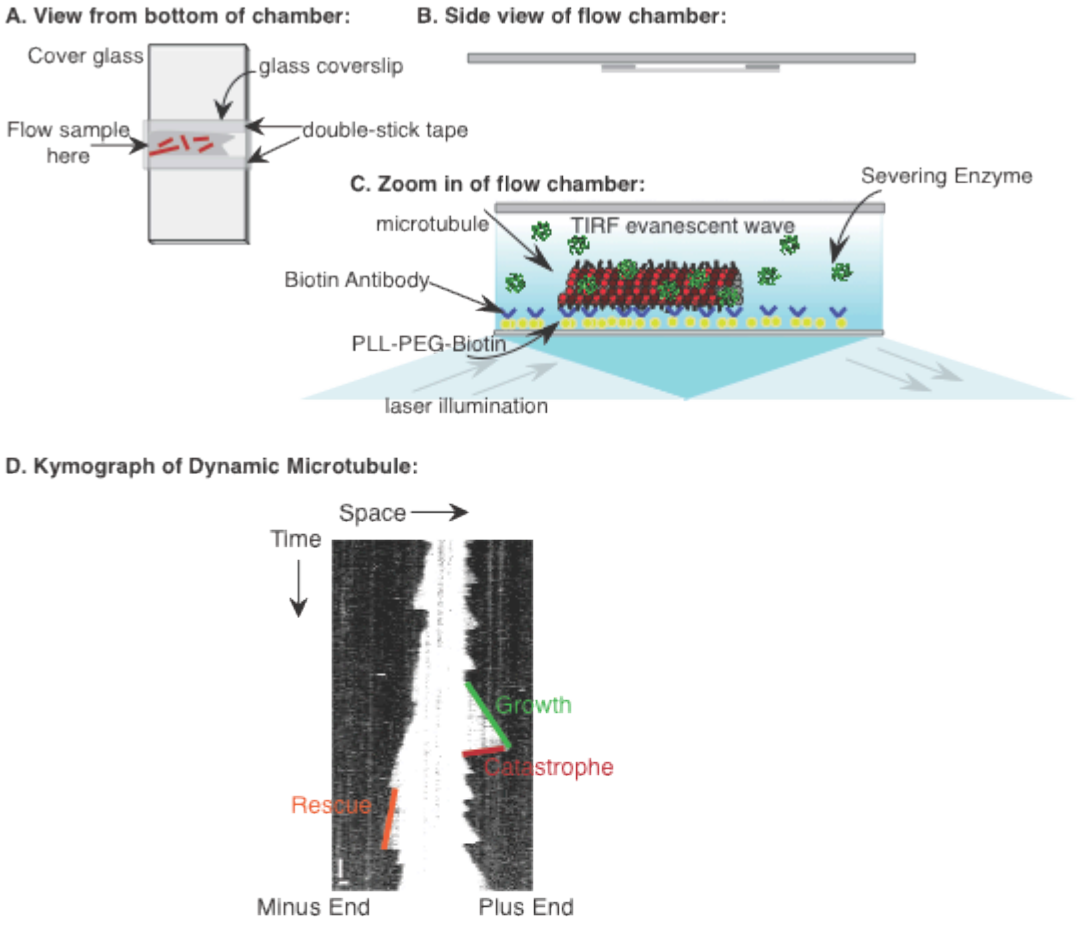

Figure 4.1 Chamber Diagram and Kymograph Analysis.

A) Diagram of flow chamber created with double-stick tape, coverslip, and glass slide. We flowed the sample in one side of the chamber and wicked the excess liquid from the other end to draw the sample through. (**B**) Side view of the chamber. (**C**) Zoom in of the side of the flow chamber. We adhered the microtubules to the surface of the chamber using an antibody to biotin. Once the severing enzyme is added to the chamber, we can image using epifluorescence, or Total Internal Reflection Fluorescence (TIRF) microscopy as depicted. In TIRF microscopy, the laser is directed in and reflected out of the chamber at the same angle allowing for less background fluorescence and better resolution of single molecules. (**D**) Example kymograph of a dynamic microtubule. The kymograph is a space-time plot with distance in the x direction and time in the y direction. The origin is at the top, left corner. Examples of growth, catastrophe and rescue events are depicted on the kymograph. The scale bars are 60 seconds in the y direction and 1 μm in the x direction.

4.2.2 Dynamic instability with destabilizing MAPs

In previous chapters we explored katanin's regulation of stabilized microtubules. However, many microtubule in vivo are required to be dynamic in order to perform necessary functions. To investigate how katanin regulates dynamic microtubules, we performed microtubule dynamic instability assays with 7 μM, 10 μM, 20 μM free tubulin and 0 nM - 1 μM katanin (p60). These assays provide information about how katanin and tubulin concentration change microtubule dynamics by measuring specific parameters (Fig. 4.1C). The measurements are made from kymographs, which are space-time plots. The x direction portrays the distance parallel to the dynamic filament, and the y direction is the time axis (Fig. 4.1C). Layering successive images of the filament next to each other over time reveals when the microtubule polymerized and depolymerized. The origin of the kymograph is located at the top, left corner.

From the kymographs, it is simple to directly measure the growth rates, time spent growing, shrinking, paused, and the amount of polymer added during growth or lost during shrinkage (Fig. 4.1D). We can also quantify the number of catastrophes and rescues per second to get a "catastrophe frequency" or a "rescue frequency" (Fig. 4.1D). Rescues are only defined as when a shrinking microtubule begins to grow again before shrinking all the way back to the seed (Fig. 4.1D). All this information together can yield answers about how dynamic the microtubules are under different conditions. Even prior to making measurements, qualitatively, we can see differences between kymographs in conditions with different amounts of tubulin and katanin (Fig. 4.2). It is clear from the kymographs that when there is more tubulin present in the dynamic instability assay there are more growth and catastrophe events and the microtubules tend to be more dynamic overall. However, it is less clear, quantitatively, how katanin affects changes in dynamics in this assay.

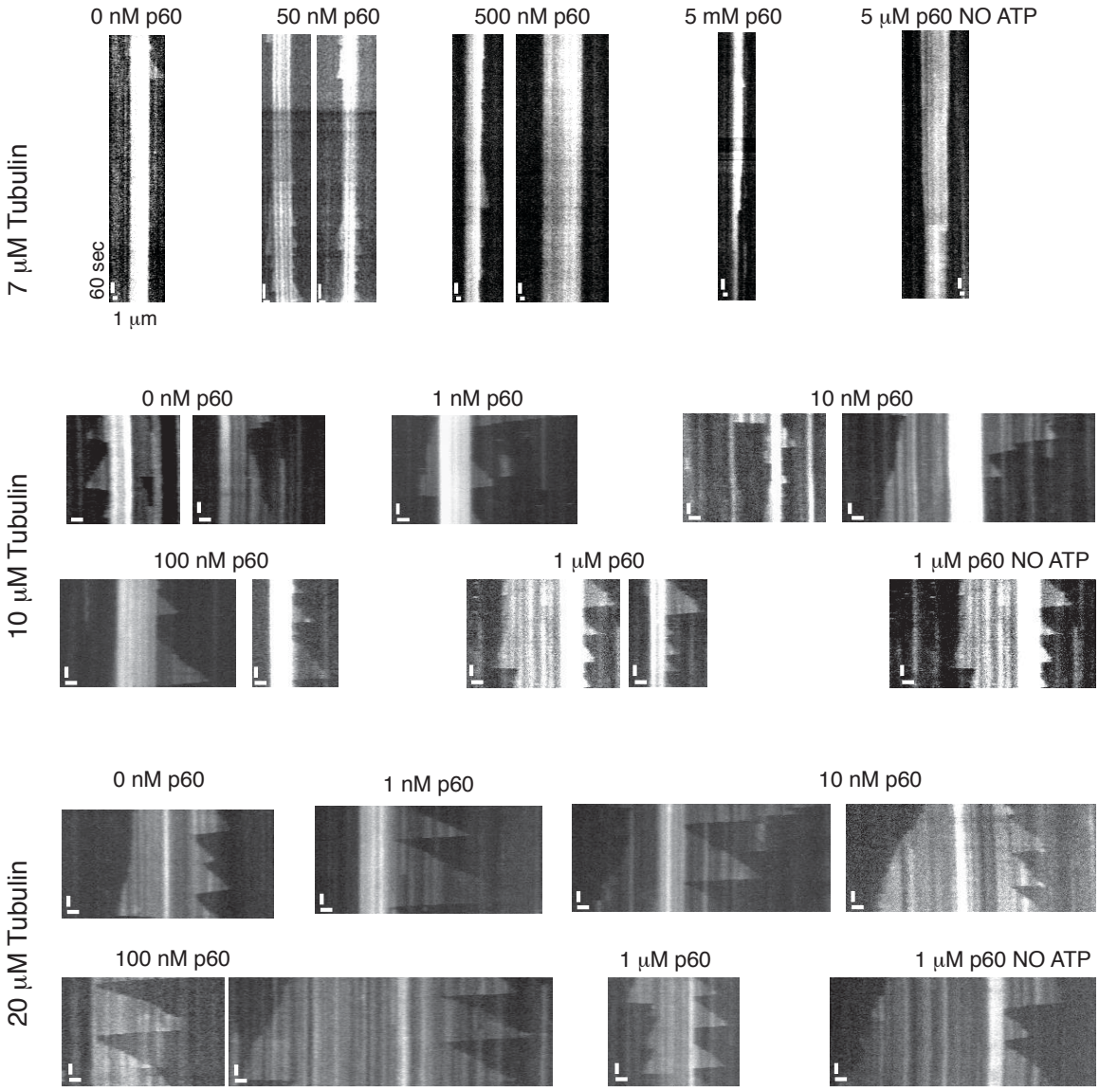

Figure 4.2 Representative Time Series of Dynamic Microtubules with Katanin.

Time series of representative dynamic microtubules at tubulin concentration of 7 μM, 10 μM, 20 μM with increasing concentrations of katanin. The kymograph is a space time plot with space in the x direction and time in the y direction. The scale bars are 60 seconds in the y direction and 1 μm in the x direction.

The first parameter we measured was the overall growth rate of each of the microtubule ends. We find that microtubules are dynamic at both ends and can display different behavior on each end. The difference between the plus-end and the minus-end is the plus end has faster growth rates, than the minus end over all tubulin concentrations (Fig. 4.3). However, since it can be difficult to distinguish which end is the plus end under some conditions, we plotted the average of all microtubule ends, as well as the average of all minus ends and all plus ends separately. Initially, for the average growth rates, 7 μM tubulin has a slightly higher growth rate than higher concentrations of tubulin (Fig. 4.3A). This is true for the "plus end" (Fig. 4.3B), the more dynamic end, and the "minus end" (Fig. 4.3C). However, in assays with p60, the 7 μM tubulin growth rate decreases both overall and at each of the respective ends. The qualitative evidence from the kymographs (Fig. 4.2) agree with this measurement. In fact, there are fewer growth events overall when more p60 is added to 7 μM tubulin dynamic assays. However, in assays with 10 μM or 20 μM tubulin the growth rate actually increases when increasing concentrations of p60 are added to the assays. This effect is most prominent on the plus ends of the microtubules, however, there is still an increase in the growth rate on the minus ends as well. Interestingly, there is only a slight increase in 10 μM assays, while the rate is increased to a greater extent in assays with 20 μM tubulin. In conditions with high concentrations of p60, but no ATP, there is still an increase in growth rate at 20 μM tubulin, however, at lower tubulin concentrations of 10 μM or 7 μM, the growth rates are the same or decreased. These results suggest that both p60 and tubulin concentration can alter the growth rate of dynamic microtubules. Under the minimal polymerization conditions, where microtubules are less dynamic, p60 causes a decrease in growth rate. As the tubulin concentration is increased, p60 causes an increase in the overall growth rates.

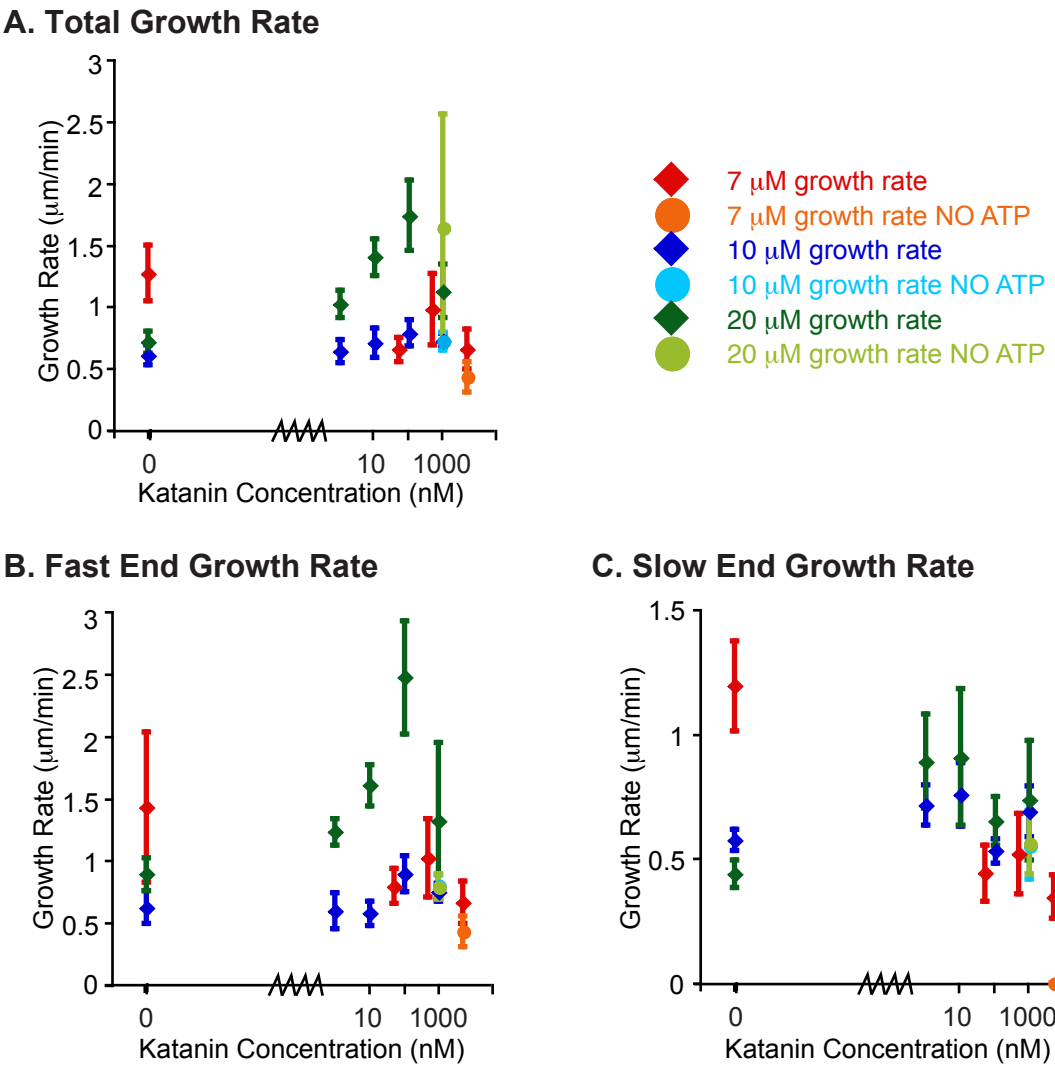

Figure 4.3 Growth Rates of Dynamic Microtubules with Katanin.

(**A**) Plot of total growth rates of both ends of the microtubules combined for each tubulin and katanin concentration. The growth rate is represented as µm/min. Red diamonds are 7 µM tubulin growth rates +/- katanin. N values are as follows: 7 µM tubulin (N=67), + 50 nM p60 (N=40), + 500 nM p60 (N=41), + 5 µM p60 (N=72). Orange circle is 7 µM + 5 µM p60 with no ATP (N=16). Dark blue diamonds are 10 µM tubulin growth rates +/- katanin. N values are as follows: 10 µM tubulin (N=72), + 1 nM p60 (N=76), + 10 nM p60 (N=76), + 100 nM p60 (N=147), + 1 µM katanin (N=55). Blue circles is 10 µM + 5 µM p60 with no ATP (N=172). Dark green diamonds are 20 µM growth rates +/- katanin. N values are as follows: 20 µM tubulin (N=144), + 1 nM p60 (N=39), + 10 nM p60 (N=39), + 100 nM p60 (N=83), + 1 µM p60 (N=206). Light green is 20 µM tubulin + 1 µM p60 with no ATP (N=39). (**B**) Quantification of the growth rates at the plus end/faster growing end of the microtubule. N values are as follows: 7 µM tubulin (N=21), + 50 nM p60 (N=24), + 500 nM p60 (N=38), + 5 µM p60 (N=70), 7 µM + 5 µM p60 with no ATP (N=16), 10 µM tubulin (N=67), + 1 nM p60 (N=60), + 10 nM p60 (N=70), + 100 nM p60 (N=134), + 1

μM katanin (N=49), 10 μM + 5 μM p60 with no ATP (N=116), 20 μM tubulin (N=96), + 1 nM p60 (N=17), + 10 nM p60 (N=27), + 100 nM p60 (N=49), + 1 μM p60 (N=136), 20 μM tubulin + 1 μM p60 with no ATP (N=23). (**C**) Quantification of the growth rates at the minus end of the microtubule. N values are as follows: 7 μM tubulin (N=46), + 50 nM p60 (N=16), + 500 nM p60 (N=3), + 5 μM p60 (N=2), 7 μM + 5 μM p60 with no ATP (N=10), 10 μM tubulin (N=40), + 1 nM p60 (N=36), + 10 nM p60 (N=31), + 100 nM p60 (N=56), + 1 μM katanin (N=25), 10 μM + 5 μM p60 with no ATP (N=56), 20 μM tubulin (N=47), + 1 nM p60 (N=21), + 10 nM p60 (N=12), + 100 nM p60 (N=33), + 1 μM p60 (N=66), 20 μM tubulin + 1 μM p60 with no ATP (N=15). The error bars represent the standard error of the mean.

We can also measure the length in μm of each growth event. This would provide information about whether the microtubules were growing fast for short amounts of time, or even possibly if there was a constraint on the overall growth lengths. The growth lengths of microtubules without p60 are similar across all three tubulin concentration of 7 μM, 10 μM, and 20 μM (Fig. 4.4A). Similar to the growth rate data, we find that there is a decrease in the growth length on both ends of the microtubule at low tubulin concentrations (Fig. 4.4B-C). Dynamic instability with 10 μM tubulin only resulted in a slight increase in growth length at high levels of p60. However, like the growth rates, dynamic instability with 20 μM tubulin had an increase in the growth lengths with increasing p60 on both ends of the microtubule. This evidence shows that microtubules have similar growth lengths overall all tubulin concentrations without any p60. When p60 is added to the assays, it causes a decrease in growth length at low tubulin concentrations and a slight increase in growth length at 10 μM tubulin and a significant length increase at 20 μM tubulin.

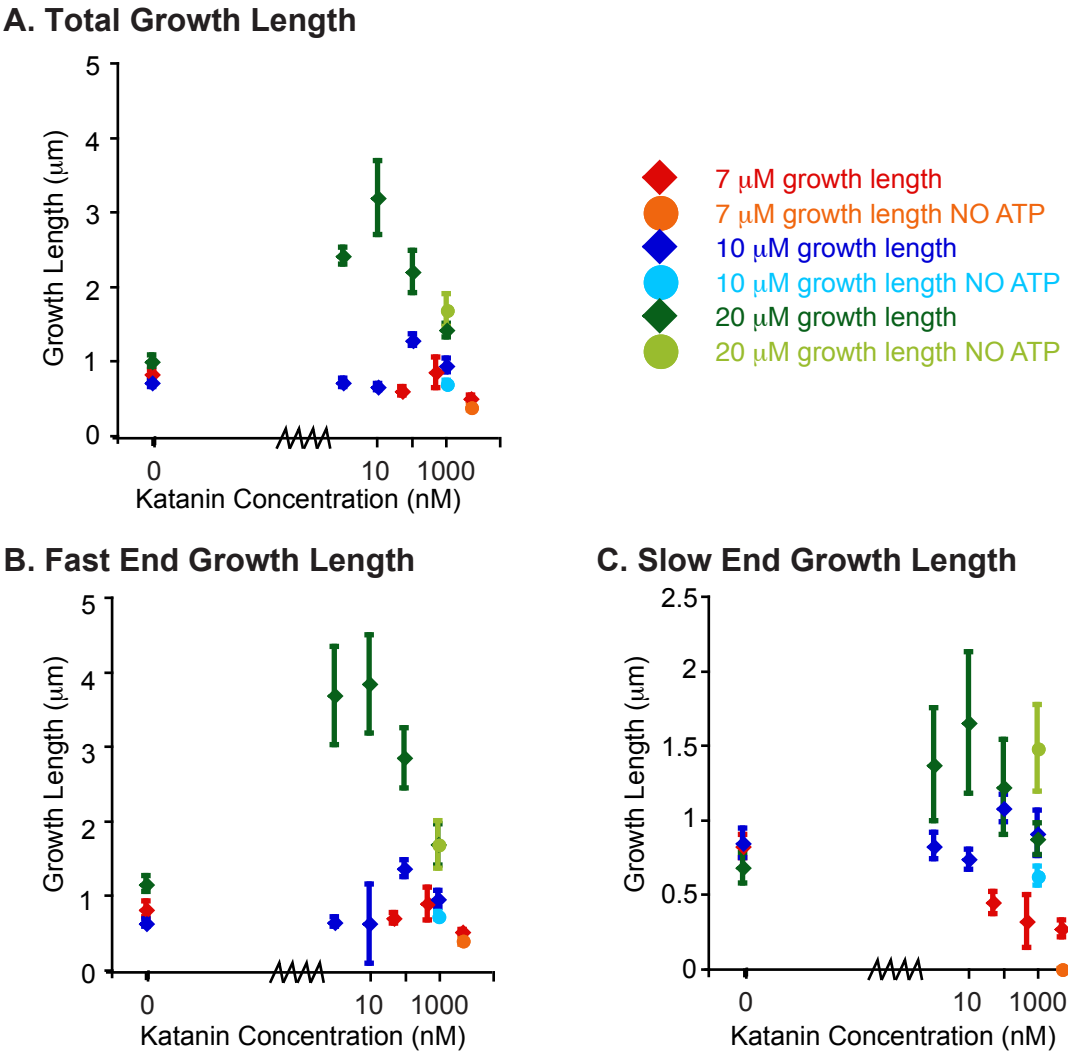

Figure 4.4 Growth Length of Dynamic Microtubules with Katanin.

(**A**) Plot of total growth length of both ends of the microtubules combined for each tubulin and katanin concentration. The growth length data is represented as μm. Red diamonds are 7 μM tubulin growth rates +/- katanin. N values are as follows: 7 μM tubulin (N=67), + 50 nM p60 (N=40), + 500 nM p60 (N=41), + 5 μM p60 (N=72). Orange circle is 7 μM + 5 μM p60 with no ATP (N=16). Dark blue diamonds are 10 μM tubulin growth lengths +/- katanin. N values are as follows: 10 μM tubulin (N=72), + 1 nM p60 (N=76), + 10 nM p60 (N=76), + 100 nM p60 (N=147), + 1 μM katanin (N=55). Blue circles is 10 μM + 5 μM p60 with no ATP (N=172). Dark green diamonds are 20 μM growth rates +/- katanin. N values are as follows: 20 μM tubulin (N=144), + 1 nM p60 (N=39), + 10 nM p60 (N=39), + 100 nM p60 (N=83), + 1 μM p60 (N=206). Light green is 20 μM tubulin + 1 μM p60 with no ATP (N=39). (**B**) Quantification of the growth lengths at the plus end/faster growing end of the microtubule. N values are as follows: 7 μM tubulin (N=21), + 50 nM p60 (N=24), + 500 nM p60 (N=38), + 5 μM p60 (N=70), + 5 μM p60 with no ATP (N=16),10 μM tubulin (N=67), + 1 nM p60 (N=60), + 10 nM p60 (N=70), + 100 nM p60 (N=134), + 1 μM katanin (N=49), + 5 μM p60 with no ATP (N=116), 20 μM tubulin

(N=96), + 1 nM p60 (N=17), + 10 nM p60 (N=27), + 100 nM p60 (N=49), + 1 μM p60 (N=136), + 1 μM p60 with no ATP (N=23). (**C**) Quantification of the growth lengths at the minus end of the microtubule. N values are as follows: 7 μM tubulin (N=46), + 50 nM p60 (N=16), + 500 nM p60 (N=3), + 5 μM p60 (N=2), + 5 μM p60 with no ATP (N=10), 10 μM tubulin (N=40), + 1 nM p60 (N=36), + 10 nM p60 (N=31), + 100 nM p60 (N=56), + 1 μM katanin (N=25), + 5 μM p60 with no ATP (N=56), 20 μM tubulin (N=47), + 1 nM p60 (N=21), + 10 nM p60 (N=12), + 100 nM p60 (N=33), + 1 μM p60 (N=66), + 1 μM p60 with no ATP (N=15). The error bars represent the standard error of the mean.

The shrinkage rate is often too fast to measure, so we cannot accurately quantify this rate. However, a related parameter is the shrinkage length. This provides us information about the average distance a microtubule shrinks back. Initially, the shrinkage distance is longest under 20 μM tubulin conditions without any katanin, both on average and for both individual ends of the microtubules (Fig. 4.5A). 7 μM and 10 μM tubulin have similar shrinkage lengths. When 1 nM to 1 μM p60 is added to the dynamic instability assays with 20 μM tubulin, the shrinkage length doubles (Fig. 4.5A). This is true for each individual end of the microtubule as well (Fig. 4.5B-C). Interestingly, this rate is even longer than the growth lengths. This would suggest that perhaps there are multiple growth events before the microtubule begins to shrink back. In dynamic assays with 10 μM tubulin, the average shrinkage length increases slightly. The shrinkage length on the plus ends of the microtubule remain similar across all p60 concentrations, however, the minus end displays an increase in shrinkage length with increasing enzyme concentrations. 7 μM tubulin dynamic assays on average and on both ends displayed a decrease in shrinkage length, although decrease was more prominent at the minus ends of the microtubules. Under all tubulin conditions, the shrinkage lengths were shorter without any ATP.

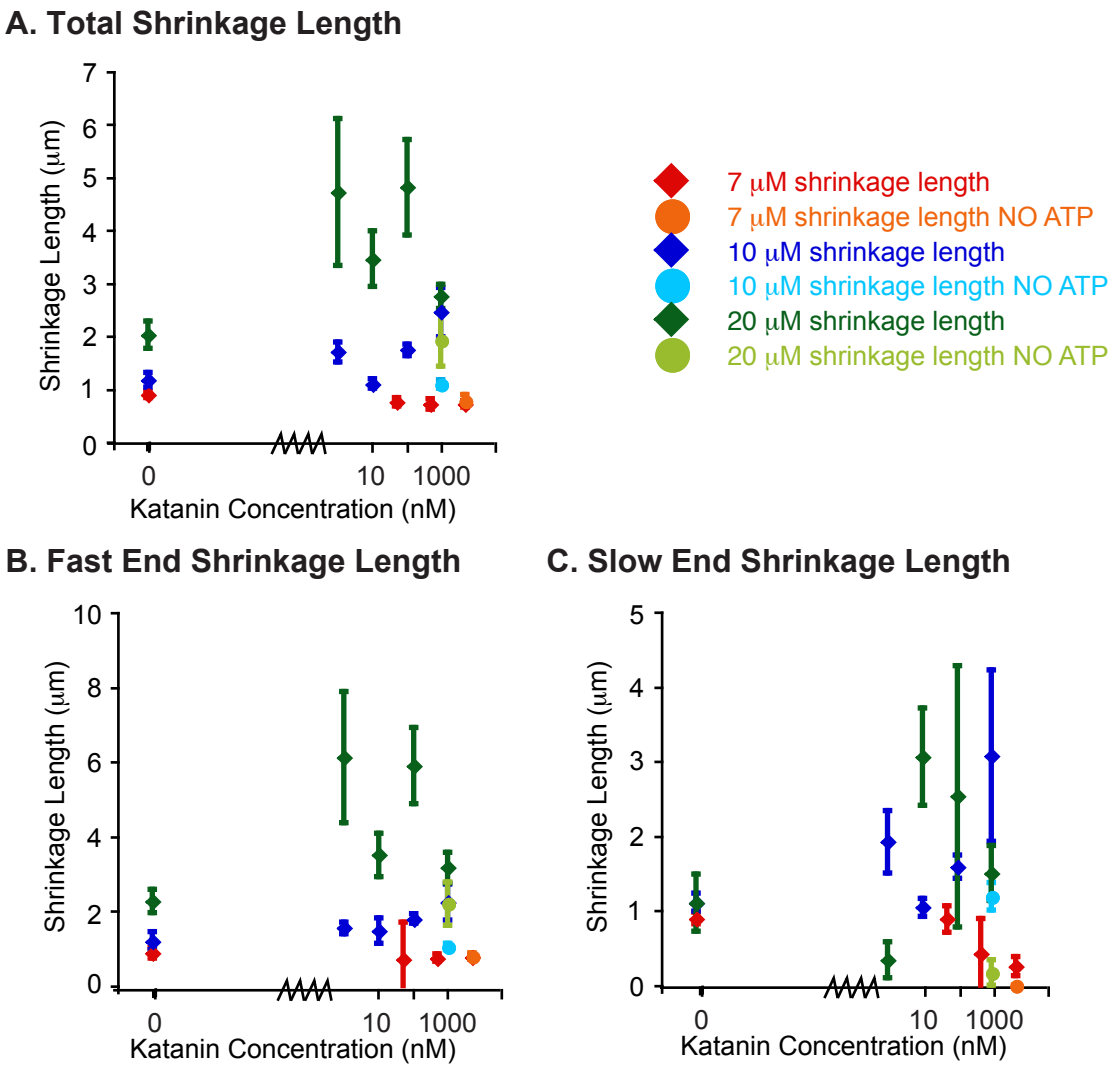

Figure 4.5 Shrinkage Length of Dynamic Microtubules with Katanin.

(**A**) Plot of total shrinkage length of both ends of the microtubules combined for each tubulin and katanin concentration. The shrinkage length data is represented as μm. Red diamonds are 7 μM tubulin shrinkage lengths +/- katanin. N values are as follows: 7 μM tubulin (N=43), + 50 nM p60 (N=20), + 500 nM p60 (N=29), + 5 μM p60 (N=35). Orange circle is 7 μM + 5 μM p60 with no ATP (N=7). Dark blue diamonds are 10 μM tubulin shrinkage lengths +/- katanin. N values are as follows: 10 μM tubulin (N=72), + 1 nM p60 (N=76), + 10 nM p60 (N=76), + 100 nM p60 (N=147), + 1 μM katanin (N=55). Blue circles is 10 μM + 5 μM p60 with no ATP (N=96). Dark green diamonds are 20 μM shrinkage lengths +/- katanin. N values are as follows: 20 μM tubulin (N=72), + 1 nM p60 (N=13), + 10 nM p60 (N=24), + 100 nM p60 (N=29), + 1 μM p60 (N=102). Light green is 20 μM tubulin + 1 μM p60 with no ATP (N=16). The error bars represent the standard error of the mean. (**B**) Quantification of the shrinkage lengths at the plus end/faster growing end of the microtubule. N values are as follows: 7 μM tubulin (N=11), + 50 nM p60 (N=15), + 500 nM p60 (N=26), + 5 μM p60 (N=32), + 5 μM p60 with no ATP (N=7), 10 μM tubulin (N=37), + 1 nM p60 (N=46), + 10 nM p60 (N=21), + 100 nM p60 (N=103), + 1 μM katanin (N=40), 10 μM + 5 μM p60 with no ATP (N=75), 20 μM tubulin (N=57), +

1 nM p60 (N=9), + 10 nM p60 (N=21), + 100 nM p60 (N=19), + 1 μM p60 (N=76), + 1 μM p60 with no ATP (N=13). The error bars represent the standard error of the mean. (**C**) Quantification of the shrinkage lengths at the minus end of the microtubule. N values are as follows: 7 μM tubulin (N=32), + 50 nM p60 (N=5), + 500 nM p60 (N=3), + 5 μM p60 (N=3), 7 μM + 5 μM p60 with no ATP (N=0), 10 μM tubulin (N=35), + 1 nM p60 (N=30), + 10 nM p60 (N=24), + 100 nM p60 (N=44), + 1 μM katanin (N=15), + 5 μM p60 with no ATP (N=21), 20 μM tubulin (N=14), + 1 nM p60 (N=3), + 10 nM p60 (N=3), + 100 nM p60 (N=9), + 1 μM p60 (N=25), + 1 μM p60 with no ATP (N=3). The error bars represent the standard error of the mean.

Catastrophe frequency is a measure of the number of times the microtubule shrinks all the way back to the seed. Often times, destabilizers will cause microtubules to catastrophe more frequently (Vaart, Akhmanova, and Straube 2009). The overall number of catastrophes at 20 μM tubulin is higher initially than 7 μM or 10 μM tubulin (Fig. 4.6A). The number of catastrophes decreases with low p60 concentration, however, at higher concentrations the catastrophe frequency is similar to the control (Fig 4.6A). This pattern holds for both the average number of catastrophes and each individual end (Fig. 4.6B-C). The catastrophe frequency increases in 10 μM assays on the plus ends, but decreases on the minus end (Fig 4.6B-C). 7 μM tubulin assays also have fewer catastrophes initially, and the number decreases with increasing p60 on both the plus and minus ends. The total number of catastrophes likely decreases with 7 μM tubulin because there are fewer dynamic events overall with more p60 (Fig. 4.2). From the kymographs, it is clear that dynamic assays with 10 μM tubulin displayed more dynamic events on the plus ends (Fig. 4.2).

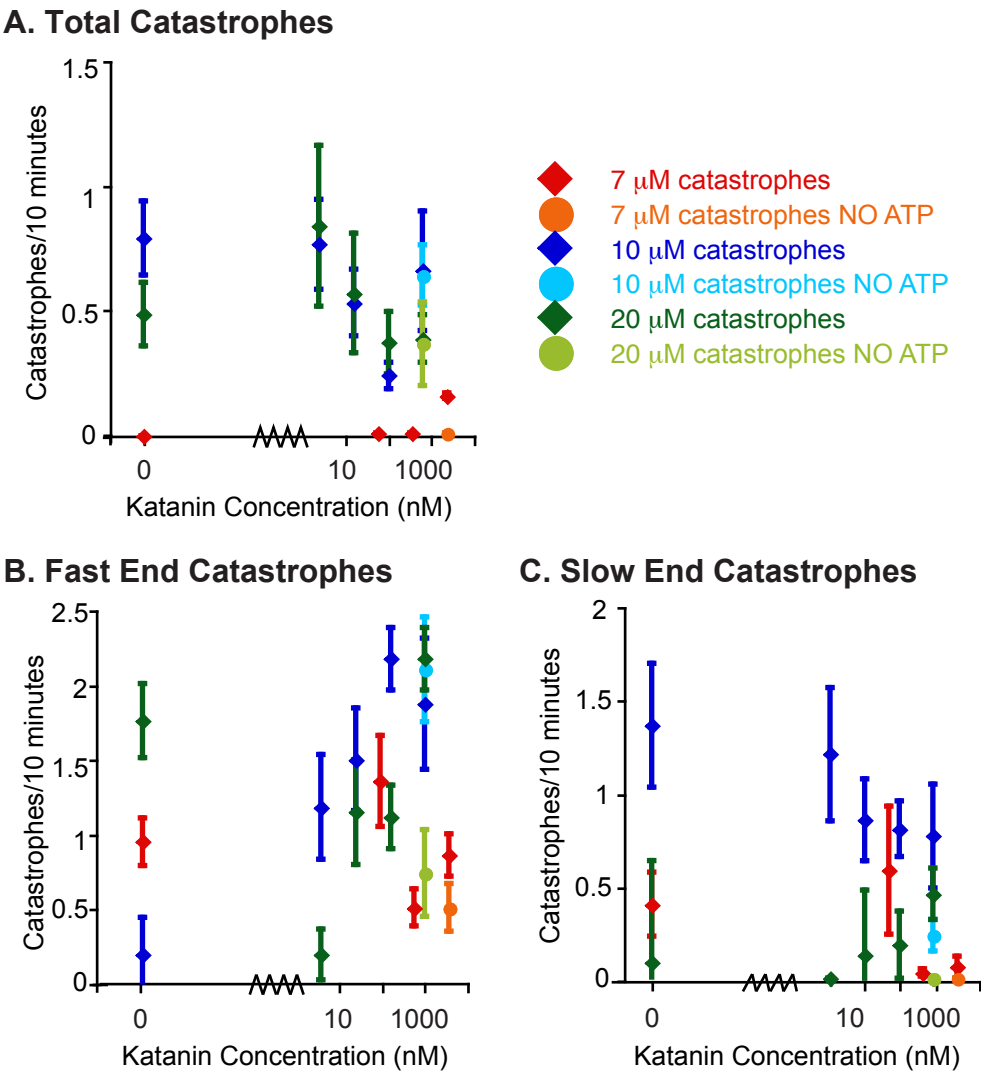

Figure 4.6 Frequency of Catastrophes on Dynamic Microtubules with Katanin.

(**A**) Plot of frequency of catastrophes on both ends of the microtubules combined for each tubulin and katanin concentration. The catastrophe frequency data is represented as # of catastrophes/10 minutes. N values are as follows: 7 μM tubulin (N=22), + 50 nM p60 (N=8), + 500 nM p60 (N=44), + 5 μM p60 (N=45), 7 μM + 5 μM p60 with no ATP (N=22), 10 μM tubulin (N=107), + 1 nM p60 (N=97), + 10 nM p60 (N=101), + 100 nM p60 (N=190), + 1 μM katanin (N=73), + 5 μM p60 with no ATP (N=172), 20 μM tubulin (N=50), + 1 nM p60 (N=12), + 10 nM p60 (N=16), + 100 nM p60 (N=22), + 1 μM p60 (N=66), + 1 μM p60 with no ATP (N=14). (**B**) Quantification of the catastrophe frequency at the plus end/faster growing end of the microtubule. N values are as follows: 7 μM tubulin (N=11), + 50 nM p60 (N=4), + 500 nM p60 (N=22), + 5 μM p60 (N=22), + 5 μM p60 with no ATP (N=11), 10 μM tubulin (N=37), + 1 nM p60 (N=19), + 10 nM p60 (N=21), + 100 nM p60 (N=41), + 1 μM katanin (N=13), 10 μM + 5 μM p60 with no ATP (N=26), 20 μM tubulin (N=25), + 1 nM p60 (N=6), + 10 nM p60 (N=8), + 100 nM p60 (N=11), + 1 μM p60 (N=33), + 1 μM p60 with no ATP (N=7). (**C**) Quantification of the catastrophe frequency at the minus end of the microtubule. N values are as follows: 7

μM tubulin (N=11), + 50 nM p60 (N=4), + 500 nM p60 (N=22), + 5 μM p60 (N=23), + 5 μM p60 with no ATP (N=11), 10 μM tubulin (N=22), + 1 nM p60 (N=19), + 10 nM p60 (N=21), + 100 nM p60 (N=41), + 1 μM katanin (N=13), 10 μM + 5 μM p60 with no ATP (N=26), 20 μM tubulin (N=25), + 1 nM p60 (N=6), + 10 nM p60 (N=8), + 100 nM p60 (N=11), + 1 μM p60 (N=33), + 1 μM p60 with no ATP (N=7). The error bars represent the standard error of the mean.

The last parameter we measured is the frequency of rescue. We defined a rescue as an event where, after a shrinking event, the microtubule begins to grow again before it reaches the seed (Fig.4.1D). The overall number of rescues over all tubulin concentrations is higher on the plus end than the minus end (Fig. 4.7B-C). The average of both ends as well as each end individual microtubule end has a decrease in the number of rescues with p60 regardless of tubulin concentration (Fig. 4.7A-C). At 7 μM tubulin, there are no rescues without p60, which does not change as p60 is added. This is not surprising given that there are fewer dynamic events with 7 μM tubulin.

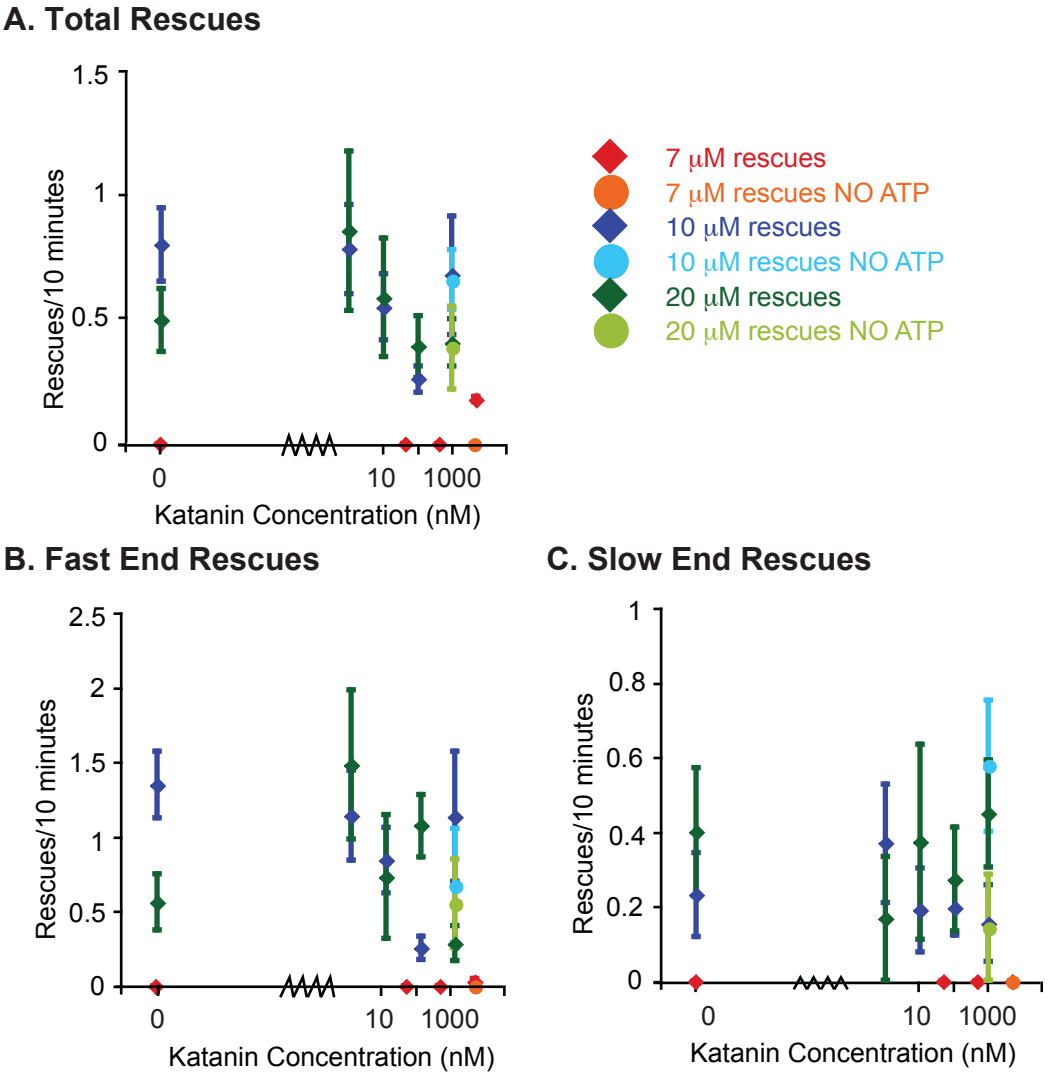

Figure 4.7 Frequency of Rescues on Dynamic Microtubules with Katanin.

(**A**) Plot of frequency of rescues on both ends of the microtubules combined for each tubulin and katanin concentration. The rescue frequency data is represented as # of rescues/10 minutes. Red diamonds are 7 μM tubulin rescue frequencies +/- katanin. N values are as follows: 7 μM tubulin (N=22), + 50 nM p60 (N=8), + 500 nM p60 (N=44), + 5 μM p60 (N=45), + 5 μM p60 with no ATP (N=22), 10 μM tubulin (N=72),+ 1 nM p60 (N=76), + 10 nM p60 (N=76), + 100 nM p60 (N=147), + 1 μM katanin (N=55), + 5 μM p60 with no ATP (N=96), 20 μM tubulin (N=50), + 1 nM p60 (N=12), + 10 nM p60 (N=16), + 100 nM p60 (N=22), + 1 μM p60 (N=66), + 1 μM p60 with no ATP (N=14). (**B**) Quantification of the rescue frequency at the plus end/faster growing end of the microtubule. N values are as follows: 7 μM tubulin (N=11), + 50 nM p60 (N=4), + 500 nM p60 (N=22), + 5 μM p60 (N=22), + 5 μM p60 with no ATP (N=11), 10 μM tubulin (N=22), + 1 nM p60 (N=19), + 10 nM p60 (N=21), + 100 nM p60 (N=41), + 1 μM katanin (N=13), + 5 μM p60 with no ATP (N=28), 20 μM tubulin (N=25), + 1 nM p60 (N=6), + 10 nM p60

(N=8), + 100 nM p60 (N=11), + 1 μM p60 (N=33), + 1 μM p60 with no ATP (N=7). (**C**) Quantification of the rescue frequency at the minus end of the microtubule. N values are as follows: 7 μM tubulin (N=11), + 50 nM p60 (N=4), + 500 nM p60 (N=22), + 5 μM p60 (N=22), 5 μM p60 with no ATP (N=11), 10 μM tubulin (N=22), + 1 nM p60 (N=19), + 10 nM p60 (N=21), + 100 nM p60 (N=41), + 1 μM katanin (N=13), + 5 μM p60 with no ATP (N=26), 20 μM tubulin (N=25), + 1 nM p60 (N=6), + 10 nM p60 (N=8), + 100 nM p60 (N=22), + 1 μM p60 (N=33), + 1 μM p60 with no ATP (N=7). The error bars represent the standard error of the mean.

The percentage of time spent growing, shrinking, and paused provides more information about the overall dynamics of the microtubules. As expected from the other parameters we measured, and from previous studies, we observed that when there is more free tubulin in the assays the microtubules are more dynamic. In the control dynamic instability assays, the microtubules growing with 20 μM tubulin spent more time both growing and shrinking than at 10 μM, or 7 μM tubulin (Fig. 4.8). This was true for both the minus and the plus ends of the microtubules. When katanin was added into the assay, there was little effect at the higher tubulin concentrations of tubulin, however, at 7 μM tubulin, there was an increase in the time spent growing and shrinking with 50 nM katanin. Any higher concentrations of katanin resulted in similar dynamics to the control. At the minus ends of microtubules grown with 7 μM tubulin we observed a different pattern. With 50 nM katanin, there was a decrease in the amount of time spent shrinking, but at 500 nM and 5 μM katanin, there was almost no time spent growing or shrinking. This is consistent with the other parameters we measured as well, because we observed few catastrophes and no rescues under higher katanin concentrations (Fig. 4.6 and 4.7).

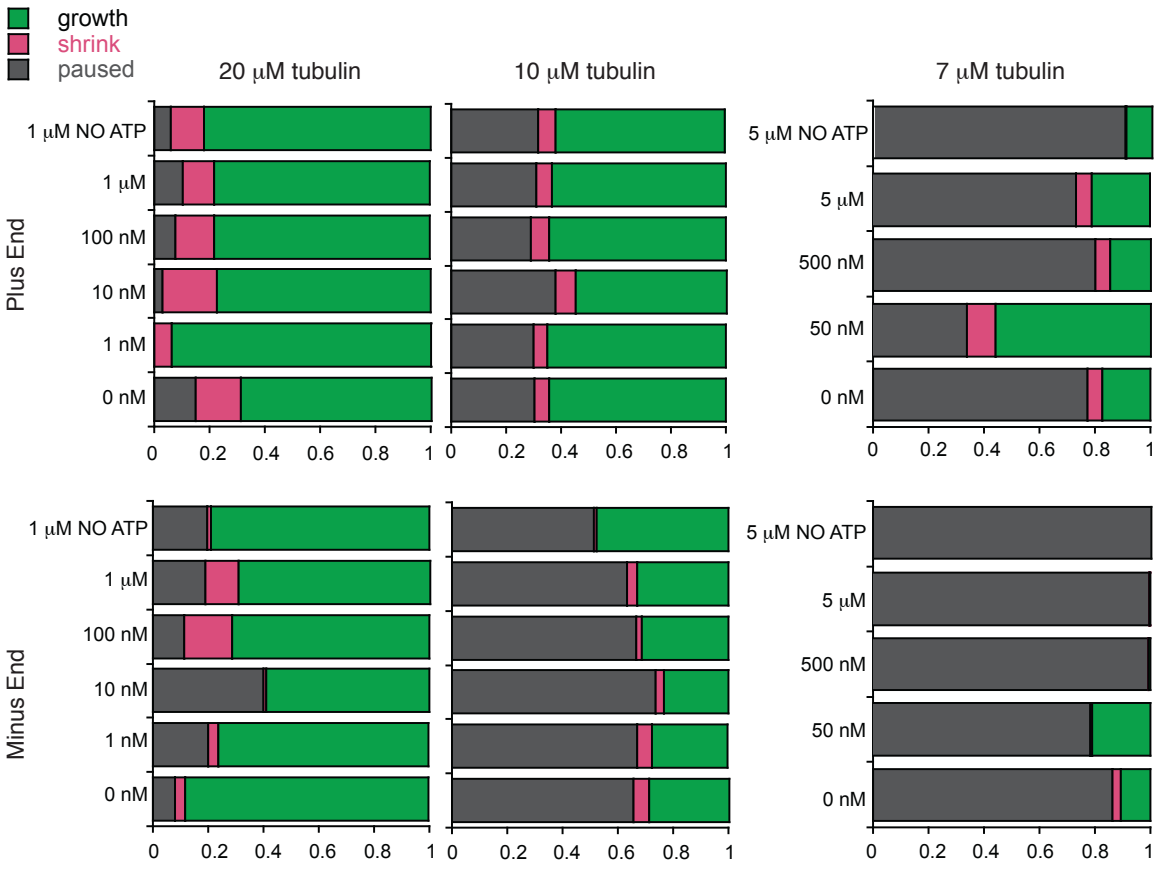

Figure 4.8 Time Spent Growing, Shrinking, or Paused.

Quantification of the fraction of overall time spent growing shrinking, or paused. N values are as follows: 7 μM tubulin (N=11), + 50 nM p60 (N=4), + 500 nM p60 (N=22), + 5 μM p60 (N=23), + 5 μM p60 with no ATP (N=10), 10 μM tubulin (N=22), + 1 nM p60 (N=19), + 10 nM p60 (N=21), + 100 nM p60 (N=41), + 1 μM katanin (N=13), + 5 μM p60 with no ATP (N=28), 20 μM tubulin (N=23), + 1 nM p60 (N=6), + 10 nM p60 (N=8), + 100 nM p60 (N=11), + 1 μM p60 (N=32), + 1 μM p60 with no ATP (N=7).

4.2.3 Stabilizing MAPs on Taxol-stabilized microtubules

Our end goals was to explore microtubule dynamics with stabilizing MAPs, such as tau 4RL, and destabilizing MAPs, like katanin. We showed that katanin can cause microtubules to become more dynamic. Dynamic instability assays have been performed with tau previously (Levy et al. 2005). It has been hypothesized that katanin's severing activity could be inhibited by tau, as a result of studies done in neurons (Qiang et al. 2006). However, there has not been any exploration of tau and katanin's interactions on microtubules in vitro. Therefore, we set up severing assays with Taxol-stabilized microtubules, p60, and increasing amounts of tau 4RL. Qualitatively, we can see that severing assays with just tau on microtubules, does not produce any breaks in the microtubules (Fig. 4.9A). In the control severing assays with only p60, the microtubules were completely destroyed in less than a minute. However, when p60 + 5 nM, 25 nM, 100 nM, 500 nM, 1 μM, or 1.5 μM tau were added to severing assays, there were few detectable severing events, and the microtubules were not completely destroyed by the end of the assay (Fig. 4.9A). This visual evidence is confirmed by loss of polymer quantification. We compared the fluorescence intensity of the microtubules at the beginning of the assay to the fluorescence of the microtubules at each frame. This provided us with information about the fraction of the microtubule remaining over the course of the assay. The loss of polymer data shows that katanin completely destroys microtubules, but tau can effectively inhibit this severing activity. Even at low concentrations of 5 nM tau, the severing activity is effectively inhibited (Fig. 4.9B). When the loss of polymer data is fit to a line or exponential decay, we can find the characteristic decay time for each condition. This characteristic decay time corresponds to how long it would take for microtubules to be completely destroyed. All conditions with tau had relatively long decay times that were beyond the length of the assay (Fig. 4.9C).

This fits well with both the loss of polymer data and the qualitative evidence.

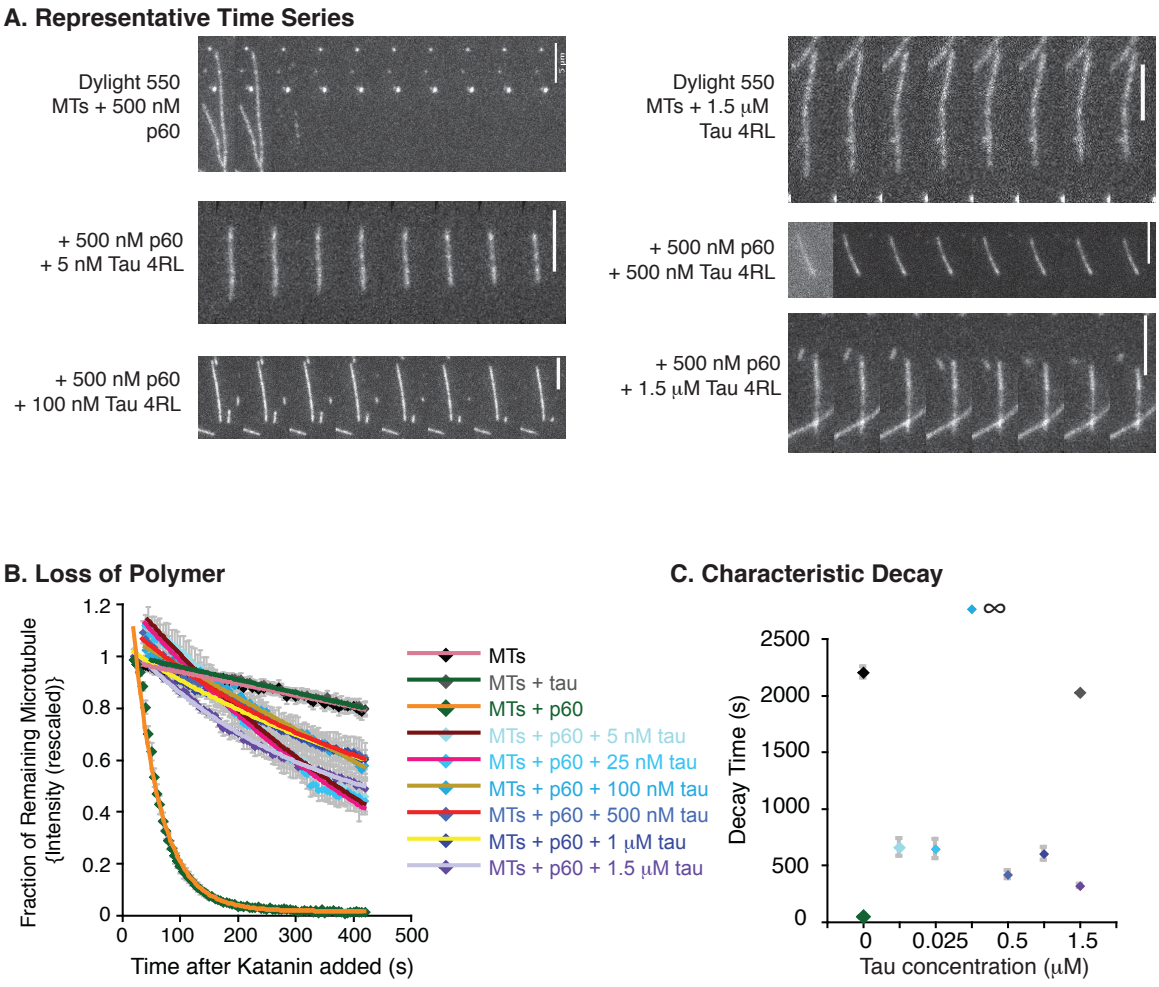

Figure 4.9 Loss of Polymer on Taxol-stabilized Microtubules with Tau and Katanin.

(**A**) Representative time series of Taxol-stabilized microtubules with katanin and 0 nM, 5 nM, 25 nM, 100 nM, 500 nM, 1 μM, 1.5 μM tau 4RL. The scale bars are as indicated. (**B**) Quantification of overall loss of polymer over time. The data is fit is fit to exponential decay, or linear functions. N values are as follows: Taxol-stabilized MTs (N=40), Taxol-stabilized MTs + 1.5 μM Tau (N=34), Taxol-stabilized MTs + p60 (N=89), Taxol-stabilized MTs + p60 + 5 nM tau (N=28), Taxol-stabilized MTs + p60 + 25 nM tau (N=64), Taxol-stabilized MTs + p60 + 100 nM tau (N=27), Taxol-stabilized MTs + p60 + 500 nM tau (N=36), Taxol-stabilized MTs + p60 + 1 μM tau (N=56), Taxol-stabilized MTs + p60 + 1.5 μM tau (N=65). Error bars represent the standard error of the mean. (**C**) Quantification of the characteristic decay times. The times were found from the fits to data in (B). The error bars represent the error associated with the fit.

4.2.4 Dynamic Instability with 7 μM tubulin + katanin + tau

We have shown that katanin destroys Taxol-stabilized microtubules, and tau has a stabilizing effect on microtubules. Katanin can cause dynamic microtubules at 10 μM or 20 μM tubulin concentrations to be more dynamic and tau can cause an increase in microtubule growth length as well as a decease in the number of catastrophes (Levy et al. 2005). However, the interactions of tau and katanin on dynamic microtubules have not been characterized yet. Therefore, we designed a set of experiments to test their interactions. We polymerized dynamic microtubules with a low concentration of tubulin, 7 μM, in order to better distinguish the effects of the MAPs on the microtubule dynamics. We added katanin concentrations of 50 nM, 500 nM, and 5 μM as well as 25 nM and 100 nM tau in different combinations. The tau concentrations are substantially lower than concentrations used previously in dynamic assays because we wanted to ensure that if there was competition between p60 and tau, we would be able to distinguish changes in the microtubule dynamics. In figure 4.9, we observed that there was a substantial decrease in the effectiveness of katanin severing on Taxol-stabilized microtubules at tau concentrations of 5 nM.

Interestingly, we observed a qualitative difference when just tau was added to the assays. The microtubules are more dynamic on both ends (Fig. 4.10). When just p60 is added to the 7 μM tubulin, as previously described, we observed more dynamics at 50 nM p60, but virtually no dynamics at 500 nM or 5 μM p60 (Fig 4.10). In dynamic instability assays with tau and p60 the microtubules were more dynamic than 7 μM tubulin alone, however, the dynamics decreased with increasing concentration of p60 (Fig 4.10). We observed no growth events and both depolymerization and severing at higher concentrations of p60 when combined with 100 nM tau, however, we observed no severing under any of the other conditions.

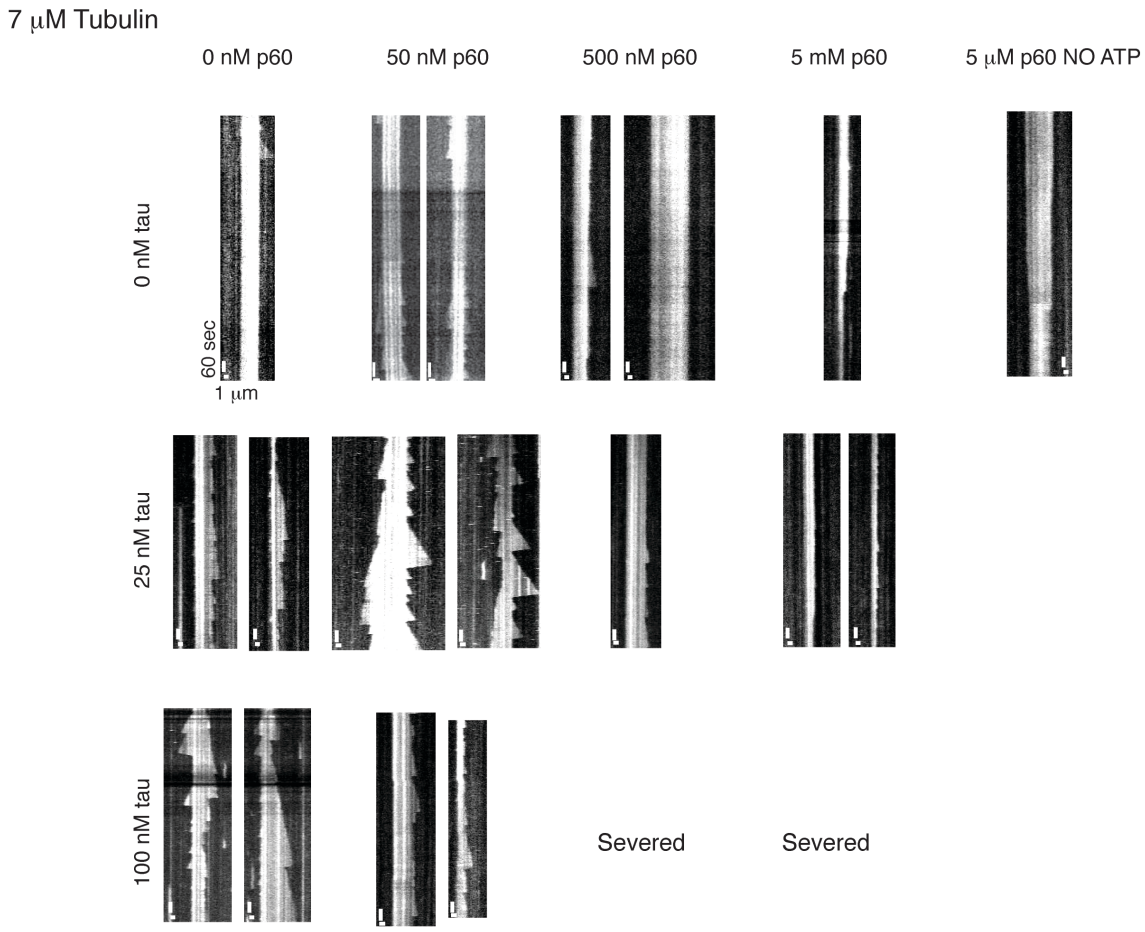

Figure 4.10 Representative Time Series of Dynamic Microtubules with Katanin and Tau.

Time series of representative dynamic microtubules at tubulin concentration of 7 μM and 0 nM, 50 nM, 500 nM, or 5 μM katanin and 0 nM, 25 nM or 100 nM tau. The kymograph is a space time plot with space in the x direction and time in the y direction. The scale bars are 60 seconds in the y direction and 1 μm in the x direction.

We can compare the parameters that are measured from the kymographs, in order to distinguish how tau and katanin can work together to regulate dynamic microtubules. The first parameter we measured was the growth rate. We quantified the average growth rates (Fig. 4.11A), the growth rates for the plus end (Fig. 4.11B), and the minus end (Fig. 4.11C). The growth rates with tau are lower both on average as well as on both ends of the microtubules (Fig. 4.11A). However, the rates increase with higher tau concentrations. When 25 nM tau and p60 are both added to the assays, the growth rate decreases and is similar to the rate with p60 alone (Fig. 4.11A). The rates are lower than p60 alone on the plus ends (Fig. 4.11B) of the microtubules and slightly higher than p60 alone on the minus ends of microtubules (Fig. 4.11C). When the tau concentration is increased to 100 nM, the growth rates are still lower than the 7 μM control, but the remain unchanged when 50 nM p60 is added. We also observed that with 100 nM tau there seems to be little change to the growth rates.

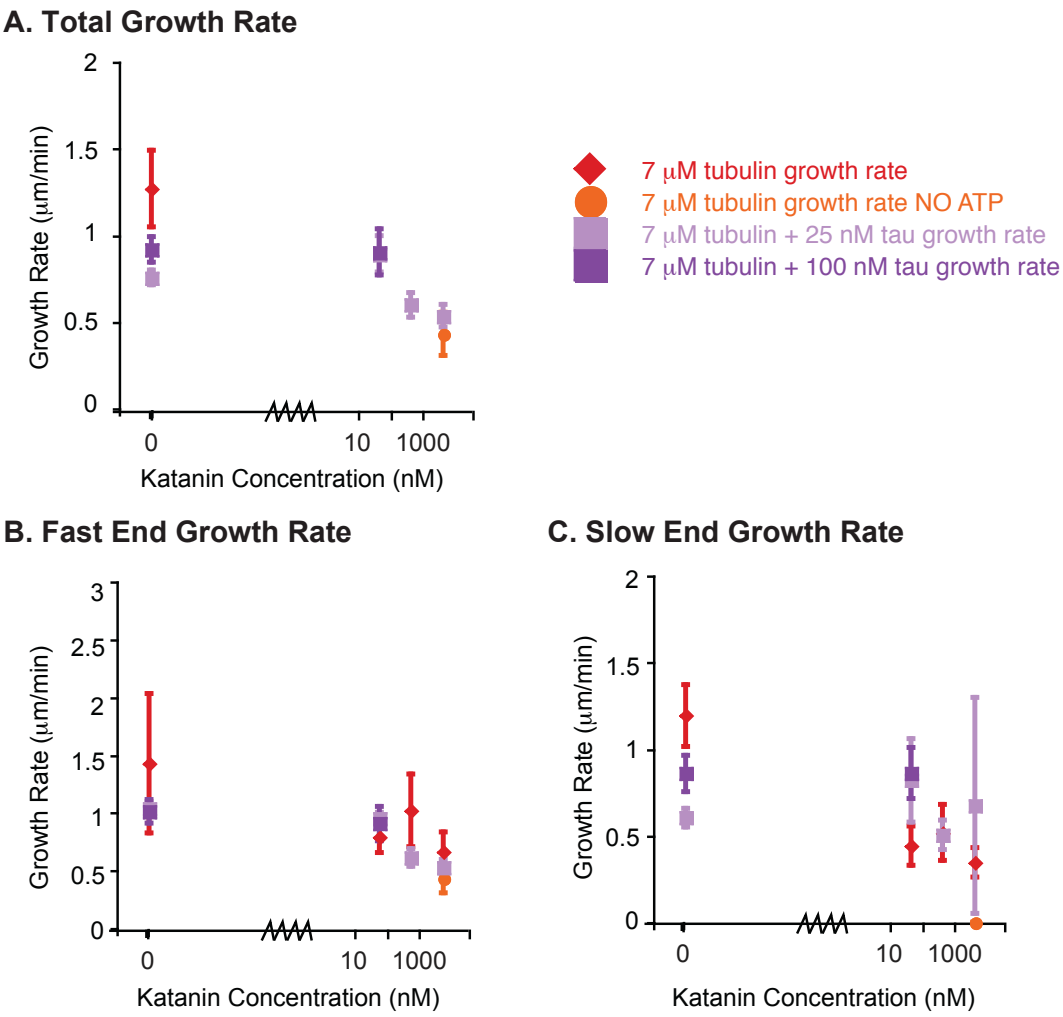

Figure 4.11 Growth Rates of Dynamic Microtubules with Katanin and Tau.

(**A**) Plot of total growth rates of both ends of the microtubules combined for each katanin and tau concentration with 7 µM tubulin. The growth rate is represented as µm/min. Red diamonds are 7 µM tubulin growth rates +/- katanin. N values are as follows: Taxol-stabilized MTs (N=67), 50 nM p60 (N=40), 500 nM p60 (N=41), 5 µM p60 (N=72). Orange circle is 5 µM p60 + no ATP (N=16). Light purple square is 25 nM tau +/- p60: 25 nM tau (N=297), 25 nM tau + 50 nM p60 (N=269), 25 nM tau + 500 nM p60 (N=173), 25 nM tau + 5 µM p60 (N=65). Purple square is 100 nM tau +/- p60: 100 nM tau (N=500), 100 nM tau + 50 nM p60 (N=125). (**B**) Quantification of the growth rates on the plus ends of the microtubules. Taxol-stabilized MTs (N=21), 50 nM p60 (N=24), 500 nM p60 (N=38), 5 µM p60 (N=70), 5 µM p60 + no ATP (N=16), 25 nM tau (N=104), 25 nM tau + 50 nM p60 (N=155), 25 nM tau + 500 nM p60 (N=154), 25 nM tau + 5 µM p60 (N=63),100 nM tau (N=196), 100 nM tau + 50 nM p60 (N=114). (**C**) Quantification of the growth rates on the minus ends of the microtubules. Taxol-stabilized MTs (N=46), 50 nM p60 (N=16), 500 nM p60 (N=3), 5 µM p60 (N=2), 5 µM p60 + no ATP (N=10), 25 nM tau (N=193), 25 nM tau + 50 nM p60 (N=115), 25 nM tau + 500 nM p60 (N=19), 25 nM tau + 5 µM p60 (N=2),100 nM tau (N=304), 100 nM tau + 50 nM p60 (N=11). Error bars represent the standard error of the mean.

The growth length with 25 nM tau is slightly decreased from the 7 μM tubulin control (Fig. 4.12A). 100 nM tau does not change the average growth length from the 7 μM tubulin control on average or at either end of the microtubule. Katanin p60 on its own decreases the growth lengths with increasing amounts of the enzyme. When tau and p60 are added to dynamic microtubules together, the length of microtubule growth shortens (Fig. 4.12A-C). However, the length still remains above the 7 μM tubulin control on the minus end. Interestingly, 25 nM tau + 50 nM p60 causes an increase in microtubule growth lengths. This result agrees with the kymographs, which show there are longer growth events at these concentrations (Fig. 4.10). The results suggest that there are shorter growth events with p60 or with p60 + tau.

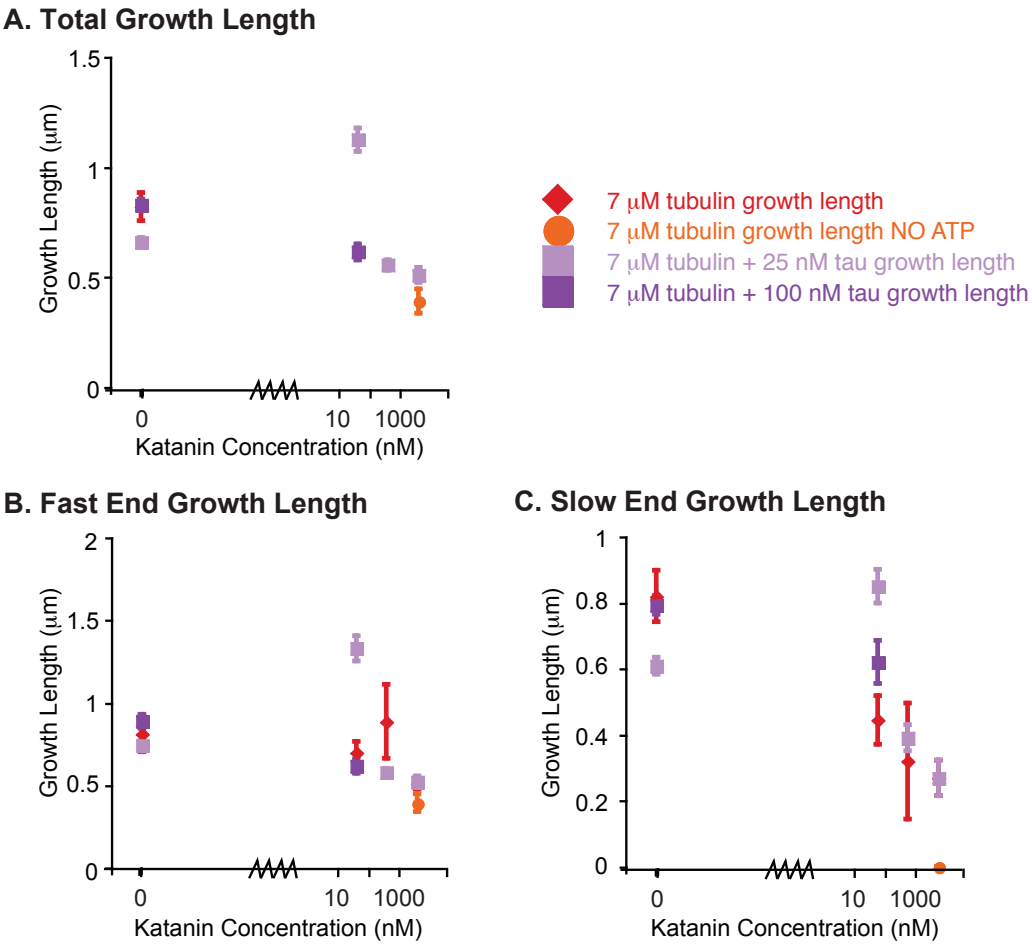

Figure 4.12 Growth Lengths of Dynamic Microtubules with Katanin and Tau.

(**A**)Plot of total growth lengths of both ends of the microtubules combined for each katanin and tau concentration with 7 μM tubulin. The growth length is represented in μms. Red diamonds are 7 μM tubulin growth length +/- katanin. N values are as follows: Taxol-stabilized MTs (N=67), 50 nM p60 (N=40), 500 nM p60 (N=41), 5 μM p60 (N=72). Orange circle is 5 μM p60 + no ATP (N=16). Light purple square is 25 nM tau +/- p60: 25 nM tau (N=297), 25 nM tau + 50 nM p60 (N=269), 25 nM tau + 500 nM p60 (N=173), 25 nM tau + 5 μM p60 (N=65). Purple square is 100 nM tau +/- p60: 100 nM tau (N=500), 100 nM tau + 50 nM p60 (N=125). (**B**) Quantification of the growth lengths on the plus ends of the microtubules. Taxol-stabilized MTs (N=21), 50 nM p60 (N=24), 500 nM p60 (N=38), 5 μM p60 (N=70), 5 μM p60 + no ATP (N=16), 25 nM tau (N=104), 25 nM tau + 50 nM p60 (N=155), 25 nM tau + 500 nM p60 (N=154), 25 nM tau + 5 μM p60 (N=63),100 nM tau (N=196), 100 nM tau + 50 nM p60 (N=114). (**C**) Quantification of the growth lengths on the minus ends of the microtubules. Taxol-stabilized MTs (N=46), 50 nM p60 (N=16), 500 nM p60 (N=3), 5 μM p60 (N=2), 5 μM p60 + no ATP (N=10), 25 nM tau (N=193), 25 nM tau + 50 nM p60 (N=115), 25 nM tau + 500 nM p60 (N=19), 25 nM tau + 5 μM p60 (N=2),100 nM tau (N=304), 100 nM tau + 50 nM p60 (N=11). Error bars represent the standard error of the mean.

Similar to the growth length, the shrinkage length can provide information about how far the microtubules are shrinking back after growth events. This information could distinguish whether there are multiple growth events prior to the shrinkage events. This could be the case if the average shrinkage length is longer than the average growth length. However, our results indicate that the lengths are similar to that of the growth lengths (Fig. 4.12 and Fig. 4.13). Dynamic instability with 25 nM tau causes shorter shrinking lengths on average than the 7 μM tubulin control. 100 nM tau displayed similar lengths as the 7 μM control. The shrinkage lengths decreased with 25 nM tau and p60, with the exception of 50 nM p60, which displayed an increase in length with respect to both the 7 μM control and 25 nM tau alone. 100 nM tau + 50 nM p60 did not display any significant change in shrinkage length with respect to 100 nM tau alone or the 7 μM tubulin control.

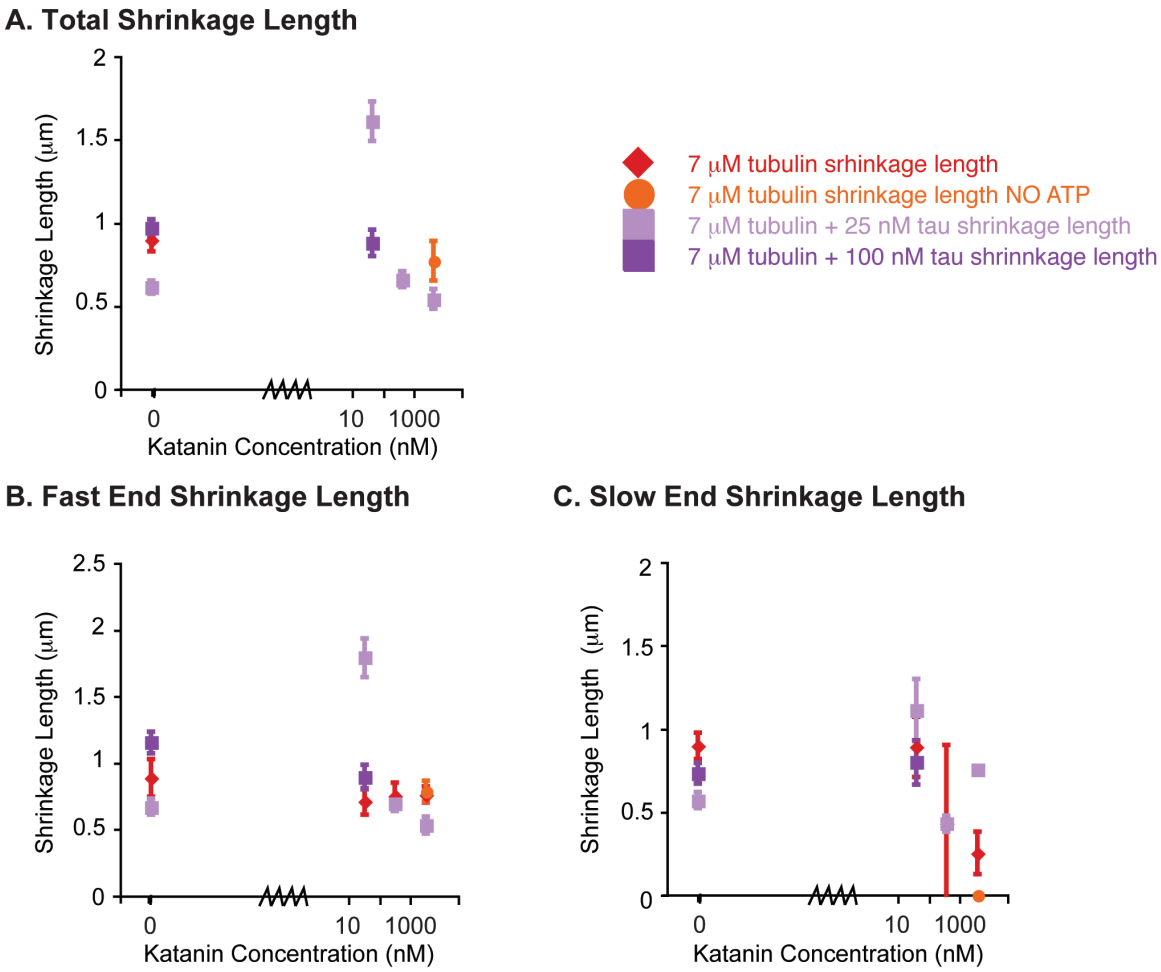

Figure 4.13 Shrinkage Lengths of Dynamic Microtubules with Katanin and Tau.

(**A**) Plot of total shrinkage lengths of both ends of the microtubules combined for each katanin and tau concentration with 7 μM tubulin. The shrinkage length is represented in mms. Red diamonds are 7 μM tubulin shrinkage length +/- katanin. N values are as follows: Taxol-stabilized MTs (N=43), 50 nM p60 (N=20), 500 nM p60 (N=29), 5 μM p60 (N=35). Orange circle is 5 μM p60 + no ATP (N=7). Light purple square is 25 nM tau +/- p60: 25 nM tau (N=113), 25 nM tau + 50 nM p60 (N=120), 25 nM tau + 500 nM p60 (N=72), 25 nM tau + 5 μM p60 (N=22). Purple square is 100 nM tau +/- p60: 100 nM tau (N=193), 100 nM tau + 50 nM p60 (N=78). (**B**) Quantification of the shrinkage lengths on the plus ends of the microtubules. Taxol-stabilized MTs (N=11), 50 nM p60 (N=15), 500 nM p60 (N=26), 5 μM p60 (N=32), 5 μM p60 + no ATP (N=7), 25 nM tau (N=48), 25 nM tau + 50 nM p60 (N=89), 25 nM tau + 500 nM p60 (N=62), 25 nM tau + 5 μM p60 (N=21),100 nM tau (N=108), 100 nM tau + 50 nM p60 (N=65). (**C**) Quantification of the shrinkage lengths on the minus ends of the microtubules. Taxol-stabilized MTs (N=32), 50 nM p60 (N=5), 500 nM p60 (N=3), 5 μM p60 (N=5), 5 μM p60 + no ATP (N=10), 25 nM tau (N=65), 25 nM tau + 50 nM p60 (N=31), 25 nM tau + 500 nM p60 (N=10), 25 nM tau + 5 μM p60 (N=1),100 nM tau (N=85), 100 nM tau + 50 nM p60 (N=13). Error bars represent the standard error of the mean.

The catastrophe frequency changes significantly with the addition of the either tau or p60. 25 nM or 100 nM tau increased the catastrophe frequency, 100 nM to a greater extent than 25 nM tau. This was true of both ends of the microtubule. Previously, we showed that katanin could both increase or decrease the catastrophe frequency depending on the tubulin concentration (Fig. 4.6). At 7 μM tubulin we observed that the catastrophe frequency is decreased with respect to the no katanin control with the exception of the lowest katanin concentration (Fig. 4.6). The catastrophe frequency with 25 nM tau and p60 remains constant on the plus end above p60 concentrations of 50 nM (Fig. 4.14B). However, on the minus ends, the catastrophe frequency decreases with p60 concentration (Fig. 4.14C). When we increased the tau concentration to 100 nM in combination with p60, the catastrophe frequency decreased at both ends of the microtubules (Fig. 4.14B-C).

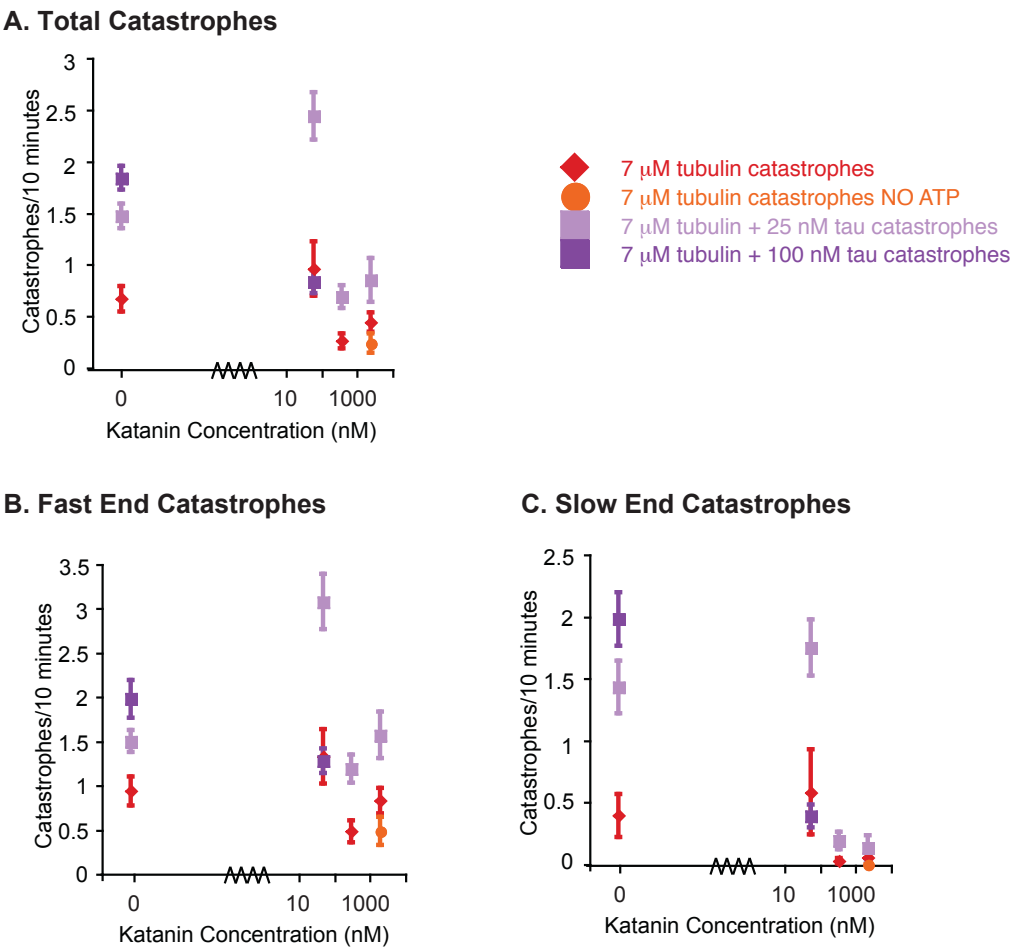

Figure 4.14 Catastrophe Frequencies of Dynamic Microtubules with Katanin and Tau.

(**A**) Plot of total catastrophe frequencies of both ends of the microtubules combined for each katanin and tau concentration with 7 μM tubulin. The catastrophe frequency is represented in # of catastrophes/min. Red diamonds are 7 μM tubulin catastrophe frequency +/- katanin. N values are as follows: Taxol-stabilized MTs (N=22), 50 nM p60 (N=8), 500 nM p60 (N=44), 5 μM p60 (N=45). Orange circle is 5 μM p60 + no ATP (N=22). Light purple square is 25 nM tau +/- p60: 25 nM tau (N=43), 25 nM tau + 50 nM p60 (N=25), 25 nM tau + 500 nM p60 (N=50), 25 nM tau + 5 μM p60 (N=20). Purple square is 100 nM tau +/- p60: 100 nM tau (N=64), 100 nM tau + 50 nM p60 (N=36). (**B**) Quantification of the catastrophe frequencies on the plus ends of the microtubules. Taxol-stabilized MTs (N=11), 50 nM p60 (N=4), 500 nM p60 (N=22), 5 μM p60 (N=22), 5 μM p60 + no ATP (N=11), 25 nM tau (N=22), 25 nM tau + 50 nM p60 (N=13), 25 nM tau + 500 nM p60 (N=25), 25 nM tau + 5 μM p60 (N=10), 100 nM tau (N=32), 100 nM tau + 50 nM p60 (N=18). (**C**) Quantification of the catastrophe frequencies on the minus ends of the microtubules. Taxol-stabilized MTs (N=11), 50 nM p60 (N=4), 500 nM p60 (N=22), 5 μM p60 (N=23), 5 μM p60 + no ATP (N=11), 25 nM tau (N=21), 25 nM tau + 50 nM p60 (N=12), 25 nM tau + 500 nM p60 (N=25), 25 nM tau + 5 μM p60 (N=10),100 nM tau(N=32), 100 nM tau + 50 nM p60 (N=18). Error bars represent the standard error of the mean.

We showed the rescue frequency was affected by tubulin concentration (Fig. 4.7). The rescue frequency decreased with increasing p60 concentration at tubulin concentrations of 10 μM and 20 μM (Fig. 4.7). In dynamic assays with 7 μM tubulin we observed virtually no rescues in the control or with p60 (Fig. 4.7). With 25 nM or 100 nM tau in dynamic assays, there was a slight increase in the rescue frequency on average and on the plus end (Fig. 4.15A-B). When p60 was added in combination with tau, there was an increase in the rescue frequency (Fig. 4.15A-B). The most significant change was on the plus end with 50 nM p60.

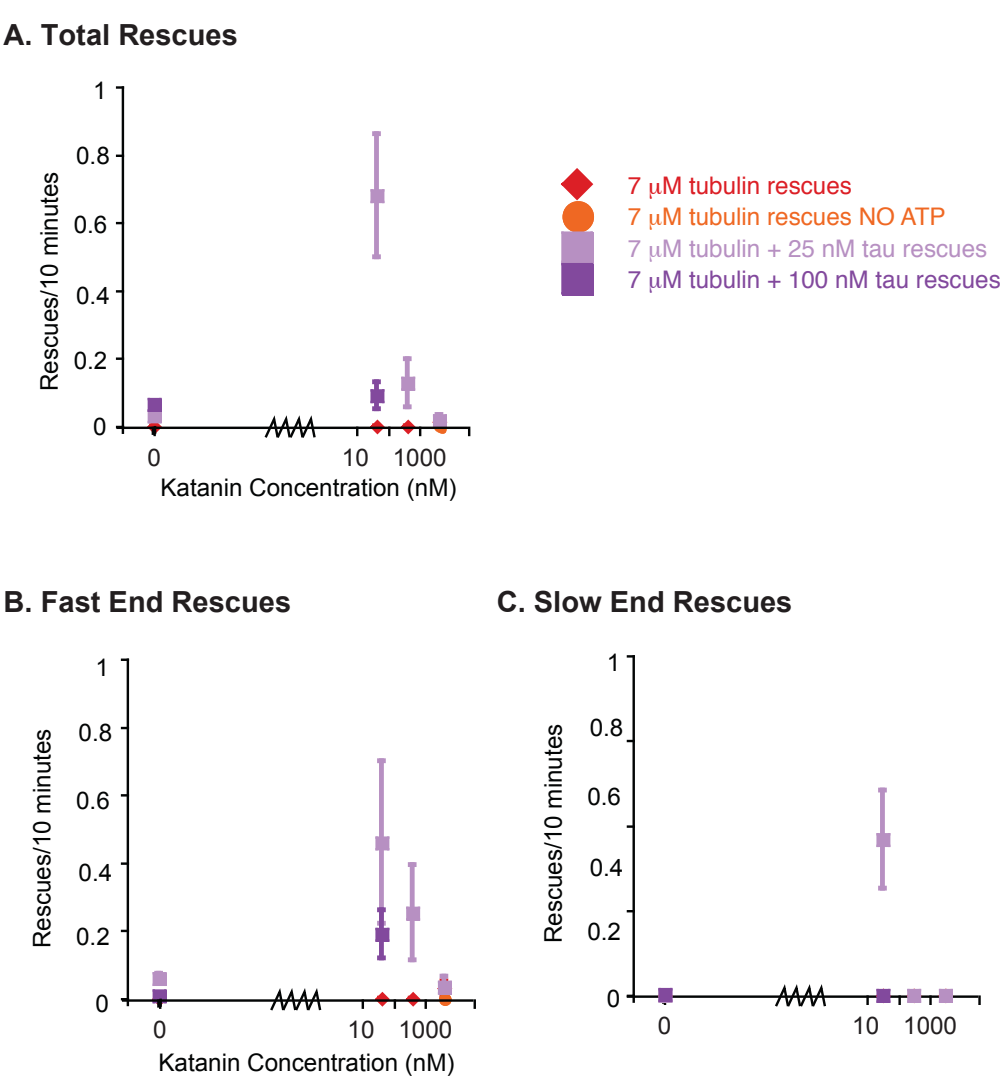

Figure 4.15 Rescue Frequencies of Dynamic Microtubules with Katanin and Tau.

(**A**) Plot of total rescue frequencies of both ends of the microtubules combined for each katanin and tau concentration with 7 μM tubulin. The rescue frequency is represented in # of rescues/min. Red diamonds are 7 μM tubulin rescue frequency +/- katanin. N values are as follows: Taxol-stabilized MTs (N=22), 50 nM p60 (N=8), 500 nM p60 (N=44), 5 μM p60 (N=45). Orange circle is 5 μM p60 + no ATP (N=22). Light purple square is 25 nM tau +/- p60: 25 nM tau (N=43), 25 nM tau + 50 nM p60 (N=25), 25 nM tau + 500 nM p60 (N=50), 25 nM tau + 5 μM p60 (N=20). Purple square is 100 nM tau +/- p60: 100 nM tau (N=64), 100 nM tau + 50 nM p60 (N=36). (**B**) Quantification of the rescue frequencies on the plus ends of the microtubules. Taxol-stabilized MTs (N=11), 50 nM p60 (N=4), 500 nM p60 (N=22), 5 μM p60 (N=22), 5 μM p60 + no ATP (N=11), 25 nM tau (N=22), 25 nM tau + 50 nM p60 (N=13), 25 nM tau + 500 nM p60 (N=25), 25 nM tau + 5 μM p60 (N=10), 100 nM tau (N=32), 100 nM tau + 50 nM p60 (N=18). (**C**) Quantification of the rescue frequencies on the minus ends of the microtubules. Taxol-

stabilized MTs (N=11), 50 nM p60 (N=4), 500 nM p60 (N=22), 5 μM p60 (N=23), 5 μM p60 + no ATP (N=11), 25 nM tau (N=21), 25 nM tau + 50 nM p60 (N=12), 25 nM tau + 500 nM p60 (N=25), 25 nM tau + 5 μM p60 (N=10),100 nM tau (N=32), 100 nM tau + 50 nM p60 (N=18). Error bars represent the standard error of the mean.

Despite having all these parameters to measure, it is difficult to determine how tau and p60 alter the microtubule dynamics. A better measure of the changes that occur may be the overall dynamicity. We chose to plot this as percentage of time the microtubules spent growing, shrinking, or paused, as this would show us if there were changes in overall time spent in each state. Figure 4.16 portrays this data and may give a clearer understanding of how each of the MAPs are altering the dynamics. Microtubules grown with 7 μM tubulin spend most of their time at both ends paused. The addition of 25 nM or 100 nM tau significantly increases the amount of time both growing and shrinking at both ends of the microtubule, consistent with the kymographs, where we observed more dynamic events (Fig. 4.10). 50 nM katanin also results in an increase in the time growing and shrinking on the plus ends of microtubules, but also causes the microtubule to become less dynamic on the minus end and spend more time paused. Adding 500 nM or 5 μM katanin to the assay causes the dynamics to be similar to the 7 μM tubulin control on the plus end, however, virtually abolishes any dynamic events on the minus end. Combining tau and katanin results in significantly more time growing and shrinking on the plus end than in the control. However, the minus end becomes mostly paused with katanin concentrations above 50 nM. As we showed previously, 100 nM tau + 500 nM p60 or 5 μM p60 resulted in depolymerization and severing. These results suggest that both katanin and tau can cause microtubules to become more dynamic at this tubulin concentration, however, it is highly dependent on the concentration of the MAPs in the assays. Overall, the microtubules spend more time growing and shrinking on the plus end and more time paused on the plus end, with katanin or a combination of katanin and tau.

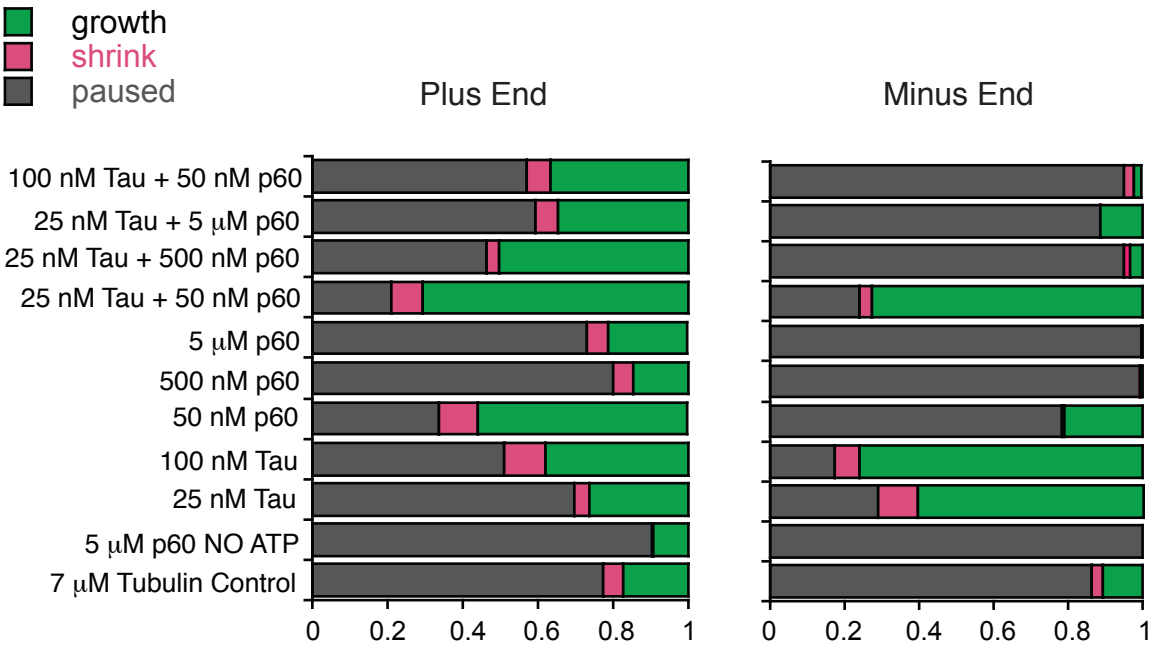

Figure 4.16 Fraction of Time Spent Growing, Shrinking, or Paused.

Quantification of the fraction of time spent growing, shrinking, or paused. N values are as follows: 7 μM tubulin control (N=11), 50 nM p60 (N=4), 500 nM p60 (N=22), 5 μM p60 (N=23), 5 μM p60 + no ATP (N=10), 25 nM tau (N=22), 25 nM tau + 50 nM p60 (N=13), 25 nM tau + 500 nM p60 (N=25), 25 nM tau + 5 μM p60 (N=10),100 nM tau (N=29), 100 nM tau + 50 nM p60 (N=18).

4.3 Discussion

In this chapter we have confirmed that tubulin concentration affects all of the parameters of dynamic instability. An increase in tubulin concentration causes an increase in growth rate, growth length, and shrinkage length (Fig. 4.3, 4.4, 4.5). Higher tubulin concentrations can result in higher catastrophe and rescue frequencies as well (Fig. 4.6, 4.7). Increasing the tubulin concentration causes microtubules to be more dynamic and causes the microtubules to spend a larger fraction of time growing and shrinking, and less time paused.

Adding katanin into dynamic instability assays caused an increase in growth rate and length, as well as shrinkage length (Fig. 4.3, 4.4, 4.5). However, katanin had different effects on the catastrophe and rescue rates at different tubulin concentrations. At 7 μM tubulin, there were very few catastrophes and rescues regardless of the katanin concentration (Fig. 4.6). At 10 μM tubulin, there was an increase in catastrophes at the plus end and decrease at the minus end (Fig. 4.7). Katanin in assays with 20 μM tubulin on the contrary resulted in a decrease in the catastrophe frequency. The rescue frequency on average decreased overall for both 10 μM and 20 μM tubulin assays with katanin. However, there was not a significant change in the fraction of time spent growing and shrinking except at the 7 μM tubulin concentration (Fig. 4.8). At 7 μM, there was an increase in fraction of time growing and shrinking with 50 nM katanin, but this fraction decreased on both ends above this katanin concentration.

Previously, tau has been described as a stabilizing MAP. We found that adding tau to severing assays resulted in a decrease in the overall loss of polymer, even at low concentrations of tau (Fig. 4.9). This suggests that tau is able to protect microtubules from p60. It has been shown previously in dynamic assays with 15 μM tubulin, that tau increases growth rates and decreases the catastrophe frequency at concentrations of

0.27 μM and above (Levy et al. 2005). We chose to do experiments with tau at lower concentrations and found that tau makes microtubules more dynamic. We found that tau decreased the growth rate slightly, however, the growth and shrinkage lengths remained similar to the control (Fig. 4.11, 4.12, 4.13). There was also an increase in both the catastrophe and rescue frequencies at the concentrations used (Fig. 4.14, 4.15) and the fraction of time and growing and shrinking was significantly increased with respect to the controls (Fig. 4.16).

To understand how stabilizing and destabilizing MAPs may work together to regulate microtubule dynamics, we performed dynamic instability assays with tau and katanin as well. Overall, we observed an increase in dynamics with 50 nM katanin and tau, however, as the katanin concentration increased, there were fewer dynamic events and less time spent growing and shrinking (4.10, 4.16).

Conclusions

Our results are not as conclusive as previous studies with destabilizing MAPs that clearly stopped growth off of microtubules completely, or caused more frequent catastrophes (Gardner et al. 2011; Montenegro Gouveia et al. 2010). In cells, katanin is found in places with dynamic microtubules, especially mitosis and meiosis, and it likely plays a part in regulating microtubule dynamics (Vale 1991; Buster, McNally, and McNally 2002; K. McNally et al. 2006; K. McNally et al. 2014). There are several reasons why we may not have observed a large effect on microtubule dynamics. In chapter 3, we demonstrated that katanin severing activity is greatly inhibited by free tubulin. The concentrations of tubulin required for inhibition are far below the critical concentrations of tubulin (Schiff, Fant, and Horwitz 1979; Shelanski, Gaskin, and Cantor 1973). Therefore, it is difficult to test whether the tubulin is causing a decrease in effect. Another option is

that p80, katanin p60's partner protein, could play a role in targeting p60 to microtubules for effective regulation. This possibility seems highly probably since it is necessary for targeting p60 to the correct locations in cells. In the future it would be interesting to further explore how p80 may change p60's regulation of microtubules.

4.4 Methods

4.4.1 Katanin Purification.

We received the pMAL-c5x-*X.* laevis p60 from the Heald lab. We used an IPTG inducible expression system was used for expression and purification. The plasmid was transformed into BL21 Competent *E. coli* (New England BioLabs). An LB starter culture was grown overnight and added to a 500mL culture the next day. This culture was grown at 37°C until it reached an OD of 0.8 and then it was induced with 1 mM IPTG. The culture was allowed to continue to grow at 16°C for 16 hours. The cells were lysed in resuspension buffer (20 mM Hepes pH 7.7, 250 mM NaCl, 0.5 mM BME, 10% glycerol, 0.25 mM ATP) via sonication. The lysate was incubated with amylose resin (New England BioLabs) for 1-2 hours. The lysate/resin mixture was added to the column and allowed to enter the column completely. Once excess lysate had passed through the column, the column was washed twice with 20 mL of resuspension buffer. Then the protein is eluted in elution buffer (20 mM Hepes pH 7.7, 250 mM NaCl, 0.5 mM BME, 10% glycerol, 0.25 mM ATP, 10 mM Maltose). The approximate concentration was obtained by a Bradford assay.

4.4.2 Tau Purification

We purified tau using an IPTG inducible expression system. The plasmid was

transformed into BL21 Competent *E. coli* (New England BioLabs). An LB starter culture was grown overnight and added to a 500mL culture the next day. This culture was grown at 37°C until it reached an OD of 0.6, and then it was induced with 1 mM IPTG for 4-6 hours. The cells were lysed in PEM-100 by sonication. The lysates were boiled with 500 mM NaCl in PEM-100 for 30 minutes and pelleted to remove all precipitated proteins. The supernatant, containing tau, was buffer exchanged into PEM-100 and the approximate concentrations was obtained by a gel.

4.4.3 GMPCPP Stabilized Seeds

To perform dynamic instability in vitro, we require a seed to nucleate microtubule growth is a particular location. We made seed from 1:1:10 rhodamine:biotin:unlabeled tubulin dimers in PEM-100. We spun down the solution remove aggregates. We polymerized tubulin in the presence of 1 mM GMPCPP at 37°C for 30 minutes. Then the microtubules were centrifuged again and resuspended in GMPCPP and warm PEM-100. The seeds were sheared four times and left at 37°C until they were used.

4.4.4 Dynamic Instability Assays

All assays will be performed in a flow chamber with ethanol cleaned slides and coverslips biologically cleaned with an acid wash as previously described (Appendix B.2) (Montenegro Gouveia et al. 2010).

Similar to the procedure previously used (Montenegro Gouveia et al. 2010), we first added 0.2 mg/mL PLL-PEG-Biotin to the chamber and incubated for 5 minutes. Next, we washed with PEM-100 and added 1 mg/mL streptavidin for 5 minutes. Then 0.125 mg/mL(1:400 dilution) of biotinylated rhodamine seeds was flowed into the chamber and incubated for 5 minutes. The chamber was blocked for non-specific interactions with 1 mg/mL K-casein in PEM-100. Finally, the elongation mix was added

(4.7 mM GTP, 0.048 mM DTT, 0.2 mg/mL K-casein, 0.28% methyl cellulose, 14.29 μg/μL glucose, 0.5 mg/ml glucose oxidase, 0.5 mg/mL catalase) in PEM-100 with tubulin dimers at 10 μM, 15 μM, or 20 μM, depending on the experiments. This will be added to the chamber right before imaging.

4.4.5 Data Analysis

The data was analyzed from kymographs generated in ImageJ using the multiple kymograph plugin. From the kymographs properties such as growth rate, and length, shrinkage length, catastrophe, and rescue frequency were calculated.

CHAPTER 5

CLOSING REMARKS AND FUTURE DIRECTIONS

5.1 Closing Remarks

Regulation of microtubules is essential in order for microtubules to undergo the changes necessary for diverse cellular functions. It has been previously shown that katanin is necessary for regulation of microtubules in a variety of organisms because when it is mutated some abnormalities that occur are: elongated spindles in meiosis (Buster, McNally, and McNally 2002; K. McNally et al. 2006; K. McNally et al. 2014), cortical arrays are not organized properly (Nakamura, Ehrhardt, and Hashimoto 2010; Q. Zhang et al. 2013), and neuronal development does not proceed properly (Ahmad et al. 1999; Yu et al. 2008). Despite the characterization of katanin thus far, it is still unclear how katanin targets microtubules for severing, and how this severing activity is regulated by other factors in the cell.

In this dissertation we use *in vitro* single molecule approaches to further elucidate how katanin regulates microtubules in vitro. The information we have gathered in these experiments should help inform future studies both in vitro and vivo, so we can better elucidate the complex regulatory network of both microtubules and its regulators.

5.1.1 Katanin's Regulation of Microtubule Defects.

We hypothesized that katanin targeted microtubules with defects based on previous theoretical and experimental evidence (Davis et al. 2002; Díaz-Valencia et al. 2011). We created "high salt" microtubules, which are characterized by fewer protofilaments (thinner width, and higher curvature) with more protofilament shifts and seam defects. We also made microtubules that were missing the CTTs of tubulin. We performed severing assays on both types of microtubules, as well as our "normal"

microtubules, Taxol-stabilized microtubules, and analyzed the overall loss of polymer for each. We were able to conclude that: (1) Katanin does not have a preference for microtubules with seam defects. Further, katanin is not sensitive to the width or curvature of the microtubules. (2) Katanin cannot sever microtubules without the CTTs of tubulin, however, it is capable of depolymerizing these microtubules in an ATP-dependent manner. (3) Katanin's severing and ATPase activity is ATP-concentration dependent. The depolymerization activity requires minimal ATP, and is not ATP-concentration dependent.

5.1.2 Katanin's Severing Activity is Inhibited by Tubulin.

There has been very little work characterizing katanin's interactions with other cellular components. Previous work has shown that spastin is inhibited by both tubulin and the CTTs of tubulin (White et al. 2007; Roll-Mecak and Vale 2008). We hypothesized that katanin may also be inhibited by tubulin and tubulin CTTs. In order to test this hypothesis, we performed severing experiments with katanin and tubulin as well as with the beta and alpha CTTs. We were able to conclude: (1) Katanin is inhibited by free tubulin. (2) Katanin recognizing the sequence and not the shape of tubulin. (3) The CTTs of beta are more effective than free tubulin at inhibiting severing. Alpha tubulin tails are less effective than beta tails. (4) Detyrosinated-alpha tubulin is not as effective at inhibiting severing, which suggests possible regulation of severing by tubulin post-translational modifications. These findings open new directions to explore in terms of regulating severing activity.

5.1.3 Dynamic Microtubule Regulation by Katanin p60 and Tau.

Regulation of dynamic microtubules requires both stabilizers and destabilizers *in vivo*. Tau's regulation of katanin severing activity on stable or dynamic microtubules has

yet to be shown in vitro. We performed severing assays with tau and katanin and showed that even low concentrations of tau were able to substantially inhibit severing activity. We found that katanin's regulation of dynamics was complicated and not conclusive. Katanin made microtubules more dynamic at low concentrations, and eliminated most dynamic events at high concentrations. However, we observed no severing events by katanin on dynamic microtubules. When katanin and tau were added together to dynamic assays, we again observed more dynamics at low concentrations of katanin and tau, fewer dynamic events at higher concentrations of the MAPs. We did observe depolymerization and severing with 100 nM tau and 500 nM - 5 μM katanin. We were able to conclude that tau does regulate severing activity on stable microtubules. We also observed that at low concentration of katanin or tau and katanin the microtubules were more dynamic, however, further work needs to be done to conclusively determine how these MAPs work together to regulate dynamic microtubules.

5.2 Future Directions

Using an in vitro system with microtubules characterized by more frequent seam defects I have shown that katanin does not prefer to sever this type of defect. However, I believe that katanin must have a targeting mechanism. In the future it would be interesting to explore further what katanin is targeting. While it could be difficult to create other microtubules with defects, such as holes in the lattice, this is a likely target for microtubule severing enzymes as it would be a weaker area of the microtubule. We could also utilize microtubules with post-translational modifications. There is some published evidence that katanin targets microtubules with specific post-translational modifications (Sharma et al. 2007; Lacroix et al. 2010; Sudo and Baas 2010). Creating

these microtubules and using them in severing assays could indicate whether katanin indeed targets post-translation modifications. This could also give further information about katanin is regulated in cells. Since most tubulin we purify from pig brains has a mixture of alpha and beta isoforms and post-translational modifications (Alexander et al. 1991), katanin could be targeting modifications and not defects specifically. However, this would not account for the more frequent severing at locations where microtubules have end-to-end annealed. Future work needs to be done to further differentiate katanin's targeting mechanism on Taxol-stabilized microtubules, and how this would translate *in vivo*.

We have also shown that katanin p60 severing activity on Taxol-stabilized microtubules is effectively inhibited by low concentrations of free tubulin due to katanin preferentially binding to the free tubulin over the microtubule. Of the CTTs we tested, beta-tubulin CTT constructs are the best inhibitors of this severing activity, and detyrosinated alpha-tubulin CTT constructs are the least effective. However, there are many open questions remaining. The first question that needs to be addressed, is how katanin can remain functional in cells if it is so sensitive to free tubulin. We have suggested several possible explanations that need to be explored further. First, the regulatory partner protein p80 could target p60 to microtubules. Since p80 has been shown previously to enhance severing activity and is known to be targeted to centrosomes, this could be one plausible explanation (K. P. McNally, Bazirgan, and McNally 2000). In the future, it is important to further characterize the p60/p80-microtubule interaction with free tubulin. Other important experiments would be to further characterize post-translational modifications of p60 itself, as well as how post-translational modifications may modify p60's targeting mechanisms. It is very plausible that phosphorylation of katanin could modify its severing activity. It has been shown

previously to negatively regulate severing activity in some species of Xenopus and there are additional predicted modification sites that have not been confirmed yet (Whitehead, Heald, and Wilbur 2012). In addition to phosphorylation of p60, post-translational modification of tubulin could also regulate the severing activity. This is especially interesting since katanin was not as inhibited as effectively by the detyrosinated tubulin tail constructs. It would be interesting to test the katanin's severing activity on fully detyrosinated microtubules in vitro. Since other post-translational modifications have been suggested to enhance katanin severing activity (Sharma et al. 2007; Lacroix et al. 2010; Sudo and Baas 2010), acetylated and polyglutamylated microtubules should also be tested individually in severing assays.

Our dynamic instability experiments with p60 and tau have showed that both MAPs can make microtubules more dynamic, and these dynamics are enhanced at low concentrations of both together. However, these experiments have shown that there is still uncertainty about how katanin regulates dynamic microtubules. We observed that katanin was not able to sever dynamic microtubules. Since the severing activity we observe in vitro is robust on Taxol-stabilized microtubules, this was surprising. In the dynamic instability assays we used 7 μM- 20 μM tubulin, and we showed in chapter 3 that katanin was inhibited by free tubulin so this could be one reason we observed this phenomenon. Similar experiments with p80 and p60 need to be performed on dynamic microtubules to further characterize the interactions of katanin with dynamic microtubules. It is likely, that p60 is binding to the free tubulin instead of the microtubules and therefore is unable to sever the microtubules. P80 could help target p60 to the microtubules and will likely change the severing activity we were observing. Adding tau or other MAPs, such as Map4, could also provide additional information about regulation of dynamic microtubules. It is also possible that katanin acts as a microtubule

depolymerizer *in vivo* and therefore would not sever the dynamic microtubules. There is no direct evidence of microtubules being severing *in vivo*, the evidence for severing is the appearance of many short microtubules (Srayko et al. 2006). If katanin p60 is still unable to sever dynamic microtubules with p80 present, its role as a depolymerizer would be a very attractive theory.

The studies presented in this dissertation have begun to address how katanin regulates microtubule dynamics on both stable and dynamic microtubules. Despite the progress that we have made towards understanding how katanin targets microtubules, there are many questions that remain unanswered. The experiments outlined here would further out understanding of how katanin regulates microtubule dynamics, and begin to address how stabilizers and destabilizers work together to regulate dynamics in the cell.

APPENDIX A

TABLES OF FIT PARAMETERS

	Linear approximation m1*(1-(x/m2))+m3							
	m1	error	m2	error	m3	error	chisq	R2
Figure 2.3								
Taxol MTs	1.0139	0.00173	2724.9	48.293			0.0054	0.9704
Taxol MTs + E306Q-Xl-p60	0.97088	0.00197	4177.9	75.532			0.00546	0.94977
Figure 2.5								
High Salt MTs + E306Q-Xl-p60	0.98327	0.0024	2091.8	37.605			0.00672	0.97014
Figure 2.9								
Subtilisin MTs	0.00335	8381.1	34.806	9E+07	1.0664	8381.1	0.01137	0.40657
Figure 2.13								
Taxol MTs	0.37792	20155	1324.5	7E+07	0.5334	20155	0.00436	0.95985
Taxol MTs + E306Q-Xl-p60	0.34181	49812	299.83	4E+07	0.677	49812	0.02715	0.98079

	Single Exponential m1+m2*exp(-x/m3)							
	m1	error	m2	error	m3	error	Chisq	R2
Figure 2.3								
Taxol MTs + WT-Xl-p60	0.12647	0.05255	0.7446	0.0147	69.559	2.7227	0.07025	0.97544
Figure 2.5								
High Salt MTs	0.71739	0.00785	0.5196	0.0319	97.207	9.1879	0.05133	0.91551
High Salt MTs + WT-Xl-p60	0.17428	0.00394	0.8456	0.0246	53.445	2.124	0.04854	0.97327
Figure 2.9								
Subtilisin MTs + E306Q-Xl-p60	0.71298	0.07505	0.3121	0.0683	506.08	189.03	0.0134	0.90507
Subtilisin MTs + WT-Xl-p60	0.49444	0.00867	0.5439	0.0212	106.47	8.5026	0.05919	0.93912
Figure 2.13								
0 mM ATP	-2.5173	5.4022	3.5131	5.4022	3072.2	5065.4	0.10351	0.93383
28 μM ATP	0.20784	0.02118	0.8457	0.0179	312.98	13.815	0.01092	0.99536
100 μM ATP	-0.4928	0.20634	1.5361	0.2035	1022.3	167.73	0.01219	0.99375
500 μM ATP	0.1217	0.0127	1.1204	0.0202	116.16	5.4368	0.11953	0.97861
2 mM ATP	-0.0089	0.00955	1.2042	0.0097	146.76	3.8696	0.03359	0.9949
5 mM ATP	-0.7472	0.24445	1.8106	0.2406	1055.5	174.3	0.01127	0.24445
10 mM ATP	0.46967	0.00914	0.6006	0.0072	186.39	7.6831	0.01379	0.99135
20 mM ATP	-1.2801	0.39967	2.3457	0.3964	1574	309.39	0.00487	0.99706

Table A.1 Fits for Data in Chapter 2

	Linear approximation m1*(1-(x/m2))					
	m1	error	m2	error	chisq	R2
Figure 1						
MTs	0.94828	0.00396	1194.7	20.368	0.02816	0.96624
MTs + tubulin	1.0394	0.00321	2693.6	85.159	0.01852	0.91137
MTs + Xl-p60 + 6 μM tubulin	1.0455	0.00484	4374.5	337.65	0.03294	0.6575
MTs + Xl-p60 + 10 μM tubulin	1.1203	0.00436	1891.1	49.545	0.02682	0.93543

	Single Exponential m1+m2*exp(-x/m3)							
	m1	error	m2	error	m3	error	Chisq	R2
Figure 1								
MTs + Xl-p60	0.00983	0.00492	1.5889	0.0342	55.69	1.5357	0.06962	0.98734
MTs + Xl-p60 + 500 nM tubulin	0.01417	0.00564	3.5494	0.2809	25.321	1.2551	0.14198	0.95683
MTs + Xl-p60 + 1 μM tubulin	0.01559	0.00859	1.3122	0.0084	160.14	3.5921	0.01457	0.99722

Table A.2 Fits for Data in Figure 3.7

Microtubules Alone, fit equation: $I(t) = I_0\left(1 - t/\tau\right)$					
$I_0 = 0.998 \pm 0.002$	$\tau = 2140 \pm 50$ s			$\chi^2 = 0.0052$	$R^2 = 0.97$
MTs + Xl-p60, fit equation: $I(t) = I_0 \exp\left(-t/\tau\right) + I_\infty$					
$I_0 = 2.32 \pm 0.03$	$\tau = 0.022 \pm 0.001$ s	$I_\infty = 43.0 \pm 0.4$		$\chi^2 = 0.0028$	$R^2 = 0.999$
MTs + GFP-Hu-p60, fit equation: $I(t) = I_1 \exp\left(-t/\tau_1\right) + I_2 \exp\left(-t/\tau_2\right)$					
$I_1 = 3.7 \pm 0.1$	$\tau_1 = 30.7 \pm 0.7$ s	$I_2 = 0.191 \pm 0.001$	$\tau_2 = 470 \pm 40$ s	$\chi^2 = 0.0065$	$R^2 = 0.997$

Table A.3 Fits for Data in Figure 3.2

Association Rate, fit equation: $k\left(\left[c\right]\right)=k_{\max}\frac{\left[c\right]}{C_{1/2}+\left[c\right]}$			
k_{max} = 0.145 ± 0.008 1/s	$C_{1/2}$ = 50 ± 10 nM	χ^2 = 0.00025	R^2 = 0.91
First Severing Rate, fit equation: $k\left(\left[c\right]\right)=k_{\max}\frac{\left[c\right]}{C_{1/2}+\left[c\right]}$			
k_{max} = 0.17 ± 0.05 1/s	$C_{1/2}$ = 300 ± 160 nM	χ^2 = 0.00051	R^2 = 0.89
Severing Activity Rate, fit equation: $k\left(\left[c\right]\right)=k_{\max}\frac{\left[c\right]}{C_{1/2}+\left[c\right]}$			
k_{max} = 0.10 ± 0.01 1/s	$C_{1/2}$ = 80 ± 40 nM	χ^2 = 0.00046	R^2 = 0.77
Total Severing Rate, fit equation: $k\left(\left[c\right]\right)=k_{\max}\frac{\left[c\right]}{C_{1/2}+\left[c\right]}$			
k_{max} = 0.057 ± 0.006 1/s	$C_{1/2}$ = 130 ± 40 nM	χ^2 = 0.000047	R^2 = 0.93
Ratio of Severing Activity Rate to First Severing Rate (average)			
average = 1.0	Standard deviation = 0.2		
Maximum GFP-Katanin Intensity, fit equation: $I\left(\left[c\right]\right)=I_{\max}\frac{\left[c\right]}{C^*+\left[c\right]}$			
I_{max} = 1000 ± 600	C* = 80 ± 20	χ^2 = 970000	R^2 = 0.95

Table A.4 Fits for Data in Figure 3.4

Microtubules + p60, fit equation: $I(t) = I_1 \exp\left(-t/\tau_1\right) + I_2 \exp\left(-t/\tau_2\right)$					
$I_1 = 0.7 \pm 0.1$	$\tau_1 = 18 \pm 5$ s	$I_2 = 0.40 \pm 0.06$	$\tau_2 = 360 \pm 80$ s	$\chi^2 = 1.1$	$R^2 = 0.69$
Microtubules + p60 + 50 nM tubulin, fit equation: $I(t) = I_0 \exp\left(-t/\tau\right) + I_\infty$					
$I_0 = 0.50 \pm 0.01$	$\tau = 220 \pm 12$ s	$I_\infty = 0.52 \pm 0.01$		$\chi^2 = 0.01$	$R^2 = 0.99$
Microtubules + p60 + 500 nM tubulin, fit equation: $I(t) = I_0\left(1 - t/\tau\right)$					
$I_0 = 1.032 \pm 0.004$	$\tau = 4600 \pm 300$ s			$\chi^2 = 0.018$	$R^2 = 0.75$
Microtubules + p60 + 1 μM tubulin, fit equation: $I(t) = I_0\left(1 - t/\tau\right)$					
$I_0 = 0.979 \pm 0.002$	$\tau = 3700 \pm 100$ s			$\chi^2 = 0.0037$	$R^2 = 0.94$
Microtubules + p60 + 6 μM tubulin, fit equation: $I(t) = I_0\left(1 - t/\tau\right)$					
$I_0 = 0.150 \pm 0.005$	$\tau = 190 \pm 20$ s	$I_\infty = 0.870 \pm 0.007$		$\chi^2 = 0.0054$	$R^2 = 0.94$
Microtubules + p60 + 10 μM tubulin, fit equation: $I(t) = I_0 \exp\left(-t/\tau\right) + I_\infty$					
$I_0 = 0.079 \pm 0.005$	$\tau = 130 \pm 30$ s	$I_\infty = 0.927 \pm 0.005$		$\chi^2 = 0.0074$	$R^2 = 0.76$
Maximum GFP-Katanin Intensity, fit equation: $I([c]) = I_\infty \exp\left(-[c]/C^*\right)$					
$I_0 = 3400 \pm 300$		C* = 3100 ± 900 nM		$\chi^2 = 350000$	$R^2 = 0.96$

Table A.5 Fits for Data in Figure 3.6

Microtubules + p60, fit equation: $I(t) = I_1 \exp\left(-t/\tau_1\right) + I_2 \exp\left(-t/\tau_2\right)$					
I_1 = 4800 ± 100	τ_1 = 14.2 ± 0.4 s	I_2 = 900 ± 20	τ_2 = 390 ± 30 s	χ^2 = 140000	R^2 = 0.99
Microtubules + p60 + 50 nM tubulin, fit equation: $I(t) = I_1 \exp\left(-t/\tau_1\right) + I_2 \exp\left(-t/\tau_2\right)$					
I_1 = 180 ± 70	τ_1 = 20 ± 1 s	I_2 = 370 ± 40	τ_2 = 210 ± 30 s	χ^2 = 100000	R^2 = 0.98
Microtubules + p60 + 500 nM tubulin, fit equation: $I(t) = I_1 \exp\left(-t/\tau_1\right) + I_2 \exp\left(-t/\tau_2\right)$					
I_1 = 420 ± 10	τ_1 = 27 ± 2 s	I_2 = 160 ± 10	τ_2 = 500 ± 100 s	χ^2 = 110000	R^2 = 0.98
Microtubules + p60 + 1 μM tubulin, fit equation: $I(t) = I_1 \exp\left(-t/\tau_1\right) + I_2 \exp\left(-t/\tau_2\right)$					
I_1 = 1170 ± 30	τ_1 = 17.2 ± 0.7 s	I_2 = 240 ± 20	τ_2 = 140 ± 10 s	χ^2 = 150000	R^2 = 0.994
Microtubules + p60 + 6 μM tubulin, fit equation: $I(t) = I_1 \exp\left(-t/\tau_1\right) + I_2 \exp\left(-t/\tau_2\right)$					
I_1 = 990 ± 30	τ_1 = 12.8 ± 0.5 s	I_2 = 160 ± 10	τ_2 = 87 ± 5 s	χ^2 = 5000	R^2 = 0.995
Microtubules + p60 + 10 μM tubulin, fit equation: $I(t) = I_1 \exp\left(-t/\tau_1\right) + I_2 \exp\left(-t/\tau_2\right)$					
I_1 = 1000 ± 30	τ_1 = 19.6 ± 0.9 s	I_2 = 80 ± 40	τ_2 = 60 ± 10 s	χ^2 = 4000	R^2 = 0.998
Maximum GFP-Katanin Intensity, fit equation: $\tau([c]) = \tau_0 \exp\left(-[c]/C^*\right) + \tau_\infty$					
τ_0 = 1000 ± 30 s	C* = 1400 ± 700 nM	τ_∞ = 70 ± 10 s		χ^2 = 320	R^2 = 0.98

Table A.6 Fits for Data in Figure 3.9

Microtubules alone, fit equation: $I(t) = I_0\left(1 - t/\tau\right)$					
$I_0 = 0.984 \pm 0.002$	$\tau = \infty$ s			$\chi^2 = 0.0035$	$R^2 = 0.427$
Microtubules + p60, fit equation: $I(t) = I_1 \exp\left(-t/\tau_1\right) + I_2 \exp\left(-t/\tau_2\right)$					
$I_1 = 3.5 \pm 0.2$	$\tau_1 = 28.2 \pm 0.8$ s	$I_2 = 0.084 \pm 0.007$	$\tau_2 = 700 \pm 200$ s	$\chi^2 = 0.003$	$R^2 = 0.996$
Microtubules + p60 + 50 nM tubulin, fit equation: $I(t) = I_0 \exp\left(-t/\tau\right) + I_\infty$					
$I_0 = 0.52 \pm 0.03$	$\tau = 51 \pm 2$ s	$I_\infty = 0.755 \pm 0.001$		$\chi^2 = 0.0028$	$R^2 = 0.98$
Microtubules + p60 + 50 nM tubulin denatured tubulin, fit equation: $I(t) = I_0\left(1 - t/\tau\right)$					
$I_0 = 1.031 \pm 0.002$	$\tau = 2860 \pm 80$ s			$\chi^2 = 0.0036$	$R^2 = 0.95$
Microtubules + p60 + 50 nM tubulin denatured subtilisin-treated tubulin, fit equation: $I(t) = I_1 \exp\left(-t/\tau_1\right) + I_2 \exp\left(-t/\tau_2\right)$					
$I_1 = 3.2 \pm 0.2$	$\tau_1 = 33 \pm 1$ s	$I_2 = 0.3 \pm 0.01$	$\tau_2 = 480 \pm 40$ s	$\chi^2 = 0.0050$	$R^2 = 0.997$

Table A.7 Fits for Data in Figure 3.11

Microtubules alone, fit equation: $I(t) = I_0\left(1 - t/\tau\right)$					
I_0 = 0.984 ± 0.002	$\tau = \infty$ s			χ^2 = 0.0035	R^2 = 0.427
Microtubules + p60, fit equation: $I(t) = I_1 \exp\left(-t/\tau_1\right) + I_2 \exp\left(-t/\tau_2\right)$					
I_1 = 3.5 ± 0.2	τ_1 = 28.2 ± 0.8 s	I_2 = 0.084 ± 0.007	τ_2 = 700 ± 200 s	χ^2 = 0.003	R^2 = 0.996
Microtubules + p60 + 50 nM tubulin, fit equation: $I(t) = I_0 \exp\left(-t/\tau\right) + I_\infty$					
I_0 = 0.52 ± 0.03	τ = 51 ± 2 s	I_∞ = 0.755 ± 0.001		χ^2 = 0.0028	R^2 = 0.98
Microtubules + p60 + 50 nM βCTT-BSA, fit equation: $I(t) = I_0 \exp\left(-t/\tau\right) + I_\infty$					
I_0 = 0.101 ± 0.007	τ = 130 ± 20 s	I_∞ = 0.877 ± 0.005		χ^2 = 0.0032	R^2 = 0.85
Microtubules + p60 + 50 nM αCTT-BSA, fit equation: $I(t) = I_0 \exp\left(-t/\tau\right) + I_\infty$					
I_1 = 0.39 ± 0.01	τ = 86 ± 4 s	I_∞ = 0.661 ± 0.003		χ^2 = 0.0029	R^2 = 0.98
Microtubules + p60 + 50 nM ΔY-αCTT-BSA, fit equation: $I(t) = I_1 \exp\left(-t/\tau_1\right) + I_2 \exp\left(-t/\tau_2\right)$					
I_1 = 1.8 ± 0.2	τ_1 = 26 ± 1 s	I_2 = 0.646 ± 0.004	τ_2 = 1270 ± 40 s	χ^2 = 0.0018	R^2 = 0.995

Table A.8 Fits for Data in Figure 3.13

APPENDIX B

PROTOCOLS

B.1 Silanization of Coverslips

*It is important to clean the racks and glass containers thoroughly before silanization.
*Do not let anything that is not dry come in contact with the silane.
*Rinse container 3X with water then 3X with ddH_2O for each step.

Clean Coverslips:
1. Immerse the coverslips in 100% acetone for 1 hour.
2. Immerse the coverslips in 100% ethanol for 10 minutes.
3. Rinse 3X in ddH_2O for 5 minutes each.
4. Immerse the coverslips in 0.1M KOH for 15 minutes (prepare just before use).
5. Rinse 3X in ddH_2O for 5 minutes each.
6. Air Dry Coverslips.

Silanization of Coverslips:
1. Once cleaned coverslips have dried completely, immerse in 2% DDS (dimethyldichlorosilane) for 5 minutes.
2. Use a funnel to pour the silane solution back into the bottle to reuse.
3. Immerse the coverslips in 100% ethanol for 5 minutes.
4. Immerse the coverslips in another 100% ethanol for 5 minutes.
5. Rinse 3X in ddH_2O for 5 minutes each.
6. Air Dry.

B.2 Acid Washed Coverslips

Use this method of cleaning coverslips for dynamic instability if coating with PLL-PEG-BIOTIN. It came from (Montenegro Gouveia et al. 2010).

1. Place coverslips in thoroughly cleaned racks and place the racks in the clean glass container.
2. Add Isopropanol to the glass container and cover completely with parafilm.
3. Sonicate in the water bath sonicator for 20 minutes.
4. Wash 3Xwith ddH_2O for 5 minutes each.
5. Add 1M KCl and cover the container with parafilm completely.
6. Sonicate in the water bath sonicator for 20 minutes.
7. Wash 3X with ddH_2O for 5 minutes each.

B.3 Nitrocellulose Coverslips

*Nitrocellulose coverslips are used for the gliding assays with actin and microtubules. These should be made fresh each week, and/or if possible kept in a humidor.

1. Wash a 2 L beaker thoroughly with soap and water. Rinse the beaker 3X with water then 3X with ddH_2O.
2. Fill the beaker with ddH_2O to about ¾ full.
3. Add 300 μL of nitrocellulose. Make sure to eject the liquid as fast as possible below the surface of the water.
4. Allow a layer of nitrocellulose film to completely form on the surface of the water. This will take 20-30 minutes.
5. Adhere coverslips to 10 mM plate (like used for bacterial plates) with a drop of water. About 7 square coverslips will fit on the surface.
6. Once the film has formed, place the plate, coverslip side down, on the film and quickly turn it over to avoid double layers of nitrocellulose (involves pushing one side under the water).
7. Let the coverslips dry in a covered location.

B.4 Tubulin Purification

Stock Solutions:	PM Buffer (200mL)	PMG Buffer (200mL)
200mM PIPES	100mL	76mL
200mM EGTA	2mL	2mL
100mM $MgSO_4$	2mL	2mL
Glycerol (from bottle)	-------	116mL

	Super PMG (200mL)
1M PIPES	16mL
1M $MgSO_4$	2mL
200mM EGTA	2mL
13.7M Glycerol	175.2mL

*When brains arrive, bring these items cold room: PM and 10 ultra centrifuge tubes (red caps) on ice, kimwipe, gloves, bag for brain junk, funnel, 1L beaker.
*Make sure the ultra centrifuge and 50.2 Ti rotor are cooling to 2^{o}C.

1X Pellets:

1. Clean pig brains (We usually use 3) and put in pre-tared 1L beaker.
   Remove meniscus, etc. (use kimwipe to help clean)
2. Weigh cleaned brains: _____g
3. Add brain parts into the blender.
   Add 0.5mL PM buffer per 1g of brain. Volume of PM: _____mL
4. Pulse blender until brains are homogenized.
   (~5 seconds/pulse to prevent mixture from heating up)
5. Pour homogenized brains into ultra centrifuge tubes.
   (Bring over 8-10 to the cold room)
6. Balance tubes.
7. Centrifuge at 100,000 xg for 45 minutes at 2^{o}C with 50.2 Ti rotor.
   *If too much brain material, you may need to do a second spin. Leave the centrifuge tubes with brains on ice until done with spins.
8. Pour supernatant into 500mL graduated cylinder.
   *Use pasteur pipette to get all the supernatant.
   Volume of sup: _____mL
9. Add same volume of PMG to the supernatant (1:1 PMG:supernatant ratio)
   *If supernatant volume is greater than 100mL, add ½ volume of sup as super PMG
10. Add GTP to final concentration of 1mM.
    _____mL of 100mM GTP stock
11. Cover graduated cylinder with parafilm and mix by inverting.
12. Put sup into new ultra centrifuge tubes and balance.
13. Polymerize MTs for 45 minutes at 37^{o}C in water bath.
14. Set ultra centrifuge to 37^{o}C, place T865 rotor in 37^{o}C incubator to warm up.
15. Centrifuge at 100,000 xg in T865 rotor for 45 minutes at 37^{o}C.

(can drop freeze and store at -80^{o}C or continue)

2X Pellets:

1. Add PM to pellets using 1/5 volume of original homogenate (1X pellets, step 3)
   Volume of PM Buffer added: _____mL
2. Using a thin, pointed spatula, scrape pellet off side of centrifuge tube and into PM buffer
   Lightly shake tube to make sure pellet is loose
   Quickly dump PM buffer + pellet into 15mL dounce in ice slurry
   Repeat for each pellet
3. Homogenize pellets in ice cold dounce until no large chunks seen (will be cloudy)
   Homogenize on ice every 2-3 minutes, for a total of 30 minutes (avoid excessive bubbling)
4. Put homogenized tubulin into ultra (T865) centrifuge tubes
5. Centrifuge 100,000 xg for 30 minutes at 2°C
6. Pour sup into graduated cylinder and approximate volume
   Volume of supernatant: _____mL
7. Add PMG buffer 1:1 with supernatant
   Add _____mL PMG
8. Add GTP to final concentration of 1mM
   Add _____μL 100mM GTP stock
9. Parafilm cylinder and mix by inverting
10. Put supernatant into new ultra T865 centrifuge tubes and incubate 45 minutes at 37°C in water bath
11. Centrifuge at 37°C for 45 minutes at 100,000 xg
12. Remove most of sup, leaving a small amount to cover pellets
13. Drop freeze pellets in liquid nitrogen and store at -80°C

High Salt Purification:

1. Quickly thaw 2X pellets in 37°C water bath.
2. Remove excess supernatant that froze with pellet
3. Take 2X pellets (should be 2) and homogenize with dounce in 5mL PM buffer for 30 minutes on ice. Homogenize on ice every 2-3 minutes, for a total of 30 minutes, avoid excessive bubbling.
4. Spin at 100,000 xg at 4°C (T865 rotor) for 30 minutes
5. Save supernatant and add:
   0.5 M PIPES
   10% DMSO
   1 mM GTP
   2 mM EGTA
   1 mM $MgSO_4$
6. Incubate at 37°C for 10 minutes.
7. Spin 20 minutes at 20,000 xg at 37°C (T865 rotor).
   *Turn on the small ultra centrifuge to cool down.
8. Using dounce, homogenize pellet in 4mL PEM-100 on ice for 30 minutes
9. Spin 30 minutes at 100,000 xg at 4°C in the **small** ultra centrifuge.
10. Save supernatant as high salt purified tubulin.

*Depending on the gel of the purification, the high salt purification may need to be done more than once.

11. Bring tubulin to 5 mg/mL using PEM-100.
12. Aliquot and drop freeze in liquid nitrogen, store in -80^{o}C.

B.5 Tubulin Labeling

BUFFERS:

5X BRB-80	High pH Cushion	Labeling Buffer
400 mM PIPES 8.6	0.1 M NaHEPES, pH 8.6	0.1 M NaHEPES, pH
5 mM $MgCl_2$	1 mM $MgCl_2$	1 mM $MgCl_2$
5 mM EGTA	1 mM EGTA	1 mM EGTA
pH 6.8 with KOH	60% (v/v) glycerol	40% (v/v) glycerol

Quench	Low pH Cushion	PEM-100
2X BRB-80	60% (v/v) glycerol	100 mM Na-PIPES
100 mM K-Glutamate	in 1X BRB-80	1 mM $MgSO_4$
40% (v/v) glycerol		1 mM EGTA
		pH 6.8

1. Thaw high salt purified tubulin: _____mg in _____mL.
2. Add MgCl2 to 4 mM: _____μL of 1M stock.
3. Add GTP to 1 mM: _____μL of 100 mM stock.
4. Incubate on ice for 5 minutes.
5. Warm to 37°C in the water bath.
   *Use ultra centrifuge tubes.
6. Add DMSO to 10% final concentration: _____μL.
   *Add in 2 steps, mix gently but thoroughly.
7. Incubate at 37°C (water bath) for 45 minutes.
8. Warm 15mL high pH cushion in a 25 mL centrifuge tube to 37°C.
9. Layer MTs onto cushion (with cut 1mL pipette tip).
10. Spin for 35 minutes in T865 rotor at 53,000 rpm (285,500 xg) at 37°C.
11. Dissolve 1mg of dye into 50μL DMSO.
    (We usually use DyLight 650 NHS Ester, Prod #62265, Thermo Scientific).
12. Warm 3 mL Labeling Buffer to 37°C.
13. After spin, remove the supernatant above the cushion.
14. Rinse supernatant-cushion interface 2 times (1mL each) with warm Labeling Buffer.
15. Remove cushion.
16. Resuspend pellet in 600μL warm Labeling Buffer using cutoff large pipette tip.
    *Keep tubulin warm during resuspension.
    *Continue resuspending until no chunks of tubulin are visible.
17. Add the dye to the tubulin (should be 10-20 fold molar excess of dye to tubulin)
    *Can estimate tubulin concentration by assuming 70% recovery of starting tubulin. We usually use all the dye.
18. Incubate at 37°C for 45 minutes.
    *Gently vortex mixture every 2-3 minutes during labeling reaction. There will be bubbles. Try to minimize as much as possible.
19. Warm 1mL Quench to 37°C and warm 5mL Low pH cushion in 10mL centrifuge tube to 37°C.
20. Add equal volume of Quench to labeling reaction and mix well.
21. Incubate 5 minutes at 37°C.
22. Layer labeling reaction onto low pH cushion.

23. Centrifuge 35 minutes at 50,000 rpm (225,600 xg) in 50Ti rotor at 37°C.
24. Warm 3 mL 1x BRB-80 to 37°C,
25. Remove the supernatant from above the cushion.
26. Rinse the supernatant-cushion interface 2 times with 1 mL warm 1x BRB-80.
27. Remove cushion.
28. Rinse pellet with 1 mL warm 1x BRB-80.
29. Resuspend pellet in 800μL of ice cold PEM-100 using cutoff large pipette tip.
30. Transfer resuspended chunks of the pellet to a small ice cold dounce (1-2mL volume) in an ice cold water bath.
31. Resuspend pellet by gentle douncing until suspension is uniform.
    *Continue douncing every 2-3 minutes for total time of 30 minutes.
32. Spin depolymerized tubulin for 20 minutes at 71,000 rpm (227,000 xg) in small ultra at 4°C.
33. Transfer supernatant to a new tube and estimate volume: _____μL.
34. Add: BRB-80 to 1x: _____μL of 5x stock
    $MgCl_2$ to 4 mM: _____μL of 1M stock
    GTP to 1 mM: _____μL of 100 mM stock
35. Incubate on ice for 5 minutes.
36. Warm to 37°C for 2 minutes.
37. Add ½ volume of glycerol (33% v/v final) and mix well.
38. Incubate 45 minutes at 37°C.
39. Warm 5 mL Low pH cushion in 10 mL centrifuge tube to 37°C.
40. Layer MTs onto cushion.
41. Spin 35,000 rpm (110,600 xg) in 50Ti rotor at 37°C for 35 minutes.
42. Warm 4 mL 1x BRB-80 to 37°C.
43. After spin, remove supernatant above the cushion.
44. Rinse the supernatant-cushion interface 2 times with 1 mL 1x BRB-80.
45. Remove the cushion.
46. Rinse pellet 2 times with 1 mL 1x BRB-80 to remove residual glycerol.
47. Resuspend pellet in 300μL ice cold PEM-100 using cut large pipette tip.
    *Pellet should resuspend easily.
48. Transfer to dounce and homogenize in ice water slurry for 20-30 minutes.
49. Transfer to small ultra centrifuge tubes.
50. Spin for 15 minutes at 144,400 xg in small ultra at 4°C.
51. Recover supernatant and bring to 5 mg/mL final concentration.
52. Aliquot and drop freeze in LN_2.

Calculate Protein Concentration:

$$\text{Protein Concentration (M)} = \frac{[A_{280} - (A_{max} \times CF)]}{\varepsilon_{protein}} \times \text{dilution factor}$$

$\varepsilon_{tubulin\ @\ 280nm} = 115{,}000\ M^{-1}\,cm^{-1}$
$CF = A_{280}$ of fluorophore / A_{max} of fluorophore

Calculate Degree of Labeling:

$$\text{Moles dye per mole protein} = \frac{A_{max} \text{ of labeled protein} \times \text{dilution factor}}{\varepsilon_{fluor} \times \text{protein concentration (M)}}$$

B.6 SF9 Katanin Purification

Notes:
*Use 10 % protease-free sucrose in the whole process to stabilize the protein.
*Before elution use cheap ATP from Fisher, but for elution, buffer exchange and assays use ATP for enzyme dynamics analysis from calbiochem.
*There are two severing buffers. Buffer I is for buffer exchange only, Buffer II is for scope or pellet assays.

Resuspension Buffer I (make up at least 600 mL):

50	mM	Tris
250	mM	NaCl
5	mM	$MgCl_2$
10	%	Sucrose
20	mM	Imidazole
50	μM	ATP*
1	mM	PMSF*
7	mM	bME*

* pH to around 7.0 using HCL before adding ATP, PMSF, bME. Add ddH2O to 600 ml.
*Add just before use to 90 mL of Resuspension buffer to make it complete.

Resuspension Buffer II/Severing Buffer (used for imaging):

20	mM	Hepes
100	mM	NaCl
3	mM	$MgCl_2$
10	%	Sucrose

*pH to 7.0

1. Pellet cells at 5000 rpm for 15 min at 4°C.
2. Resuspend cells in 20 mL Resuspension Buffer (+ATP 50 μM + bME + PMSF). For 500 mL culture make 600 mL RB.
3. Homogenize cells using a french press- three passes. (Bring to Tom Maresca's lab: pipette gun, 10 ml pipette, isopropanol, Resuspended cells, Buffer +ATP, Parafilm, ddH2O, paper towels.) Centrifuge at 30,000 xg for 45 minutes at 4 °C.
4. Separate the super and add washed Ni+ Agarose beads. Incubate for 2 hrs at 4 °C with rocking.
5. Pellet beads.
6. Prepare Wash Buffer (100 mL RB+ ATP 200 μM +50 μL bME). Wash bound beads 2x with 20 mM Imidazole and 5x with 40 mM Imidazole, for the last wash transfer to a column.
7. Make Elution Buffer – 10 ml (Add Imidazole to final concentration of 0.5 M + 9 ml RB + 5 μL bME + 100 μL PMSF + 7 μL ATP from Calbiochem.)
8. (In column) Elute the protein with 0.5 M EB (0.5 ml-1 ml fractions, ~3 elutions). Incubate 5-10 min. before the first elution at 4 °C.
9. Do a dot blot and pool elutions with protein.
10. Buffer exchange eluted protein fraction into severing buffer I (20 mM Hepes, PH7, 300 mM NaCl, 3 mM MgCl2, 5 mM DTT, 50 μM ATP, 10 % sucrose) in buffer exchange columns. Minimize the volume to about 50 μL. Check the concentration.

B.7 Bacterial Katanin Purification

Resuspension Buffer:
20 mM Hepes pH 7.7
250 mM NaCl
10% glycerol
*0.5 mM BME
*0.25 mM Mg*ATP (pH 7!)
*1 mM PMSF
*Protease inhibitors:
2 mg/mL Aprotinin
2 mg/mL Pepstatin
2 mg/mL Leupeptin
* Add Day of to 50 mL of Resuspension buffer

Katanin Activity Buffer (KAB):
20 mM Hepes pH 7.7
2 mM $MgCl_2$
10 % glycerol

Day 1:
7. Transform p60 into BL21 cells. Plate on Amp plates.

Day 2:
7. Pick 3 colonies and start 3 overnight start cultures with Ampicillin and Chloramphenicol.
8. Make up 3x 400 mL of LB.
1 L LB:
10 g NaCl
10 g tryptone
5 g yeast extract

Day 3:
1. Add Ampicillin and Chloramphenicol to flasks of LB. Antibiotics are made up for a 1:1000 dilution into cultures.
2. Add starter cultures to flasks of LB. Should be 1:100 dilution so for 1 L add 10 mL of starter culture.
3. Grow cultures in shaking incubator at 37 C until it reaches an O.D. of 0.8. This usually takes about 6 hours.
4. Add 1 mM IPTG (1 M stock) to the culture. Bring the culture to Tom Maresca's Lab and grow in the shaker at 16 C for 15-18 hours. Lab code: 7995

Day 4:
1. Pellet bacteria at 5,000 rpm for 15 min. DO NOT FREEZE.
2. Make up 50ml of resuspension buffer.
*Remember to add Protease inhibitors as well.
1. Resuspend pellets in 15 ml of Resuspension Buffer.
2. Lyse cells using the sonicator every 20 seconds for 20 seconds for a total of 3 minutes.
3. Transfer sonicated lysate to red capped centrifuge tube.
4. Centrifuge in T865 at 13,000 rpm for 30 minutes.
5. Incubate lysate with ~1 ml bed volume of amylose resin for ~1.5-2 hours at 4C.

*Wash resin before in column/resuspension buffer 3x. 2x with water, 1x with resuspension buffer at 3,000 RPM for 5 minutes each.

6. Pour lysate into column and wash with ~20 mL of resuspension buffer.
7. Elute with 10 mM Maltose in resuspension buffer (50 µL of 1 M maltose to 5mL of completed resuspension buffer).
8. Perform bradford to get concentration.

B.8 Tau Purification

Day 1:
Transform Tau into Rosetta cells.

Day 2:
Set up overnight culture.

1. Take plate out of 37°C incubator, parafilm and store in the deli case fridge.
2. Set up 5 mL starter culture (5 mL LB + 5 μL AMP + colony from plate).
3. Leave in 37°C incubator overnight to grow.
4. Make 400 mL 2xYT in 1 L flask and autoclave.

Day 3:
Start growing culture and Induce.

1. Add 5 mL starter culture to 400 mL of 2xYT in 1L Flask.
2. Grow culture until it reaches an O.D. of 0.6-1.0
3. Take gel sample- "Uninduced sample"
4. Add 1 M IPTG (final concentration: 1 mM).
5. Incubate for 3-4 hours at 37°C.
6. Take gel sample- "Induced sample".
11. Centrifuge cultures in 500 mL centrifuge bottles at 5,0000 RPM for 15 minutes, 4°C.
12. Resuspend pellet in 5-10 mL of PEM-100 + 1 mM PMSF. The pellet can be stored in 50mL conical in the freezer at this point.

Day 4:
Purification.

1. Thaw pellets on ice.
2. Sonicate 3x for 1 minute each at power level 3, rest for 1 minute.
3. Centrifuge in tabletop centrifuge at top speed for 10 minutes.
4. Place supernatant in a new microcentrifuge tube.
5. Take "lysed" sample for gel.
6. Add 500 mM NaCl to supernatants.
1. Boil samples for 20 minutes in heat block by gel station. Poke holes in tops of the tubes so they don't "pop".
2. Take "boiled" sample for gel.
3. Centrifuge samples at 13,000 RPM in the tabletop centrifuge for 30 minutes at 4°C.
10. Take sample of supernatant for gel.
11. Buffer exchange samples with NAP-5 column to remove salt. (May need to concentrate with spin column after.)
12. Freeze in aliquots in -80°C.

Day 5:

Gels for concentration and to check purity.

(A) Run gels of samples from purification steps.

(B) Run gel with BSA standards to get concentration of Tau.

Experiments to test protein:

(A) Test whether Tau bundles microtubules and over what concentration range.

(B) Pelleting assays with microtubules to make sure that Tau is binding to microtubules as it should.

B.9 Taxol-stabilized Microtubule Polymerization

1. Mix labeled tubulin with unlabeled tubulin. (I have been using microtubules that are 20% labeled).
2. Centrifuge at 90,000 rpm for 10 minutes at 4°C.
3. Transfer supernatant to 1.5mL tube.
4. Add GTP (stock is at 100 mM) to 1 mM.
5. Incubate at 37°C in the incubator for 20 minutes.
6. Add 50 μM Taxol (stock is at 2 mM).
7. Incubate at 37°C in the incubator for 20 minutes.
8. Centrifuge 10 minutes in tabletop centrifuge at 14,000 rpm, room temp.
9. Resuspend pellet in original volume of PEM + 50 μM Taxol.

We usually use the microtubules at a 1:100 dilution.

<u>1:100 Microtubule Dilution</u>

98 μL PEM-100
1 μL 2 mM Taxol
1 μL 5mg/mL polymerized microtubules

B.10 High Salt Microtubule Polymerization

1. Mix labeled tubulin with unlabeled tubulin. (I have been using microtubules that are 20% labeled).
2. Centrifuge at 90,000 rpm for 10 minutes at 4°C.
3. Transfer supernatant to 1.5mL tube.
4. Add GTP (stock is at 100 mM) to 1 mM and NaCl to 580 mM (stock is at 5M).
5. Incubate at 37°C in the incubator for 20 minutes.
6. Add 50 μM Taxol (stock is at 2 mM).
7. Incubate at 37°C in the incubator for 20 minutes.
8. Centrifuge 10 minutes in tabletop centrifuge at 14,000 rpm, room temp.
9. Resuspend pellet in original volume of PEM + 50 μM Taxol.

B.11 Subtilisin-Treated Taxol-stabilized Microtubule Polymerization

1. Mix labeled tubulin with unlabeled tubulin. (I have been using microtubules that are 20% labeled).
2. Centrifuge at 90,000 rpm for 10 minutes at 4°C.
3. Transfer supernatant to 1.5mL tube.
4. Add GTP (stock is at 100 mM) to 1 mM.
5. Incubate at 37°C in the incubator for 20 minutes.
6. Add 50 μM Taxol (stock is at 2 mM).
7. Incubate at 37°C in the incubator for 20 minutes.
8. Add 4 mg/mL subtilisin.
9. Incubate at 37°C for 45 minutes.
10. Add 4 mM PMSF.
11. Incubate at room temperature for 15 minutes.
12. Centrifuge for 30 minutes, 27°C, at 16,000 xg.
13. Resuspend pellet in original volume of PEM + 50 μM Taxol + 1 mM GTP.

*It is best to use these microtubules within a few days of making them.

B.12 Severing Assay

* Chambers are assembled on glass slides that have been washed with 70% ethanol. Use doublestick tape to make a chamber with a silanized coverslip.

1. Flow in 2% anti-tubulin antibody (0.4 μL YL1/2 tubulin antibody + 9.6 μL PEM-100. Incubate 5 minutes.
2. Flow in 5% F-127. Incubate for 5 minutes.
3. Flow in 1:100 MTs. Incubate 5-7 minutes.
4. Flow in KAB-rxn #1 buffer.
5. Image 3 minutes.
6. Flow in Katanin in KAB-rxn buffer #2 (1:10 katanin:rxn buffer).

KAB-rxn Buffer 1:

2 μL	0.5% F-127
1 μL	DTT (1 M stock)
1 μL	BSA (100 mg/mL stock)
0.5 μL	Taxol (2 mM stock)
0.8 μL	ATP (50 mM stock)
1 μL	glucose (300 mg/mL stock)
1 μL	deoxy
12.7 μL	KAB
20 μL TOTAL	

KAB-rxn Buffer 2:

2 μL	0.5% F-127
1 μL	DTT (1 M stock)
1 μL	BSA (100 mg/mL stock)
0.5 μL	Taxol (2 mM stock)
0.8 μL	ATP (50 mM stock)
1 μL	glucose (300 mg/mL stock)
1 μL	deoxy
2 μL	Katanin (10x stock)
10.7 μL	KAB
20 μL TOTAL	

B.13 Dynamic Instability Assay

Microtubule seeds:
43 μL unlabeled tubulin 5mg/mL
3 μL rhodamine tubulin (resuspended in 4 μL Pem-100 initially)
4 μL biotin tubulin (resuspended in 4 μL of PEM-100 initially)

1. Centrifuge in microultra for 10 min. at 4C, 90,000 RPM
2. Take off supernatant and put in a new 1.5mL centrifuge tube and add 5uL of 10mM GMPCPP.
3. Incubate at 37°C for 30 minutes.
4. Pellet seeds in tabletop centrifuge at 14,000 RPM for 15 minutes at 35°C.
5. Remove supernatant and resuspend in warm GMPCPP + PEM-100 (heat in 37°C water bath during previous step). (45uL PEM-100 + 5uL GMPCPP)
6. Shear seeds 4 times with hamilton syringe.
7. Store at 37C until ready to use.

Elongation Mix: -start after seeds are ready
29 μL of 5 mg/mL unlabeled tubulin
1L 5 mg/mL rhodamine tubulin

1. Centrifuge at 90,000 RPM for 10 minutes, 4°C.
2. Transfer to a 1.5 mL tube because ultra tubes sink to the bottom of the ice bucket!

Lasts about 4-5 hours.

Chambers:
-Use acid washed coverslips.

Experiments:
3. Flow in 7 μL of 0.2 mg/mL PLL-PEG-Biotin. Incubate for 5 minutes.
4. Wash chamber with PEM-100.
5. Flow in 7 μL 1 mg/mL streptavidin.
6. Add 7 μl of 1:400 seeds. Shear 2x before using. Incubate for 5 minutes.
7. Flow in 7 μL 1 mg/mL κ-casein.
8. Flow in elongation 1 (without any MAPs). Image.
9. Flow in elongation 2 (with MAPs). Image.

Example Elongation:

_____ tubulin (μM)
_____ PEM-100
1μL 0.1M GTP
1μL 1M DTT
0.4μL 10mg/mL K-casein
0.5μL 2M KCl
3μL 2% methyl cellulose
1μL 300 mg/mL glucose
1μL deoxy
0.42μL 0.1M ATP
0.5μL 0.1M PC
1.75μL 1 mg/mL CPK
_____ katanin
_____ MAP
21ul total

B.14 ATPase Assays

ATPase mix for 25 reactions:

10 μL	100 mM ATP (pH 7.0)
5 μL	100 mM PEP
10 μL	LDH/PK (stock from bottle)
1 μL	100 mM NADH
224 μL	KAB
250 μL TOTAL	

1. Make up a 2x solution of katanin + MTs in KAB.
2. Add 10 μL of the katanin solution to each well of the plate. Make sure to have a 20 μL buffer control and a 10 μL buffer control to test the ATPase mix is working properly.
3. Make up the ATPase mix with everything except for the NADH.
4. Incubate the plate in the plate reader at 30°C and the ATPase mix at 30°C as well.
5. Add the NADH to the ATPase mix.
6. Use a repeat pipetter to put 10 μL of the ATPase mix into each of the wells.
7. Start reading the plate at 340 nm every 5 seconds.

B.15 Actin/MT Gliding Assay

Buffers:

Actin Buffer (10x):
250 mM Imidazole
250 mM KCl
40 mM $MgCl_2$
10 mM EGTA
*pH to 7.4

Myosin Buffer (10x):
3 M KCL
250 mM Imidazole
10 mM EGTA
40 mM $MgCl_2$
* Add 1mM DTT to 1x before experiments

1:100 MTs:
1 μL MTs
1 μL 2mM Taxol
98 μL PEM-100

Chamber Wash:
45 μL PEM-100
2.5 μL BSA (100 mg/mL stock)
1.5 μL Taxol (2 mM stock)
1 μL DTT (1 M stock)

1. Make a 10 μL flow chamber on nitrocellulose coated coverslips.
2. Flow in 10 μL of 1:9 kinesin:myosin mixture. Incubate for 5 minutes.
3. Flow in 10 μL wash buffer: 45 μL 1x Actin Buffer + 2.5 mg/mL BSA (100 mg/mL) + 1.5 μL Taxol (2 mM stock) + 1 μL DTT (1 M stock).
4. Flow in 10 μL of microtubules.
5. Flow in 10 μL wash buffer: 45 μL 1x Actin Buffer + 2.5 mg/mL BSA (100 mg/mL) + 1.5 μL Taxol (2 mM stock) + 1 μL DTT (1 M stock).
6. Flow in 10 μL of actin.
7. Flow in motility mix:

Motility Mix:
3 μL 3% methyl cellulose
1 μL DTT (1 M stock)
0.5 μL BSA (10 mg/mL stock)
1 μL glucose (300 mg/mL stock)
0.5 μL Taxol (2 mM stock)
0.4 μL ATP (100 mM stock)
0.5 μL PC (100 mM stock)
1.75 μL CPK (1 mg/mL stock)
1 μL Deoxy
10.35 μL Actin Buffer
20 μL TOTAL

8. Image- 500 msec exposure, every 5 seconds for 5 minutes.

BIBLIOGRAPHY

Ahmad, F J, W Yu, F J McNally, and P W Baas. 1999. “An Essential Role for Katanin in Severing Microtubules in the Neuron.” *The Journal of Cell Biology* 145 (2): 305–15.

Al-Bassam, Jawdat, Hwajin Kim, Gary Brouhard, Antoine van Oijen, Stephen C Harrison, and Fred Chang. 2010. “CLASP Promotes Microtubule Rescue by Recruiting Tubulin Dimers to the Microtubule.” *Developmental Cell* 19 (2): 245–58. doi:10.1016/j.devcel.2010.07.016.

Al-Bassam, Jawdat, Mark van Breugel, Stephen C Harrison, and Anthony Hyman. 2006. “Stu2p Binds Tubulin and Undergoes an Open-to-Closed Conformational Change..” *The Journal of Cell Biology* 172 (7): 1009–22. doi:10.1083/jcb.200511010.

Alexander, J E, D F Hunt, M K Lee, J Shabanowitz, H Michel, S C Berlin, T L MacDonald, R J Sundberg, L I Rebhun, and A Frankfurter. 1991. “Characterization of Posttranslational Modifications in Neuron-Specific Class III Beta-Tubulin by Mass Spectrometry..” *Proceedings of the National Academy of Sciences of the United States of America* 88 (11): 4685–89.

Alper, Joshua D, Franziska Decker, Bernice Agana, and Jonathon howard. 2014. “The Motility of Axonemal Dynein Is Regulated by the Tubulin Code.” *Biophysical Journal* 107 (12). The Authors: 2872–80. doi:10.1016/j.bpj.2014.10.061.

Amos, L A, and J Löwe. 1999. “How Taxol Stabilises Microtubule Structure.” *Chemistry & Biology* 6 (3): R65–R69.

Amos, Linda A, and Daniel Schlieper. 2005. “Microtubules and Maps.” In *Advances in Protein Chemistry*, 71:257–98. Advances in Protein Chemistry. Elsevier. doi:10.1016/S0065-3233(04)71007-4.

Audebert, S, A Koulakoff, Y Berwald-Netter, F Gros, P Denoulet, and B Eddé. 1994. “Developmental Regulation of Polyglutamylated Alpha- and Beta-Tubulin in Mouse Brain Neurons..” *Journal of Cell Science* 107 (Pt 8) (August): 2313–22.

Audebert, S, E Desbruyères, C Gruszczynski, A Koulakoff, F Gros, P Denoulet, and B Eddé. 1993. “Reversible Polyglutamylation of Alpha- and Beta-Tubulin and Microtubule Dynamics in Mouse Brain Neurons..” *Molecular Biology of the Cell* 4 (6): 615–26.

Baas, Peter W, and Liang Qiang. 2005. “Neuronal Microtubules: When the MAP Is the Roadblock.” *Trends in Cell Biology* 15 (4): 183–87. doi:10.1016/j.tcb.2005.02.001.

Barisic, M, R Silva e Sousa, S K Tripathy, M M Magiera, A V Zaytsev, A L Pereira, C Janke, E L Grishchuk, and H Maiato. 2015. “Microtubule Detyrosination Guides Chromosomes During Mitosis.” *Science (New York, NY)*, April. doi:10.1126/science.aaa5175.

Bartolini, F. 2005. “Identification of a Novel Tubulin-Destabilizing Protein Related to the Chaperone Cofactor E.” *Journal of Cell Science* 118 (6): 1197–1207. doi:10.1242/jcs.01719.

Belmont, L D, and T J Mitchison. 1996. “Identification of a Protein That Interacts with Tubulin Dimers and Increases the Catastrophe Rate of Microtubules..” *Cell* 84 (4): 623–31.

Bobinnec, Y, A Khodjakov, L M Mir, C L Rieder, B Eddé, and M Bornens. 1998. “Centriole Disassembly in Vivo and Its Effect on Centrosome Structure and Function in Vertebrate Cells..” *The Journal of Cell Biology* 143 (6): 1575–89.

Bohm, K J, W Vater, P Steinmetzer, and E Unger. 1990. “Effect of Sodium Chloride on Microtubule Assembly.” *Acta Histochemica Supplementband* 39 (January): 365–71.

Bosch Grau, M, G Gonzalez Curto, C Rocha, M M Magiera, P Marques Sousa, T Giordano, N Spassky, and C Janke. 2013. “Tubulin Glycylases and Glutamylases Have Distinct Functions in Stabilization and Motility of Ependymal Cilia.” *The Journal of Cell Biology* 202 (3): 441–51. doi:10.1007/s00415-006-0245-5.

Brandt, R, and G Lee. 1993. “Functional Organization of Microtubule-Associated Protein Tau. Identification of Regions Which Affect Microtubule Growth, Nucleation, and Bundle Formation in Vitro.” *The Journal of Biological Chemistry* 268 (5): 3414–19.

Brouhard, Gary J, Jeffrey H Stear, Tim L Noetzel, Jawdat Al-Bassam, Kazuhisa Kinoshita, Stephen C Harrison, Jonathon howard, and Anthony A Hyman. 2008. “XMAP215 Is a Processive Microtubule Polymerase.” *Cell* 132 (1): 79–88. doi:10.1016/j.cell.2007.11.043.

Brown, A, Y Li, T Slaughter, and M M Black. 1993. “Composite Microtubules of the Axon: Quantitative Analysis of Tyrosinated and Acetylated Tubulin Along Individual Axonal Microtubules.” *Journal of Cell Science* 104 (Pt 2) (February): 339–52.

Burk, D H, B Liu, R Zhong, W H Morrison, and Z H Ye. 2001. “A Katanin-Like Protein Regulates Normal Cell Wall Biosynthesis and Cell Elongation.” *The Plant Cell* 13 (4): 807–27.

Buster, Dan, Karen McNally, and Francis J McNally. 2002. “Katanin Inhibition Prevents the Redistribution of Gamma-Tubulin at Mitosis.” *Journal of Cell Science* 115 (Pt 5): 1083–92.

Cambray-Deakin, M A, and R D Burgoyne. 1987. “Posttranslational Modifications of Alpha-Tubulin: Acetylated and Detyrosinated Forms in Axons of Rat Cerebellum.” *The Journal of Cell Biology* 104 (6): 1569–74.

Caplow, M, J Shanks, and R L Ruhlen. 1988. “Temperature-Jump Studies of Microtubule Dynamic Instability.” *The Journal of Biological Chemistry* 263 (21): 10344–52.

Charafeddine, Rabab A, Joy Makdisi, David Schairer, Brian P O apos Rourke, Juan D Diaz-Valencia, Jason Chouake, Allison Kutner, et al. 2015. “Fidgetin-Like 2: A Microtubule Based Regulator of Wound Healing.” April. Nature Publishing Group, 1–10. doi:10.1038/jid.2015.94.

Chau, Miu-Fun, Monte J Radeke, Concepción de Inés, Isabel Barasoain, Lori A Kohlstaedt, and Stuart C Feinstein. 1998. “The Microtubule-Associated Protein Tau Cross-Links to Two Distinct Sites on Each A and B Tubulin Monomer via Separate Domains.” *Biochemistry* 37 (51): 17692–703. doi:10.1021/bi9812118.

Chen, J, Y Kanai, N J Cowan, and N Hirokawa. 1992. “Projection Domains of MAP2 and Tau Determine Spacings Between Microtubules in Dendrites and Axons.” *Nature* 360 (6405): 674–77. doi:10.1038/360674a0.

Choudhary, Chunaram, Chanchal Kumar, Florian Gnad, Michael L Nielsen, Michael Rehman, Tobias C Walther, Jesper V Olsen, and Matthias Mann. 2009. “Lysine Acetylation Targets Protein Complexes and Co-Regulates Major Cellular Functions.” *Science (New York, NY)* 325 (5942): 834–40. doi:10.1126/science.1175371.

Clandinin, T R, and P E Mains. 1993. “Genetic Studies of Mei-1 Gene Activity During the Transition From Meiosis to Mitosis in Caenorhabditis Elegans.” *Genetics* 134 (1): 199–210.

Clark-Maguire, S, and P E Mains. 1994. “Mei-1, a Gene Required for Meiotic Spindle Formation in Caenorhabditis Elegans, Is a Member of a Family of ATPases.” *Genetics* 136 (2): 533–46.

Cleveland, D W, S Y Hwo, and M W Kirschner. 1977. “Purification of Tau, a Microtubule-Associated Protein That Induces Assembly of Microtubules From Purified Tubulin.” *Journal of Molecular Biology* 116 (2): 207–25.

Conde, Cecilia, and Alfredo Cáceres. 2009. “Microtubule Assembly, Organization and Dynamics in Axons and Dendrites.” *Nature Reviews. Neuroscience* 10 (5): 319–32. doi:10.1038/nrn2631.

Curmi, P A, S S Andersen, S Lachkar, O Gavet, E Karsenti, M Knossow, and A Sobel. 1997. “The Stathmin/Tubulin Interaction in Vitro.” *The Journal of Biological Chemistry* 272 (40): 25029–36.

Davis, Liza J, David J Odde, Steven M Block, and Steven P Gross. 2002. “The Importance of Lattice Defects in Katanin-Mediated Microtubule Severing in Vitro.” *Biophysical Journal* 82 (6): 2916–27. doi:10.1016/S0006-3495(02)75632-4.

Desai, A, and T J Mitchison. 1997. “Microtubule Polymerization Dynamics.” *Annual Review of Cell and Developmental Biology* 13: 83–117. doi:10.1146/annurev.cellbio.13.1.83.

Dias, D P, and R A Milligan. 1999. “Motor Protein Decoration of Microtubules Grown in High Salt Conditions Reveals the Presence of Mixed Lattices.” *Journal of Molecular Biology* 287 (2): 287–92. doi:10.1006/jmbi.1999.2597.

Díaz-Valencia, Juan Daniel, Margaret M Morelli, Megan Bailey, Dong Zhang, David J Sharp, and Jennifer L Ross. 2011. “Drosophila Katanin-60 Depolymerizes and Severs at Microtubule Defects.” *Biophysical Journal* 100 (10): 2440–49. doi:10.1016/j.bpj.2011.03.062.

Ross, J.L., and R. Dixit 2010. Multiple color single molecule TIRF imaging and tracking of MAPs and motors. Methods. Cell. Biol. 95:521-542.

Dymek, Erin E, Paul A Lefebvre, and Elizabeth F Smith. 2004. “PF15p Is the Chlamydomonas Homologue of the Katanin P80 Subunit and Is Required for Assembly of Flagellar Central Microtubules.” *Eukaryotic Cell* 3 (4): 870–79. doi:10.1128/EC.3.4.870-879.2004.

Eckert, Thomas, Doan Tuong-Van Le, Susanne Link, Lena Friedmann, and Günther Woehlke. 2012. “Spastin's Microtubule-Binding Properties and Comparison to Katanin.” *PloS One* 7 (12): e50161. doi:10.1371/journal.pone.0050161.

Eckert, Thomas, Susanne Link, Doan Tuong-Van Le, Jean-Philippe Sobczak, Anja Gieseke, Klaus Richter, and Günther Woehlke. 2012. “Subunit Interactions and Cooperativity in the Microtubule-Severing AAA ATPase Spastin.” *The Journal of Biological Chemistry* 287 (31): 26278–90. doi:10.1074/jbc.M111.291898.

Elbaum-Garfinkle, S, G Cobb, J T Compton, X H Li, and E Rhoades. 2014. “Tau Mutants Bind Tubulin Heterodimers with Enhanced Affinity.” *Proceedings of the National Academy of Sciences of the United States of America* 111 (17): 6311–16. doi:10.1073/pnas.1315983111.

Ehrhardt, David W, and Sidney L Shaw. 2006. “Microtubule Dynamics and Organization in the Plant Cortical Array..” *Annual Review of Plant Biology* 57: 859–75. doi:10.1146/annurev.arplant.57.032905.105329.

Fan, J, A D Griffiths, A Lockhart, R A Cross, and L A Amos. 1996. “Microtubule Minus Ends Can Be Labelled with a Phage Display Antibody Specific to Alpha-Tubulin.” *Journal of Molecular Biology* 259 (3): 325–30. doi:10.1006/jmbi.1996.0322.

Fouquet, J P, B Eddé, M L Kann, A Wolff, E Desbruyères, and P Denoulet. 1994. “Differential Distribution of Glutamylated Tubulin During Spermatogenesis in Mammalian Testis.” *Cell Motility and the Cytoskeleton* 27 (1): 49–58. doi:10.1002/cm.970270106.

Frickey, Tancred, and Andrei N Lupas. 2004. “Phylogenetic Analysis of AAA Proteins.” *Journal of Structural Biology* 146 (1-2): 2–10. doi:10.1016/j.jsb.2003.11.020.

Fukushima, Nobuyuki, Daisuke Furuta, Yuji Hidaka, Ryutaro Moriyama, and Toshifumi Tsujiuchi. 2009. “Post-Translational Modifications of Tubulin in the Nervous System.” *Journal of Neurochemistry* 109 (3): 683–93. doi:10.1111/j.1471-4159.2009.06013.x.

Gard, D L, and M W Kirschner. 1987a. “A Microtubule-Associated Protein From Xenopus Eggs That Specifically Promotes Assembly at the Plus-End.” *The Journal of Cell Biology* 105 (5): 2203–15.

Gard, D L, and M W Kirschner. 1987b. “Microtubule Assembly in Cytoplasmic Extracts of Xenopus Oocytes and Eggs.” *The Journal of Cell Biology* 105 (5): 2191–2201.

Gardner, Melissa K, Marija Zanic, Christopher Gell, Volker Bormuth, and Jonathon Howard. 2011. “Depolymerizing Kinesins Kip3 and MCAK Shape Cellular Microtubule Architecture by Differential Control of Catastrophe.” *Cell* 147 (5): 1092–1103. doi:10.1016/j.cell.2011.10.037.

Gerhard, Hiller, and Klaus Weber. 1978. “Radioimmunoassay for Tubulin: a Quantitative Comparison of the Tubulin Content of Different Established Tissue Culture Cells and Tissues.” *Cell*.

Gigant, B, P A Curmi, C Martin-Barbey, E Charbaut, S Lachkar, L Lebeau, S Siavoshian, A Sobel, and M Knossow. 2000. “The 4 a X-Ray Structure of a Tubulin:Stathmin-Like Domain Complex.” *Cell* 102 (6): 809–16.

Goode, Bruce L, Paul E Denis, Dulal Panda, Monte J Radeke, Herb P Miller, and Leslie Wilson. 1997. “Functional Interactions Between the Proline-Rich and Repeat Regions of Tau Enhance Microtubule Binding and Assembly.” *Molecular Biology of the Cell* 8 (February): 353–65.

Gottesman, S, E Roche, Y Zhou, and R T Sauer. 1998. “The ClpXP and ClpAP Proteases Degrade Proteins with Carboxy-Terminal Peptide Tails Added by the SsrA-Tagging System.” *Genes & Development* 12 (9): 1338–47.

Gundersen, G G, and J C Bulinski. 1986. “Distribution of Tyrosinated and Nontyrosinated Alpha-Tubulin During Mitosis.” *The Journal of Cell Biology* 102 (3): 1118–26.

Gundersen, Gregg G, Edgar R Gomes, and Ying Wen. 2004. “Cortical Control of Microtubule Stability and Polarization.” *Current Opinion in Cell Biology* 16 (1): 106–12. doi:10.1016/j.ceb.2003.11.010.

Haar, ter, E, R J Kowalski, E Hamel, C M Lin, R E Longley, S P Gunasekera, H S Rosenkranz, and B W Day. 1996. “Discodermolide, a Cytotoxic Marine Agent That Stabilizes Microtubules More Potently Than Taxol.” *Biochemistry* 35 (1): 243–50. doi:10.1021/bi9515127.

Hallak, M E, J A Rodriguez, H S Barra, and R Caputto. 1977. “Release of Tyrosine From Tyrosinated Tubulin. Some Common Factors That Affect This Process and the Assembly of Tubulin.” *FEBS Letters* 73 (2): 147–50.

Hamel, Ernest, Dan L Sackett, Dionisios Vourloumis, and K C Nicolaou. 1999. “The Coral-Derived Natural Products Eleutherobin and Sarcodictyins a and B: Effects on the Assembly of Purified Tubulin with and Without Microtubule-Associated Proteins and Binding at the Polymer Taxoid Site.” *Biochemistry* 38 (17): 5490–98. doi:10.1021/bi983023n.

Hammond, Jennetta W, Dawen Cai, and Kristen J Verhey. 2008. “Tubulin Modifications and Their Cellular Functions.” *Current Opinion in Cell Biology* 20 (1): 71–76. doi:10.1016/j.ceb.2007.11.010.

Hartman, J J, and R D Vale. 1999. “Microtubule Disassembly by ATP-Dependent Oligomerization of the AAA Enzyme Katanin.” *Science (New York, NY)* 286 (5440): 782–85.

Hartman, J J, J Mahr, K McNally, K Okawa, A Iwamatsu, S Thomas, S Cheesman, J Heuser, R D Vale, and F J McNally. 1998. “Katanin, a Microtubule-Severing Protein, Is a Novel AAA ATPase That Targets to the Centrosome Using a WD40-Containing Subunit.” *Cell* 93 (2): 277–87.

Hirose, Keiko, Juan Fan, and Linda A Amos. 1995. “Re-Examination of the Polarity of Microtubules and Sheets Decorated with Kinesin Motor Domain.” *Journal of Molecular Biology* 251 (3): 329–33. doi:10.1006/jmbi.1995.0437.

Horio, T, and H Hotani. 1986. “Visualization of the Dynamic Instability of Individual Microtubules by Dark-Field Microscopy.” *Nature* 321 (6070): 605–7. doi:10.1038/321605a0.

Hoskins, J R, M Pak, M R Maurizi, and S Wickner. 1998. “The Role of the ClpA Chaperone in Proteolysis by ClpAP.” *Proceedings of the National Academy of Sciences of the United States of America* 95 (21): 12135–40.

Hotani, H, and T Horio. 1988. “Dynamics of Microtubules Visualized by Darkfield Microscopy: Treadmilling and Dynamic Instability.” *Cell Motility and the Cytoskeleton* 10 (1-2): 229–36. doi:10.1002/cm.970100127.

Howell, Bonnie J, Niklas Larsson, Martin Gullberg, and L Cassimeris. 1999. “Dissociation of the Tubulin-Sequestering and Microtubule Catastrophe-Promoting Activities of Oncoprotein 18/Stathmin.” *Molecular Biology of the Cell* 10 (January): 105–18.

Howes, S C, G M Alushin, T Shida, M V Nachury, and E Nogales. 2014. “Effects of Tubulin Acetylation and Tubulin Acetyltransferase Binding on Microtubule Structure.” *Molecular Biology of the Cell* 25 (2): 257–66. doi:10.1091/mbc.E13-07-0387.

Hu, Wen F, Oz Pomp, Tawfeg Ben-Omran, Andrew Kodani, Katrin Henke, Ganeshwaran H Mochida, Timothy W Yu, et al. 2014. “Katanin P80 Regulates Human Cortical Development by Limiting Centriole and Cilia Number.” *Neuron* 84 (6). Elsevier Inc.: 1240–57. doi:10.1016/j.neuron.2014.12.017.

Hyman, A A, S Salser, D N Drechsel, N Unwin, and T J Mitchison. 1992. “Role of GTP Hydrolysis in Microtubule Dynamics: Information From a Slowly Hydrolyzable Analogue, GMPCPP..” *Molecular Biology of the Cell* 3 (10): 1155–67.

Ishikawa, T, F Beuron, M Kessel, S Wickner, M R Maurizi, and A C Steven. 2001. “Translocation Pathway of Protein Substrates in ClpAP Protease..” *Proceedings of the National Academy of Sciences of the United States of America* 98 (8): 4328–33. doi:10.1073/pnas.081543698.

Iwaya, Naoko, Yohta Kuwahara, Yoshie Fujiwara, Natsuko Goda, Takeshi Tenno, Kohei Akiyama, Shogo Mase, et al. 2010. “A Common Substrate Recognition Mode Conserved Between Katanin P60 and VPS4 Governs Microtubule Severing and Membrane Skeleton Reorganization.” *The Journal of Biological Chemistry* 285 (22): 16822–29. doi:10.1074/jbc.M110.108365.

Janke, C. 2014. “The Tubulin Code: Molecular Components, Readout Mechanisms, and Functions.” *The Journal of Cell Biology* 206 (4): 461–72. doi:10.1158/0008-5472.CAN-05-1270.

Janke, Carsten, and Matthias Kneussel. 2010. “Tubulin Post-Translational Modifications: Encoding Functions on the Neuronal Microtubule Cytoskeleton.” *Trends in Neurosciences* 33 (8): 362–72. doi:10.1016/j.tins.2010.05.001.

Johjima, Ai, Kentaro Noi, Shingo Nishikori, Hirotsugu Ogi, Masatoshi Esaki, and Teru Ogura. 2015. “Microtubule Severing by Katanin P60 AAA+ ATPase Requires the C-terminal Acidic Tails of Both A- and B-Tubulins and Basic Amino Acid Residues in the AAA+ Ring Pore.” *The Journal of Biological Chemistry*, March, jbc.M114.614768. doi:10.1074/jbc.M114.614768.

Jourdain, L, P Curmi, A Sobel, D Pantaloni, and M F Carlier. 1997. “Stathmin: a Tubulin-Sequestering Protein Which Forms a Ternary T2S Complex with Two Tubulin Molecules.” *Biochemistry* 36 (36): 10817–21. doi:10.1021/bi971491b.

Karabay, Arzu, Wenqian Yu, Joanna M Solowska, Douglas H Baird, and Peter W Baas. 2004. “Axonal Growth Is Sensitive to the Levels of Katanin, a Protein That Severs Microtubules.” *The Journal of Neuroscience : the Official Journal of the Society for Neuroscience* 24 (25): 5778–88. doi:10.1523/JNEUROSCI.1382-04.2004.

Kim, Myung Hee, Tomasz Cierpicki, Urszula Derewenda, Daniel Krowarsch, Yuanyi Feng, Yancho Devedjiev, Zbigniew Dauter, et al. 2003. “The DCX-Domain Tandems of Doublecortin and Doublecortin-Like Kinase.” *Nature Structural Biology* 10 (5): 324–33. doi:10.1038/nsb918.

Kolb, Hartmuth C, M G Finn, and K Barry Sharpless. 2001. “Click Chemistry: Diverse Chemical Function From a Few Good Reactions.” *Angewandte Chemie (International Ed. in English)* 40 (11): 2004–21.

Kollman, Justin M, Andreas Merdes, Lionel Mourey, and David A Agard. 2011. “Nrm3209.” *Nature Reviews Molecular Cell Biology* 12 (11). Nature Publishing Group: 709–21. doi:10.1038/nrm3209.

Komarova, Yulia, Christian O De Groot, Ilya Grigoriev, Susana Montenegro Gouveia, E Laura Munteanu, Joseph M Schober, Srinivas Honnappa, et al. 2009. “Mammalian End Binding Proteins Control Persistent Microtubule Growth.” *The Journal of Cell Biology* 184 (5): 691–706. doi:10.1083/jcb.200807179.

Konishi, Yoshiyuki, and Mitsutoshi Setou. 2009. “Tubulin Tyrosination Navigates the Kinesin-1 Motor Domain to Axons.” *Nature Neuroscience* 12 (5): 559–67. doi:10.1038/nn.2314.

Kreis, T E. 1987. “Microtubules Containing Detyrosinated Tubulin Are Less Dynamic.” *The EMBO Journal* 6 (9): 2597–2606.

L'Hernault, S W, and J L Rosenbaum. 1985. “Chlamydomonas Alpha-Tubulin Is Posttranslationally Modified by Acetylation on the Epsilon-Amino Group of a Lysine.” *Biochemistry* 24 (2): 473–78.

Lacroix, Benjamin, Juliette van Dijk, Nicholas D Gold, Julien Guizetti, Gudrun Aldrian-Herrada, Krzysztof Rogowski, Daniel W Gerlich, and Carsten Janke. 2010. “Tubulin Polyglutamylation Stimulates Spastin-Mediated Microtubule Severing.” *The Journal of Cell Biology* 189 (6): 945–54. doi:10.1083/jcb.201001024.

Le, Doan Tuong-Van, Thomas Eckert, and Günther Woehlke. 2013a. “Computer Simulation of Assembly and Co-Operativity of Hexameric AAA ATPases.” *PloS One* 8 (7): e67815. doi:10.1371/journal.pone.0067815.

Lechtreck, Karl-Ferdinand, Travis J Gould, and George B Witman. 2013. “Flagellar Central Pair Assembly in Chlamydomonas Reinhardtii.” *Cilia* 2 (1): 15. doi:10.1186/2046-2530-2-15.

Levy, Sasha F, Adria C Leboeuf, Michelle R Massie, Mary Ann Jordan, Leslie Wilson, and Stuart C Feinstein. 2005. “Three- and Four-Repeat Tau Regulate the Dynamic Instability of Two Distinct Microtubule Subpopulations in Qualitatively Different Manners. Implications for Neurodegeneration.” *The Journal of Biological Chemistry* 280 (14): 13520–28. doi:10.1074/jbc.M413490200.

Li, S, J Finley, Z J Liu, S H Qiu, H Chen, C H Luan, M Carson, et al. 2002. “Crystal Structure of the Cytoskeleton-Associated Protein Glycine-Rich (CAP-Gly) Domain.” *The Journal of Biological Chemistry* 277 (50): 48596–601. doi:10.1074/jbc.M208512200.

Lohret, T A, F J McNally, and L M Quarmby. 1998. “A Role for Katanin-Mediated Axonemal Severing During Chlamydomonas Deflagellation.” *Molecular Biology of the Cell* 9 (5): 1195–1207.

Long, B H, J M Carboni, A J Wasserman, L A Cornell, A M Casazza, P R Jensen, T Lindel, W Fenical, and C R Fairchild. 1998. “Eleutherobin, a Novel Cytotoxic Agent That Induces Tubulin Polymerization, Is Similar to Paclitaxel (Taxol).” *Cancer Research* 58 (6): 1111–15.

Lopus, Manu, Cristina Manatschal, Rubén M Buey, Sasa Bjelic, Herbert P Miller, Michel O Steinmetz, and Leslie Wilson. 2012. “Cooperative Stabilization of Microtubule Dynamics by EB1 and CLIP-170 Involves Displacement of Stably Bound P(I) at Microtubule Ends.” *Biochemistry* 51 (14): 3021–30. doi:10.1021/bi300038t.

Loughlin, Rose, Jeremy D Wilbur, Francis J McNally, François J Nédélec, and Rebecca Heald. 2011. “Katanin Contributes to Interspecies Spindle Length Scaling in Xenopus.” *Cell* 147 (6): 1397–1407. doi:10.1016/j.cell.2011.11.014.

Löwe, J, H Li, K H Downing, and E Nogales. 2001. “Refined Structure of Aβ-Tubulin at 3.5 Å Resolution.” *Journal of Molecular Biology* 313 (5): 1045–57. doi:10.1006/jmbi.2001.5077.

Maccioni, R B, C I Rivas, and J C Vera. 1988. “Differential Interaction of Synthetic Peptides From the Carboxyl-Terminal Regulatory Domain of Tubulin with Microtubule-Associated Proteins.” *The EMBO Journal* 7 (7): 1957–63.

Mains, P E, K J Kemphues, S A Sprunger, I A Sulston, and W B Wood. 1990. “Mutations Affecting the Meiotic and Mitotic Divisions of the Early Caenorhabditis Elegans Embryo..” *Genetics* 126 (3): 593–605.

Mandelkow, E M, E Mandelkow, and R A Milligan. 1991. “Microtubule Dynamics and Microtubule Caps: a Time-Resolved Cryo-Electron Microscopy Study.” *The Journal of Cell Biology* 114 (5): 977–91.

Mandelkow, Eva-Maria, R Schultheiss, R Rapp, M Muller, and Eckhard Mandelkow. 1986. “On the Surface Lattice of Microtubules: Helix Starts, Protofilament Number, Seam, and Handedness.” *Journal of Cell Science* 102 (March): 1067=1073.

Manna, Tapas, Srinivas Honnappa, Michel O Steinmetz, and Leslie Wilson. 2008. “Suppression of Microtubule Dynamic Instability by the +TIP Protein EB1 and Its Modulation by the CAP-Gly Domain of P150glued.” *Biochemistry* 47 (2): 779–86. doi:10.1021/bi701912g.

Mao, C X, Y Xiong, Z Xiong, Q Wang, Y Q Zhang, and S Jin. 2014. “Microtubule-Severing Protein Katanin Regulates Neuromuscular Junction Development and Dendritic Elaboration in Drosophila.” *Development (Cambridge, England)* 141 (5): 1064–74. doi:10.1242/dev.097774.

Margolis, R L, and L Wilson. 1978. “Opposite End Assembly and Disassembly of Microtubules at Steady State in Vitro.” *Cell* 13 (1): 1–8.

Matsuyama, Akihisa, Tadahiro Shimazu, Yuko Sumida, Akiko Saito, Yasuhiro Yoshimatsu, Daphné Seigneurin-Berny, Hiroyuki Osada, et al. 2002. “In Vivo Destabilization of Dynamic Microtubules by HDAC6-Mediated Deacetylation.” *The EMBO Journal* 21 (24): 6820–31.

McCullough, Brannon R, Elena E Grintsevich, Christine K Chen, Hyeran Kang, Alan L Hutchison, Arnon Henn, Wenxiang Cao, et al. 2011. “Cofilin-Linked Changes in Actin Filament Flexibility Promote Severing.” *Biophysical Journal* 101 (1). Biophysical Society: 151–59. doi:10.1016/j.bpj.2011.05.049.

McCullough, Brannon R, Laurent Blanchoin, Jean-Louis Martiel, and Enrique M De La Cruz. 2008. “Cofilin Increases the Bending Flexibility of Actin Filaments: Implications for Severing and Cell Mechanics.” *Journal of Molecular Biology* 381 (3): 550–58. doi:10.1016/j.jmb.2008.05.055.

McDermott, C, K White, K Bushby, and P Shaw. 2000. “Hereditary Spastic Paraparesis: a Review of New Developments.” *Journal of Neurology, Neurosurgery, and Psychiatry* 69 (2): 150–60.

McNally, F. 2000. “Capturing a Ring of Samurai.” *Nature Cell Biology*. doi:10.1038/71385.

McNally, F J, and R D Vale. 1993. “Identification of Katanin, an ATPase That Severs and Disassembles Stable Microtubules.” *Cell* 75 (3): 419–29.

McNally, F J, and S Thomas. 1998. “Katanin Is Responsible for the M-Phase Microtubule-Severing Activity in Xenopus Eggs.” *Molecular Biology of the Cell* 9 (7): 1847–61.

McNally, F J, K Okawa, A Iwamatsu, and R D Vale. 1996. “Katanin, the Microtubule-Severing ATPase, Is Concentrated at Centrosomes.” *Journal of Cell Science* 109 (Pt 3) (March): 561–67.

McNally, K P, O A Bazirgan, and F J McNally. 2000. “Two Domains of P80 Katanin Regulate Microtubule Severing and Spindle Pole Targeting by P60 Katanin.” *Journal of Cell Science* 113 (Pt 9) (May): 1623–33.

McNally, K, E Berg, D B Cortes, V Hernandez, P E Mains, and F J McNally. 2014. “Katanin Maintains Meiotic Metaphase Chromosome Alignment and Spindle Structure in Vivo and Has Multiple Effects on Microtubules in Vitro.” *Molecular Biology of the Cell* 25 (7): 1037–49. doi:10.1091/mbc.E13-12-0764.

McNally, Karen Perry, Dan Buster, and Francis J McNally. 2002. “Katanin-Mediated Microtubule Severing Can Be Regulated by Multiple Mechanisms.” *Cell Motility and the Cytoskeleton* 53 (4): 337–49. doi:10.1002/cm.10080.

McNally, Karen, Anjon Audhya, Karen Oegema, and Francis J McNally. 2006. “Katanin Controls Mitotic and Meiotic Spindle Length.” *The Journal of Cell Biology* 175 (6): 881–91. doi:10.1083/jcb.200608117.

Mitchison, T J. 1993. “Localization of an Exchangeable GTP Binding Site at the Plus End of Microtubules..” *Science (New York, NY)* 261 (5124): 1044–47.

Mitchison, T J, and M W kirschner. 1984. “Dynamic Instability of Microtubule Growth.” *Nature* 312 (5991): 237–42.

Montenegro Gouveia, Susana, Kris Leslie, Lukas C Kapitein, Rubén M Buey, Ilya Grigoriev, Michael Wagenbach, Ihor Smal, et al. 2010. “In Vitro Reconstitution of the Functional Interplay Between MCAK and EB3 at Microtubule Plus Ends.” *Current Biology : CB* 20 (19): 1717–22. doi:10.1016/j.cub.2010.08.020.

Mukherjee, Suranjana, Juan Daniel Diaz-Valencia, Shannon Stewman, Sylvain Monnier, Uttama Rath, Ana B Asenjo, Rababa charafeddine, et al. 2012. “Human Fidgetin Is a Microtubule Severing Enzyme and Minus-End Depolymerase That Regulates Mitosis.” *Cell Cycle (Georgetown, Tex)* 11 (12): 1–8.

Murata, Takashi, Seiji Sonobe, Tobias I Baskin, Susumu Hyodo, Seiichiro Hasezawa, Toshiyuki Nagata, Tetsuya Horio, and Mitsuyasu Hasebe. 2005. “Microtubule-Dependent Microtubule Nucleation Based on Recruitment of Γ-Tubulin in Higher Plants.” *Nature Cell Biology* 7 (10): 961–68. doi:10.1038/ncb1306.

Nakamura, Masayoshi, and Takashi Hashimoto. 2009. “A Mutation in the Arabidopsis Gamma-Tubulin-Containing Complex Causes Helical Growth and Abnormal Microtubule Branching.” *Journal of Cell Science* 122 (Pt 13): 2208–17. doi:10.1242/jcs.044131.

Nakamura, Masayoshi, David W Ehrhardt, and Takashi Hashimoto. 2010. “Microtubule and Katanin-Dependent Dynamics of Microtubule Nucleation Complexes in the Acentrosomal Arabidopsis Cortical Array.” *Nature Cell Biology* 12 (11): 1064–70. doi:10.1038/ncb2110.

Nath, J P, G R Eagle, and R H Himes. 1986. “Studies on the Exchangeable Nucleotide Binding Site of Tubulin.” *Annals of the New York Academy of Sciences* 466: 482–95.

Newton, Cori N, Michael Wagenbach, Yulia Ovechkina, Linda Wordeman, and Leslie Wilson. 2004. “MCAK, a Kin I Kinesin, Increases the Catastrophe Frequency of Steady-State HeLa Cell Microtubules in an ATP-Dependent Manner in Vitro.” *FEBS Letters* 572 (1-3): 80–84. doi:10.1016/j.febslet.2004.06.093.

Nogales, E, M Whittaker, R A Milligan, and K H Downing. 1999. “High-Resolution Model of the Microtubule.” *Cell* 96 (1): 79–88.

Nogales, E, S G Wolf, and K H Downing. 1998. “Structure of the Alpha Beta Tubulin Dimer by Electron Crystallography.” *Nature* 391 (6663): 199–203. doi:10.1038/34465.

Ogawa, Tadayuki, Ryo Nitta, Yasushi Okada, and Nobutaka Hirokawa. 2004. “A Common Mechanism for Microtubule Destabilizers-M Type Kinesins Stabilize Curling of the Protofilament Using the Class-Specific Neck and Loops.” *Cell* 116 (4): 591–602.

Peris, L, M Wagenbach, L Lafanechere, J Brocard, A T Moore, F Kozielski, D Job, L Wordeman, and A Andrieux. 2009. “Motor-Dependent Microtubule Disassembly Driven by Tubulin Tyrosination.” *The Journal of Cell Biology* 185 (7): 1159–66. doi:10.1083/jcb.105.1.265.

Peris, Leticia, Manuel Thery, Julien Fauré, Yasmina Saoudi, Laurence Lafanechère, John K Chilton, Phillip Gordon-Weeks, et al. 2006. “Tubulin Tyrosination Is a Major Factor Affecting the Recruitment of CAP-Gly Proteins at Microtubule Plus Ends.” *The Journal of Cell Biology* 174 (6): 839–49. doi:10.1083/jcb.200512058.

Qiang, Liang, Wenqian Yu, Athena Andreadis, Minhua Luo, and Peter W Baas. 2006. “Tau Protects Microtubules in the Axon From Severing by Katanin.” *The Journal of Neuroscience : the Official Journal of the Society for Neuroscience* 26 (12): 3120–29. doi:10.1523/JNEUROSCI.5392-05.2006.

Qiang, Liang, Wenqian Yu, Mei Liu, Joanna M Solowska, and Peter W Baas. 2010. “Basic Fibroblast Growth Factor Elicits Formation of Interstitial Axonal Branches via Enhanced Severing of Microtubules.” *Molecular Biology of the Cell* 21 (2): 334–44. doi:10.1091/mbc.E09-09-0834.

Rasi, M Qasim, Jeremy D K Parker, Jessica L Feldman, Wallace F Marshall, and Lynne M Quarmby. 2009. “Katanin Knockdown Supports a Role for Microtubule Severing in Release of Basal Bodies Before Mitosis in Chlamydomonas.” *Molecular Biology of the Cell* 20 (1): 379–88. doi:10.1091/mbc.E07-10-1007.

Reed, Nathan A, Dawen Cai, T Lynne Blasius, Gloria T Jih, Edgar Meyhofer, Jacek Gaertig, and Kristen J Verhey. 2006. “Microtubule Acetylation Promotes Kinesin-1 Binding and Transport.” *Current Biology* 16 (21): 2166–72. doi:10.1016/j.cub.2006.09.014.

Robson, S J, and R D Burgoyne. 1989. “Differential Localisation of Tyrosinated, Detyrosinated, and Acetylated Alpha-Tubulins in Neurites and Growth Cones of Dorsal Root Ganglion Neurons.” *Cell Motility and the Cytoskeleton* 12 (4): 273–82. doi:10.1002/cm.970120408.

Rogowski, Krzysztof, FranÃ ois Juge, Juliette van Dijk, Dorota Wloga, Jean-Marc Strub, Nicolette Levilliers, Daniel Thomas, et al. 2009. “Evolutionary Divergence of Enzymatic Mechanisms for Posttranslational Polyglycylation.” *Cell* 137 (6). Elsevier Inc.: 1076–87. doi:10.1016/j.cell.2009.05.020.

Roll-Mecak, Antonina, and Francis J McNally. 2010. “Microtubule-Severing Enzymes.” *Current Opinion in Cell Biology* 22 (1): 96–103. doi:10.1016/j.ceb.2009.11.001.

Roll-Mecak, Antonina, and Ronald D Vale. 2005. “The Drosophila Homologue of the Hereditary Spastic Paraplegia Protein, Spastin, Severs and Disassembles Microtubules.” *Current Biology : CB* 15 (7): 650–55. doi:10.1016/j.cub.2005.02.029
.

Roll-Mecak, Antonina, and Ronald D Vale. 2006. “Making More Microtubules by Severing: a Common Theme of Noncentrosomal Microtubule Arrays?” *The Journal of Cell Biology* 175 (6): 849–51. doi:10.1083/jcb.200611149.

Roll-Mecak, Antonina, and Ronald D Vale. 2008. “Structural Basis of Microtubule Severing by the Hereditary Spastic Paraplegia Protein Spastin.” *Nature* 451 (7176): 363–67. doi:10.1038/nature06482.

Rosenberg, Kenneth J, Jennifer L Ross, H Eric Feinstein, Stuart C Feinstein, and Jacob Israelachvili. 2008. “Complementary Dimerization of Microtubule-Associated Tau Protein: Implications for Microtubule Bundling and Tau-Mediated Pathogenesis.” *Proceedings of the National Academy of Sciences of the United States of America* 105 (21): 7445–50. doi:10.1073/pnas.0802036105.

Rostovtseva, Tatiana K, Kely L Sheldon, Elnaz Hassanzadeh, Claire Monge, Valdur Saks, Sergey M Bezrukov, and Dan L Sackett. 2008. “Tubulin Binding Blocks Mitochondrial Voltage-Dependent Anion Channel and Regulates Respiration.” *Proceedings of the National Academy of Sciences of the United States of America* 105 (48): 18746–51. doi:10.1073/pnas.0806303105.

Schiff, P B, J Fant, and S B Horwitz. 1979. “Promotion of Microtubule Assembly in Vitro by Taxol.” *Nature* 277 (5698): 665–67.

Schuyler, S C, and D Pellman. 2001. “Microtubule ‘Plus-End-Tracking Proteins’: the End Is Just the Beginning.” *Cell* 105 (4): 421–24.

Schweers, O, E Schönbrunn-Hanebeck, A Marx, and E Mandelkow. 1994. “Structural Studies of Tau Protein and Alzheimer Paired Helical Filaments Show No Evidence for Beta-Structure.” *The Journal of Biological Chemistry* 269 (39): 24290–97.

Serrano, L, E Montejo de Garcini, M A Hernández, and J Avila. 1985. “Localization of the Tubulin Binding Site for Tau Protein.” *European Journal of Biochemistry / FEBS* 153 (3): 595–600.

Sharma, N, J Bryant, D Wloga, R Donaldson, R C Davis, M Jerka-Dziadosz, and J Gaertig. 2007. “Katanin Regulates Dynamics of Microtubules and Biogenesis of Motile Cilia.” *The Journal of Cell Biology* 178 (6): 1065–79. doi:10.1083/jcb.200704021.

Shelanski, M L, F Gaskin, and C R Cantor. 1973. “Microtubule Assembly in the Absence of Added Nucleotides.” *Proceedings of the National Academy of Sciences of the United States of America* 70 (3): 765–68.

Shipley, Krista, Mohammad Hekmat-Nejad, Jennifer Turner, Carolyn Moores, Robert Anderson, Ronald Milligan, Roman Sakowicz, and Robert Fletterick. 2004. “Structure of a Kinesin Microtubule Depolymerization Machine.” *The EMBO Journal* 23 (7): 1422–32. doi:10.1038/sj.emboj.7600165.

Sirajuddin, Minhajuddin, Luke M Rice, and Ronald D Vale. 2014. “Regulation of Microtubule Motors by Tubulin Isotypes and Post-Translational Modifications.” *Nature Cell Biology* 16 (4): 335–44. doi:10.1038/ncb2920.

Snyder, J P, J H Nettles, B Cornett, K H Downing, and E Nogales. 2001. “The Binding Conformation of Taxol in Beta-Tubulin: a Model Based on Electron Crystallographic Density.” *Proceedings of the National Academy of Sciences of the United States of America* 98 (9): 5312–16. doi:10.1073/pnas.051309398.

Song, Y H, and E Mandelkow. 1993. “Recombinant Kinesin Motor Domain Binds to Beta-Tubulin and Decorates Microtubules with a B Surface Lattice..” *Proceedings of the National Academy of Sciences of the United States of America* 90 (5): 1671–75.

Srayko, M, D W Buster, O A Bazirgan, F J McNally, and P E Mains. 2000. “MEI-1/MEI-2 Katanin-Like Microtubule Severing Activity Is Required for Caenorhabditis Elegans Meiosis.” *Genes & Development* 14 (9): 1072–84.

Srayko, Martin, Eileen T O'toole, Anthony A Hyman, and Thomas Müller-Reichert. 2006. “Katanin Disrupts the Microtubule Lattice and Increases Polymer Number in C. Elegans Meiosis.” *Current Biology : CB* 16 (19): 1944–49. doi:10.1016/j.cub.2006.08.029.

Steinmetz, M O, R A Kammerer, W Jahnke, K N Goldie, A Lustig, and J van Oostrum. 2000. “Op18/Stathmin Caps a Kinked Protofilament-Like Tubulin Tetramer.” *The EMBO Journal* 19 (4): 572–80. doi:10.1093/emboj/19.4.572.

Stewart, Andrea, Asako Tsubouchi, Melissa M Rolls, W Daniel Tracey, and Nina Tang Sherwood. 2012. “Katanin P60-Like1 Promotes Microtubule Growth and Terminal Dendrite Stability in the Larval Class IV Sensory Neurons of Drosophila.” *The Journal of Neuroscience : the Official Journal of the Society for Neuroscience* 32 (34): 11631–42. doi:10.1523/JNEUROSCI.0729-12.2012.

Stoppin-Mellet, Virginie, Jérémie Gaillard, and Marylin Vantard. 2002. “Functional Evidence for in Vitro Microtubule Severing by the Plant Katanin Homologue.” *The Biochemical Journal* 365 (Pt 2): 337–42. doi:10.1042/BJ20020689.

Stoppin-Mellet, Virginie, Jérémie Gaillard, and Marylin Vantard. 2006. “Katanin's Severing Activity Favors Bundling of Cortical Microtubules in Plants.” *The Plant Journal : for Cell and Molecular Biology* 46 (6): 1009–17. doi:10.1111/j.1365-313X.2006.02761.x.

Sudo, Haruka, and Peter W Baas. 2010. “Acetylation of Microtubules Influences Their Sensitivity to Severing by Katanin in Neurons and Fibroblasts.” *The Journal of Neuroscience : the Official Journal of the Society for Neuroscience* 30 (21): 7215–26. doi:10.1523/JNEUROSCI.0048-10.2010.

Sudo, Haruka, and Peter W Baas. 2011. “Strategies for Diminishing Katanin-Based Loss of Microtubules in Tauopathic Neurodegenerative Diseases.” *Human Molecular Genetics* 20 (4): 763–78. doi:10.1093/hmg/ddq521.

Sudo, Haruka, and Yoshiro Maru. 2008. “LAPSER1/LZTS2: a Pluripotent Tumor Suppressor Linked to the Inhibition of Katanin-Mediated Microtubule Severing.” *Human Molecular Genetics* 17 (16): 2524–40. doi:10.1093/hmg/ddn153.

Tournebize, R, A Popov, K Kinoshita, A J Ashford, S Rybina, A Pozniakovsky, T U Mayer, C E Walczak, E Karsenti, and A A Hyman. 2000. “Control of Microtubule Dynamics by the Antagonistic Activities of XMAP215 and XKCM1 in Xenopus Egg Extracts..” *Nature Cell Biology* 2 (1): 13–19. doi:10.1038/71330.

Toyo-Oka, Kazuhito, Shinji Sasaki, Yoshihisa Yano, Daisuke Mori, Takuya Kobayashi, Yoko Y Toyoshima, Suzumi M Tokuoka, et al. 2005. “Recruitment of Katanin P60 by Phosphorylated NDEL1, an LIS1 Interacting Protein, Is Essential for Mitotic Cell Division and Neuronal Migration.” *Human Molecular Genetics* 14 (21): 3113–28. doi:10.1093/hmg/ddi339.

Trinczek, Bernhard, Jacek Biernat, Karlheinz Baumann, Eva-Maria Mandelkow, and Eckhard Mandelkow. 1995. “Domains of Tau Protein, Differental Phosphorylation, and Dynamic Instability of Microtubules.” *Molecular Biology of the Cell* 6 (December): 1887–1902.

Truslove, Gillian M. 1956. “The Anatomy and Development of the Fidget Mouse.” *Journal of Genetics* 54 (1). Springer: 64–86.

Vaart, Babet van der, Anna Akhmanova, and Anne Straube. 2009. “Regulation of Microtubule Dynamic Instability.” *Biochemical Society Transactions* 37 (5): 1007. doi:10.1042/BST0371007.

Vale, R D. 1991. “Severing of Stable Microtubules by a Mitotically Activated Protein in Xenopus Egg Extracts.” *Cell* 64 (4): 827–39.

Vasquez, R J, D L Gard, and L Cassimeris. 1994. “XMAP From Xenopus Eggs Promotes Rapid Plus End Assembly of Microtubules and Rapid Microtubule Polymer Turnover.” *The Journal of Cell Biology* 127 (4): 985–93.

Vitre, Benjamin, Frédéric M Coquelle, Claire Heichette, Cyrille Garnier, Denis Chrétien, and Isabelle Arnal. 2008. “EB1 Regulates Microtubule Dynamics and Tubulin Sheet Closure in Vitro.” *Nature Cell Biology* 10 (4): 415–21. doi:10.1038/ncb1703.

Walker, R A, E T O'Brien, N K Pryer, M F Soboeiro, W A Voter, H P Erickson, and E D Salmon. 1988. “Dynamic Instability of Individual Microtubules Analyzed by Video Light Microscopy: Rate Constants and Transition Frequencies.” *The Journal of Cell Biology* 107 (4): 1437–48.

Walker, R A, N K Pryer, and E D Salmon. 1991. “Dilution of Individual Microtubules Observed in Real Time in Vitro: Evidence That Cap Size Is Small and Independent of Elongation Rate.” *The Journal of Cell Biology* 114 (1): 73–81.

Wang, Hong-Wei, and Eva Nogales. 2005. “Nucleotide-Dependent Bending Flexibility of Tubulin Regulates Microtubule Assembly.” *Nature Cell Biology* 435 (7044): 911–15. doi:10.1038/nature03606.

Waterman-Storer, C M, and E D Salmon. 1997. “Microtubule Dynamics: Treadmilling Comes Around Again.” *Current Biology* 7 (6): R369–72.

Wegner, A. 1976. “Head to Tail Polymerization of Actin.” *Journal of Molecular Biology* 108 (1): 139–50.

Weisenberg, R C, W J Deery, and P J Dickinson. 1976. “Tubulin-Nucleotide Interactions During the Polymerization and Depolymerization of Microtubules.” *Biochemistry* 15 (19): 4248–54.

White, Susan Roehl, Katia J Evans, Jeffrey Lary, James L Cole, and Brett Lauring. 2007. “Recognition of C-terminal Amino Acids in Tubulin by Pore Loops in Spastin Is Important for Microtubule Severing.” *The Journal of Cell Biology* 176 (7): 995–1005. doi:10.1083/jcb.200610072.

Whitehead, Evan, Rebecca Heald, and Jeremy D Wilbur. 2012. “N-terminal Phosphorylation of P60 Katanin Directly Regulates Microtubule Severing.” *Journal of Molecular Biology*, November, –. doi:10.1016/j.jmb.2012.11.022.

Witte, H, D Neukirchen, and F Bradke. 2008. “Microtubule Stabilization Specifies Initial Neuronal Polarization.” *The Journal of Cell Biology* 180 (3): 619–32. doi:10.1002/(SICI)1097-0169(1998)41:1<18::AID-CM2>3.0.CO;2-B.

Wloga, D, and J Gaertig. 2010. “Post-Translational Modifications of Microtubules.” *Journal of Cell Science* 124 (1): 154–54. doi:10.1242/jcs.083576.

Yang, Hsin-ya, Karen McNally, and Francis J McNally. 2003. “MEI-1/Katanin Is Required for Translocation of the Meiosis I Spindle to the Oocyte Cortex in C Elegans.” *Developmental Biology* 260 (1): 245–59.

Ye, Xiangcang, Yu-Chen Lee, Michel Choueiri, Khoi Chu, Chih-Fen Huang, Wen-Wei Tsai, Ryuji Kobayashi, Christopher J Logothetis, Li-Yuan Yu-Lee, and Sue-Hwa Lin. 2011. “Aberrant Expression of Katanin P60 in Prostate Cancer Bone Metastasis.” *The Prostate*, June. doi:10.1002/pros.21431.

Yu, Wenqian, Joanna M Solowska, Liang Qiang, Arzu Karabay, Douglas Baird, and Peter W Baas. 2005. “Regulation of Microtubule Severing by Katanin Subunits During Neuronal Development.” *The Journal of Neuroscience : the Official Journal of the Society for Neuroscience* 25 (23): 5573–83. doi:10.1523/JNEUROSCI.0834-05.2005.

Yu, Wenqian, Liang Qiang, Joanna M Solowska, Arzu Karabay, Sirin Korulu, and Peter W Baas. 2008. “The Microtubule-Severing Proteins Spastin and Katanin Participate Differently in the Formation of Axonal Branches.” *Molecular Biology of the Cell* 19 (4): 1485–98. doi:10.1091/mbc.E07-09-0878.

Zanic, Marija, Per O widlund, Anthony A Hyman, and Jonathon Howard. 2013. “Synergy Between XMAP215 and EB1 Increases Microtubule Growth Rates to Physiological Levels.” *Nature Cell Biology* 15 (6): 688–93. doi:10.1038/ncb2744.

Zhang, Dong, Gregory C Rogers, Daniel W Buster, and David J Sharp. 2007. “Three Microtubule Severing Enzymes Contribute to the ‘Pacman-Flux’ Machinery That Moves Chromosomes.” *The Journal of Cell Biology* 177 (2): 231–42. doi:10.1083/jcb.200612011.

Zhang, Dong, Kyle D Grode, Shannon F Stewman, Juan Daniel Diaz-Valencia, Emily Liebling, Uttama Rath, Tania Riera, et al. 2011. “Drosophila Katanin Is a Microtubule Depolymerase That Regulates Cortical-Microtubule Plus-End Interactions and Cell Migration.” *Nature Cell Biology* 13 (4): 361–70. doi:10.1038/ncb2206.

Zhang, Pingbo, Yu Wang, Hiromi Sesaki, and Miho Iijima. 2010. “Proteomic Identification of Phosphatidylinositol (3,4,5) Triphosphate-Binding Proteins in Dictyostelium Discoideum.” *Proceedings of the National Academy of Sciences of the United States of America* 107 (26): 11829–34. doi:10.1073/pnas.1006153107.

Zhang, Quan, Erica Fishel, Tyler Bertroche, and Ram Dixit. 2013. “Microtubule Severing at Crossover Sites by Katanin Generates Ordered Cortical Microtubule Arrays in Arabidopsis.” *Current Biology* 23 (21). Elsevier Ltd: 2191–95. doi:10.1016/j.cub.2013.09.018.